



TECHNISCHE
UNIVERSITÄT
WIEN
Vienna University of Technology

DISSERTATION

Novel biocompatible materials for *in vivo* two-photon polymerisation

Ausgeführt zum Zwecke der Erlangung des akademischen Grades eines Doktors der technischen Wissenschaften unter der Leitung von

Ao. Univ. Prof. Dipl.-Ing. Dr. mont. Jürgen Stampfl

am

Institut für Werkstoffwissenschaft und Werkstofftechnologie (E308)

Eingereicht an der Technischen Universität Wien

Fakultät für Maschinenwesen und Betriebswissenschaften

von

Dipl.-Ing. Jan Torgersen

0425694 / E786-740

Gobergasse 89/12, 1130 Wien, Österreich

Wien, am 22. März 2013

1 Kurzfassung

Zweiphotonenpolymerisation (2PP) ist eine vielseitig anwendbare laserbasierte Fertigungstechnik, die es ermöglicht, 3D Strukturen mit Mikro- und Nanometerpräzision herzustellen. Die Strukturen können dabei direkt nach einem computergenerierten Design (CAD) additiv aufgebaut werden. Für die 2PP benötigt man stark fokussiertes, femtosekunden-gepulstes Laserlicht. Die Wellenlänge der verwendeten Laser liegt normalerweise im nahen Infrarotbereich. Licht dieser Wellenlängen wird von biologischem Gewebe nur minimal absorbiert und verursacht bei moderaten Pulsenergien keine zellulären Schäden. Theoretisch kann also 2PP in direktem Kontakt mit lebendem Gewebe und Zellen erfolgen. Mithilfe von biokompatiblen Formulierungen könnten so bioaktive Konstrukte geschaffen werden, die dynamisch modellierbar sind und ähnliche topografische, chemische und mechanische Anreize wie die natürliche extrazelluläre Matrix (EZM) geben. Mittels 2PP könnte man so bestimmte Elemente dieser Umgebung verändern, ohne auf andere Faktoren Einfluss zu nehmen. Um diese Möglichkeiten auszuschöpfen, müssen jedoch zwei Einschränkungen der 2PP überwunden werden: die langen Prozesszeiten und die geringe Verfügbarkeit von passenden, für die 2PP optimierten photopolymerisierbaren Formulierungen.

In dieser Doktorarbeit beschreiben wir das Design und die Realisierung eines experimentellen Aufbaus für die 2PP, der es erlaubt, neuartige wasserbasierte Formulierungen zu verarbeiten. Hydrogelstrukturen können mit Schreibgeschwindigkeiten von über 100 mm/s aufgebaut werden, die bisher höchsten Schreibgeschwindigkeiten in der 2PP. Zusätzlich können diese Strukturen *in vivo*, in Gegenwart von lebenden biologischem Gewebe und Zellen geformt werden. Mithilfe eigens entwickelter, wasserlöslicher 2PP-Photoinitiatoren (PI) konnten wir Akrylat-Monomere in Formulierungen mit über 80% Wassergehalt vernetzen. Da diese Monomere eine Tendenz zur Michael-Addition an Proteine zeigen, untersuchten wir auch die Verarbeitbarkeit von Vinylester- und Vinylkarbamat-Monomeren. Im Gegensatz zu Akrylaten, die in potentiell toxische Polyacrylsäure zerfallen, degradieren Vinylester und Vinylkarbamat-Polymere zu biokompatiblen Polyvinylalkohol. Effiziente Thiol/-en-Chemie erlaubte uns, CAD-Präzisionsbauteile aus biokompatibler modifizierter Gelatine und Hyaluronsäure aufzubauen. In Toxizitätsanalysen untersuchten wir den Einfluss einzelner Komponenten von akrylatbasierten Formulierungen auf den Modellorganismus *C. elegans*. Schlussendlich zeigten wir 2PP in direktem Kontakt mit lebenden Nematoden.

2 Abstract

Two-photon polymerisation (2PP) is a versatile laser fabrication technique that allows the creation of 3D structures at micro- and nanometre precision. The structures are created additively in direct accordance to a computer-aided design (CAD). It requires tightly focused fs-pulsed light sources usually operating in the near infrared (NIR) wavelength range. In this region, biological tissues exhibit a window of transparency and only absorb light minimally. When operating below a certain pulse energy threshold, the laser light does not cause any cellular damage. This theoretically allows inducing 2PP in the presence of living biological tissues and cells. Suitable biocompatible formulations that can render bioactive constructs would potentially allow building a dynamic environment with topographical, chemical and mechanical cues similar to that of the natural extracellular matrix (ECM). In that way, 2PP would allow to alter key elements of this environment without changing any other influencing factors. To explore these possibilities, 2PP has to overcome two main limitations, the slow process speeds and the lack of available optimised formulations.

In this thesis, we report the design and realisation of a 2PP experimental setup, which allows fabricating hydrogel structures from novel water-based formulations. Writing speeds of above 100 mm/s are feasible, which is the highest speed reported in 2PP. Moreover, the presented components have the potential to be formed *in vivo*, in the presence of living cells and tissues. Using water-soluble two-photon optimised photoinitiators (PI), we could effectively cross-link acrylates in formulations of up to 80% water content. As acrylates show a tendency towards Michael addition to proteins, we explored the use of vinyl ester and vinyl carbonate monomers for 2PP. In contrast to acrylic polymers, which form potentially toxic poly (acrylic acid), vinyl ester and carbonate polymers form biocompatible poly (vinyl alcohol) during degradation. Efficient thiol-ene chemistry enabled us to cross-link modified Gelatine and Hyaluronic Acid hydrogel precursors to form precise biocompatible constructs in good accordance to CAD. Using model organisms of type *C. elegans*, we performed lethal concentration assays exposing the animals to the components of one selected hydrogel formulation. Finally, as a proof-of-concept, we performed 2PP directly in the presence of a living nematode.

3 Content

1	Kurzfassung	2
2	Abstract.....	3
3	Content	4
4	Acknowledgement	6
5	Introduction	8
6	Additive Manufacturing Technologies	10
6.1	Photopolymerisation.....	11
6.1.1	Photoinitiator	12
6.1.2	Cross-linking of monomers.....	13
6.2	Lithography based AMT	15
7	Multi-photon absorption and related processes	19
7.1	Two-photon polymerisation	22
7.2	Photoinitiators and two-photon efficiency	24
7.3	Optical Elements in systems for two-photon lithography.....	29
7.3.1	Femtosecond pulsed laser	29
7.3.2	Acousto-optic modulator.....	31
8	State-of-the-art 2PP-structured hydrogels	33
8.1	Cell encapsulation in hydrogel constructs.....	34
8.2	Additive manufacturing of hydrogels.....	34
8.3	Commercially available, water-soluble, two-photon photoinitiators	36
8.4	Biopolymers	39
8.4.1	Synthetic polymers as hydrogel precursors	39
8.4.2	Native proteins/ protein precursors.....	42
8.4.3	Modified natural polymers as hydrogel precursors	45
9	Processed Materials.....	45
9.1	Photoinitiators	45
9.1.1	Organo-soluble PIs	46
9.1.2	Water-soluble PIs.....	47
9.2	Precursors.....	48
9.2.1	Synthetic precursors	48
9.2.2	Natural based precursors	50
10	Experimental setups for 2PP.....	53
10.1	Micro 3-dimensional structuring device	53
10.2	2PP Micro Processing system Mipro	54
10.2.1	Power Adjustment.....	56

10.2.2	Beam expander.....	59
10.2.3	Galvano-scanner.....	59
10.2.4	Camera for online observation	61
10.2.5	X-Y-Z- axes system and formulation container	61
10.2.6	The control software.....	62
10.2.7	Photographs.....	63
10.3	Microscope objectives	64
11	Structuring experiments	68
11.1	Preparation for 2PP structuring	68
11.2	Speed-power screening via lattice array	69
11.3	Preparation for investigations in the laser scanning microscope.....	70
12	Material screening	72
12.1	Organo-soluble 2PP Initiators.....	72
12.2	Water-soluble 2PP Initiators	76
12.3	Synthetic Precursor Screening	85
12.3.1	Polyethylene glycol diacrylate (PEGda).....	86
12.3.2	Polyethylene glycol dimethacrylate (PEGdma).....	94
12.3.3	Formulation three	95
12.3.4	Hexandioic acid divinyl ester (4VE)	96
12.3.5	Polyethylene glycol vinyl ester (PEGve)	97
12.3.6	Glycerol Trivinyl Carbonate (GVC)	98
12.4	Modified Natural Precursor Screening.....	99
12.4.1	Assessment of photochemical reactions in protein cross-linking	99
12.4.2	Hydrolysed Gelatine Vinyl Ester (GHve).....	101
12.4.3	Hyaluronic Acid Vinyl Ester (HAvE)	109
13	Toxicity analysis.....	111
13.1	Biocompatibility of monomers and initiators.....	112
13.1.1	Preparation and Experimentation	112
13.1.2	Analysis.....	113
13.1.3	Results of LC assay	115
13.2	Photodamage.....	116
14	In-Vivo writing	118
15	Perspectives	120
16	Conclusion.....	122
17	Abbreviations	124
18	Literature	126
19	Curriculum Vitae	136

4 Acknowledgement

I thank...

...my supervisor ao. Univ. Prof. DI Dr. mont. Jürgen Stampfl for his great support in every respect. He gave me full freedom for realising my projects, supported me in my decisions and paved the way for my future development. Apart from his technical expertise and his management skills that were essential for this project, he has a very good hand for providing a good working atmosphere, in which every employee gets incentives to voluntarily work rather than being forced to. The own personal development was in the foreground, which, together with the right team, always made the work very pleasant, interesting and diversified. I can say that Prof. Stampfl was my best employer so far and I enjoyed working at the Institute of Materials Science every day.

...ao. Univ. Prof. DI Dr. techn. Robert Liska, my second examiner and head of our close collaborators from the Institute of Applied Synthetic Chemistry. As the reader of this thesis will notice, all results of this work only came up as his and our department worked together. Prof. Robert Liska's expertise, his ideas and his ability to express chemical issues understandably were a key for the successP of this project.

... Peter Gruber Bsc. for working with me on the Mipro setup. His programming work and his expertise in electronics formed the basis of a very fast, reproducible and easy-to-use machine that provides great functionality. Without him, this work would not have been possible. To my view, employing Peter Gruber was my best decision during this thesis. Peter Gruber is a very interested, talented and helpful person. I hope, he will continue to to have joy in work during his ongoing PhD thesis and I wish him all the best for his future.

... my collaborators Xiao-Hua Qin and Zhiquan Li from the Institute of Applied Synthetic Chemistry. Xiao-Hua Qin made outstanding work in modifying biopolymers for their use in 2PP. A major result and novelty of this thesis was the fabrication of constructs from his materials. Likewise, without the initiators from Zhiquan Li, these findings would not have been possible either.

... Dr. Aleksandr Ovsianikov for very fruitful discussions and for his good advice. He is a real expert in two-photon polymerisation and is always informed on the latest development in this field. His knowledge and his ideas were essential for this work.

...my colleagues and friends Dr. Thomas Koch, DI Christoph Schoberleiter, DI Franziska Stadlbauer, DI Simon Gruber, DI Markus Hatzenbichler, Dr. Klaus Cicha, Dr. Klaus Stadlmann, DI Gerald Mitteramskogler, DI Robert Gmeiner, Dr. Ruth Felzmann, Christoph Balka, DI Adrienne Wilke, DI Peter Dorfinger and Dr. Ruth Markut-Khol for the perfect working atmosphere and the very interesting discussions on sundry topics especially during lunch break. I really enjoyed working with them all.

... Prof. Mag. Dr. Verena Jantsch-Plunger, Dr. Antoine Baudrimot, Mag. Thomas Machacek, Mag. Alexander Woglar and Christian Pflügl from the Department of Chromosome Biology, University of Vienna, for their collaboration and their assistance with the toxicity tests on *Caenorhabditis elegans*. The results of the last two sections of this thesis developed from this very fruitful collaboration. I regret that we did not get funding for a common project, as I liked working together with them.

... my father Dr. Helge Torgersen for reading through my manuscripts and my PhD thesis. He helped me a lot structuring the text and expressing myself in my writing. I learned a lot during the discussions with him and I attribute my language skills and ability to write largely to him.

...my girlfriend Julia Hein for being very patient and understanding concerning long working hours, for always being interested in my work, no matter how boring or incomprehensible and for being on my side during the last two years. Moreover, I thank her for deciding to join me working abroad.

...my cousin Mag. Ludwig Fliesser, who recommended me image and video editing software that were essential for the toxicity analysis and the press release. Furthermore, I thank him for giving me insight into image processing as well as for his very creative ideas in evaluating experiments.

...my brother Sven Torgersen, my mother Christine Torgersen and my friends for supporting me, for being patient and interested in what I was doing. They provided me the necessary background to relax and gave me the sometimes very necessary view from the distance.

This quite comprehensive acknowledgement illustrates that this interdisciplinary work originated from many people from very different fields. I hesitate to attribute the reported findings solely to myself. In the following thesis, I will use the “we” term, whenever I use the active form, indicating that this work developed from the involvement of all people mentioned above. In that way I want to show my appreciation for all my supporters, collaborators, helpers and friends without them this work would not have been possible.

5 Introduction

Additive manufacturing (AM) allows creating parts additively directly in accordance with a computer-aided design. The big advantage of this technique is its small batch size, which cannot be reached with any other manufacturing processes. Every individual structure can be customised. In some cases, also several different parts can be created in one batch.

This advantage rendered AM widely used in biomedical applications, where implants are created according to data from clinical imaging like magnetic resonance or computer tomography. However, conventional AM technologies (AMT) have resolutions in the tens of micrometre range. A construct like the native extracellular matrix (ECM), has micro-features organised in a 3D continuum proceeding from the micro- to the macro-scale (REF). To really resemble these features, an AMT is required that allows resolutions below one μm while still being able to create mm to cm sized constructs.

Two-photon polymerisation (2PP) is a novel AMT that uses pulsed near infrared (NIR) laser light to trigger polymerisation of a liquid formulation. Due to the nonlinear two-photon absorption (2PA) effect, the polymerisation only occurs in the confined area of the focal point of a high magnification, high numerical aperture microscope objective. Due to this nonlinearity, the feature sizes are much smaller than in conventional AMT. Moreover, as polymerisation only occurs in the focal point, the polymerisation is not limited to the surface of the formulation. In contrast to other AMTs, thus, 2PP does not require a layer-by-layer approach. 3D features can be directly created tracing the focal point into the volume of the formulation.

For biomedical applications, 2PP offers another advantage. As biological tissues exhibit a window of transparency at the wavelength of the applied laser, the light only causes minimal stress for tissues and cells. In two-photon microscopy, which is based on the same working principle, high-resolution pictures can be taken deep inside living biological tissue without causing cellular damage. Hence, with 2PP, it would be theoretically possible to create high-resolution constructs in a topographical similarity to the ECM directly in the presence of cells and tissues. This synthetic environment can then be tuned dynamically to observe the interactions with cells and tissues.

These are exciting prospects indeed. However, for exploiting the possibilities, 2PP has to overcome two main limitations. First, as 2PP constructs are built from very thin polymeric lines, the fabrication of constructs in biologically relevant size takes hours or even days. For significant biological assays, a large number of constructs are needed. Current fabrication times limit the use of 2PP for this purpose. Second, there are only a limited number of formulations commercially available so far, all of them exclusively soluble in organic solvents only. However, for successful polymerisation in the presence of biological tissues and cells hydrophilic precursors are needed that can render biocompatible hydrogel constructs, i.e. polymers swollen by water. Ideally, these precursors are based on synthetic or naturally derived biomaterials that not only are inert to cells but also support their proliferation and differentiation.

In this PhD thesis, we addressed both aspects; the long processing time and the limited availability of 2PP optimised biocompatible formulations. Thus, we designed a novel 2PP system intended to increase the fabrication speed. Secondly, we screened water-based formulations efficiently convertible into hydrogels. Finally, we tested these materials regarding their biocompatibility and their potential for biomedical applications.

This PhD thesis is divided into two parts. In the first section, we will provide a short overview over existing AM technologies and their differentiation from 2PP. Then a theoretical description

on the components involved in a 2PP will be given and the working principle of necessary devices involved will be explained. Furthermore, the reader will gain knowledge about the composition of a polymerisable formulation and will get an overview over existing work on biocompatible 2PP materials.

In the second section, we will present the design, composition and capabilities of the 2PP experimental system we built in the course of this thesis. On this system, we screened novel water-soluble two-photon initiators and ranked them regarding their efficiency. We will investigate the 2PP processability of novel biocompatible hydrogels based on natural and synthetic components. Finally, the reader will get an insight on the biocompatibility and feasibility for *in situ* fabrication of the presented formulations.

6 Additive Manufacturing Technologies

The general principle of additive manufacturing (AM) is to create a 3D object by successively adding cross-sections of defined thickness on top of each other. An AM technology (AMT) can convert 3D computer aided designs (CADs) into single slices and assemble a part physically adding these slices in the right order. The system works without user interaction and thus combines computer aided design with manufacturing (CAD-CAM). In contrast to other manufacturing technologies, the material properties of the object evolve simultaneously to its geometry during the fabrication. AMT are processes in which [1]:

- the slices are generated from CAD files that are universal to all AMTs (STL¹ format),
- no tooling is required,
- mechanical properties evolve simultaneously to the geometry and
- workpieces can be generally created in any direction. As it inherently adheres to the building platform, it is not necessary to clamp the pieces as in conventional machining processes.

Formerly, AMT was known as Rapid Prototyping. Its initial use was to quickly create simple objects meaningful for a particular related product. These objects supported the design process without being necessarily applicable. In recent years, however, AMTs became feasible for direct manufacturing of end-products.

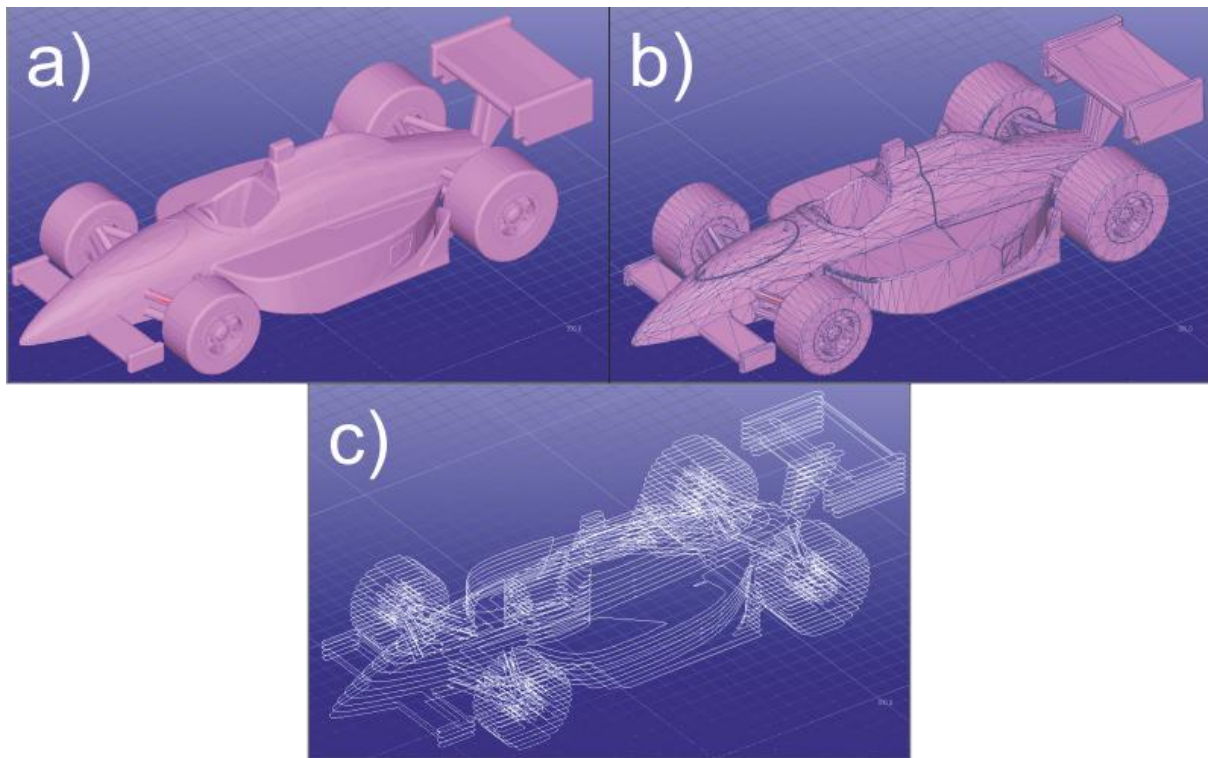


Figure 1 a) CAD of an indy racecar, b) approximation of the surface via a net of triangles (STL) and c) generation of layered cross-sections for subsequent AM

¹ The STL file format is a data interface approximating a 3D object's surface via triangles. Three end points and the associated surface normal describe each triangle. The smaller the triangles, the more the model matches to its intended design. Smaller triangles, in turn, increase the file size and complicate computer processing. The STL is the common standard in AMT and in various other CAM applications and is saved binary or in ASCII code.

The underlying physical principle classifies AMTs into different groups. They can be roughly divided into technologies that generate from the solid, liquid and gas phase [1]. Generation from the solid phase includes:

- melting and solidification of powder, powder mixtures or granulates (sintering or melting processes),
- cutting or milling out from foils, ribbons or boards,
- melting and solidifying hard materials (extrusion) and
- adhesion of granulates or powders via binders (3D printing).

Forming objects from the gas phase includes:

- physical separation from aerosols and
- chemical separation from the gas phase

Finally, the generation of objects from the liquid phase includes laser or lamp assisted photopolymerisation. In our group, we specialized on the latter process. The underlying AM principle is called photolithography based AM. In the next chapter, we will discuss the main composition of photopolymerisable formulations and explain their overall polymerisation principle based on common components.

6.1 Photopolymerisation

A photopolymerisable formulation typically consists of a reactive diluent, a cross-linker and a photoinitiator. However, most formulations contain additional components (Figure 2) all influencing its reactivity, viscosity, reaction mechanism and the properties of the resulting polymer [2][3]:

- High molecular weight monomers, i.e. **cross-linkers** with more than one reactive group define the mechanical properties of the resulting polymer.
- Mono- and multifunctional **reactive diluents** affect the number of reactive groups, decrease the viscosity of the formulation and additionally tune the mechanical properties.
- A **photoinitiator** that meets the emission spectra of the used light source efficiently creates radicals upon its activation.
- A **solvent** swells the polymer network decreasing the stiffness and strength of the obtained structure.
- **Filler materials** influence the Young's modulus² and/or other functional properties of the final polymer structure.
- If the monomers are very reactive, **inhibitors** can prevent premature polymerisation scavenging formed radicals.
- **Bioactive stimuli** can be added to the formulation. These substances are major determinants for cell behaviour and can be conjugated to the scaffold material [5].

Adding solvents and filler materials decrease the shrinkage during polymerisation to obtain better shape accuracy and reduce internal stresses.

² The Young's modulus is also known as tensile modulus or elastic modulus. It is a value describing the stiffness of an elastic material. It is calculated as the ratio between stress and strain along an axis in the linear range, where Hooke's law can be applied [4].

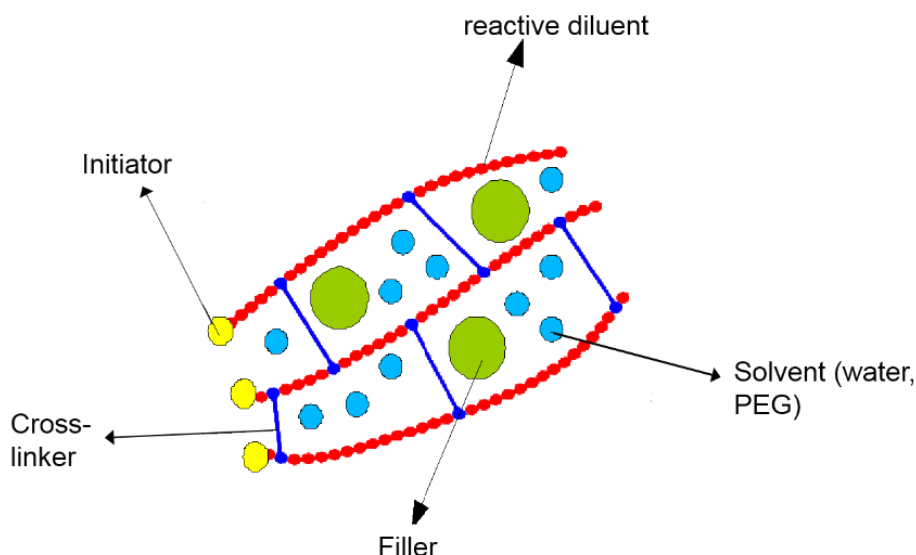


Figure 2 Basic building block of photopolymerisable formulations used for lithography based AMT [2]

In photopolymerisation, initiators dissolve into radicals that break the double bonds of the monomers (cross-linkers and reactive diluents) and start the solidification in the radical chain reaction polymerisation. In the following section, we will explain the mechanisms of the PIs' decay into radicals and the process of radical chain growth polymerisation.

6.1.1 Photoinitiator

PIs are the key substance of photopolymerisable formulations. They are UV or VIS sensible and convert radiation energy into chemical energy dissolving into radicals [6] (Figure 6a), molecules that have unpaired electrons on an otherwise open shell configuration. As they are highly reactive, they can react with another molecule breaking its double bonds [7]. This **initiation** step starts the free radical polymerisation chain reaction.

In conventional photopolymerisation, one absorbed photon elevates the PI molecule from a lower (S_0) to a higher and short-lived (S_1) vibrational energy level, both of them being singlet states with spin zero.³ Rather than immediately decaying to the ground state simply emitting fluorescence or converting the energy into internal heat, the PI decays to a long-lived triplet state via inter system crossing. The spin of the molecule is now one.⁴ Depending on the molecule, the PI in the excited triplet state can create radicals via the monomolecular type 1 or the bimolecular type 2 mechanism of radical formation.

³ The spin is measured in reduced Planck's constant

⁴ Triplet is referred to the three possibilities for the secondary spin quantum number (1,0,-1).

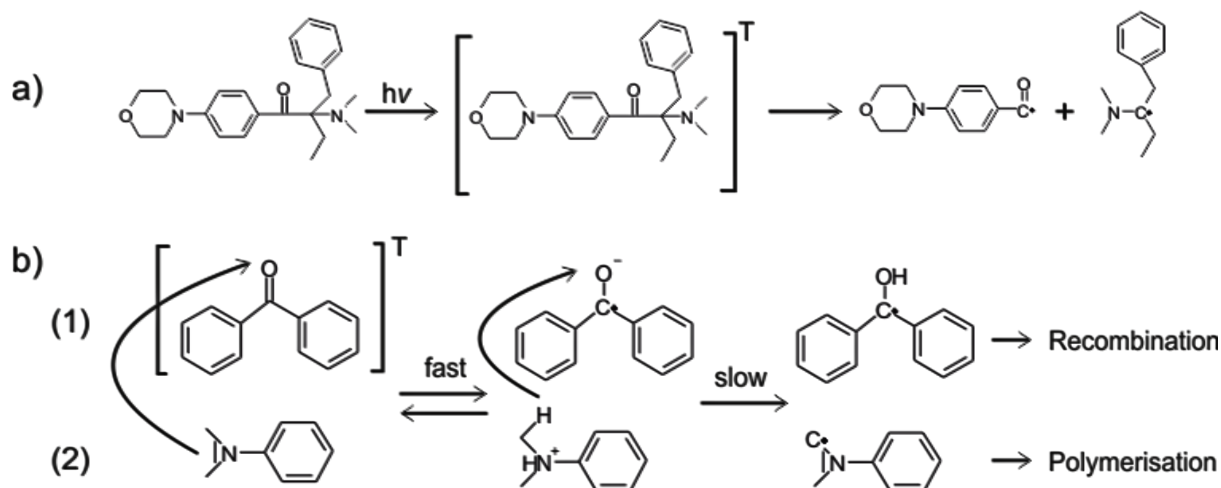


Figure 3 a) type I initiator Irgacure 369 cleaves from the excited triplet state forming two radicals that can start polymerisation b) an amine (2) quickly transfers an electron to the type II initiator benzophenone (1); proton transfer leads to a reactive amine that can start polymerisation. The PI itself recombines [8].

α - or β -cleavage leads to photo-fragmentation and radical formation of type I PIs. This usually takes place next to an aromatic carbonyl group and thus results in the formation of one or two benzoyl radicals, which are capable of starting the polymerisation. One typical example of a α -cleavage initiator is Irgacure 369 (Figure 3a).

Chromophores such as benzophenones and analogues as well as donors (co-initiators) such as alcohols, ethers and amines are the basis of bimolecular type II PIs. They create radicals via hydrogen abstraction or electron transfer. In hydrogen abstraction, a benzophenone in the triplet state, for example, abstracts hydrogen from an alcohol, ether or amine. Whereas the formed alcohol, ether or amine radicals start the polymerisation, benzophenone radicals recombine to form a non-reactive dimer. Figure 3b shows the latter type II reaction. An electron is abstracted from the amine (2) and transferred to the excited ketone (1). Subsequent proton transfer renders reactive amine radicals that can start the polymerisation. The benzophenone radicals recombine. Beside amines, ethers or alcohol, also monomers or the formed polymer chains can serve as donors [9][8][10].

For 1PP, the reaction mechanism of type I initiators is usually more efficient. It is much simpler and requires shorter excited state lifetimes not necessitating any interaction with another molecule. For 2PP, however, type I initiators are rare as shifting their absorption spectra is complicated. The design of 2PIs will be addressed in section 7.2.

6.1.2 Cross-linking of monomers

Radicals formed in the initiation process (Figure 6a) cross-link viscous monomers to form a polymer. In the simplest case, a photopolymerisable formulation consists of only one type of monomer and the PI. Figure 4 shows the cross-linking of acrylates (AC), common monomers in photopolymerisation. In the **propagation** step (Figure 4b), the PI radicals break the double bonds of the carbonyl group and add onto the acrylate monomers rendering the nearest carbon a radical. The formed molecule can add another acrylate, which creates another anchor point on the molecule.

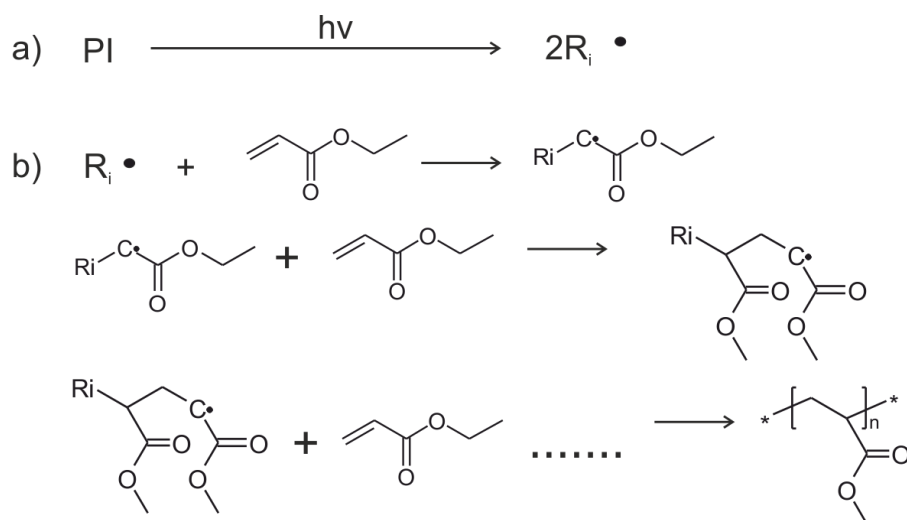


Figure 4 The principle of Initiation (a) and Propagation (b), modified from [6] and [11]

This process continues until a chain **termination** reaction occurs. Recombination (Figure 5(1)) involves two unpaired electrons from two reactive molecules that bond together to form a non-reactive molecule. In **disproportionation** (Figure 5(2)), a radical attaches to a single C-H bond from another reactive molecule. Both reaction partners can form two non-reactive molecules, one with a single and one with a double bond at the end of the chain. Termination can also happen through random incidentally existent inhibitors such as aerial oxygen. This is a common challenge in stereolithography (see section 6.2). The radical chain propagation terminates integrating a peroxide group.

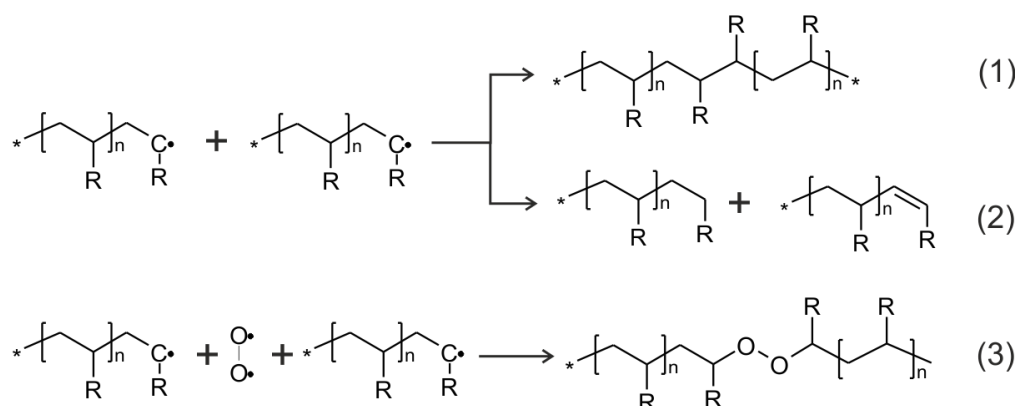


Figure 5 Termination through Recombination (1) and Disproportionation (2) or oxygen inhibition (3), modified from [6] and [11]

Branched polymers develop via **chain transfer** reactions (Figure 6). A reactive chain transfers its unpaired electron to a random unreactive C-H bond anywhere in the middle of the reaction partner's chain. While this terminates the chain growth of the considered molecule, it creates a reactive anchor point in the chain of the reaction partner. As other molecules attach, a new chain starts to propagate leaving a branched polymeric structure [11].

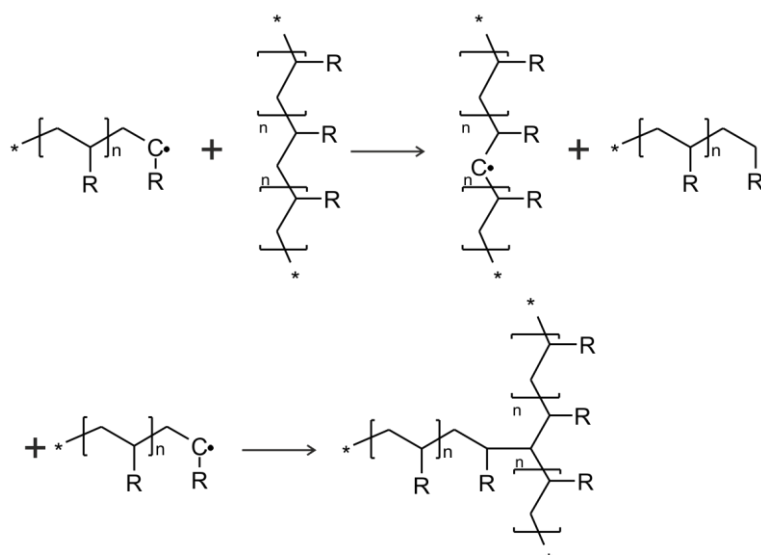


Figure 6 Chain transfer, R stands for the acrylate branch modified from [6] and [11]

Photopolymerisation based AMT restricts the curing of the formulation to the respective layered cross-sections of the CAD (see Figure 1c). It can be distinguished between different lithography based AMTs regarding their way of spatially controlling the exposure [1]. In the following section, we will present laser-scanning and photomask based AMT.

6.2 Lithography based AMT

Laser-scanning based stereolithography (SLA) is the oldest and most widely used AMT. Figure 7 shows a principal scheme. Typically, a UV laser beam with small diameter passes an acousto-optic modulator (AOM) which turns it on and off. A galvanoscanner containing two rotating mirrors deflects the laser beam before it reaches the surface of a photopolymerisable formulation. Both, the AOM and the galvanoscanner, are computer-controlled. The beam moves on the surface of the specimen according to the cross-sections of the CAD. As the fabrication starts, the first layer cures to a defined depth. It sticks on the computer-driven building platform, which moves away from the surface. The coating system delivers new liquid material and the illumination starts again. The depth of curing is slightly larger than the movement to ensure cross-linking with unreacted functional groups of the previous layer. This ensures good adherence. The procedure repeats until the desired solid object reaches its intended extent. In STL writing speeds of 0.2-0.5 m/s are possible [2].

After fabrication, the operator removes the part from the building platform and cleans it from excess liquid formulation. This requires chemical developers or water (depending on the type of formulation). Afterwards, it is necessary to drain the finished part. In many cases, STL produces parts not fully polymerised. These “green part” are post-cured with UV light to improve their mechanical properties [12]. Subtractive post-processing like machining, grinding, sandblasting, metallizing and/or painting is possible to a certain extent.

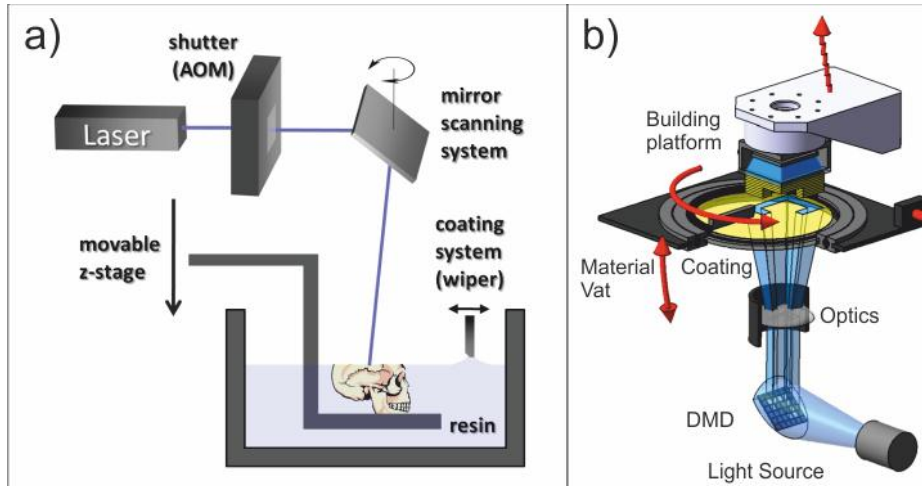


Figure 7 Comparison between a) Laserscanning SLA [6] and b) DLP [13]

Among all commercial AMTs, laser-scanning is still the most accurate. Only the diameter of the laser beam limits the X- and Y- resolution. Hence, today, the laser beam usually passes a focusing device before it reaches the formulation increasing available resolution and providing more energy per unit area. A resolution of 5 μm in the X- and Y- plane and 10 μm in the Z- direction have been reported processing hybrid sol-gel materials without further post-processing [2]. During the fabrication process, the parts have relatively low strength. Recoating, internal tensions and/or the part's self-weight can easily deform overhanging structures or cantilevers. These geometries require supporting during the building process (Figure 8). Another disadvantage of laser-scanning and its related bottom-up structuring procedure is the related exposure of the surface to the surrounding environment. Oxygen inhibition might hinder the polymerisation process and reduce the obtainable part quality making it necessary to provide an adequate surrounding (e.g. nitrogen).

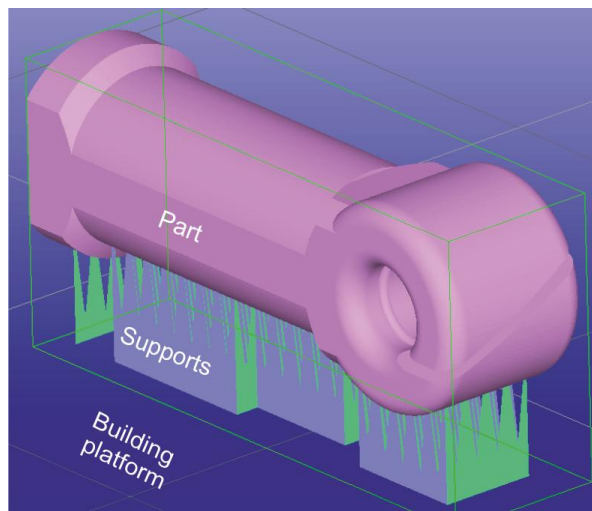


Figure 8 CAD part of yarn guide with supports

Figure 7b illustrates a photomask lithography based AMT: Here, the machine fabricates the object top-down rather than bottom-up projecting light on a transparent, non-adhering plate from underneath. The building platform dips into the formulation from above. On one side, this eventually increases the mechanical forces during the separation from the bottom plate after the illumination. On the other, it ensures a smooth surface and prevents oxygen from reaching the polymerising surface. In addition, for low-viscous formulations, recoating is not required. In

contrast to laserscanning, the dynamic masks can cure the entire cross-section of the part at once. When using high power light sources, this reduces the process time significantly. Exploiting the full extent of the building platform, the process speed measure is vertical mm/h.

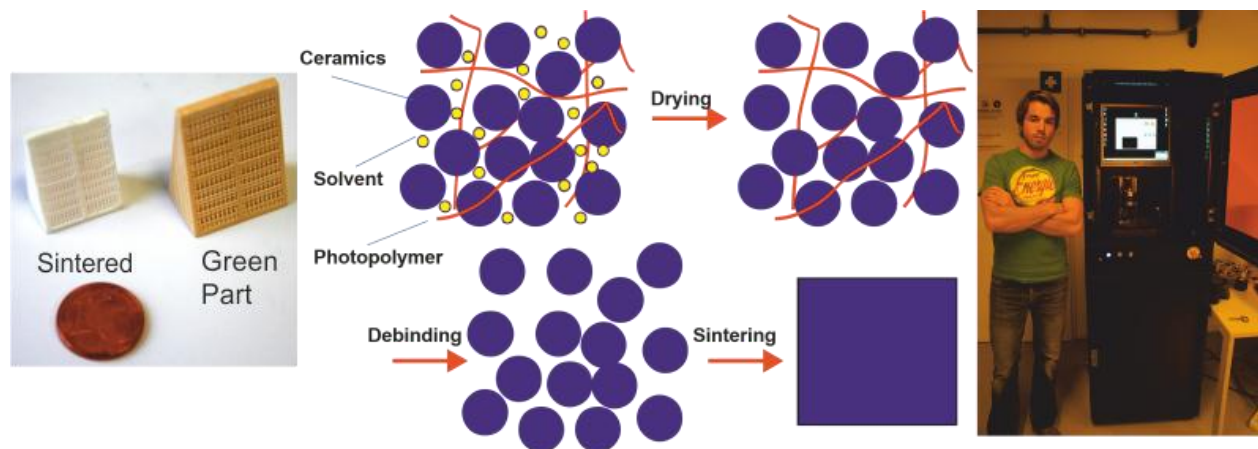


Figure 9 DLP of ceramic materials [13]

One can distinguish between lamp-mask and projector mask processes. The former includes a transparent mask on which the full cross-section of the part is displayed. Strong UV lamps shine through the mask and cure the behind liquid formulation at desired spots. The latter (Figure 7) uses a video beamer to image the cross-section onto the surface to be exposed. In this technology, a digital light projector (DLP), consisting an array of micro-mirrors (digital mirror device), projects a 2D pixel-pattern onto the transparent plate. Depending on the focusing objective and the amount of micro-mirrors, the resolution can be up to 40 μm laterally and 15 μm in Z [13]. Our group uses this technique to process formulations filled with ceramic particles (Figure 9). The “green part”, which is obtained after fabrication, is an organic matrix containing ceramic particles. Thermal treatment including drying, debinding and sintering ensures the removal of this matrix. This facilitates the AM fabrication of fully dense ceramic parts. It was possible to fabricate alumina, bioglass and β -tricalciumphosphate objects [13].

Similar to stereolithography, 2PP is a laser-scanning approach, too. The experimental setups can be similar to that of Figure 7a. However, as fabrication is not limited to the surface of the formulation, the focal point can be moved anywhere in the volume leaving cured polymer along its trace [11][14]. Any arbitrary 3D shape can thus be “recorded” into the volume (see Figure 10). The basic building unit, where the polymerisation takes place (volumetric pixel or voxel) can be regarded as “3D pen”, with which a polymeric line can be created anywhere in the volume of a formulation.

The resolution can be down to 65 nm [15] as the non-linearity of 2PA provides the possibility to reduce the size of the polymerised volume below the diffraction limit [14]. Figure 10 shows a comparison between STL and 2PP fabrication. The former is limited to the surface, whereas in the latter allows to trace the focal volume (volumetric pixel or voxel) through the formulation leaving a complex polymeric structure.

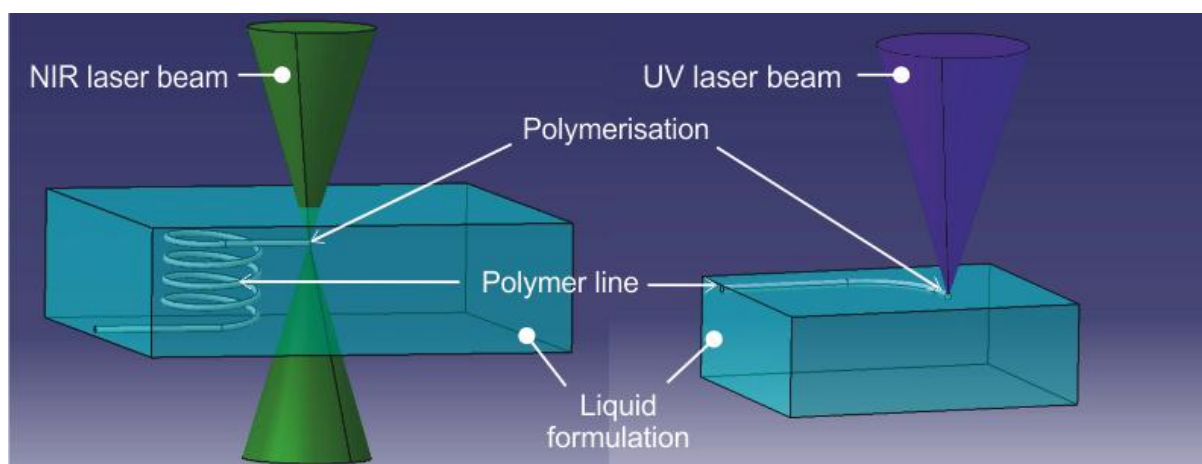


Figure 10 Right image: 2PP is limited to the focal point of a microscope objective; Left image: STL is limited to the surface and requires layer-by-layer manufacturing [11].

Hence, as first AMT, 2PP offers true 3D polymerisation without the need of a layer-by-layer fabrication procedure. All shortcomings related to the surface formation such as high viscosities of the formulation (leading to high surface tensions), the necessity of recoating, the need of supporting material and oxygen inhibition can be discarded.

For any photopolymerisable formulation it is necessary to define a minimum threshold irradiation (energy and/or time), that is required for starting polymerisation. Likewise, a maximum threshold exists, where high-energy doses lead to bubble formation and subsequent damage to the polymer. Apart from the magnification and the numerical aperture of a microscope objective, also the irradiation dose regulated by laser power and scanning speed determines the voxel size.

The unique features of 2PP are an effect of a nonlinear activation principle, substantially different from one-photon activation in other lithography based AMT. The nonlinearity of this principle places very specific demands to the hardware and chemistry involved in 2PP. Conventionally, 1PA optimised compounds were used for 2PP, too. However, this resulted in inefficient cross-linking and therefore long process times, a major drawback of 2PP. To face this challenge, it is indispensable to optimise the components of photopolymerisable formulations for 2PP specific needs. Furthermore, we also have to use hardware that is able to rapidly trace the focal point inside the volume of an optimised formulation. Appropriate light sources and fast switching devices are necessary. They facilitate an efficient supply of laser intensity precisely at CAD defined spots inside the volume.

To accommodate 2PP requirements, it is worth to look at this nonlinear two-photon absorption effect from a theoretical side. Its basic physical principle and its history of origin will be topics of the next chapter. The reader will get to know other application than 2PP based on the same two-photon absorption (2PA) effect. Furthermore, we will get a little deeper into 2PP applications in particular.

The structure-property relationship of two-photon absorbing molecules will be part of the next chapter's second section. Describing the efficiency measure two-photon absorption cross-section (δ), we will explain a two-photon absorbing molecule's composition and explain in which way different groups of the molecule contribute to this efficiency value. Finally, we will investigate how a molecule's δ is related to its feasibility as efficient two-photon PI.

In the third section of the next chapter, we will explain the basic principle of the light sources used in this work. The reader will get to know femtosecond pulsed lasers and related devices used for beam adjustment.

7 Multi-photon absorption and related processes

Multi-photon absorption is a process proposed by Göppert-Mayer (1931) [16] and experimentally proven by Kaiser and Garrett with the development of the Laser [17]. The combination of several photons can excite a molecule to an energy electronic state higher than that caused by one photon only. The frequencies of the photons can be different but must sum up to the resonance frequency of the molecule⁵. The simplest version of Göppert-Mayer's prediction is two-photon absorption (2PA), the underlying principle of two-photon polymerisation (2PP). In 2PA, two photons interact with a molecule producing an energy state similar to an excitation with one photon of higher energy (see Figure 11) [19].

$$\Delta E = h * \nu_{IR1} + h * \nu_{IR2} \quad 1$$

where ΔE is the energy gap between two energy states of a molecule, h is the Planck's constant and ν are the oscillation frequencies of the photons. After a non-radiative decay, different photochemical processes can be started. Intersystem crossing (ISC) to the excited triplet state and energy or electron transfer are important pathways for photoinitiators. Some molecules return to the ground state via up-converted emission of one photon of shorter wavelength and higher energy [20].

The 2PA differs from the one-photon absorption (1PA) in the resonance time of the molecule. In a 1PA, the electric field of the photon is in resonance with the molecule for a longer period; it oscillates in phase with the polarisation resulting in a finite transition probability. In 2PA, however, the molecule is only in resonance for a short time rendering no probability for a 1PA [21]. This depends on the photons interacting with a molecule nearly simultaneously (within a time frame of 10^{-15} s [16]).

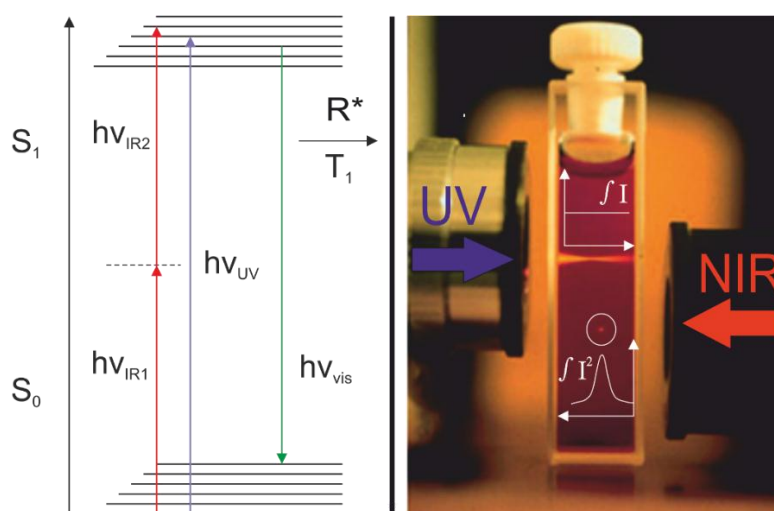


Figure 11 Left: Jablonski diagram⁶ of the 1PA and 2PA process resulting in the production of reactive species or fluorescence (adapted from [8]); Right: Fluorescence in a Rhodamine B solution caused by a UV photon (1PA) and by 2 NIR photons (2PA) (modified from [23])

⁵ There are two 2PA processes called degenerate and non-degenerate describing 2PA with two photons of similar frequencies and with two photons of different frequencies. However, research has focused on degenerate 2PA processes due to available light sources [18].

⁶ The Jablonski diagram illustrates possible transitions of valence electrons between different electronic states of a molecule. The transitions to different energy states are plotted vertically, whereas the horizontal plane groups transitions with changes in spin multiplicity [22].

Following Lambert-Beer's law for one photon absorption (1PA), the absorption of a light beam in 2PA can be written as:

$$\frac{dI}{dz} = -N\alpha_2 I^2 = -N\delta FI \quad 2$$

where I is the intensity, z the wavelength in the media, N the volume referred chromophor number and α_2 a molecular coefficient for 2PA [21]. In contrast to 1PA, the probability of 2PA depends quadratically on the laser intensity. Under tight focusing of a pulsed laser, the absorption is limited to the focal point as the number of molecules excited decreases rapidly with the distance from the intensity maximum [19]. This results in spatial resolutions below the diffraction limit of light (down to 65 nm [15]) within a confined 3D volume inside a medium [18]. For the wavelengths of the photons involved in a 2PA, the materials used are transparent.

A good comparison between 1PA and 2PA is given in the right image of Figure 11. A UV laser is focused into a Rhodamine B solution. The sample is excited over the whole length of the beam rendering a double cone like fluorescence. The smallest diameter of this fluorescing volume is in the focal point of the microscope objective. If we focus a femtosecond pulsed near-infrared (NIR) laser emitting at 100 kHz repetitions rate and 800 nm wavelength into the same sample, we only get a fluorescence in the focal volume, where the square of intensity is sufficient to cause 2PA. In any other plane of the sample, the intensity is not sufficient and no fluorescence is obtained.

Today, the principle of 2PA is used in various applications including optical power limiting [24][25], up-converted lasing [26], 3D data storage [27], optical tweezers [28], fluorescence microscopy, 2D and 3D micro-fabrication.

In **optical power limiting**, generally, a large change in an optical input signal, leads to a small change in the output only. Besides effects such as reverse saturable absorption, non-linear refraction and optically triggered scattering, also 2PA allows such a characteristic. Optical power limiting is used to design materials for optical eye protection. Whereas under normal conditions, these materials possess high transmission, a rapid change in their optical properties proceeds under the influence of intense radiation (e.g. laser light). The material loses its transparency and protects the eye from potential damage making such materials attractive for safety goggles. The power limiting effect can also be used to suppress fluctuations and stabilise a light source [29].

In **up-converted lasing**, a shorted wavelength (UV) lasing output with a longer wavelength (NIR or IR) pump source is produced via a multistep 1PA or a direct 2PA excitation. A 1PA was obtained in earth doped materials, whereas semiconductor crystals, dye solutions and dye doped materials could be excited via 2PA [30]. Compared to other frequency up-conversion techniques, multistep 1PA and 2PA does not require a phase-match, facilitates the use of semiconductor lasers as pump sources [29] and allows to adopt waveguides and fiber configurations [26].

For **3D optical data storage**, a medium is used that exhibits a change in its properties upon 2PA. Changes such as different absorbance, fluorescence or refractive index can be used to save data. Using appropriate read and write beams and precise mechanics for accessing data points in 3D, storage densities of up to 10^{12} bits/cm³ were reported [29]. Furthermore, low cost storage materials such as PMMA can be used [31].

Optical tweezers offer a non-invasive method for manipulating dielectric particles *in situ*, in the presence of living biological tissue. Object sizes from 25 nm to tens of microns can be

manipulated using the optical gradient force. For tweezering, cw lasers are as efficient as pulsed lasers. Yet fs-pulsed lasers offer the opportunity to observe 2PA effects in trapped objects [28].

In **fs-laser surgery**, a pulsed laser is tightly focused inside biological tissue to disrupt or cut specific regions using multiphoton ionization. The high intensity of the fs laser pulse promotes free electrons that act for avalanche ionization. These electrons absorb energy from the electromagnetic field of the laser pulse rendering laser-induced optical breakdown and the generation of high density plasma [32]. The ionization is limited to the focal point. The area of ablation is small and can be adjusted using different NA objectives [33]. This principle was used, for example, to disrupt subcellular organelles [32] and ablate cytoskeletal filaments [33] and mitochondria in living cells. Furthermore, the recovery of model organisms could be studied cutting single axons of the model organism *Caenorhabditis elegans* [34].

Two-photon fluorescence microscopy (2PM) is widely used to create 3D images of tissues and cells without compromising their viability. It was first demonstrated by Denk et al. in 1990 [35]. The specimen to be observed is stained with a fluorescent 2PA dye or integrates fluorophores that can be excited via 2PA. A scanning mechanism deflects the laser beam to raster over a plane of the volume to be imaged. A photodetector collects optical signals from the excited fluorescing molecules. The electrical signals obtained can be converted to a digital image. Repeating this process over several successive planes along the optical axis, a 3D image of the specimen is created. As with all 2PA processes, the absorption and subsequent emission is limited to the focal point rendering high lateral resolution; spatial filtering with a confocal aperture might not be needed. As average laser power is lower than in a respective 1PA and biological materials exhibit a window of transparency in the NIR wavelength region, the penetration depth can be higher than in conventional confocal fluorescence microscopy. Helmchen et al., for example, reported the high resolution imaging of biological tissues up to several 100 μm deep in various organs of living animals [36]. Furthermore, NIR light excitation facilitates to use the entire visible spectrum for detecting. It is thus possible to use different colour fluorophores in different tissues to obtain better contrast and multi-colour images [29]. Figure 12 shows a 2PM image taken deep in the neo cortex of a living transgenic mouse as well as images for functional studies of kidneys.

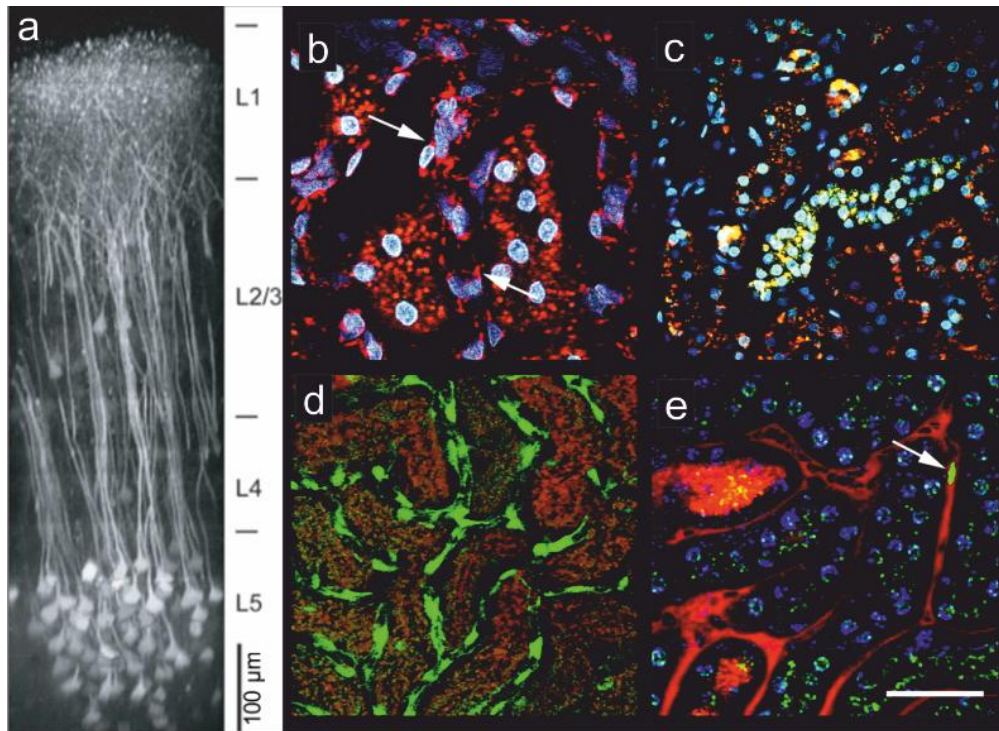


Figure 12 *In vivo* 2PM imaging of a) an intact mouse neocortex obtained deep in a transgenic mouse expressing clomeleon⁷, fluorescence image stack [36]; b) a living rat's kidney after intravenous injection of rhodamine R6 and Hoechst 33342 showing accumulation of rhodamine in the mitochondria of endothelial cells (white arrows); c) a living rat's kidney showing fluorescein dextran fluorescence of the endosomes of proximal tubule cells, the orange fluorescence indicates the location of tubular lumens (fluorescence of Sudan black-stained castor oil); d) projection of a living transgenic mouse's 3D vasculature of the kidney, renal cortical proximal tubules with brown autofluorescent inclusions surround the vasculature network; e) single frame image of a mouse's kidney transplanted with bone marrow cells expressing GFP and labelled with fluorescein and rhodamine dextran, the arrow indicates a leukocyte; white scale bar resembles 25 µm in b), 50 µm in c) and 40 µm in d) and e) [37]

7.1 Two-photon polymerisation

Two-photon polymerisation (2PP) is an additive manufacturing technology (AMT) for the fabrication of complex 3D parts with micro- and nanometre scale resolution. Similar to 2PM, photosensitive chromophores inside photopolymerisable formulations are excited in the focal point of a microscope objective. Via the interaction with monomers, the formed reactive species trigger two-photon induced chain-reaction polymerisation in the focal point. Tracing the focal point (volumetric pixel or voxel) through the formulation, 3D polymer lines are created (see section 6.2).

Research groups have already used it for a wide variety of purposes. However, the technology has a high potential for industrial applications, too, where resolution, complex geometries and three-dimensionality are important. Let us take Photonic Crystal fabrication as an example. Being the optical analogue of semiconductors, Photonic Crystals are periodic microstructures that affect the propagation of electromagnetic waves. In the repeating small units of high and low dielectric constants, certain wavelengths (modes and bands) can propagate whereas others (photonic band gaps) cannot. The design of high efficient waveguides with sharp bends,

⁷ Clomeleon is a genetically encoded chloride indicator [36].

low-threshold lasers and superprisms is likely to involve such structures. The periodicity of these crystals should match the wavelength of interest [38].

The resolution of these state-of-the-art technologies is feasible, however, these processes require many complicated and time-consuming steps. The manufacturing has been realised using self-organizing colloidal particles, which tend to give close packing lattices and little room for forming the lattice type. Hole drilling via lithography and subsequent wet etching gives small depth-to width ratios and no satisfactory 3D lattices. Electrochemical etching of porous silicon as in semiconductor processing is expensive and complicated; no structures with more than a few periods are obtainable. 2PP, in contrast, can produce 3D structures with lattices of any arbitrary 3D shape and complexity opening the door for polymer based photonic crystals for various optoelectronic applications [38].

Fabricating PCs is certainly not the only promising application of 2PP. Researchers have used this technique to fabricate photonic crystals [39][40][41], microfluidics [42][43], micro-electrical and micromechanical systems [44][45] as well as polymer based optical waveguides [46][47][48].

The manufacturing of biocompatible structures is another promising application. 2PP allows the exact reconstruction of cell specific sites in 3D at micro- and nanometre precision [49][50][51]. Furthermore, it is possible to operate at IR and NIR wavelengths, where biological tissues exhibit a window of transparency. This limits potential compromising photo-chemical stress for living tissue and cells and thus renders 2PP materials to be formed *in vivo*, providing a dynamic microenvironment⁸ [52][50].

Another aspect is the versatility of 2PP systems. It was reported that the same experimental system used for 2PP can be used for 2PA based applications like tweezer [53] and/or for 2PM imaging [54]. With small adaptations, other 2PA tasks might also be possible.

However, 2PP has still some limitations. First, it requires long fabrication times reducing its operating efficiency. Second, the required devices, especially fs-pulsed Ti:Sapphire lasers, are expensive hampering potential interested parties to invest. Third, only a few companies provide complete 2PP systems, most groups use adapted and potentially not optimised 2PMs for 2PP. Finally, available photopolymers are not optimised for 2PP. Research groups usually use compounds known from 1PA based lithography, which suffer from limited absorption in a 2PA reducing their efficiency for this purpose. For biomedical applications in particular, efficient formulations are required that convert into water-soluble polymers without compromising the viability of biological tissues.

In the next section, we will focus on the latter problem. We will see how a molecule has to be designed to efficiently absorb two photons that render them in a higher electronic state. Furthermore, we will see, how efficient absorption is related to the efficient generation of radicals for 2PP.

⁸ The reader will find more on the potential of 2PP for biomedical applications in section 8.

7.2 Photoinitiators and two-photon efficiency

To design an efficient photoinitiator, a molecule is needed that efficiently absorbs two photons to convert into a higher energy state. In this state, it should convert all the energy for creating radicals. In this section, we want to describe a molecule with high two-photon absorption capabilities. Then we want to know, if such a molecule is also an efficient two-photon PI.

To theoretically investigate a molecule's absorption behaviour, we can consider the intensity as photon flux:

$$F = \frac{I}{h\nu} \left[\frac{\text{Photons}}{\text{s*cm}^2} \right] \quad 3$$

($h\nu$ is the photon energy). If the light is plane polarised, the molecular 2PA cross-section δ (equation 2) for the transition from the ground state S_0 to the excited state S_1 (Figure 11) at the maximum of a 2PA band can be written as:

$$\delta_{max} = \frac{2\pi h\nu^2}{\epsilon_0^2 n^2 c^2} \left(\frac{n^2+2}{3} \right)^4 \left(\frac{1}{\Gamma} \right) S_{12} \quad 4$$

using a Lorentzian line shape function. Γ is the half-width at half-maximum of the 2PA band in energy units, n the refractive index, c the speed of light and $\epsilon_0 = 1/\mu_0 c^2$, the vacuum permittivity [55]. δ defines the efficiency of a molecule for 2PA as analogue to the linear absorption coefficient. It is measured in Göppert-Meyer (GM) units [$10^{-50} \text{ cm}^4 \text{ s photon}^{-1}$] [56]. The term S_{12} is the energy gap between the states S_0 and S_1 (Figure 11) and can be written as:

$$S_{01} = \left[\sum_i \frac{\langle \mu_{0i} \mu_{01} \rangle}{(E_{0i} - h\nu)} \right]^2 \quad 5$$

μ_{xy} is the amplitude of the oscillating dipole moment induced by the electric field of a light wave in resonance causing a transition from x to y . If all moments μ_{1i} and μ_{i2} are parallel, the result of equation 5 is 1/5, which is true for almost all molecules with large δ [21]. Equation 4 can thus be written as:

$$S_{12} = \frac{1}{5} \left[\left(\frac{\Delta \mu_{01} \mu_{01}}{h\nu} \right)^2 + \sum_{i \neq 12} \left(\frac{\mu_{0i}^2 \mu_{i1}^2}{(E_{0i} - h\nu)^2} \right) \right] \quad 6$$

defining the dipolar (first) and the two-photon (second) term contributing to the energy gap. Designing an efficient 2PA molecule, therefore, theoretically refers to maximising these two terms. This can be achieved through various molecule design considerations.

Generally, 2PA molecules consist of electron donors (D) and electron acceptors (A) coupled to a conjugated chromophore (π , see Figure 13). A charge is displaced during a transition from the donor's highest (HOMO) to the acceptor's lowest (LUMO) occupied molecular orbital [21]. The optical field of the first photon drives the polarisation μ_{01} with the superposition of the HOMO and LUMO wave function. Its intrinsic frequencies differ by ν , the wavelength of one photon.

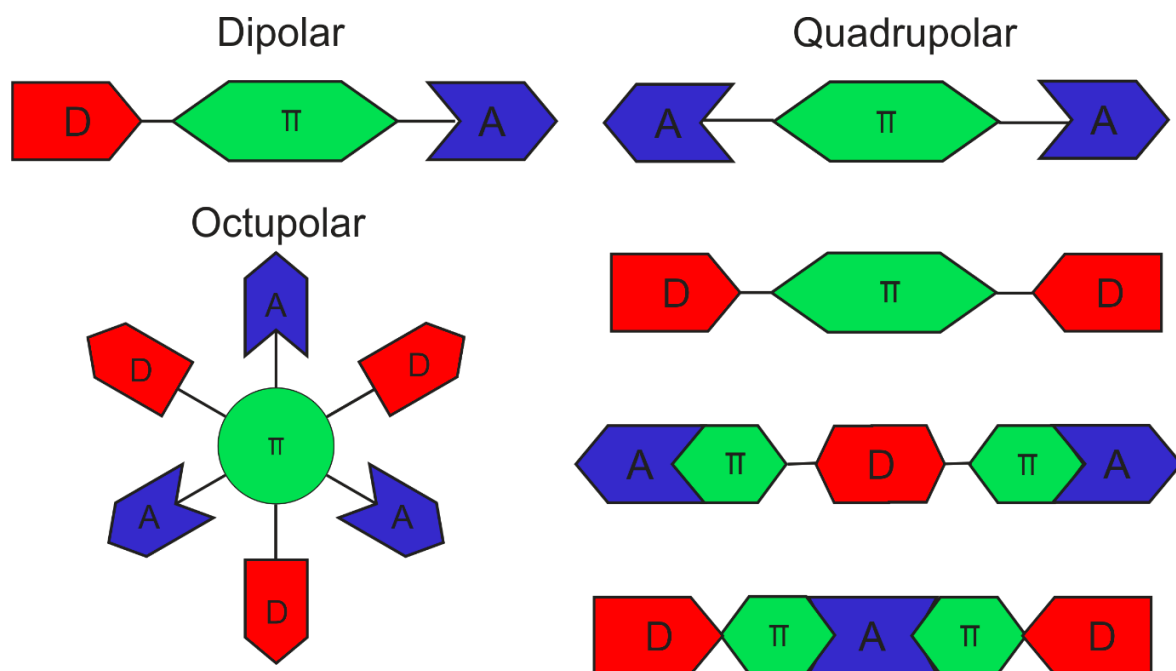


Figure 13 TPA chromophores schematics (D=donor, π =conjugated bridge, A=acceptor) [10]

At a phase separation of π , a **centrosymmetric** molecule (e.g. D- π -A- π -D, Figure 13) has a maximum displacement. One side of the molecule has a high, the other a low amplitude, which renders large dynamic dipole moments (second term in equation 6). The dipolar term, however, is low. This can be explained regarding a schematic 1PA and 2PA excitation diagram of a centrosymmetric molecule (Figure 14). The ground state's (S_0) and the excited state's (S_1) wave functions are symmetric to the centre of inversion. The intermediate state (B), reachable with 1PA, is antisymmetric [21]. 1PA transitions from S_0 to B and from B to S_1 are allowed involving two photons of frequencies differing from the ones involved in a 2PA. In 2PA, however, the excitation to S_1 proceeds via a non-stationary virtual state existing only 1-10 fs long [57]. The intermediate state differs by Δ from the non-stationary virtual state and determines the magnitude of the decoupling term $E_{0i}-h\nu$ (denominator of the second two-photon term in equation 6). The smaller Δ , the closer the intermediate state to the virtual state and the larger the two-photon term in equation 6. Though the frequencies of the photons involved differ, a transient presence of state B in a 2PA of a centrosymmetric molecule, can lead to an excitation to S_1 involving a photon of wavelength ν . Quadrupolar and octupolar (Figure 13) molecules are popular efficient chromophores as they are effective and easier prepared than higher branched derivatives [10].

For a **non-centrosymmetric** molecule (e.g. D- π -A, Figure 13), the first dipolar term is non-zero and the transition from S_0 to S_1 is allowed for both 1PA and 2PA. An intermediate state B cannot exist between S_0 to S_1 . It would be higher or equal S_1 , making Δ large. The two-photon term decreases relatively to the dipolar term (second and first term of equation 6, respectively). The transition moments μ_{0i} in a centrosymmetric molecule will be much larger than the polarisation μ_{01} in a non-centrosymmetric molecule as the latter is only effectively polarised in one optical cycle. Thus these molecules usually have lower δ than their centrosymmetric counterparts [21].

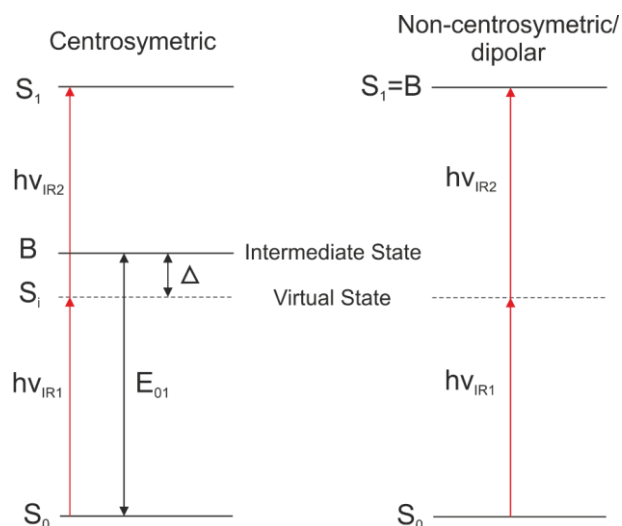


Figure 14 2PA Jablonski diagrams of centrosymmetric and non-centrosymmetric molecules, adapted from [21]

Since intramolecular charge-transfer is the “driving force” for 2PA, **electron-donor and/or electron-acceptor** groups in the centre and as end groups of the molecule increase the transition moments. As end groups, especially dialkyl and diarylaminogroups are popular donors [21], whereas oxygen groups (-OR) are usually less efficient (see Figure 15 molecules 1 and 2). Electron deficient heterocycles are efficient acceptors. D- π -D and D- π -A- π -D structures are generally more efficient than A- π -A and A- π -D- π -A systems (see Figure 15 molecules 3 and 4) [58]. Donor and acceptor groups in the centre also influence an efficient push-pull system. For example, introducing electron-withdrawing nitrile groups to the central core can increase δ substantially (Figure 15, molecules 5 and 6).

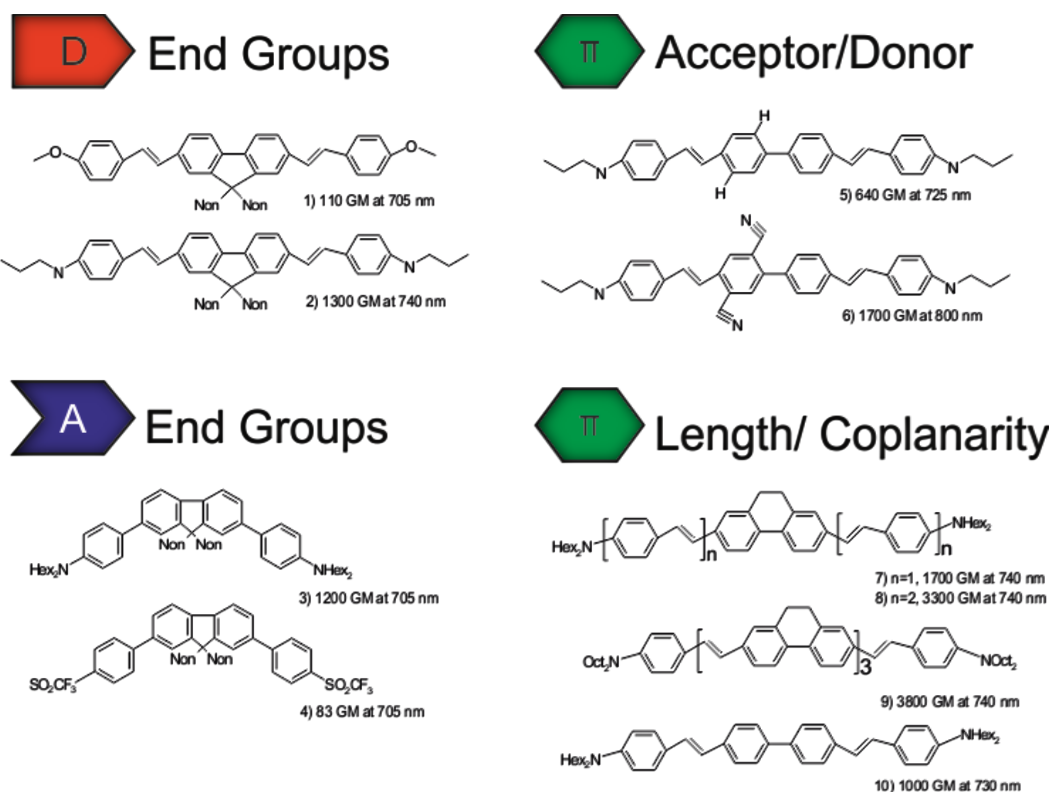


Figure 15 Different Influence of donor and acceptor groups and π -conjugation length on δ , D=donor, A=acceptor, π = π -conjugated bridge, adapted from [21]

The **π -delocalisation** based on the length of its π -conjugated bridge and its coplanarity extends the charge separation and enhances the efficiency of intramolecular charge transfer. As the distance of the charge displacement increases during transition, the moments μ_{xy} are expected to scale with the length of a linear chromophore, or more exactly, the number of its π -electrons ($\mu_{xy} \propto N_e$). However, increasing the conjugation length limits the coherence of the wavefunction due to limited coplanarity. μ_{xy} has a maximum. The impact of the chromophore's length on the δ is shown in Figure 15, molecules seven, eight and nine. Overlapping π -orbitals with strong coupling increase the 2PA activity. In relation to chromophore seven with its fixed dihydrophenanthren, molecule ten has a flexible biphenyl bridge and thus lower δ . The normalised 2PA cross-section (δ/N_e) shows the dependence of δ in relation to the π -conjugation. Figure 16 compares the structurally similar molecules five, seven, eight and nine of Figure 15. Though molecule nine has larger δ than eight, its normalised δ is lower (8: 69 and 9: 64 GM). The π -conjugation length is reached. In addition, increasing the π -conjugation shifts the absorption maximum to higher wavelengths [10].

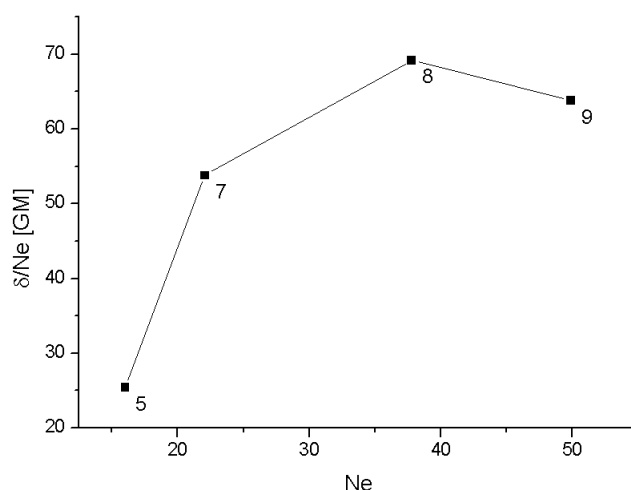


Figure 16 Normalised 2PA cross-section (δ/N_e) in relation to π -electrons for molecules 5,7,8 and 9 (Figure 15), adapted from [21]

Finally, a chromophore with **small 2PA bands** (r of equation 4) can increase δ . For centrosymmetric molecules, the band must be close to the virtual state. As it must not overlap, the 1PA band must be small, too. Squarine dyes, for example, exhibit small 2PA and 1PA bands, low decoupling energy (denominator $E_{01}-h\nu$ of equation 6) and strong transition moments μ_{i1} and μ_{oi} .

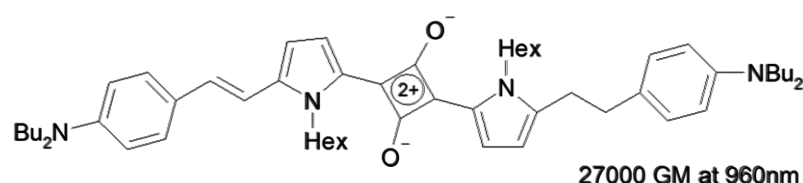


Figure 17 Squarine dye with large δ , adapted from [21]

To summarise this theoretical approach, to get large δ , we have to design a centrosymmetric D- π -A- π -D molecule with:

- Diaryl or dialkylaminogroups as donors,
- Heterocycles as acceptors,
- Large π -delocalisation,
- Good coplanarity and
- Small 2PA bands.

In addition, we have to consider the **solubility** of the chromophores and the solvent polarity as these factors additionally determine the 2PA activity as well as influence the charge transfer character of excited states. Especially planar and rigid molecules suffer from limited solubility. A combination of double bonds and benzene rings over anthracene as π -bridge and/or long aliphatic side chains increase the solubility in the formulation or solvent [10].

Though the 2PA activity of a chromophore shows the molecules' efficiency to generate excited states, it is not the only factor guaranteeing efficient 2PP. From the theoretical description and from experiments it is now evident that centrosymmetric D- π -A- π -D and A- π -D- π -A molecules generally show stronger δ than their D- π -A counterparts do. However, rather than an efficient absorption, it is the energy available in the excited state resulting from a 2PA that is important for subsequent photochemical processes. Increasing the δ with a delocalised π -system and high dipolar moments facilitates an excitation with low energy. But does it always stand for a molecule's efficiency for generating radicals for 2PP?

A high δ facilitates the creation of an excited energy state with low energy; however, this means that the excited energy level is also low. It cannot be higher than the sum of the energy levels of two photons of low energy that caused the excitation. This might not be useful for all 2PA-based applications. Moreover, high dipolar moments are a consequence of a resonance with an energy interstate of a centrosymmetric molecule. The moments are higher if the interstate is at approximately half the energy of the excited 2PA state. Yet, the resulting final state can rapidly relax to this existing lower energy interstate, which causes the photochemical processes to start from this lower energy level instead. The energy of one of the photons converts to heat, whereas in non-centrosymmetric molecules, the energies of both photons are available for subsequent photochemical processes [21]. A process of free radical polymerisation as 2PP requires a sufficient density of radicals rather than molecules in excited energy levels. δ is thus an important parameter but does not directly correlate with the 2PP sensitivity, i.e. the efficient generation of radicals. Apart from the conversion of one photon's energy to heat in centrosymmetric molecules, also other processes might compromise a PI's efficiency [59], these include (Figure 18):

- Energy conversion into fluorescence from the singlet state (F)
- Phosphorescence from the triplet state (P) and/or
- Molecule deactivation due to monomer (MQ) or radical quenching (RQ)

Hence, although plenty of 2PA active chromophores have been reported, nearly all of them are maybe suitable for fluorescence dyes in bioimaging applications [60][61] but do not induce photopolymerisation upon activation. For an effective 2PP PI, however, low fluorescence quantum yields are preferred leading to a higher population of active states to initiate subsequent polymerisation.

Lu et al., for example, compared a series of D- π -A- π -D chromophores on their 2PP activity. The compound with the lowest δ was most suitable for polymerising acrylates [62]. Rhodamine B, an efficient, commercially available sensitizer for 2PM with a δ of 200 GM, is not usable for 2PP [63]. Hence, designing an efficient 2PI involves minimising the instances of Figure 18.

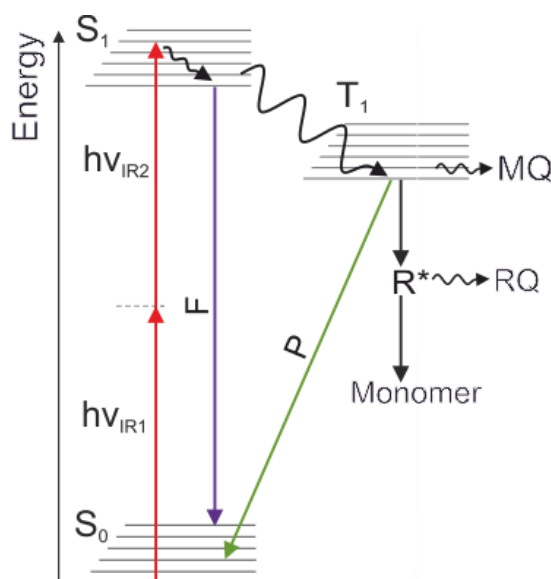


Figure 18 Jablonski diagram for 2PA and initiation efficiency reducing processes including fluorescence (F), phosphorescence (P) and deactivation from monomer (MQ) and radical quenching (RQ); S_0 , S_1 : Singlet state, T_1 : triplet state, $h\nu$: photon energy, R^* : radical(s); adapted from [59]

Moreover, experiments have to be conducted that show the PI's ability for cross-linking monomers at different writing speeds and laser powers. In the course of this thesis, we will therefore describe assessment strategies introducing the lower and the upper polymerisation threshold as well as the processing window of a photopolymerisable formulation containing PIs and monomers.

Before we can conduct these experiments, we need adequate light sources (femtosecond pulsed lasers) as well as devices that allow switching the laser beam and controlling its intensity (acousto-optic modulators). These elements will be explained in the next section.

7.3 Optical Elements in systems for two-photon lithography

7.3.1 Femtosecond pulsed laser

For activating 2PIs and subsequently initiating the polymerisation, we use a Titanium Sapphire (Ti:Sa) oscillator. These lasers use a solid-state frequency-doubled Nd:YAG (neodym doped yttrium aluminium garnet) or Nd:YLF (yttrium lithium fluoride) laser to pump a titanium ion doped corundum crystal (Al_2O_3). The broadband pump emits a range of longitudinal modes into the resonator (see Figure 19), which the Ti:Sa crystal can amplify due to its large spectral range (approximately 670-1070 nm). The crystals amplification maximum is ~ 800 nm. This allows longitudinal modes with different wavelengths to start oscillating simultaneously. If these modes have a fixed phase relationship between each other, a constructive interference pattern emerges where the total intensity results from the intensity sum of the single waves. An appropriate resonator design facilitates the amplification of only one laser pulse that circulates between the resonator mirrors. The intensity sum apart from the region of the pulse is almost zero (destructive interference). To ensure this fixed phase relationship and a proper operation, a pulsed laser requires active or passive mode-locking [64][65].

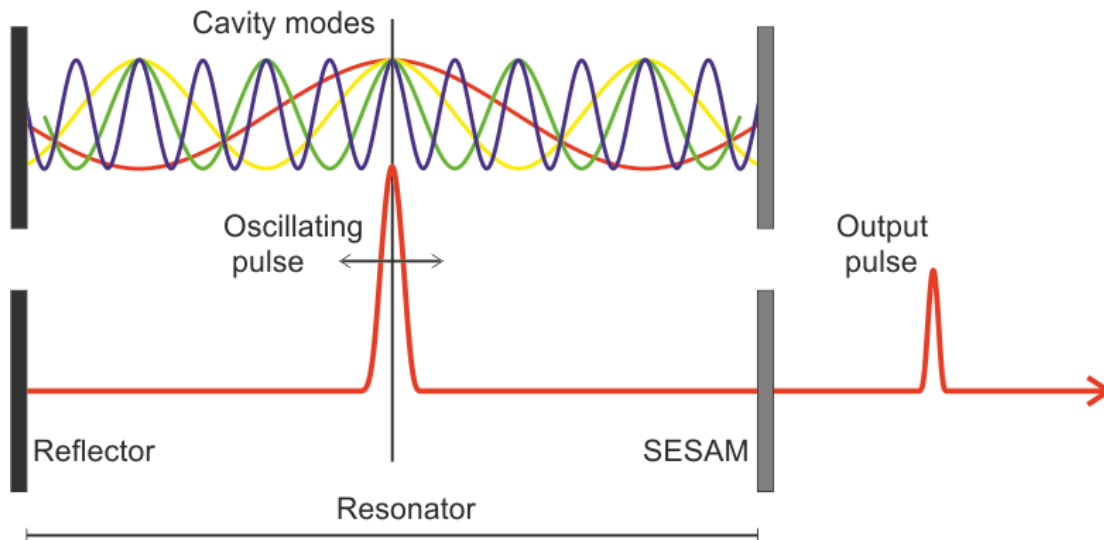


Figure 19 Principle of mode-locking, cavity modes (above) are locked in phase for constructive interference generating a pulse that travels around the cavity at the speed of light, as soon as it reaches its intensity, the SESAM releases the pulse.

In active mode-locking, intracavity gates (electro-optic or acousto-optic) block all light waves but the one of the pulse, modulating the cavity loss at the cavity frequency. This technique allows tuning the laser over its full range and facilitates femtosecond and picosecond pulses. In passive mode-locking, an intracavity element creates cw losses during operation. Usually, one exploits the Kerr⁹ behaviour of the Ti:Sa crystal as it can function as an intensity dependent focussing lens; the higher the intensity of the laser light, the narrower the lens distance. Hence, laser pulses with high intensity get more focussed than low intensity cw light. An intracavity slit or pinhole blocks the cw-light preferring the pulsed operation. The laser requires an external starter mechanism (e.g. mechanical vibration) for initiating the mode-locking. Furthermore, the nonlinear dependence on the peak limits the operation to shorter pulse widths [65].

A self-starting system requires a semiconductor output coupler, a so-called semi saturable absorber mirror (SESAM). It consists of a quantum well absorber layer incorporated into a semiconductor Bragg mirror. Such a mirror contains an alternating layer sequence of two different optical materials. Each interface contributes to a Fresnel reflection¹⁰ in two ways [64]:

- The optical path length varies by half the wavelength between each interface. Depending on their wavelength, the device forces light waves to travel different distances creating interference with other waves.
- The amplitude reflections alternate from interface to interface resulting in constructive interference and strong reflection.

The integrated quantum well absorber layer near the Bragg mirror's surface ensures beam intensity dependent absorption and reflection (Figure 20). While it causes a loss during cw operation, the absorption saturates at high peak power increasing the reflectivity. Adjusting its modulation depth (modulation amplitude divided by the mean value of a sinus signal), saturation fluence (saturation of the media from a single pulse), recovery time (recovery after a saturating pulse) and operating wavelength, a SESAM facilitates self-starting of the oscillator.

⁹ The Kerr effect is also known as quadratic electro-optic effect. A material shows has a Kerr-effect changing its refractive index directly proportional to the square of the strength of an applied electric field [66]

¹⁰ The Fresnel reflection describes in which way light gets reflected and/or transmitted at the interface between two optical materials with different refractive indices [67].

A non-tuneable pulsed industrial Ti:Sa laser usually contains a SESAM and creates nanojoule pulse energies.

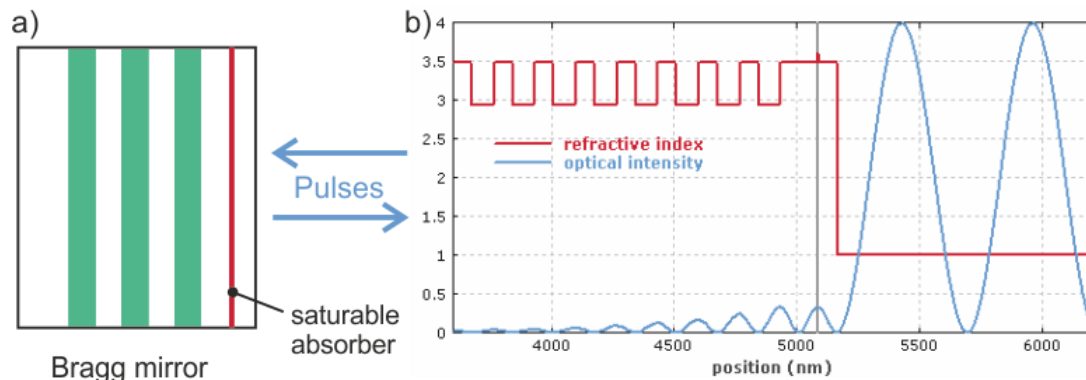


Figure 20 a) Scheme of a SESAM consisting of a Bragg mirror with an incorporated quantum well saturable absorber near the surface; b) Refractive index profile and optical intensity distribution within a SESAM, the intensity has a maximum at the absorber position within the mirror (vertical grey line) (modified from [64])

7.3.2 Acousto-optic modulator

An acousto-optic modulator (AOM) is a device for controlling the intensity, frequency and the direction of a laser beam modifying the refractive index of a transparent solid crystal (e.g. tellurium dioxide, crystalline quartz or fused silica). Following an oscillating electric signal, a piezoelectric transducer causes the attached crystal to vibrate (Figure 21).

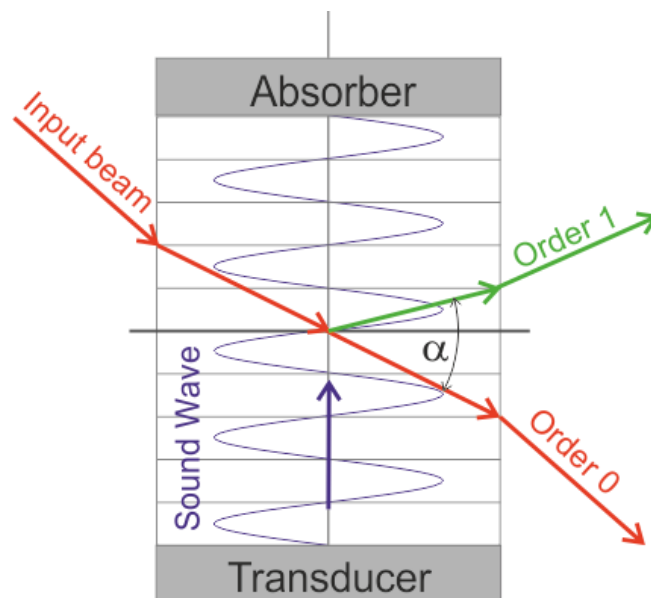


Figure 21 Scheme of an AOM; passing the sound wave, the input beam splits into several orders of diffraction, the first order propagates in a direction diverging by the Bragg angle α from the incident beam.

The periodic mechanical pressure induce sound waves inside the crystal. In that way, the crystal can function as a so-called Bragg cell diffracting and shifting the frequency of light. Increasing or decreasing the optical frequency of translucent light by the frequency of the sound wave, the incident beam splits into several beams of different intensity and propagation directions (orders of diffraction). Changing the sound wave tailors the properties of the orders. This makes AOMs versatile devices used as beam switches (sound signal on/off), intensity

controllers (sound amplitude) and scanners (sound frequency). The efficiency of diffraction is up to 95% [64].

To achieve higher bandwidths, an acoustic absorber on the opposite of the crystal can avoid standing waves and prevent reflections of the sound waves. Though this facilitates bandwidths of many megahertz, it decreases the modulation strength. By contrast, reflect the wave at the crystal's opposite promotes resonance and increases modulation strength at the expense of the bandwidth.

Dependent on the beam's polarisation, longitudinal waves (Figure 21) exhibit the highest diffraction efficiencies, whereas the less efficient acoustic shear waves operate polarisation independent. In the latter case, the acoustic wave moves in the direction of the beam.

The devices explained in this section are part of 2PP experimental setups used for the experiments of this thesis. Additionally to switching and controlling the laser intensity of the beam, these setups allow deflecting the beam before it is focused through a microscope objective. In this way, small 3D polymeric lines can be created within a liquid photopolymerisable formulation. According to section 6.2, they are arranged to form precise 3D constructs according to a CAD.

However, before we go into deeper what has been done in this thesis, we have to know what is state-of-the-art in 2PP. One of the main goals in this thesis was to find and process formulations with high water content rendering biocompatible hydrogel structures. Ideally, these formulations would allow polymerisation *in situ*, in the presence of living biological tissue and cells. Before we can start experiments, we will take an excursus in the work of fabricating hydrogels with 2PP done by research groups all over the world.

8 State-of-the-art 2PP-structured hydrogels

As mentioned in the introduction, the scope of this thesis was to find and screen novel biocompatible formulations. Before we will present the composition of the materials used in this work, we will review state-of-the-art 2PP materials for biomedical applications. The focus of this overview will also be on water-based formulations rendering hydrogel constructs. The following sections are an excerpt from a review paper submitted in December 2012 [50]. Co-authors of the following chapter are Xiao-Hua Qin, Zhiquan Li and Robert Liska (IAS), as well as Aleksandr Ovsianikov and Jürgen Stampfl (IMST).

In human tissues, most cells are embedded within an intricate meshwork of interacting collagens, proteoglycans and adhesion proteins [68]. They receive numerous signals from their natural surroundings, the extracellular matrix (ECM), which influence their behaviour. The ECM functions as a scaffold for tissue morphogenesis, provides cues for cell proliferation and differentiation, promotes the maintenance of differentiated tissues and enhances the repair response after injury [69]. It serves as a reservoir for signalling molecules and 3D substructures for cell adhesion and proliferation. Research has focused on mimicking key characteristics of the ECM to study cell responses to different mechanical, chemical and topographical cues. The composition of the natural ECMs guides the design of artificial biomaterial constructs for their use in tissue engineering [70].

As different tissues require different ECM composition and physical properties, a rational design of artificial cell environments requires various considerations. Appropriate cell support for colonization, migration, growth and differentiation has to be ensured. Furthermore, the construct must have the necessary physiochemical properties, an adequate morphology and ensure proper degradation kinetics [71]. FDA approved biomaterials are based on poly lactic acid, polycaprolactone, or poly(lactid-co-glycolide) providing good mechanical properties and controlled degradation behaviour [70]. Although these materials have advantages related to their mechanics, they are rather stiff and hydrophobic and do not provide the ideal environment for cell-ECM interactions [72][73].

Being structurally similar to the ECM, hydrogels are an appealing material for various biomedical applications such as drug delivery devices [74], contact lenses [75] and wound healing bioadhesives [76]. They contain a high content of water and hold their shapes while still being able to deform [77]. Moreover, the mechanical properties (especially the stiffness) of hydrogels are comparable to many biological tissues [3]. Due to their capability of suspending cells in 3D, supporting nutrient diffusion and dissolving gases through their open network [78][3], hydrogels are one of the most promising materials for tissue engineering. It has been reported that substitutes for skin [79], tendon [80] and cartilage [81][82] could be successfully fabricated from synthetic hydrogel constructs.

The general approach is to seed cells onto prefabricated scaffolds that support diffusion of oxygen and nutrients as well as larger ECM molecules such as collagen. For this, a wide range of hydrophilic and hydrophobic precursors can be used. The fabrication process may involve harsh solvents, toxic reactants and may proceed under nonviable environmental conditions (e.g. high temperature or non-physiological pH value) as long as the final product is biocompatible [83]. Cells are introduced to migrate into and populate the inner regions of the produced parts [84]. However, the seeding approach makes it hard to control the density and the distribution of cells [85][86]. Using biocompatible stimuli and hydrogel precursors, though, it is possible to form these materials *in situ*, in the presence of cells and tissues, allowing the encapsulation of cells during the fabrications process.

8.1 Cell encapsulation in hydrogel constructs

Cell-encapsulation offers several advantages compared to the seeding approach. Apart from achieving a better cell distribution, liquid precursor solutions with suspended cells can be directly shaped at the site of interest. The formed constructs can adhere to the surrounding without requiring adhesives or sutures [83][87]. To exploit these advantages, the gelation process must be mild and cell friendly and the final construct suitable for cell survival and tissue formation. Furthermore, the material must degrade and the degradation product must not affect cell viability. As the natural ECMs assemble and disassemble interacting with their inherent cells, researchers have tried to mimic their properties using naturally derived materials, such as fibrin [88], alginate [89], chitosan [90] and Hyaluronic Acid [91] as well as synthetic materials such as poly(ethylene glycol) (PEG) [92] and polyfumarate [93]. To control the properties of these gels (cross-linking density, hydrophobicity, swelling rate, permeability, degradability and mechanical strength), various stimuli facilitating hydrogel cross-linking in the presence of cells and tissue have been explored [77]. These include physical stimuli such as temperature, pressure and solvent composition or biochemical stimuli like pH changes or ions [94]. Light is of particular interest since it can be controlled with great ease and convenience [77]. In this regard, ECM analogues were built incorporating modified proteins and glycosaminoglycans into a single photopolymerised matrix [87]. Encapsulating mesenchymal stem cells in these matrices provided superior tissue regeneration capturing the native mechanical properties and architecture of cartilage [95]. This shows that hydrogels offer great promise in designing suitable environments that provide mechanical and chemical cues promoting cell proliferation, differentiation and tissue growth. In contrast to the porous scaffolds used in seeding approaches, however, hydrogels with encapsulated cells may limit the transport of important nutrients, oxygen and large ECM molecules such as collagen [82][83]. Besides chemical and mechanical cues, an effective ECM analogue, thus, also requires topographical similarities.

8.2 Additive manufacturing of hydrogels

To overcome the transport limitations, researchers fabricated porous architectures in hydrogel structures with highly interconnected pore networks [96]. AM provide an effective control of these complex architectures. In a very recent report, AM was used to create channels in ECM analogues creating vascular architectures aligned with endothelial cells and perfused with blood under high pressure.[97]

To create similar architectures directly in the presence of cells in a one-step approach SLA (see section 6.2) has been extensively used [3][85][98][99][100]. The ability to easily create constructs according to data from clinical imaging like magnetic resonance imaging or computer tomography renders this technique useful for biological applications [85]. Complex hydrogel constructs with well-defined porous architectures and desired mechanical functions as well as appropriate mass transport characteristics have been created leading researchers to a better understanding of cell-matrix interactions in 3D [101]. As the resolution can be adjusted down to a few micrometres [2], it is possible to produce hydrogel scaffolds with features in the order of 10-400 μm to control the structure cluster of cells as well as features >400 μm to control the interactions between multiple cell clusters [102]. Furthermore, it allows to provide necessary design criteria for zonal density variations of cells as existent in articular cartilage or meniscal- and osteochondral tissues [103].

Pore resolutions that can be obtained with SLA are relatively large compared to the dimension of a cell [104]. This can result in cell isolation and makes it necessary to cluster cells [105]. To control the environment of individual cells, resolutions in the order of 0.1-10 μm are necessary [102]. In this respect, electrospinning is a diverse technique capable of producing fibril networks with fibre diameters in the sub- μm region. Encapsulating living cells during the fabrication process has also been reported [106]. However, despite significant progress in controlling the fibre orientation [107], electrospinning does not allow the exact recapitulation of the entire matrix architecture [108]. The fabricated scaffolds are ideal substrates for growing and implanting cell monolayers. However, constructs with larger pore sizes, suitable for cell invasion after seeding have poor mechanical stability. An ideal construct has to provide micro-features organized within a 3D continuum proceeding from the micro- to the macroscale facilitating effective cell migration and proliferation [109]. Due to the uncontrollable nature of electrospinning, this technique does not meet the necessary requirements [108].

Electrospun fibril networks have been introduced in SLA fabricated scaffolds to “sieve” individual cells [104]. Bovine primary chondrocytes were more efficiently retained on AMT scaffolds containing an electrospun fibril network than on those without. However, this two-step approach increases the complexity of the fabrication process, sets new limitations and reduces reproducibility [8]. A complete understanding of the cells’ behavior in respect to topographical cues requires a one-step fabrication process that is capable of reproducibly producing defined 3D structures at multiple length scales, high resolution and in accordance to a specific design.

2PP, in contrast, can meet the necessary feature resolution requirements (see sections 0 and 6.2). In addition, 2PP relies on 2PA offering mild processing conditions using light of the NIR spectral range. In contrast to short wavelength UV light, which induces photochemical damage to biological tissues [110][111], NIR light seems to be most suitable for inducing polymerisation in the presence of cells. Proteins, DNA, melanin and hemoglobin dominate tissue absorption in the UV and visible spectral range, whereas water begins to contribute significantly at $\lambda \geq 900\text{ nm}$. At 800 nm, however, biological tissue exhibits a window of transparency where the absorption seems to be minimal [112].

However, in fs-laser surgery (section 7), the 2PA effect allows the selective ablation of components at micro- and nanometer precision without altering neighbouring structures. 2PP, too, requires NIR fs-laser pulses and similar focusing. To prevent nonspecific intracellular ablation, it is necessary to operate below a maximum threshold of 1.5 nJ using a 100x/ NA 1.4 objective at 5 $\mu\text{m/s}$ scanning speed [113][114].

Due to the lack of available formulations, complex porous scaffolds were usually produced of synthetic commercially available sol-gel formulations showing appropriate biocompatibility and no cytotoxicity [115]. However, these formulations render hydrophobic structures that cannot be swollen in water. Furthermore, post processing with organic solvents is required and the obtained scaffolds do not degrade hydrolytically.

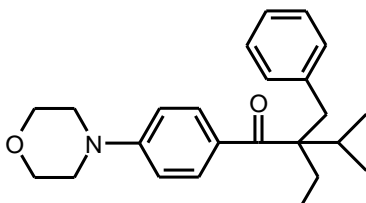
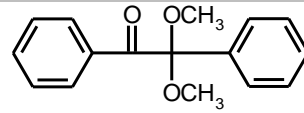
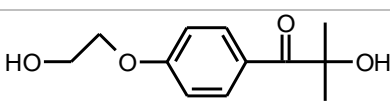
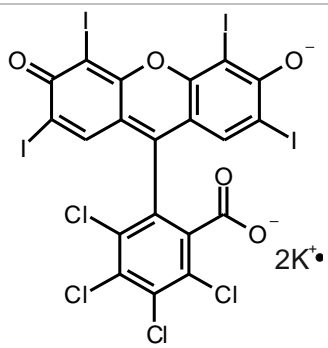
The following sections present results on 2PP of formulations containing different types of the six components mentioned in section 6.1. Natural derived, synthetic and modified natural precursors form the basis of the biopolymers. We will investigate their chemical structure, their reaction mechanism under the influence of incident light and their interplay with other components. We will present successful combinations, discuss their potential for biomedical applications and show how these materials can serve as bioinspired matrices to study cell behaviour in 3D.

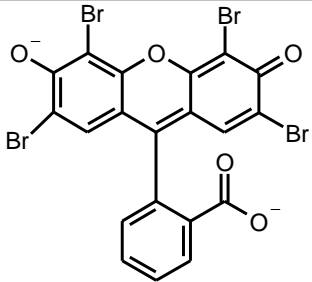
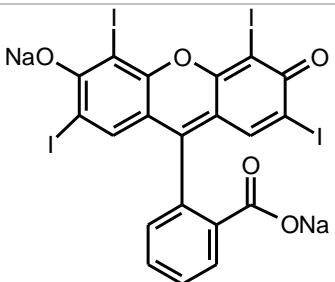
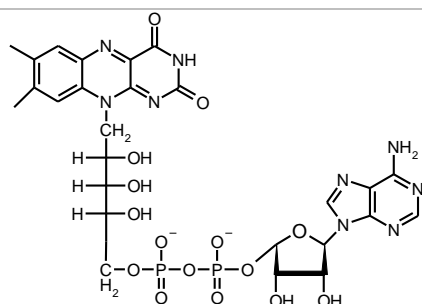
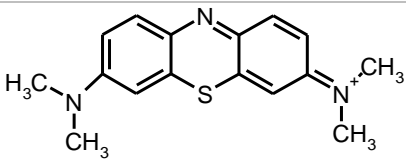
8.3 Commercially available, water-soluble, two-photon photoinitiators

As mentioned in section 7.2, highly active PIs are critical for efficient 2PP characterized by a high 2PA cross-section (δ) and high initiating efficiency leading to a broad processing window [116] and a low polymerisation threshold. Polymerisation can be done at only low excitation power and short exposure times leading to high polymerisation speeds and high quality structures.

Successful 2PP micro-fabrication of cytocompatible scaffolds is conventionally done using commercially available inorganic-organic hybrid formulations containing the UV initiator Irgacure 369 as photoinitiator [115][117][118]. Section 6.1.1 shows the molecule's radical formation mechanism. Although the δ of Irgacure 369 is small at the desired wavelength [119], the limited 2PA could be compensated by high radical formation quantum yields to ensure acceptable initiation efficiency. In Table 1, PIs for the fabrication of hydrogels via 2PP are listed. Z-scan analysis was used to measure the δ as two-photon analogue to the linear absorption coefficient [56].

Table 1 2PP PI, water solubility, availability and δ at 800 nm [50]

2PP PI	Water-soluble	σ^{2PA}	Chemical Structure	Ref.
Irgacure 369	No	7		[119]
Irgacure 651	No	28		[119]
Irgacure 2959	Yes	Not known		
Rose Bengal	Yes	10		[63]

Eosin Y	Yes	10		[63]
Erythrosin	Yes	10		[63]
Flavin adenine dinucleotide (FAD)	Yes	0.035		[120]
Methylene blue	Yes	Not known		

To form hydrogels, researchers fabricated hydrophilic constructs via 2PP of water-soluble monomers using commercial hydrophobic UV photoinitiators in the absence of water [121][122][123]. Using this approach, cells cannot be incorporated in the fabrication process since they must be kept in an aqueous suspension. Moreover, the solvent-change from fabrication to cell seeding can lead to significant structure distortions [124]. Thus, the main advantages of 2PP – the high resolution and the possibility of forming structures *in situ* without harming biological tissues – cannot be fully exploited. A strategy to improve water solubility of commercially available, hydrophobic initiators makes use of nonionic surfactants [125]. Though this approach facilitates the fabrication of hydrogel structures from an aqueous formulation, large amounts of surfactant are needed to ensure adequate initiation efficiency, which might reduce the biocompatibility. The optimisation of real water-soluble initiating systems for 2PP becomes important.

Irgacure 2959 was used for 2PP of 3D scaffolds due to its hydrophilicity and good biocompatibility [126]. However, this initiator is only suitable for 2PP at 515 nm wavelength. At this wavelength, proteins absorb the laser light increasing the chance of their denaturation [111]. Only a limited intensity can be applied in the presence of biological tissues [112] leading to lower available energy for polymerisation (see section 10.3). For 2PP at 800 nm wavelength, Jhaveri et al. increased the water solubility of a commercial

hydrophobic initiator (Irgacure 651 and AF240) using a nonionic surfactant (Pluronic F127) [125]. However, a large amount of surfactant is needed to ensure adequate initiation efficiency in aqueous condition.

Until now, the most popular hydrophilic initiation system for 2PP is a dye-amine combination. Due to suitable absorption above 400 nm and easy accessibility, commercially available hydrophilic xanthene dyes, such as rose bengal, eosin and erythrosine, were applied in 2PP of formulations with amine as co-initiator [63][127]. In this type of initiation, the dye becomes excited by simultaneous absorption of two NIR photons via a virtual state. Accessing the second excited singlet state S_2 , the molecule undergoes rapid radiationless decay to S_1 , interconverting to the long-lived triplet state with high quantum yield (Figure 22) [128][129]. Intermolecular electron transfer followed by hydrogen transfer from the amine to the excited dye generates active amine radicals to induce subsequent polymerisation. 2PP of synthetic monomers such as pentaerythritol triacrylate [127] and acrylamide [63] have been realised with dye-amine initiation systems.

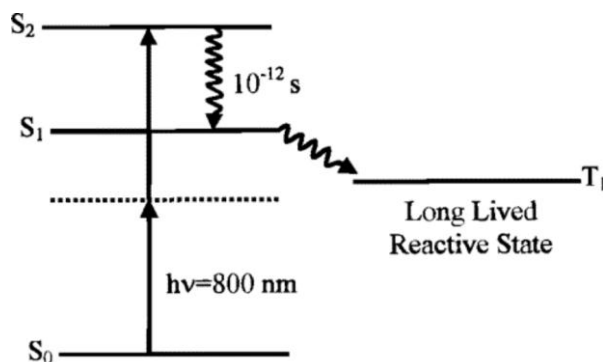


Figure 22 Energy level diagram for two-photon excitation of rose Bengal [50,128]

However, high laser intensities (~ 100 mW) and long exposure times (300–400 μ s) were required due to the small 2PA cross section (Table 1) of the dye [130]. Additionally, some intrinsic limitations derived from bimolecular systems, such as electron transfer efficiency between dye and co-initiator or the back electron transfer, would significantly decrease the initiation efficiency.

Some hydrophilic dyes, such as rose Bengal [129] and methylene blue [131][124] can also be used to directly cross-link proteins. Since the protein itself fulfils the role of a co-initiator and cross-linker at the same time, triethanolamine is not required and in fact appears to act as an inhibitor. Protein cross-linking without a co-initiator is believed to occur in one of two ways, both of which involve excitation of the dye to the T_1 state (Figure 22). The excited dye can either abstract hydrogen directly from a protein molecule to induce protein cross-linking, or transfer energy to the ground state polytriplet molecular oxygen, producing singlet molecular oxygen [128]. In the singlet oxygen mechanism, the active oxygen species continues to react with an oxidisable amino acid residue to generate an electron-deficient protein that may react with another protein's amino acid residue to form a covalent bond. The probability for this reaction depends on the type of amino acid residues on proteins. Two radicals have to be formed by 2PA to make one cross-link, which makes the process rather inefficient compared to the radical chain growth 2PP of synthetic materials (6.1.2) [123]. Furthermore, though Campagnola et al. improved rose bengal and benzophenone initiation adding co-initiators to form one molecule [132], the 2PA activity of the dyes remained low. As a result, the fabrication process still requires very long exposure times and high energies [125].

Although a full understanding of the relationship of molecular structure and two photon properties remains a big challenge until now, 2PA PIs with high δ combined with a high photoreactivity (just like for conventional 1PP PIs) seems the goal to be achieved [133]. A 2PP PI used for efficiently cross-linking hydrogels in an aqueous surrounding must meet the design criteria from section 0 and must be soluble in water. For this work, a couple of novel hydrophilic PIs were synthesised and evaluated. The reader will find more information in section 9.1.2.

8.4 Biopolymers

Despite the access to highly efficient water-soluble two-photon PIs is a prerequisite for 2PP of hydrogels, the selection of appropriate photopolymerisable monomers/macromers as hydrogel precursors is equally important. These compounds have to meet several requirements.

First, the precursor should possess sufficient water-solubility. In this regard, polyethylene glycol (PEG) based synthetic monomers as well as certain natural polymers (e.g., Hyaluronan) have drawn wide interests due to their superior hydrophilicity [134].

Second, from a biological point of view, the hydrogel precursor must meet several requirements.

- For *in vivo* 2PP, cells and tissues are exposed to the unpolymerised formulation, the polymerisation reaction and to the final polymerised structure. Hence, the unpolymerised precursors and their polymerisation reaction must be cytocompatible.
- After 2PP micro-fabrication, the precursors determine the sustainability of cell viability and further cell functions (proliferation, differentiation, etc.) [135].
- To guide cells to specific directions in 3D, additional cues should be provided. Thus an incentive for cell attachment to the polymer should be given; the materials should be bioactive.

In natural ECMs, cell attachment is regulated by the crosstalk between integrin receptors on cell membranes and integrin binding motifs (e.g., arginine-glycine-aspartic acid-RGD peptides). As known from cell encapsulation studies, naturally-derived proteins with cell-adhesive ligands (e.g., collagen, gelatin, fibrinogen) or synthetic materials with incorporated ligands are promising materials for providing similar environments [126].

Third, the photo-reactivity of hydrogel precursor plays an important role in the feasibility for 2PP. To obtain mm sized structures in a reasonable time, the formulation has to be processed at high writing speed and high pulse energies without compromising the quality of 2PP printed structures and its desired feature sizes [136].

With these criteria in mind, we present synthetic, native protein based and chemically modified natural polymers suitable for 2PP of hydrogels in the next three sections.

8.4.1 Synthetic polymers as hydrogel precursors

A suitable biomaterial must withstand the normal loads and stresses of native tissues and has to degrade while still providing a temporal support. Whereas the mechanical properties of natural derived polymers are often inferior compared to their natural counterparts [137],

the chemistry and properties of synthetic materials, in contrast, can be controlled reproducibly [138]. To meet different application specific requirements, synthetic materials are produced tuning molecular weights, blocks structures, degradable linkages and cross-linking modes. PEG is a potential key component of synthetic precursors, since it is widely used in tissue engineering and is FDA approved for various medical applications. It can be found in cosmetics, lotions, soaps and drug formulations.

Functionalising PEG with (meth)acrylates creates photopolymerisable formulations that can form hydrogels with a wide range of physical properties [138][139]. In this regard, these polymers are cytocompatible, nonimmunogenic, bio-inert to cells, tissues and drugs and inherently resistant to protein absorption [140][141]. PEG based hydrogels facilitate the exploration of mechanical (elastic modulus, mesh size), geometrical (architecture) and chemical (cell adhesions peptides) effects disregarding the polymers bioactivity as design variable [5]. Furthermore, the mechanical properties and mesh sizes of PEG based hydrogel constructs can be controlled over a wide range simply by varying the molecular weight and/or the concentration of photopolymerizable PEG [139].

Using PEG as an inert substrate, researchers identified the role of molecules for regulating specific cell-ECM interactions mediated via adhesion molecules such as fibronectin and laminin. These molecules induce the arrangement and polymerisation of the cell's cytoskeleton [142].

The group of JL West guide cells in 3D using the chemical attributes of bound growth factors within an existing PEG based hydrogel [143]. They synthesised proteolytically degradable PEG diacrylate (PEGda) monomers by introducing a collagenase-sensitive protein linker into the PEG backbone. Human dermal fibroblast clusters in fibrin hydrogels were added to a photopolymerisable PEG solution and cured under UV light in the presence of cells. A solution containing the fibronectin derived peptide arginine-glycine-aspartic acid (RGD) bound to modified PEG-acrylates was soaked into the hydrogel. After this preparation, patterns of proteins could be bound to the hydrogel locally by 2PP in the presence of a PI solution (2,2-dimethoxy-2-phenyl acetophenone in n-vinylpyrrolidone). Fibroblasts migrated out from the fibrin into the degradable PEG hydrogel networks, whereas cells entrapped in degradable PEG hydrogels without patterns stayed in the fibrin. The same group later patterned multiple peptide moieties within the same hydrogel sample [141]. Furthermore they showed the local acceleration of endothelial cells' tubulogenesis and angiogenesis by covalently binding VEGF (glycosaminoglycans also present in the native ECM) and integrin ligands to the existing hydrogel [144].

The group of KS Anseth at the University of Colorado (CO, USA) developed synthetic PEG hydrogels that can be modulated on demand. They synthesised monomers capable of polymerising in the presence of cells rendering cytocompatible hydrogel structures [145]. By introducing a nitrobenzyl ester-derived moiety into the PEG backbone (Figure 23 green part), the hydrogel can be cleaved via fs NIR light and thus spatially and temporally tuned in their physical and chemical properties. Besides these topographical cues, the group was also able to immobilize thiol-containing biomolecules within a click-based hydrogel [146]. Upon gel formation, the hydrogel was soaked with fluorescently labelled thiol-containing biomolecules together with a water-soluble PI (eosin Y). 3D biochemical patterns were created at high resolution (1 μm X/Y, 3-5 μm Z). The process was repeated to provide multiple adhesive signals relevant for many cell types. The same group synthesised biological molecules containing thiol groups for photocoupling and photolabile moieties for photocleavage to and from the PEG based hydrogel [54]. This way, they showed the photomediated introduction of cell-adhesion ligands RGD as well as their removal using different wavelengths of NIR fs laser (860 nm and 740 nm, respectively), all in the presence

of cells. Embryonic fibroblasts were seeded onto specimens containing patterned islands of RGD. Cells attached to these islands but detached within minutes upon their removal. These constructs provide a dynamic simplified synthetic environment with full spatiotemporal control where single factors can be varied selectively to explore a better understanding of cell-material interactions in the native ECM.

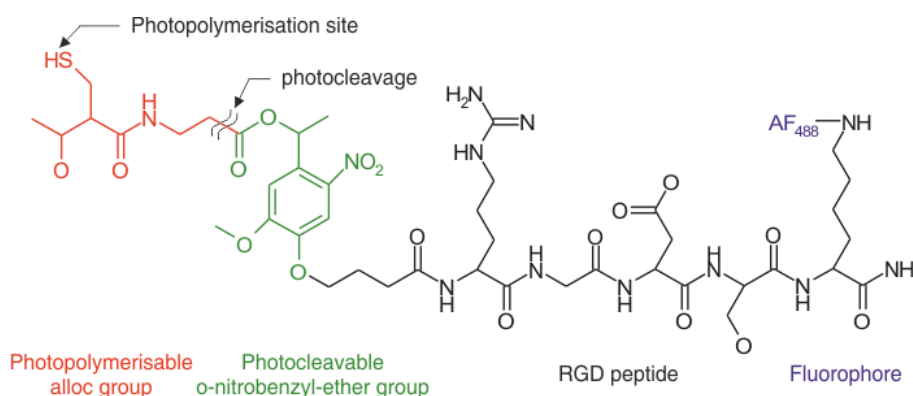


Figure 23 RGD peptide (black) fluorescently labelled with Alexa Fluor 488 (blue) bound to photocleavable *o*-nitrobenzyl ether (green) and photopolymerisable alloc groups (red); the molecule can be reversibly polymerised to a PEG based hydrogel via thiol/ene photoreaction [50,54].

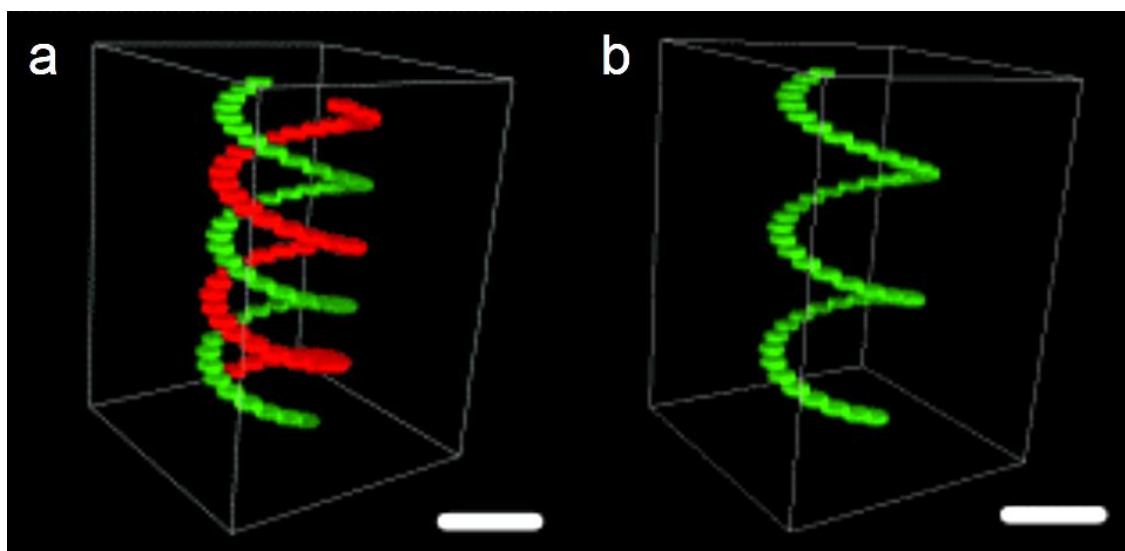


Figure 24 Two-photon patterned fluorescent peptide inside the preformed hydrogel (carried out at 850 nm wavelength) and b) after cleavage of the red marked areas (740 nm wavelength), Scale bar 200 μm , laser scanning microscopy (LSM) images [50,54]

Besides the binding of growth factors to and from existing PEG matrix, researchers have been able to build-up 3D structures and scaffolds from modified PEG monomers. So far, commercially available, water-soluble initiators were not used to cross-link modified PEG. Highly porous scaffolds out of PEGda (Mw 700) were fabricated using a commercial, organo-soluble PIs (Irgacure 369, reaction mechanism in section 6.1.1, δ in Table 1, hydrogel references in Table 2) [122] at 200 nm accuracy [123]. The unpolymerised residue could be washed away with water to render complex 3D hydrogel structures. Their cytotoxicity was evaluated using mouse fibroblasts, 3T3 cells and chondrocytes [121][123]. It could be shown that the PI content plays a key role in the biocompatibility of the constructs post fabrication.

Table 2 2PP hydrogel formulations and references

Monomer	Aqueous Formulation	Initiator	Reference
PEGda	No	Irgacure 369	[135][122][147][148]
	No	Michler's ketone	[123]
	Yes	WSPI	[49]
HA-MA/Acrylamide	No	Irgacure 369	[140]
Modified Gelatine	Yes	Irgacure 2959	[149][126]
PEGda/HEMA	Yes	AF240/Irgacure 651	[125]
BSA	Yes	Rose Bengal/modified	[128][132][150]
	Yes	Methylene blue	[53][151][152]
	Yes	FAD	[153][131]
Lypholized BSA	Yes	Eosin Y	[124]
		Methylene blue	[124]
Collagen	Yes	Modified rose bengal	[132][129]
	Yes	Riboflavin	[154]
Firbinogen	Yes	Rose Bengal	[128][155]
Fibronectin	Yes	Rose Bengal	[156]
Concanavalin A	Yes	Rose Bengal	[156]
Cytoplasmic proteins in live cells	Yes	Rose Bengal	[129]

Claiming the low δ of conventional dyes for 2PP in an aqueous surrounding (section 8.3), Jhaveri et al. dissolved commercially available hydrophobic initiators (Irgacure 651 and AF240) in water using a non-ionic, FDA approved surfactant (Pluronic F127) [125]. This way, the successful one-step additive 2PP of simple 2D structures from PEGda (Mw 575) and 2-hydroxyethyl methacrylate from formulations with water contents of up to 40 wt% was reported.

Using novel efficient water-soluble initiators (section 12.2), we processed PEG based hydrogels in a surroundings with up to 80 wt water content in the presence of living organisms. The reader will find more details in section 9.2.2, 12.3.1 and 0.

8.4.2 Native proteins/ protein precursors

Since synthetic polymers generally lack of bioactivity, commercially available natural polymers have been explored as substrates for 2PP hydrogels. In this respect, macromeres derived from natural polymers are of interest [50][140].

Campagnola and co-workers performed seminal work on 2PP fabrication of 2D simple structures by using native bovine serum albumin (BSA) [128][132]. BSA is similar to human serum albumin. It is a monomeric protein with high solubility in water and a lack of a carbohydrate moiety. Being a product of the liver, it serves as carrier of ions, fatty acids, metabolites, bilirubin, drugs and hormones [157].

The photo-induced cross-linking reaction of BSA is based on several oxidisable amino acid residues (e.g. Tyr) present in BSA [158]. A detailed mechanism (e.g., di-tyrosine cross-linking) is shown in Figure 25. The cross-linking reaction starts from the excitation of a photosensitiser into the triplet state. These photoexcited species are expected to oxidise tyrosine residues [158]. The resultant tyrosyl radical is isomerisation-stabilised and can recombine with a second tyrosyl radical from another protein nearby. Therefore, intermolecular cross-links can be formed between proteins.

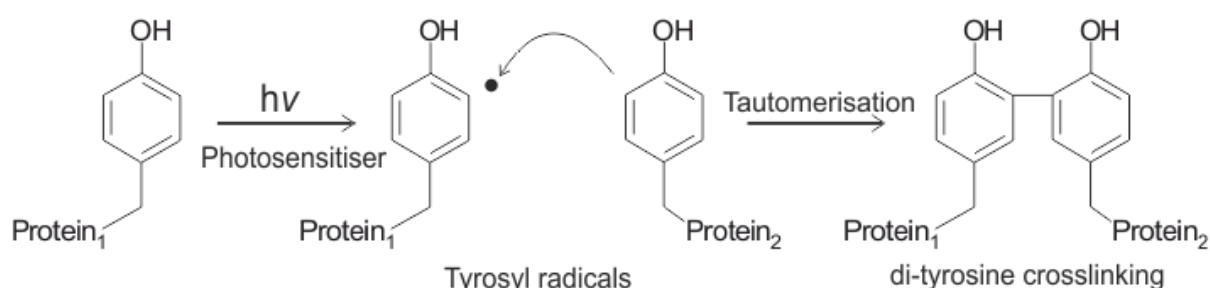


Figure 25 Mechanism of photocross-linking of native proteins [50]

Besides BSA, Campagnola's group also cross-linked other proteins with oxidisable units via 2PP. In this respect, it was possible to process native ECM proteins like collagen I [132], fibrinogen, concanavalin A and fibronectin [156]. Different native proteins contain different cell-adhesive ligands. After cross-linking the protein matrices, cell adhesion and migration could be observed in response to chemical cues provided by collagen and fibrinogen in contrast to BSA [159][155]. Also multiprotein matrices made from BSA and fibrinogen in a 1:1 molar ratio were built [155]. To isolate cellular processes, the same group later fabricated channels and compartments inside live cells (starfish oocyte) cross-linking endogenous cytoplasmic proteins [129].

The group of JB Shear from the Institute for Cellular and Molecular Biology from the University of Texas (USA) found a variety of uses to engineer biological micro-scale devices from cross-linked natural proteins. BSA and avidin microstructures were created in the presence of cortical neurons without compromising cell viability using flavin adenine dinucleotide (FAD) as photosensitizer. The neuron's contact position could be guided with micrometre-scale resolution [153]. To further explore responses of neuroblastoma-glioma cells to physiochemical cues, they later fabricated large aspect ratio structures, manipulated portable protein microparticles by fs-pulsed NIR light induced optical trapping and directly patterned enzymes on existing matrices [53]. For creating real 3D guidance, structures for dorsal root ganglions and hippocampal neuronal progenitor cells, BSA micropatterns were fabricated inside an existing Hyaluronic Acid¹¹ (HA) hydrogel. These structures were decorated with laminin-derived peptides using avidin linkages to promote cell adhesion and

¹¹ Hyaluronic Acid (HA) is an anionic nonsulfated polysaccharide existing in all tissues and body fluids of vertebrates as well as in some bacteria. It is one of the major components of the ECM and favors cell adhesion, proliferation and migration. It is widely used as wound-healing bioadhesive and is found in various cosmetics and lotions [160].

proliferation [131]. Hence, the researchers can interact with the biological tissue during its development providing physical and chemical cues.

Another approach by the Shear group was to use protein microstructures as compartments for cells and bacteria to study their behaviour in response to different stimuli. By incorporation of microscopic thickness and density gradients in cross-linked proteins containing poly(methyl methacrylate) particles, stimuli-responsive structures could be fabricated that underwent large volume changes upon changes in the pH value [151]. The fabricated microenclosures could trap, incubate and release *Escherichia coli* (*E. coli*) bacteria (Figure 26). Harper et al. could recently physically isolate single cells from their surrounding and entrap them in BSA microchambers. Cells remained accessible for chemical cues through the permeable walls of the microstructures [152]. This approach allowed studying a variety of cell functions ranging from single cell biochemistry to perturbation and analysis of small populations of cultured cells upon their exposition to chemical cues.

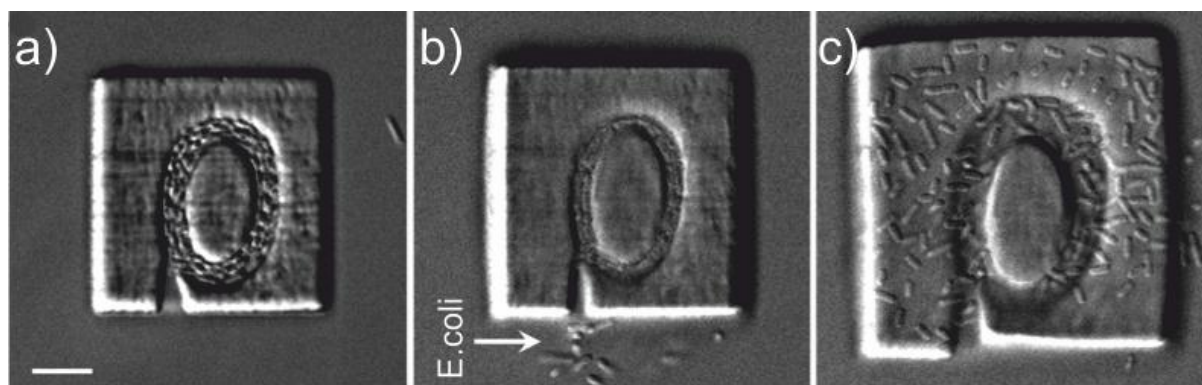


Figure 26 pH-responsive microchamber for controlled release of *E. coli* bacteria, abrupt changes in pH (from 7 to 12.2) cause temporary compression of the internal chamber, releasing a few *E. coli* (b), or eventually disrupting the substrate interface (c); differential interference contrast images [50,151]

Delicate microstructures can be fabricated out of native proteins such as BSA. The mechanical properties can be adjusted altering the laser intensity necessary for the fabrication [161]. However, the efficiency of di-tyrosine cross-linking of natural proteins is quite limited when compared to the conventional chain-growth polymerisation of synthetic polymers. In the former process, a minimum of two excited photosensitisers form two tyrosyl radicals that have to couple with each other to form only one cross-link (section 8.3). Only one radical is needed to start the chain-growth polymerisation in the latter approach, the cross-linking of synthetic based polymers. In a recent report, precise BSA structures were fabricated at a writing speed of only 6 $\mu\text{m/s}$ using a 100x NA 1.4 objective [124]. 2PP of synthetic hydrogels can proceed at 10 mm/s using a 20x NA 0.4 microscope objective, drastically reducing the fabrication time [49]. Though single cells and small cell clusters can be addressed using cross-linked natural derived polymers as precursors, the creation of millimetre-sized constructs, sizes suitable for a large variety of biological assays, is not economically feasible. To get relevant samples still promoting cell adhesion and proliferation, 2PP of natural precursors has to proceed faster.

8.4.3 Modified natural polymers as hydrogel precursors

To achieve high reactivity and good biocompatibility of 2PP formulations, researchers have turned to use chemically modified natural polymers. For instance, methacrylated Hyaluronan (HAMA) has been explored as hydrogel precursor in a recent study by Berg et al [140]. In this work, HAMA was prepared through a reaction between primary hydroxyl groups of HA and methacrylic anhydride. While the 2PP feasibility was proved in this work, writing speed (150 $\mu\text{m/s}$) was very low. Furthermore, acrylate-based monomers (20 wt % acrylamide and 1.2 wt % N, N-ethylene bisacrylamide, w/v) were added into the hydrogel precursors, presumably because the photoreactivity of the HAMA was not sufficient.

Ovsianikov et al. recently reported the 2PP of methacryamide derivatives of Gelatine (GelMOD) using Irgacure 2959 as photoinitiator [126][149]. Gelatin is a proteinaceous material hydrolytic degraded from natural collagen, the main constituent of the ECM. It is soluble in warm water and solidifies reversibly to a transparent gel upon cooling [162]. Gelatin's physiochemical properties are tailorable, it is bioresorbable *in vivo* and does not show antigenicity. Hence, this translucent, colourless and flavourless biomaterial is an ideal gelling agent for food, pharmaceuticals and cosmetics. The food legislation in Europe classifies gelatin as food with the E number 441.

For 2PP, GelMOD was prepared through an amidation reaction between ϵ -amino groups of lysine units in Gelatine and methacrylic anhydride [162]. Complex CAD based scaffolds with 3D features were fabricated allowing a bioadhesive environment with accurate 3D topography. The constructs preserved their enzymatic degradation capabilities after the fabrication. In contrast to the AM of pure proteins, the writing speed could be as high as 10 mm/s allowing for shorter fabrication times. Mesenchymal stem cells were seeded on the scaffolds, adhered and differentiated into osteogenic lineage [50].

To tackle the reactivity issue further, we synthesised the vinyl ester derivative of Gelatine (GHve) and Hyaluronic Acid (HAv), which are supposed to be more cytocompatible and enzymatically degradable. We processed them with novel 2PP optimised initiators (see section 9.1.2).

However, before we will assess their processability for 2PP, we will first briefly describe the chemical structure of the materials in this work. Section 9 will be about hydrophobic and hydrophilic PIs and precursors. We will talk about their chemical structure; give an insight on their synthesis and investigate their biocompatibility, i.e. their potential for *in vivo* polymerisation.

9 Processed Materials

9.1 Photoinitiators

In this section, we present novel, highly efficient PIs used for processing the formulations in this work. The number of optimised 2PP PIs in general was so far quite limited. Applying efficient water-soluble PIs for 2PP was not yet reported. Hence, our first strategy was to design and screen novel organo-soluble PIs and add subsequently add functional groups to make them soluble in water. Accordingly, this subchapter has two parts: In the first part, we present efficient oil-soluble PIs that form the basis of water-soluble PIs presented in the second

section. It has to be noted, that R1, one of the presented oil-soluble PIs is not a constituent of any formulations in this work. However, this molecule forms the basis of the water-soluble PI WSPI, presented in section 9.1.2, and is thus important to assess.

9.1.1 Organo-soluble PIs

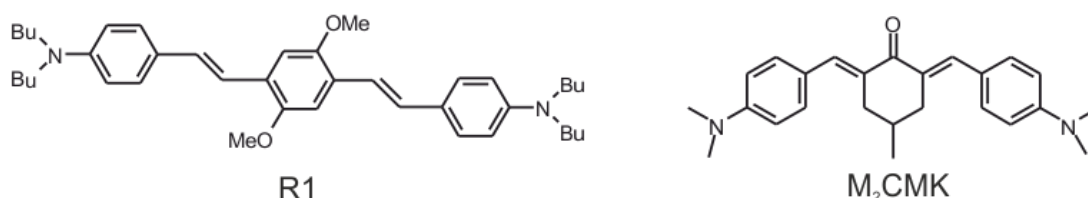


Figure 27 Organo-soluble 2PP PIs processed

R1 is a known, highly reactive D- π -D PI known from literature [163]. It consists of an electron tertiary amino electron donor and a bis(phenylbutadienyl)benzene bridge (Figure 27). Its preparation requires a multistep synthetic route. The alkoxy side groups can act as additional donors. A δ of 900 GM and at 730 nm wavelength and ns pulse duration was reported.

M₂CMK is one of recently published centrosymmetric D- π -A- π -D PIs with different member rings as central acceptor [164]. In these molecules, alkylamino groups act as donors, vinyl as π -conjugated bridge and carbonyl as central acceptor. The long conjugation length, its coplanarity and the presence of strong electron donors and central acceptors facilitate high δ . Furthermore, the molecules can be easily synthesised in a one-step synthetic routine and shows only low fluorescence quantum yields leading to a high population of active states for polymerisation. M₂CMK, in particular, is based on a benzylidene ketone with a central cyclohexanone. Analogue molecules with central cyclopentanone as acceptors have substantially higher δ due to the increased planarity and therefore higher conjugation (see section 7.2). Whereas the cyclopentanone molecule has a δ of 466 GM, M₂CMK has only 191 GM in chloroform when exposed to a 100 fs pulsed, 1 kHz repetition rate laser emitting at 800 nm wavelength.

9.1.2 Water-soluble PIs

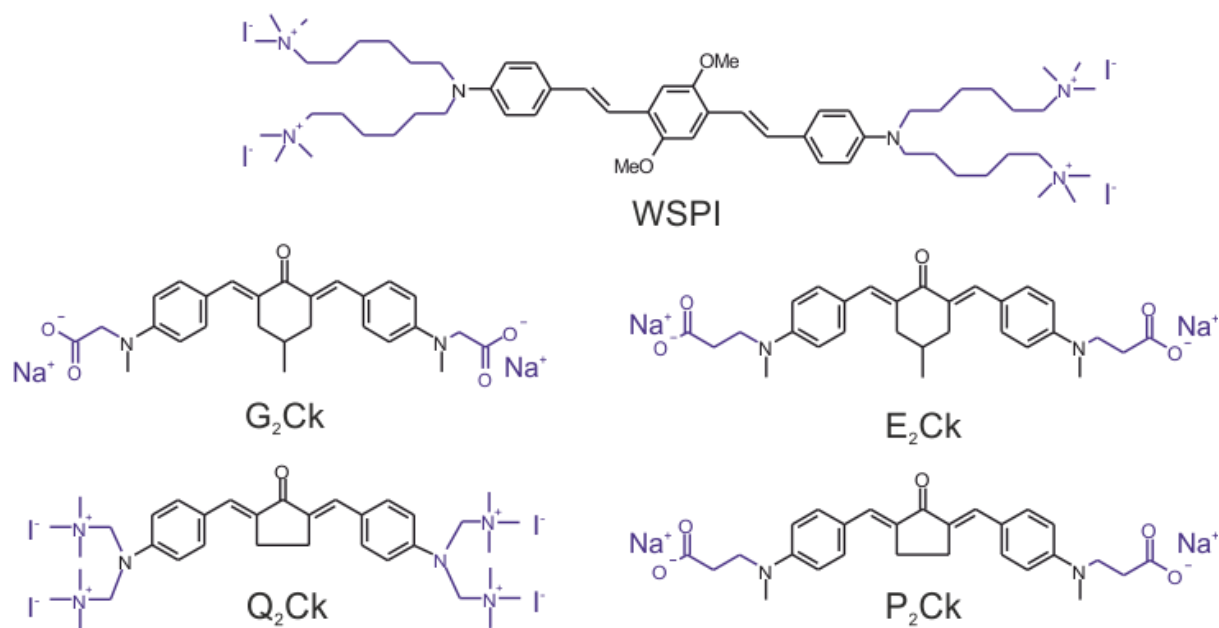


Figure 28 Water-soluble 2PP PIs, black: organo-soluble PI, blue: water-borne functional groups

To produce efficient water-soluble 2PA PIs, we modified the above described organo-soluble compounds introducing water-borne functional groups. Suitable spacers like alkyl-chains are required to avoid shifting their electronic structure.

A distyrylbenzene chromophore based on R1 with additional quaternary ammonium cations was initially synthesised to study the solvent effects on the 2PA behaviour [165]. Niklas Pucher from IAS synthesised **WSPI** (Figure 28) to employ it as potent 2PA PI with high 2PA initiation efficiency in aqueous formulation. The introduction of the ammonium cations increased the already complex preparation of R1 to a complicated six-step synthesis requiring various purification procedures. Niklas Pucher elaborately described the compound's preparation in his PhD thesis [10].

To simplify the preparation and to increase the reproducibility, Zhqiu Li and Marton Siklos from IAS synthesised a set of water-soluble PIs based on the organo-soluble M₂CMK described in the last section. Different carboxylic sodium (G₂CK, E₂CK and P₂CK) or quarternary ammonium salts (Q₂CK) were attached to the cyclic benzylidene ketone chromophores (Figure 28). The 4-methylcyclohexanone based PIs G₂CK and E₂CK are direct, water-soluble analogues of M₂CMK, whereas P₂CK has a cyclopentanone as central acceptor. P₂CK has a δ of only 176 GM at 100 fs and 800 nm laser pulses, which is substantially lower than that of its hydrophobic analogue (466 GM, see section 9.1.1). The δ is strongly dependent on the solvent and drops significantly in water likely due to interactions of the dissolved molecule with the solvent such as hydrogen bonding or changes in the chromophore geometry and/or multichromophore aggregation. However, G₂CK and E₂CK have a δ of 163 and 201 GM in water using a 100 fs pulsed, 1 kHz repetition rate amplified laser emitting at 800 nm wavelength. As M₂CMK, the hydrophobic analogue, has a δ of 191 GM in chloroform, the solvent effect seems to be weaker. The non-planarity of the cyclohexanone obviously reduces the aggregation of optical units in water and provides a steric hindrance effect. The longer alkyl chain of E₂CK enhances the electron donating ability compared to G₂CK. In addition, a red shift derived from an increasing molecule length (see section 7.2) might increase the δ at 800 nm wavelength [166]. The δ of Q₂CK is not known.

9.2 Precursors

9.2.1 Synthetic precursors

9.2.1.1 Acrylate and methacrylate formulations

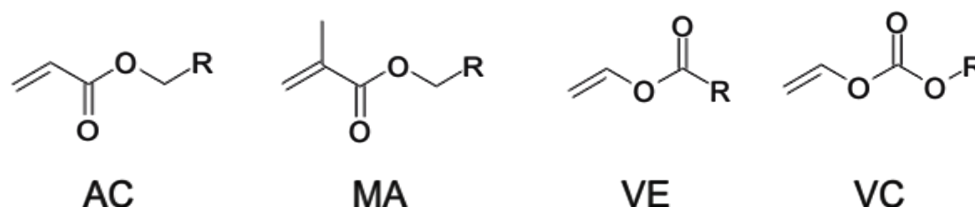


Figure 29 Chemical structure of monomers used in this work; AC: acrylate, MA: methacrylate, VE: vinyl ester and VC: vinyl carbonate

Acrylates (AC) are the most common monomers for photopolymerisation. They are based on the structure of acrylic acid consisting of a vinyl group and a carboxylic acid terminus. Acrylates and the less reactive but more biocompatible methacrylates (MA) are hydrophobic, liquid and transparent materials and polymerise to thermoplast like polymers with a wide range of physical properties. High reactivity makes them the ideal candidates for easy processable photopolymer precursors [167].

ETA-TTA is an organo-soluble 1:1 mixture of ethoxylated (20/3)-trimethylolpropanetriacrylate and trimethylolpropanetriacrylate (*ETA-TTA*), an ideally suitable 2PP formulation [49][50]. We used it for testing novel organo-soluble initiators, high-speed structuring and as reference formulation for toxicity assays.

PEGda is a commercial cross-linker consisting of a polyethylene glycol backbone functionalised with two reactive acrylate at each end. For most of the experiments in this thesis, we used PEG diacrylate (*PEGda*) with a molecular weight (*M_w*) of 700. The material is soluble in aqueous formulations. Both organo-soluble and water-soluble initiators are feasible for processing *PEGda*.

PEGdma is similar to *PEGda* besides it MA end groups. It is less reactive but more biocompatible than *PEGda*. For preliminary structuring tests, we used these precursors with *M_w*s of 600, 700, 800 and 1000.

Formulation 3 is an organo-soluble 1:1:1 mixture of the commercial monomers bisphenol A-diglycerolate dimethacrylate (Bis-GMA), diurethane dimethacrylate (UDMA) and 1,10-decanediol dimethacrylate (*D₃MA*) and is a composite formulation for restorative dentistry. We used this formulation to evaluate the performance of novel PIs for polymerising methacrylates.

Skin irritancy and toxicity of AC and MA monomers limits their use for biomedical applications. The acrylate double bond has a tendency to react via Michael addition to amino or thiol groups of proteins. Moreover, an AC polymer degrades to high *M_w* poly ((acrylic acid), which is hardly excreted from the body. The resulting local decrease of pH changes may lead to tissue necrosis [168].

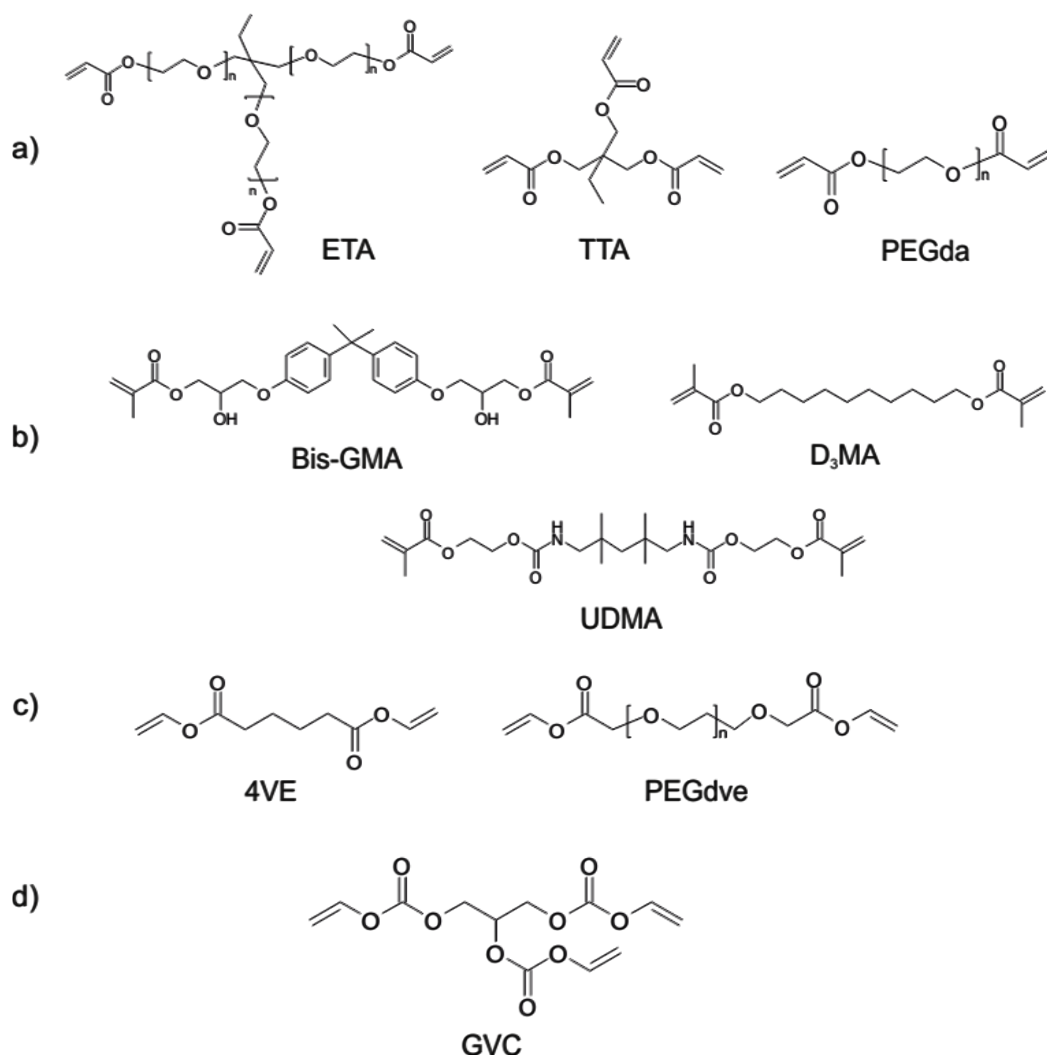


Figure 30 a) acrylate-, b) methacrylate, c) vinyl ester and d) vinyl carbonate polymer precursors used in this work.

9.2.1.2 Vinyl esters and carbonates

Vinyl esters (VE) are a series of alternative monomers with good cytocompatibility [168][169]. These monomers derive from a reaction of a vinyl donor (vinyl acetate) with carboxylic acid in the presence of a catalyst (Hg-(II)-acetate or Pd-(II)-salt) and are not commercially available [167]. Comparative cytotoxicity studies on osteoblasts proved that VE monomers are at least one or two orders of magnitude less toxic than their MA or AC references, respectively. VE polymers degrade to low Mw poly(vinyl alcohol), a common FDA approved compound of many biomaterials. In contrast to high Mw acrylic acid, released from unpolymersed AC, unpolymersed VE groups release acetaldehyde that can easily be metabolised into acetic acid in the presence of acetaldehyde dehydrogenase. In addition, VE have usually lower viscosity than ACs and MAs allowing the incorporation of various biocompatible fillers.

VE are less prone to chain-growth reactions presumably due to resonance stabilisation, their reactivity is lower than the AC references'. However, the UV polymerised AC and VE networks show similar values for indentation hardness and modulus [167].

In the course of this thesis, we tested several VE components provided from IAS including the hydrophobic and most reactive hexandioic acid divinyl ester (4VE) and two PEG based polymers functionalised with VE groups (PEG divinyl ester-PEGdve with Mws of 250 and 600).

For some formulations, we added Dithiolthreitol (DTT) as comonomer to increase the occurrence of chain transfer reactions and thus higher reactivity.

Vinyl Carbonates (VC) also exhibits similar photoreactivity and mechanical properties compared to AC references. VCs also consist of the biocompatible poly(vinyl alcohols) backbone but their synthesis is more easy and not sensitive to the presence of functional groups. A reaction of amines or alcohols with commercially available vinyl chloroformate gives the desired carbonates in high yields [170]. In contrast to VE and MA, the degradation behaviour can be easily tuned and the VC polymers do not release any acidic degradation products. In this thesis, we evaluated the trifunctional cross-linker glycerol (glycerol trivinyl carbonate - GVC) for its use in 2PP. It is a part of lipids and considered cytocompatible. The UV polymerised GVC has the highest modulus among all measured substances. It is even stiffer than the triacrylate reference TTA [6].

9.2.2 Natural based precursors

9.2.2.1 Hydrolysed Gelatine Vinyl Ester (GHve)

Xiao-Hua Qin from IAS synthesised the vinyl ester derivative of gelatin, which is supposed to be cytocompatible and enzymatically degradable (see section 8.4.3). An aminolysis reaction between ϵ -amino groups of lysine units and an excessive amount of divinyl adipate rendered low Mw gelatin (Gelatine hydrolysate - GH) functionalised with VE groups. According to proton nuclear magnetic moment analysis, the degree of substitution of amino groups with vinyl ester groups was 0.964% (~96.4 vinyl esters in 100 repeating units) [171]. As VE limits the efficiency of chain-growth reactions compared to AC, thiol-ene click chemistry should raise chain transfer reactions. Radicals generated from PIs abstract hydrogen from thiols. The resulting thiyl radicals propagate across the carbon-carbon double bonds (enes) from the VE resulting in carbon centered radicals [172]. This step-growth reaction, combines thiol and ene functional groups while still enabling all the benefits of a rapid, photoinitiated radical-mediated process [173]. Figure 31 shows the reaction mechanism.

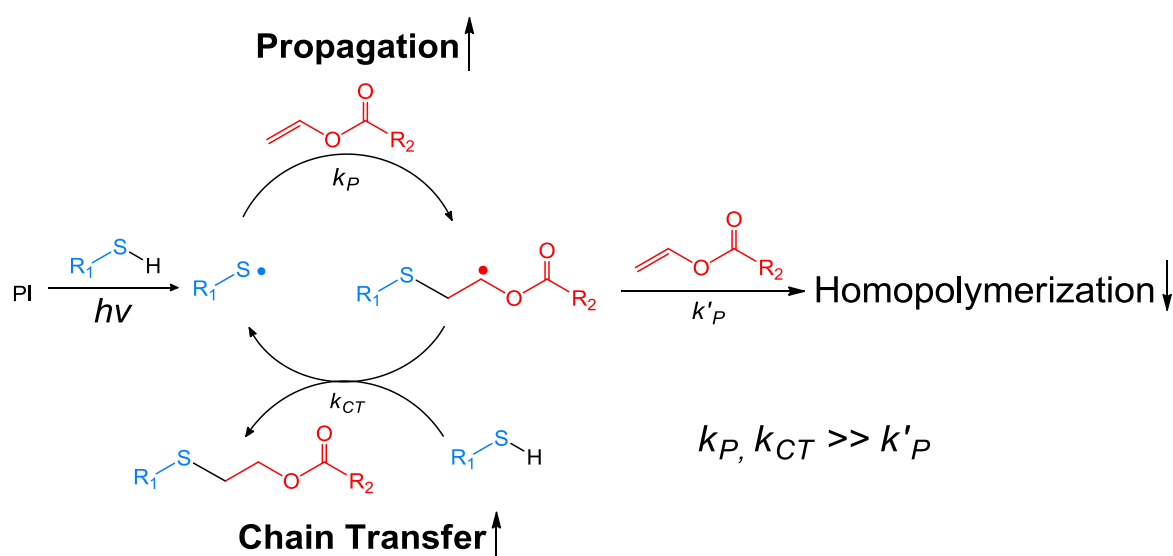


Figure 31 Mechanism of radical-mediated thiol-VE photopolymerisation [50].

To provide multiple free cysteine units for subsequent thiol-vinyl ester photo-click reactions, he selected the reduced BSA (BSA-SH) as a model macrothiol. Since the extent of cysteine units depends on the stoichiometry between disulfide bridges and reducing agents, we tested

varying ratios between thiol and -ene groups of VEs and different ratios between BSA-SH and GHve to obtain hydrogels with different mechanical properties.

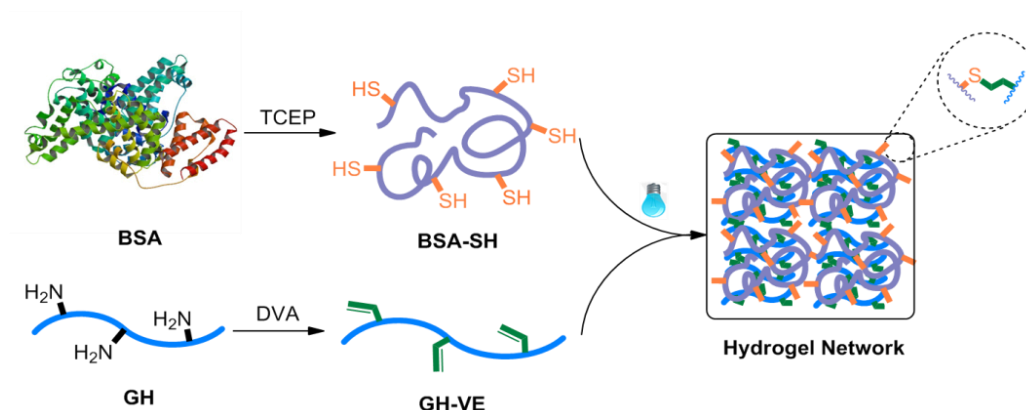


Figure 32 Schematic of GH-VE and BSA-SH photocross-linking hydrogel networks using as precursors, TCEP= tris(2-carboxyethyl)phosphine, DVA=divinyl adipate [50]

9.2.2.2 Hyaluronic Acid Vinyl Ester (HAvE)

Vinyl Esters can be bound to the OH end groups of Hyaluronic acid (HA). As this molecule provides more of these anchor points than GH, including an additional macrothiol in the formulation is not required. In addition, HA allows for a higher degree of substitution with VE and thus presumably a higher photoreactivity. Furthermore, in contrast to BSA, it is bioactive and supports cell attachment, proliferation and migration. We made preliminary structuring tests using VE derivatives of low Mw HA (HAvE) (see section 12.4.3).

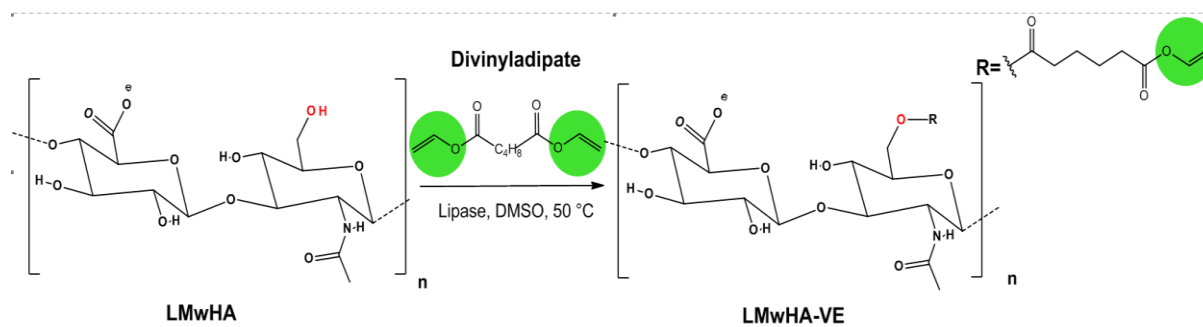


Figure 33 Synthesis of low Mw HA-ve [174]

Xiao-Hua Qin (IAS) prepared low Mw HA (Mw ~8 kilodalton) via acidic degradation of high Mw HA (~1.3 megadalton) according to an established protocol [175]. The compound was then synthesised through lipase-catalysed trans-esterification reactions between primary hydroxyl groups on HA and divinyl adipate. By carefully tuning the reaction time and stoichiometry, a wide range of substitution degree was accessible. For 2PP fabrication, we used HAvE with a substitution degree of 0.53 (53 vinyl esters in 100 repeating units) [174].

After this chapter on the photoinitiators and precursors that were used, we can now end the theory part of this thesis. We know now, how 2PP is different from other AMTs, what has to be considered in designing a two-photon absorbing molecule and how this relates to the preparation of an efficient 2PP photoinitiator. We have heard about light sources and switching devices that are required for illuminating the sample at desired spots within the volume. Moreover, we had a look in the literature, and learned which biomaterials were already

successfully processed with 2PP. After this section on the chemical structure and properties of the components used in this work, we are now at the point, where we can turn our focus to what has been done.

The next section will be about the two experimental systems that were available at the time this thesis was written. One system was available straight from the beginning. We designed the other one to face the 2PP specific challenge of long process times.

10 Experimental setups for 2PP

In this section, we will describe the two experimental setups used for the experiments of this work. At the time of writing this thesis, these two systems were available at the IMST.

10.1 Micro 3-dimensional structuring device

The micro 3-dimensional structuring device (M3DL) is a prototype manufactured by the Laser Zentrum Hannover (LZH). Klaus Stadlmann from the IMST optimised the initial design from Sven Passinger (LZH) for the scope of producing waveguide connectors for optoelectronic circuits.

Figure 34 shows the basic setup of M3DL. The 100 fs pulsed laser beam of a Ti:sapphire laser (High Q laser) emitted at 810 nm wavelength at a repetition rate of 73 MHz and 400 mW power output. It passed through an AOM. This shutter diffracted the laser beam leaving the first order waves for the polymerisation. A $\lambda/2$ wave-plate together with a polarisation dependent beam-splitter adjusted the intensity. A selectable microscope objective focused the beam into a container with photopolymerisable formulation. Two high precision air-bearing axes (Aerotech) moved the beam-focusing objective in the X- and Y-dimension. A similar air-bearing Z-axis carried the formulation container. The mirror system ensured that the X- and Y-movement was only parallel to the direction of the laser beam, so that the guidance of the beam was stable throughout the whole structuring process. For the online process observation, a camera viewed along the laser beam and got focused on the polymerisation spot through the same objective used for focusing the laser. Mounting the axes on a hard stone frame ensured appropriate damping of noises and vibrations. The whole setup's base was an optical table with an air friction damping, again to suppress vibrations. For controlling the machine, the axes and the laser intensity power meter were plugged to an electronic device, which processed the commands given by the control computer. A red LED lamp illuminated the sample preventing premature polymerisation. An extensive setup description is given elsewhere [11,176,177].

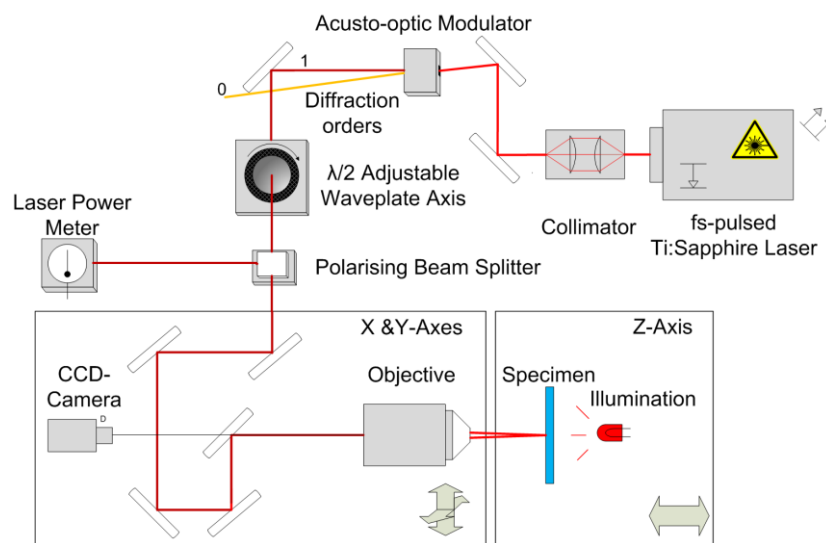


Figure 34 Setup scheme of M3DL [11].

10.2 2PP Micro Processing system Mipro

With the scope of increasing the processing speed, we designed a novel 2PP system based on an old setup from LZH. It was initially used for micro-stereolithography. A UV laser passed through an AOM used for switching the beam and adjusting the laser intensity. A galvanoscanner deflected the beam, which was focused onto the surface of the formulation using a telecentric F-theta lens. Throughout the complete scanning field, this lens kept the focal point in one plane to produce flat surface layers. Furthermore, it ensured an orthogonal entrance angle from the beam to the surface of the formulation.

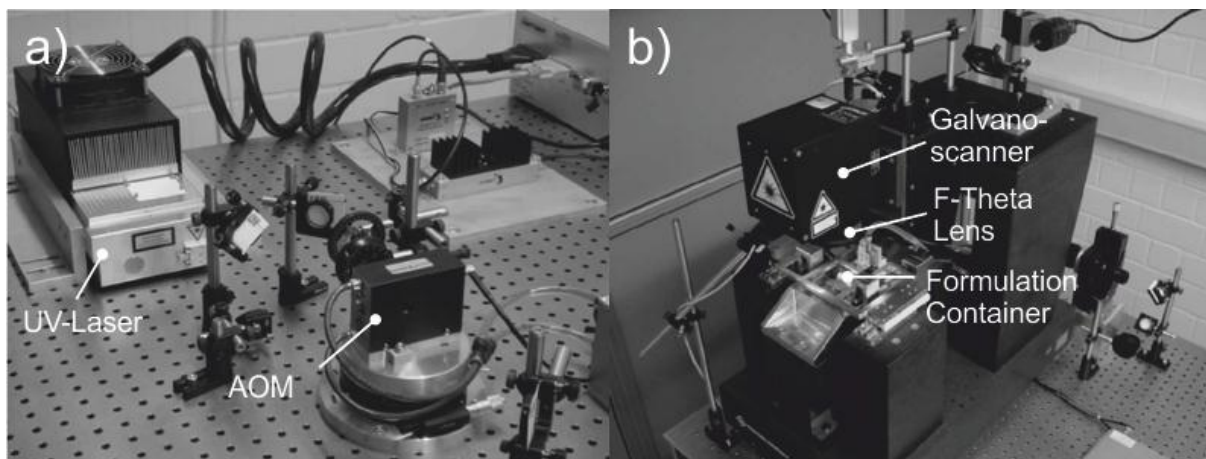


Figure 35 Microstereolithography setup Mipro, a) optical setup, b) building platform

As SLA requires a flat surface, two piezo stages (Nanomotion) moved two linear axes (Schneeberger) that carried a recoater blade. A linear encoder (Numeric Jena) measured the position of the recoater. Like other stereolithography setups, the old Mipro setup followed a bottom-up building approach, where the surface was exposed to the surrounding. A piezoelectric stage (Steinmeyer) dipped the building platform into the formulation and moved it away from the formulation's surface during the building process. To ensure a correct position of the surface and an associated constant layer thickness, another piezoelectric stage dipped a compensating volume into the formulation. As the building platform moved down, it displaced the liquid levelling up the formulation's surface. Simultaneously, the compensating volume moved up decreasing the submerged volume to the same amount as the building platform increased it ensuring a constant vertical position of the surface. Although this setup ensured a writing speed of 0.5 m/s and a resolution of 5 μm in X, Y and 10 μm in Z, it suffered from several disadvantages:

- Low convenience; it was hard to operate the vertically mounted touch-screen control panel and to access the building platform.
- Insufficient mass compensation of linear axes. The moving parts of the building platform and the compensating volume were strong and heavy. Hence, the axes had to level up a large amount of weight, which had to be compensated. The applied gas compression springs provided the intended effect but also damped the acceleration capabilities of the axes reducing the possible setup-up time for producing the next polymer layer.
- Only one large formulation container with a capacity of 79.38 cm^3 was available. Quite a large amount of formulation was necessary to produce only small polymeric parts. The excess formulation had to be disposed. For testing new formulations, this was not efficient and increased costs. In addition, as the processed organo-soluble formulations

were exposed to the surrounding, the setup required a laboratory hood to get rid of solvent fumes.

Though 2PP, in general, is a similar technique as SLA, the adaption of the old setup required a complete redesign. Two new hardware components were bought; the heart of the new setup was a laser from High Q Lasers, operating at 797.5 nm wavelength, 428 mW output power, 72 fs pulse duration and 73 MHz repetition rate. The diameter of the beam was 1.88 in X and 1.81 in Y. In addition, a new acousto-optic modulator from AA Optoelectronics permitted a diffraction efficiency of >85% and a transmission of >95% at VIS/IR. The galvano-scanner manufacturer Scanlab changed the mirrors of the device for operating at NIR wavelength. Similarly, all mirrors of the optical setup had to be changed. We tried to design a very simple setup with low complexity to circumvent resulting limitations, to increase the reproducibility of the fabricated parts and to reduce costs. After a short overview of the basic principle of the novel 2PP setup Mipro (Figure 36 and Figure 37), we will describe its optical and mechanical components and explain the underlying design reasons.

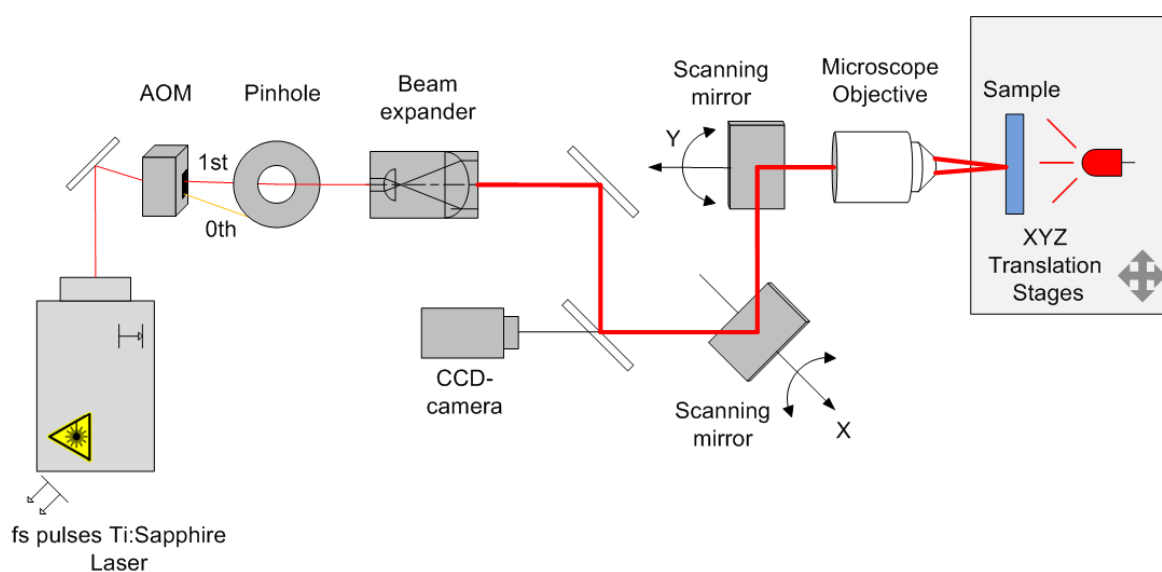


Figure 36 Scheme of the new 2PP Mipro setup

In the new setup, the laser beam passed through the AOM (Figure 36 and Figure 37-1) leaving the first order of diffraction for the structuring. The beam could be switched and controlled in its intensity by applying waves of different amplitudes inside the crystal (see description of AOMs in section 7.3.2). A pinhole (2) blocked the other beam orders from further propagation in the setup. Leaving the pinhole, the beam was expanded six times of its initial 1.8 mm diameter (3). The galvanoscanner deflected the beam before focusing it with a microscope objective (6). We could choose between three objectives differing in their magnification and numerical aperture (see section 10.3). To create 3D polymeric structures, the rotating mirrors of the galcanoscanner (5) traced the focal point inside the formulation. A clamp carried the formulation container and was mounted to a linear XYZ axes system (7). We adapted the axes from the old setup (8) and used them to position the specimen clamp for creating the third order of dimension (Z-axis) and to increase the limited field of view of the objective (see section 10.3). For online process observation, a CCD camera (9) monitored the polymerisation process. The whole setup was mounted on the old setup's hard stone frame to damp vibrations. The laser power was measured behind the AOM (10).

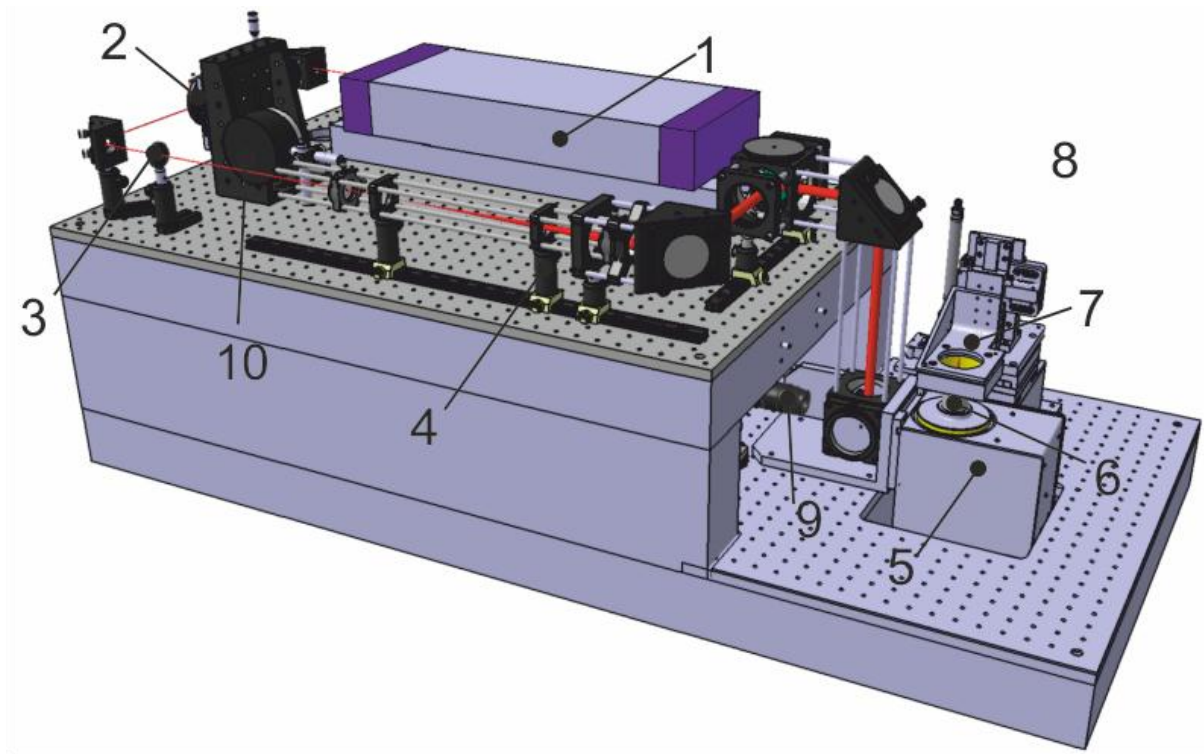


Figure 37 CAD drawing of 2PP Mipro setup; 1) Laser, 2) AOM, 3) Pinhole, 4) Beam expander, 5) Galvanoscanner, 6) Microscope objective, 7) Specimen clamp, 8) XYZ translation axes, 9) CCD camera, 10) Laser power meter.

In contrast to the M3DL setup, minimising the amount of mirrors and lenses reduced distortions of the pulse width and ensured high beam quality when focused into the specimen. Figure 37 shows a CAD of the setup.

10.2.1 Power Adjustment

In contrast to M3DL, the laser power was not measured continuously during the fabrication process. A laser power meter (Coherent) could be mounted between the pinhole and the beam expander. An automatic software routine then calibrated the power values to the analogue electric signal used for adjusting the amplitude of the acoustic wave in the AOM crystal. Once calibrated, the operator removed the power meter from the beam path and the full laser intensity of the AOM's first order could be used for structuring. No laser power was required for the measurement and the beam did not have to pass any additional optic devices.¹²

¹² For power adjustment in M3DL, the laser beam had to pass a $\lambda/2$ waveplate and a beamsplitter, increasing pulse length, costs and complexity relative to the Mipro setup.

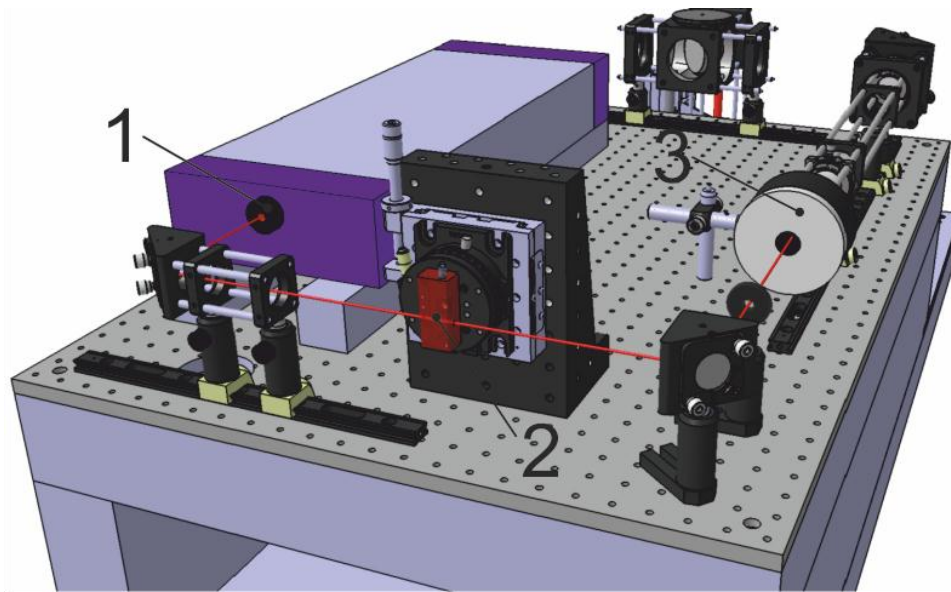


Figure 38 Power Calibration; 1) Laser, 2) AOM, 3) Power Meter

For adjusting the acoustic wave inside the AOM crystal, an analogue electric signal with a potential of 0-5V supplied an AOM driver, which generated high frequency electric waves. The transducer of the AOM converted these electric waves into acoustic waves. The electric potential dictated the amplitude of the electric waves and hence also the one of the acoustic wave. The acoustic wave, again, prompted the amount of intensity deflected (see operation principle of AOMs in section 7.3.2). This resulted in a direct correlation (Figure 39a) between applied electric potential and laser power output that was correct as long as the laser power output was constant. By pushing the electric signal to the ground, the full intensity was on the 0th order, no deflection occurred. Two electric signals were used for the intensity adjustment (height of the electric potential) and the switching (pushing the signal to the ground), respectively. The driver card of the galvano-scanner delivered these two signals.

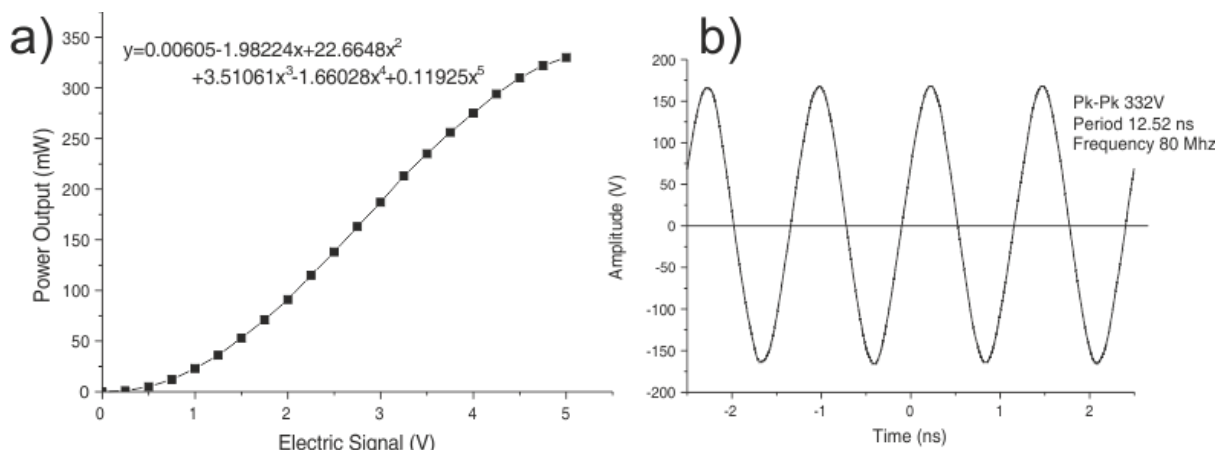


Figure 39 a) Laser Power past the AOM over electrical potential def to the AOM driver; b) electric frequency signal of the AOM driver at 3V input voltage

One was an active-low transistor-transistor logic (TTL) signal (GND or 5V) that was on high when no intensity was required. This included standby, positioning of the linear axes and positioning of the mirrors (jump mode) for creating the next polymer line(s). When it was off,

the potential of the TTL was on GND, the adjusted intensity of the laser was deflected to the first order and could be used for structuring (mark mode).

The driver card provided another analogue 0-10V signal that was independent of the operation status (mark, jump or standby modes). This signal was used for the intensity adjustment.

To convert the logic and the analog signal of the galvano-scanner driver to a single analog 0-5V signal required for the AOM driver, we designed and assembled an optical-electric transistor circuit with the following functions:

- Impedance and potential matching between galvano-scanner and AOM driver.
- Supply of sufficient current for the AOM driver.
- Optical separation of the TTL signal from the AOM driver to avoid high frequency reflections potentially causing damage to the galvano-scanner driver.
- Brief circuit times to reduce delays between mark and jump phases of the galvano-scanner.

A full elaboration of this optical circuit is beyond the scope of this thesis. Interested readers will find more information in the Mipro setup documentation. In short, we could achieve 60 ns circuit times at an average. This is already very close to the 10 ns switching capacity of the AOM. Using this circuit, the (already minimised) cable length and the inertia of the mirrors were considered as the only delaying factors between a jump and a mark phase.

For some experiments of this work, the AOM was not available since it was sent for maintenance. We used the write/read head of a hard disk for beam switching. Figure 40 shows a photograph of the adapted hard disc. When using this mechanical switch, we manually controlled the laser intensity using a continuously variable neutral density filter. We will indicate the experiments conducted with the mechanical switch in the dedicated passages.

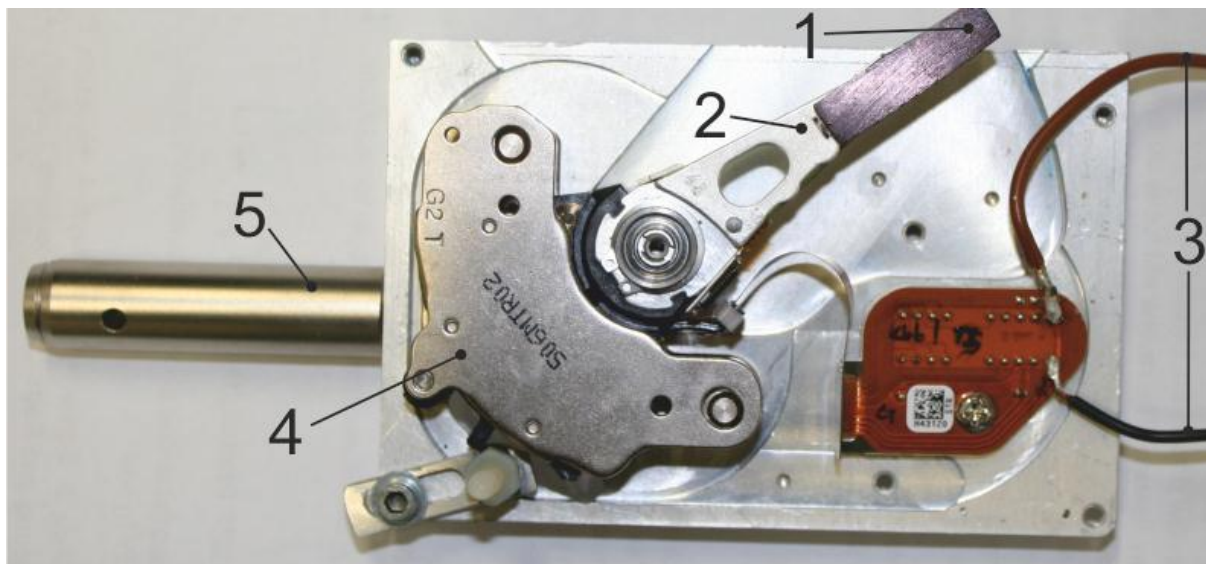


Figure 40 Mechanical laser switch based on a hard disc; 1) laser impact point, 2) read/write head used as switch, 3) connector cables for controlling the head, 4) electric coil, 5) rod for mounting

10.2.2 Beam expander

For adequate focusing, the diameter of the beam has to fill the whole back aperture of a microscope objective and its intensity distribution should be flat [19]. In the Mipro setup, the beam was expanded such that the lower intensity shares did not pass the back aperture of the microscope objective. Hence, the objective was “overfilled” and the lower intensity shares were simply cut off to ensure a flat distribution prior to focusing (see Figure 41)

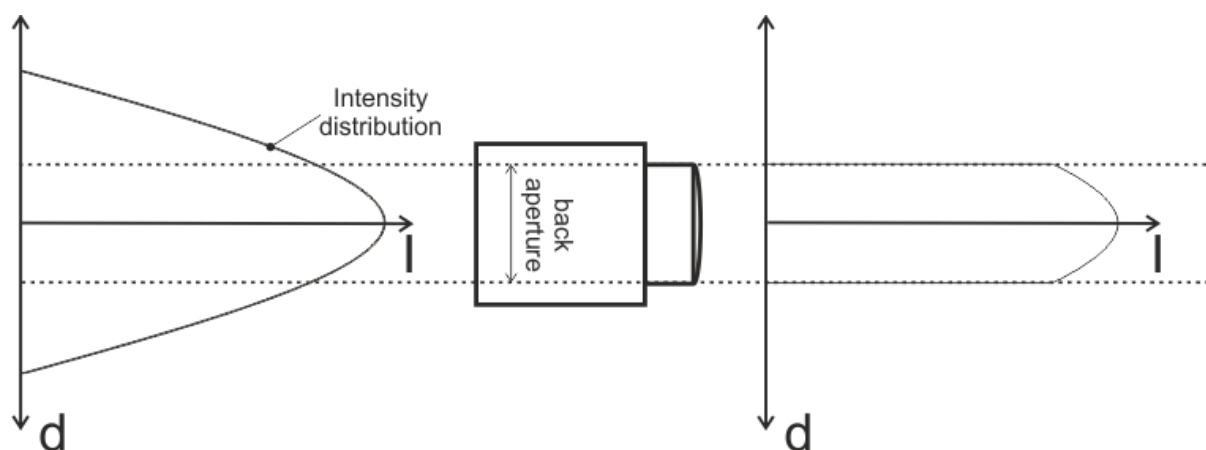


Figure 41 Cutting off the lower intensity shares of an expanded beam (left distribution) at the back aperture of a microscope objective (middle). The resulting homogeneous distribution (right distribution) ensures appropriate focusing; d =distance from the focal point, I =intensity

Using a galvano-scanner for tracing the focal point within the specimen, a wide beam with a flat distribution was required providing homogeneous intensity even at high deflection angles. This facilitated the exploitation of the microscope objective’s whole field of view for structuring. In the Mipro setup, a six-fold expansion increased the beam’s diameter to ~ 11.3 mm from its initial ~ 1.88 mm. Two plano-convex lenses were used for the expansion (see Figure 42).

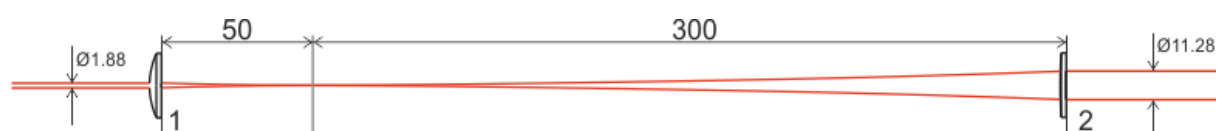


Figure 42 Beam expander consisting of two plano-convex lenses; 1) focal distance 50 mm, 2) focal distance 300 mm

After passing the first lens, the beam became narrower reaching its smallest diameter 60 mm behind the lens. Then it diverged again over a length of 300 mm. It was again collimated passing a plano-convex lens with a focal distance of 300 mm. The relationship between the focal lengths of these lenses determined the ratio of total expansion ($300/50=6$).

10.2.3 Galvano-scanner

The principle of the galvano-scanner-based movement of the focal point is straightforward. There are two rotating mirrors deflecting the laser beam before it focusing it with the microscope objective. The rotation of the mirror traces the focal point inside the liquid formulation and leaves a polymer line. Precise positioning and movement of the mirrors facilitates line-by-line scanning according to a layer of a predefined CAD (see section 6.2).

Figure 43 visualises the basic principle of this approach. The galvano-scanner used in this work, had a total travelling range of ± 32000 pixels in X and Y, respectively. The “Home” Position, where the beam was diffracted to a right angle had the coordinates X: 0 and Y: 0. The distance travelled in unit length divided by the amount of pixels defined the maximum resolution accessible with the scanner. We will define this ratio as the resolution factor. It is dependent on the magnification of the used microscope objective (see section 10.3). The maximum scanning speed of the galvano-scanner mirrors was 1000000 pixels per second. As with the travelled distance, the scanning speed in unit length was also dependent on the resolution factor.

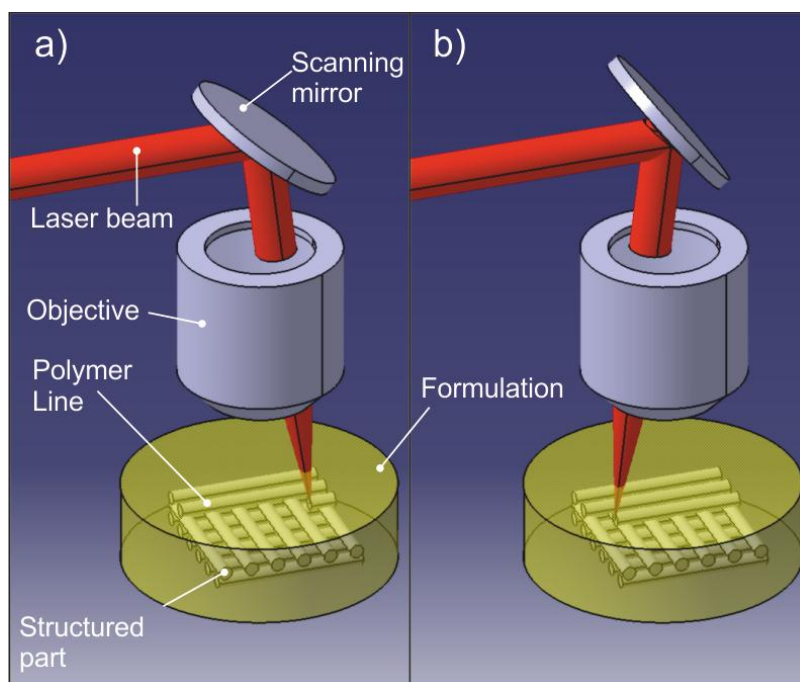


Figure 43 Basic principle of tracing the focal point with a galvoscaner mirror in 2PP; the movement from position a) to b) creates a polymer line inside the photopolymerisable formulation.

The galvano-scanner provided a set of positioning (jumping) and writing (marking) commands for controlling the mirrors. Each command described a vector to be travelled consisting of a number of equidistant pixels. The user set the pixel distance and the output period via the control software (see section 10.2.6). The timing of the mirror movement and the laser switching (see section 10.2.1) was very complex and the inertia of the mirrors played a significant role. For this task, the control of the galvano-scanner offered several user-definable delays, which ensured that turning off and on the laser happened at exactly the right time.

These delays were also important for exact positioning. As it would slow down the scanning process significantly, there was no feedback control for the position of the mirrors. To ensure precise scanning according to a user defined CAD required correct adjustment of the delay parameters. Interested readers will find appropriate values and explanations in the Mipro manual as well as in the galvano-scanner manufacturer manual.

A closer look to Figure 43 indicates a maximum mirror angle, where the beam is deflected beyond the field of view of the microscope objective. This indicates that the travelling range of the galvano-scanner was much larger than the field of view of the microscope objective. Hence, the objective not only defined the resolution but also the maximum build size accessible with the galvano-scanner. For microscope objectives used in 2PP, this is usually well below 1 mm. This also applies for the objectives used in this work, which are the topic of section 10.3.

10.2.4 Camera for online observation

For online process observation, a CCD camera (IDS imaging, Figure 44-1) was mounted to a camera objective with adjustable focus (2) (Avantar). It viewed through a half-transparent dielectric mirror (3) that deflected the NIR light but permitted light of visible wavelengths to pass. Similar to a light microscope, the camera recorded the field of view of the microscope objective, the same spot used for structuring. This allowed the operator to observe the building process online and to position the structures on the specimen. Most formulations contained fluorescent initiators that emitted green or blue light upon two-photon exposure. Generally, this already happened at intensities way below the polymerisation threshold (see section 10.3), even before polymerisation actually occurred. It allowed localising the building spot. However, in most cases the fluorescence was too bright, which caused an overexposure of the CCD camera and a merely white image on the screen. A blue filter behind the camera objective prevented the overexposure.

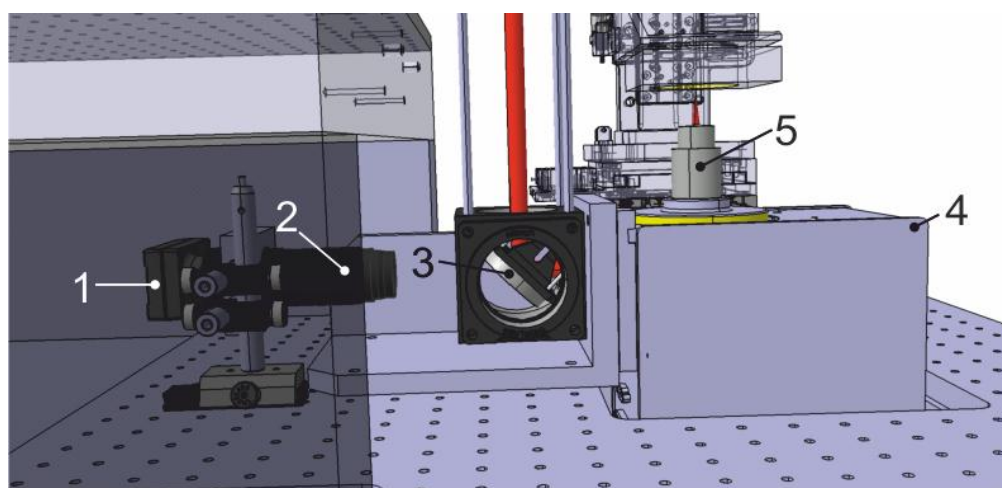


Figure 44 Realisation of online process observation; 1) CCD camera, 2) camera objective, 3) half-transparent mirror, 4) galvanoscanner, 5) objective

10.2.5 X-Y-Z- axes system and formulation container

The galvanoscanner could only build one layer of the CAD file at X- and Y-dimensions limited by the field of view of the magnifying objective used (see section 10.3). A standard microscope slide containing photopolymerisable formulation was attached to specimen clamp (Figure 45-5) from upside down. Once the fabrication of one layer was finished, a linear Z-stage moved the specimen up by the thickness of one layer until the galvanoscanner could fabricate the next layer. As the X- and Y-axes (6 and 7) of the Mipro setup carried the Z-stage, it was important to minimise the weight and to avoid an off-centre loading. This was especially important for the Y-axis being the base of the assembly and carrying the most weight. We built a lightweight stage consisting of an unmotorised linear axis (1) (Schneeberger), a piezoelectric

motor (2) (Nanomotion) and a linear Encoder (3) (Numeric Jena). An air pressure cylinder (4) (Airpel) compensated the weight of the Z-axis. In Figure 45, the encoder is not visible. It is located behind the specimen clamp. The arrow indicates its location.

For creating larger structures than the maximum build size of the respective microscope objective, we divided the CAD file into several parts of obtainable dimensions. The setup created these subparts in a sequential manner. As soon as the fabrication was finished, the scanner went into standby and the linear X- and Y-axes positioned the specimen for the creation of the next subpart. In this sequence, these subparts were stitched together to form the entire desired polymer structure.

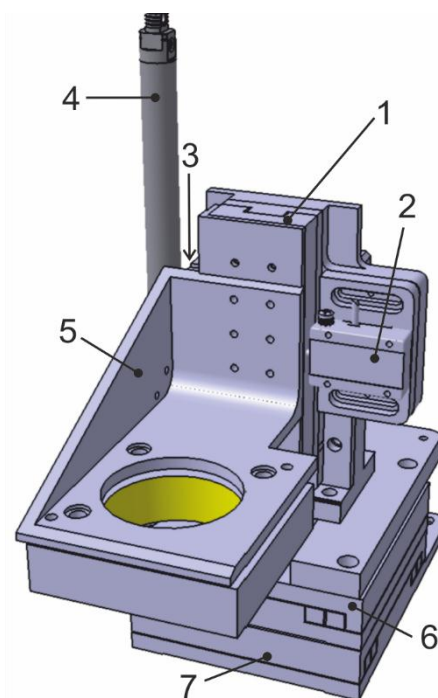


Figure 45 linear X-Y-Z stage assembly with specimen clamp; 1) Z-stage, 2) Motor, 3) Encoder, 4) air pressure cylinder, 5) specimen clamp, 6) X-axis, 7) Y-axis

10.2.6 The control software

Peter Gruber programmed the control software of the Mipro setup. It combined the control of the linear axis with the galvanoscanner driver. All axes and galvanoscanner parameters were accessible with this software. It provided various standard structures, such as lattices, lines and cylinders that could be arranged in rectangular and hexagonal shape and at a user-defined distance between the single elements. STLs were sliced based on different selectable slicing routines considering various processing modes. The software divided big STLs and processed the subparts as described in section 10.2.5.

Once the user had chosen the total structure dimensions (or an STL file with defined geometries was uploaded), she/he had to set process specific parameters including:

- Line Power: the power used to create the polymer lines of an object.
- Markspeed: the speed of the fabrication
- Line distance: the distance between the polymer lines of an object
- Layer-distance: the distance between the layers
- Number of layers

The software allowed the fabrication of several structures of the same kind at a certain distance to each other. The user could choose one of the above-described parameters to be changed by a certain amount from one element to the other. For example, it was possible to fabricate an array of similar structures differing in their line power in X and in their markspeed in Y. A qualitative analysis of these structures in the microscope facilitated a quick benchmark of different material components in the formulation. This routine was useful for PI screenings (see section 12.1 and 12.2). Under the prevalent conditions, we could identify the processing window and classify the component under investigation.

The software offered a range of other functionalities, which will not be explained in this thesis. The reader will find more information in the Mipro manual. Some experiments of this work required software tools not described in this section. The reader will find more information before the respective passages.

10.2.7 Photographs

In the last section of this brief setup description, we will show some photographs, from which the reader will get an overview on the actual realisation of the Mipro setup. Some of the components described in this section will be visible.

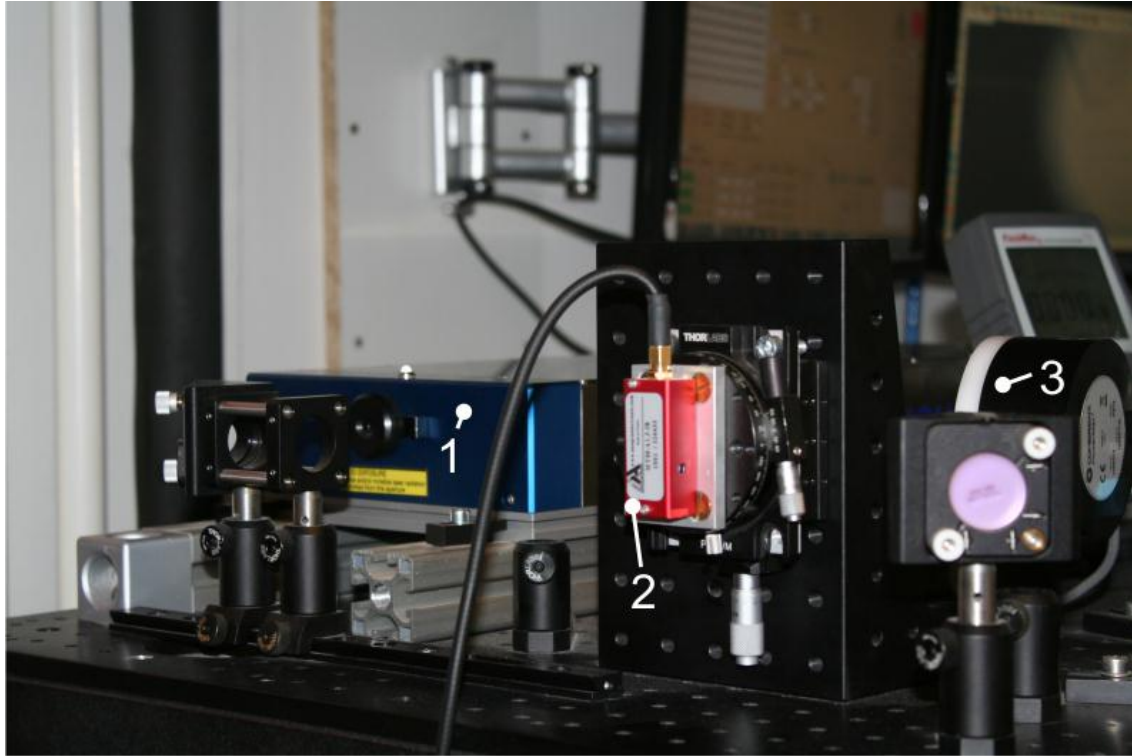


Figure 46 1) Laser, 2) acousto-optic modulator and 3) laser power meter

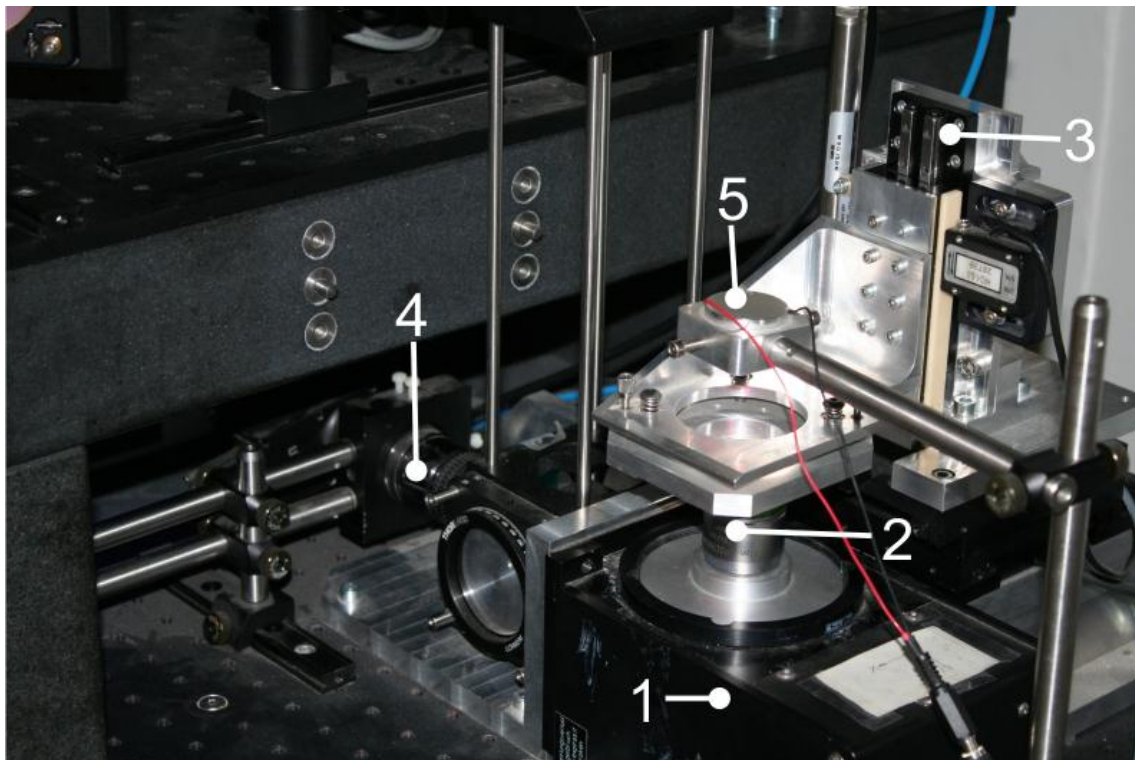


Figure 47 1) galvanoscanner, 2) microscope objective, 3) XYZ axes, 4) CCD camera and 5) sample illumination

10.3 Microscope objectives

Two objectives with equal magnification and different numerical aperture could be mounted in both of the experimental setups used in this work. Before going into their specifications, we will first theoretically describe the key parameters of microscope objectives. Furthermore, we will investigate, how these parameters determine the resolution and shape of the structures, we are going to fabricate.

Generally, a microscope objective's key parameters are its magnification (M), its numerical aperture (NA) and its working distance (WD). M describes the ratio between the appearance of an object through the objective and its real dimensions. The WD describes the objective's actual focal distance. The manufacturer usually corrects this value for its use with a thin glass coverslip (~ 0.2 mm) used in microscopy. NA is a dimensionless value for an objective's maximum angle of aperture for emitting or accepting light. It is calculated as the product of the refractive index n and the sinus of the half-angle of aperture (see Figure 48). The smallest resolvable detail is defined as the ratio between the wavelength and the numerical aperture. In air, the NA can be ~ 1 at its maximum. For achieving higher resolution, high NA objectives require immersion media like water or oil [11,176].

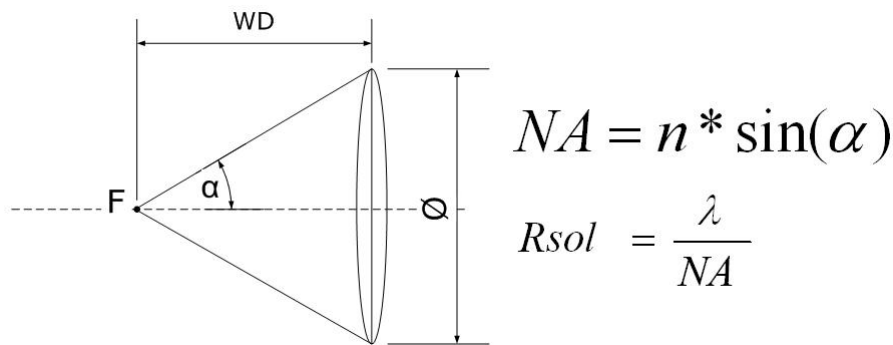


Figure 48 Explanation of the numerical aperture; F=focal point, Rsol=resolution power) [11]

In this work, two 20x magnification were used with NAs of 0.4 and 0.8, respectively. Both required no special immersion media. The objective with an NA of 0.4 was a LD Plan Neofluar. LD, here, stands for long distance. Plan refers to an installed correction of the field of curvature aberration [11]. Neofluar refers to the special optical glass of the lens ensuring high transmission for the entire visible spectrum. It had a working distance of 7.4-8.4 mm and could be adapted to various cover glass thicknesses from 0 to 1.5 mm. Its transmittance of light at 800 nm was approximately 85% according to the manufacturer Carl Zeiss [178]. In the Mipro setup, the accessible building size was ~ 600 μ m using this objective. The efficiency (ratio between the intensity measured after and before the objective) was 30%. The 20x magnification resulted in 10 pixels per μ m and a maximum scanning resolution of 100 nm. The maximum speed of the galvano-scanner was 5 m/s with this objective.

Of special interest is the theoretical maximum obtainable resolution. According to Zipfel et al., the equation for the minimum diameter that can be resolved (Figure 48) must be adapted for the use in two-photon based applications. The following equations provide a good estimate of the minimum diameter of the basic building unit in 2PP. The minimum dimensions in X and Y are [19]:

$$w_{xy} = \frac{0.302 \lambda}{\sqrt{2} NA}$$

for objectives with NAs ≤ 0.7 . The dimension in Z is:

$$w_z = \frac{0.532 \lambda}{\sqrt{2}} \left[\frac{1}{n - \sqrt{n^2 - NA^2}} \right] \quad 8$$

With an refractive index of 1 (air), the X- and Y-dimensions for the 20x NA 0.4 objective is roughly ~ 453 nm and the Z resolution is ~ 3605 nm. A structured polymer line is thus widely elongated in Z. The ratio between height and width is expectedly eight, which is in good agreement with previous experimental work [11]. The volume can be calculated as [19]:

$$V_{2PP} = \sqrt{\pi^3} w_{xy}^2 w_z \quad 9$$

and is roughly $1 \mu\text{m}^3$ for the described objective.

The other 20x magnification objective was a Plan Apochromat. Objectives of this kind have high NAs and good flatness of field. They are widely used in confocal microscopy and are recommended for 2PP. The WD was 0.55 mm. The objective was adjusted to a 0.17 mm thick cover glass. The transmission efficiency at 800 nm wavelength was $\sim 90\%$ [179]. Compared to the 20x NA 0.4 objective, we could obtain a slightly smaller building size of $\sim 550 \mu\text{m}$ in the Mipro setup. The efficiency, however, was 60%. The process speed and the maximum resolution obtainable was the same as with the NA 0.4 objective.

For $NA > 0.7$, the resolution in X- and Y is calculated as [19]:

$$w_{xy} = \frac{0.352 \lambda}{\sqrt{2} NA^{0.91}} \quad 10$$

which results in approximately 244 nm. The Z-resolution for this objective according to equation 8 is roughly 752 nm. The height-to-width ratio of the basic building unit (voxel) is then three, the expected exposed volume is with $\sim 0.06 \mu\text{m}^3$ considerably smaller than the exposed volume of the NA 0.4 objective.

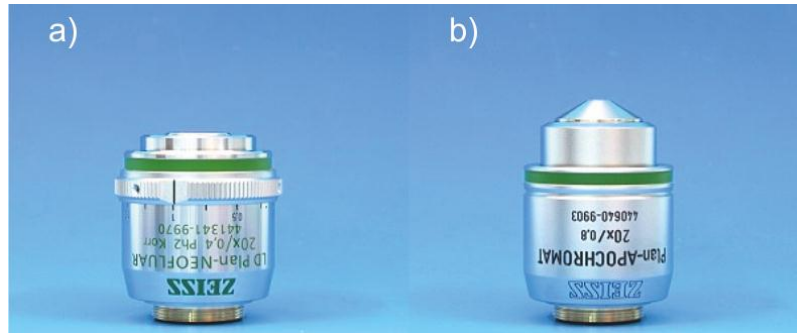


Figure 49a) LD Plan Neofluar 20x NA 0.4 [178], b) Plan-Apochromat 20x NA 0.8 [179]

The above described voxel dimensions are simply rough estimates. The probability of a 2PA and subsequent polymerisation can saturate near the focal centre while continuing to increase in the wings of the focal volume. This causes a deviation from the calculated voxel dimensions. It is thus dependent on several other factors than the NA including

- Laser power
- Pulse width
- Repetition rate
- Reactivity of the formulation

- Size of the molecules inside the formulation

Zipfel et al., for example, calculated the influence of the 2PA cross-section (δ , section 7.2) on the relative increase in 2PA excited volume in two-photon microscopy (Figure 50). Whereas the power has almost no influence in solutions containing fluorophores with a δ of 1 GM, the excited volume increases nonlinearly with the laser power in a solution containing a fluorophore with a δ of 300 GM [19].

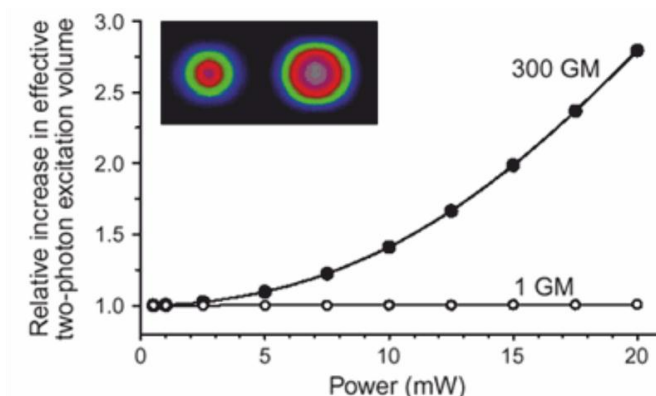


Figure 50 Increase in 2PA excited volume dependent on the laser power for a 1 GM and a 300 GM fluorophore calculated for a 1.2 NA objective, and a 200 fs pulsed 80 MHz laser source; the insert shows the lateral plane for the respective fluorophores at 20 mW [19].

In 2PP, it is possible to achieve photopolymerisation in a very small volume, significantly smaller than calculated. The laser intensity has to stay within the boundaries of polymerisation as shown in Figure 51. The irradiation fluence and/or time at which polymerisation initially occurs defines the threshold. It is dependent on all parameters described above. Precisely controlling the intensity or irradiation time allows polymerising structures at resolutions below the diffraction limit. Increasing the intensity, the voxel sizes increase as long as the upper threshold is reached, at which the formulation gets overexposed and bubbles start to form which subsequently results in damage to the polymer. Hence, it is important to stay within the boundaries of polymerisation.

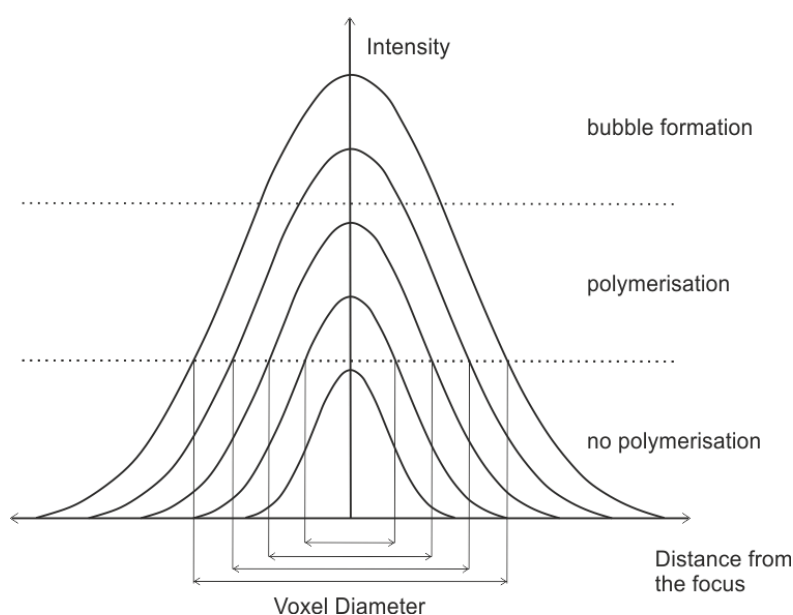


Figure 51 Effect of the laser Intensity on the voxel diameter

Varying the laser powers and writing speeds, one can benchmark a photopolymerisable formulation according to its lower and higher polymerisation threshold as well as its process window. Leaving the testing protocol similar between the tested formulations provides a useful method to compare different components regarding their reactivity. This is what we will further call material screening (section 11.2).

However, before we report on screening the components described in section 9, we will first address the necessary sample preparation protocol.

11 Structuring experiments

11.1 Preparation for 2PP structuring

As a fast screening procedure and low material consumption was favourable, we produced structures with dimensions of only below 100 μm in height. Therefore, only a small building volume was required. A suitable specimen was prepared placing a liquid formulation on a microscope slide as depicted in Figure 52.

To prevent the liquid formulation from flowing down, an 18x18x0.17 mm³ coverslip (Figure 52-3) was put at 120 μm distance from the slide (1). Two pieces of chemical resistant adhesive strip (2) specified this distance. Using another two pieces, the coverslip was attached to the layer of strip underneath (4). The space in between the slide and the coverslip constituted the building area of roughly 18x10x0.12 mm³ assuming that 4 mm of the coverslip laid on either side of the adhesive strip spacers attached to the slide. Hence, in total, the required amount of formulation was approximately 22 mm³ of unit volume.

Using a syringe (5), 30 μl of liquid formulation was applied to the microscope slide. The drop (6) was placed between the two spacers and right next to the coverslip. The liquid formulation could soak into the space between slide and coverslip. After the full building volume was completely filled up, the excess formulation not soaked into the building volume was removed. Two additional pieces of strip were attached on either side of the coverslip (7), where the building volume was exposed to the surrounding. This was especially important for water-based resins as this prevented the water from evaporation and hence the formulation from drying out and from getting unusable. The prepared specimen was then loaded into the designated clamp on the XYZ axes system. The white arrows in Figure 52d indicate, where the specimen was placed. After loading, the operator pushed down the Z-axis manually until the focal point (tip of the red triangle above the microscope objective in Figure 52d) was located in the building volume. 2PA, respectively the PIs associated fluorescence was then visible in the online process observation. The blue arrow of Figure 52 indicates the manual movement to position the focal point.

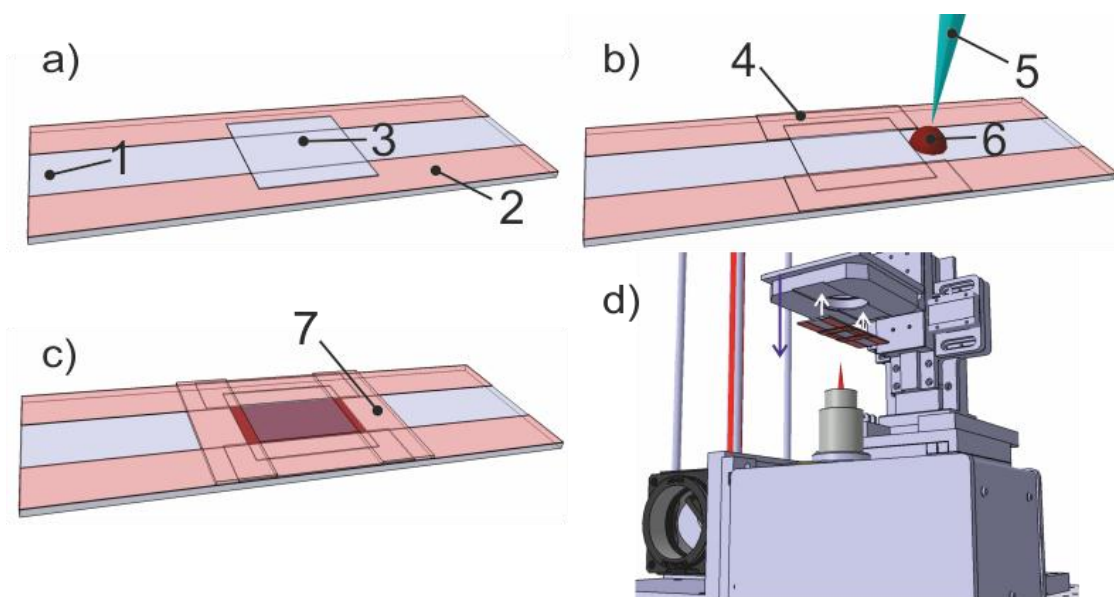


Figure 52 Specimen preparation and loading; a) strip spacers and coverglass on coverslip, b) fixation of coverglass and pipetting formulation drop next to building volume, c) sealing of building volume, d) loading of specimen onto the clamp

Next, the operator enabled the axes for software-controlled movement. She/he moved down the axis to position the focal point close to the surface of the microscope slide. This was then considered as the reference position, where the fabrication of the first structure was intended to start. The subsequent structuring process proceeded upside down. Fabricating in a layer-per-layer approach, the Z-axis moved in the positive direction stacking the individual layers on top of each other. As soon as the fabrication of one lattice was finished, the X- or Y-axis moved to the intended position for the next element. The Z-axis moved to the reference position near the microscope slide's surface. This ensured all structure's attachment to the slide and supported keeping their arrangement. The user could assign the correct markspeed and laser power values to the individual structures and further qualitatively assess the structures in the microscope.

11.2 Speed-power screening via lattice array

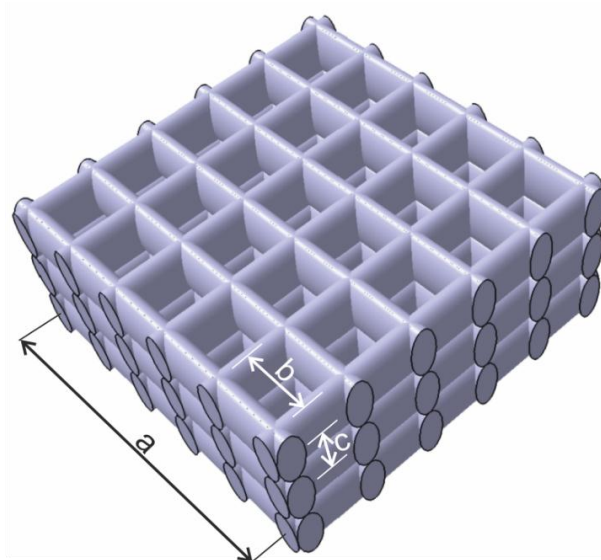


Figure 53 Lattice structure with adjustable parameters; a) base area dimension, b) line distance, c) layer distance

For evaluating the PIs and the precursors described in this work, we often employed one assessment procedure to allow better comparability between the compounds. The assessment was based on qualitatively categorising the optical appearance of standard lattice structures (see Figure 53). Unless indicated otherwise, the applied objective, the structuring parameters and the dimensions of the structure were kept constant for all assessments. We used the 20x NA 0.8 objective to fabricate lattices with an intended base area (a) of $50 \times 50 \mu\text{m}^2$. In total, 40 layers were fabricated at a layer distance (c) of $5 \mu\text{m}$. The distance between the polymer lines (b) was $10 \mu\text{m}$ resulting in six polymer lines per layer. We fabricated several similar lattice elements in an array, where the markspeed and laser power varied in X and Y, respectively.

After the fabrication process, the specimen was immersed in a suitable solvent. The adhesive strips including the coverslip were removed from the microscope slide carrying the lattices. This procedure allowed removing the unpolymerised monomer residue. A check of the structures in the light microscope (LM) gave evidence on the strength of the structure's attachment on the slide.

Attention must be paid to the attachment of the polymer structures on the glass slide. Especially acrylate-based formulations suffer from shrinkage after the development. As the

solvent evaporated, polymer structures often lost adherence to the microscope slide and could not be associated to any particular writing speed and/or laser power. In this case, a qualitative assessment was thus insufficient. Careful development including ensuring a horizontal position of the slide in a still solvent bath, careful removal of the cover glass and safe transportation and storage reduced the chances for the structure's detachment. However, in many cases, this issue could not be prevented. A functionalization of the glass slide with a methacrylic surface as described by Niklas Pucher [10], helped to strengthen the adhesion. Such a slide preparation recommend is recommended before conducting any screening.

When attached properly, the specimens manufactured in hydrophobic formulations were investigated in the Scanning Electron Microscope (FEI Philips XL30). The hydrogel structures were taken to the Laser Scanning Microscope (Zeiss LSM 700). We took pictures showing the overview of all lattices produced as well as detailed shots showing four individual lattices at once. We qualitatively assigned the produced structures to different quality categories. As the level of detail differs between the SEM and the LSM, the quality categories are different for hydrophobic and hydrophilic materials, respectively. The particular schemes will be presented in the respective following sections of this chapter.

For the LSM analysis, we wanted to keep the sample hydrated, similar like in a biological surrounding. Moreover, we wanted to keep the amount of water constant through which the structures were analysed. Using the same LSM parameters, this ensured comparable auto-fluorescence between different samples. The polymer's fluorescence intensity gave insight into its cross-linking density (see section 12.3.1.1). To ensure constant water depth to the polymeric parts, we prepared the structured samples according to the protocol described in the next section.

11.3 Preparation for investigations in the laser scanning microscope

Our intention was to observe the structures in a surrounding, which is similar to a physiological, aqueous environment. Hence, we again kept the structures in DI water for 12 hours until they reached equilibrium swelling [123], where the restoring force of the polymer network limits its swelling capability in the solvent [180]. A laser-scanning microscope (LSM) allowed direct observation of the polymer's auto-fluorescence when exposed to a cw-laser. Thus, it was possible to investigate the lattices directly in the aqueous surrounding. Drying was not required.

For transportation to the LSM and for subsequent investigation, the specimen was prepared in a similar way as for fabrication (see Figure 54). First, the slide with the attached structures was taken out of the solvent. Second, the water remaining on the slide around the structures and on the adhesive strip spacers was dried with tissues. Third, we again laid a cover glass on the spacers of the slide with the attached structures (a). After fixation of the cover glass, we obtained an observation volume of 22 mm³ (b). A drop of DI water was placed next to this volume and was soaked in (c). The sample was now ready for transportation and observation.

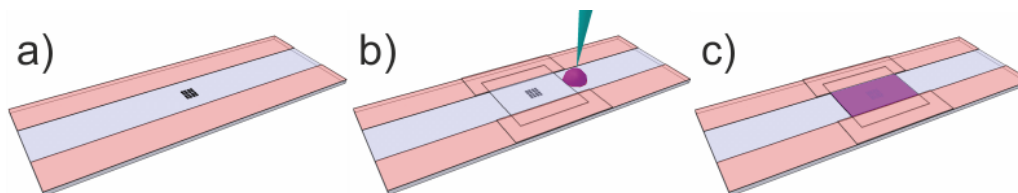


Figure 54 Sample preparation for LSM observation a) soaked structures (black) on dry slide with strip spacers, b) coverglass fixation with spacers and application of DI water drop next to the observation volume, c) volume soaks up the water, the sample is ready for transportation and observation.

After describing the experiments done, we can finally present their results. Similar as in the chapter on state-of-the-art hydrogels for 2PP, we will divide the following chapter in two parts. In the first one, we screened novel 2PP PIs described in section 9.1. The second section will deal with precursors that can render polymeric constructs. The focus here, again, will be on high process speeds and biocompatible hydrogels derived from formulations with high water content.

12 Material screening

The results of this section have to be seen from the major perspective of this thesis; to build up biocompatible hydrogel structures with 2PP at high process speeds.

Using the novel Mipro setup, we therefore first processed organo-soluble formulations. Novel PIs, synthesised at the IAS, were evaluated for their performance in high-speed 2PP manufacturing. For comparing the initiators to previously synthesised compounds, we used the standard monomers ETA and TTA in a 1:1 ratio for reference purposes. This monomer was already well established in 2PP, especially from the work of Klaus Cicha and Niklas Pucher [116,176,181,182].

Second, taking advantage of the results of the organo-soluble PI screening, we tested the water-soluble derivatives for cross-linking a standard acrylate monomer with a water-soluble PEG backbone (PEGda). The chemical structure of these monomers is described in section 9.2.1.1.

Third, in the organo-soluble precursor section, we evaluated the polymerisation efficiency of organo-soluble materials that likely can be turned into water-soluble components. In this section, we especially searched for alternatives to potentially toxic acrylates

Fourth, in the water-soluble precursors section, we increased the water content of a PEGda formulation to 80% to minimise potentially toxic influence of the monomers.

Fifth, we structured natural based polymers that were functionalised with the monomers found in the third section.

12.1 Organo-soluble 2PP Initiators

We synthesised and benchmarked 2PP PIs with different size member rings as central acceptor groups. To allow a good comparison, mostly Klaus Cicha (IMST) screened all components in markspeed-power arrays according to the aforementioned protocol [183]. These screenings were conducted with the M3DL setup at a constant writing speed of 50 $\mu\text{m/s}$. It could be shown, that especially the compound with the number 3e, here termed as M_2CMK , having the smallest δ of all investigated initiators in this study, displayed much broader ideal processing windows than other benzylidene ketone PIs with different central acceptors. The processing window was comparable to the reference PIs R1, a component requiring a more complex multiple-step synthesis (see section 9.1.1 for the chemical structure of M_2CMK and R1). As the goals of this study were not directly related to biocompatible, water-based formulations, we will highlight here only the feasibility of this compound for structuring at high writing speed on the new Mipro setup.

TTA and ETA in a 1:1 ratio (section 9.2.1.1) were mixed with M_2CMK in a concentration of 6.3×10^{-6} mol PI/g formulation (0.2 wt%). A screening according to above described protocol was performed, where we varied the writing speed from 1 to 151 mm/s in the X-plane and the laser power from 35 to 360 mW in the Y-plane. We used the 20x NA 0.8 objective for the structuring. After the fabrication process, the specimen was immersed in ethanol for 4 hours and observed in the LM. When attached properly, the dry structures were investigated in the SEM. The structures were assigned to a classification scheme introduced by Klaus Cicha [176]. The first class included good structures with straight fine lattice bars. Initiators favouring the fabrication of a large number of these structures at a wide range of laser powers and writing speeds are

considered high performing. Structures of class two have thicker bars and are slightly wavy. These slight distortions are usually attributed to the development process rather than to the fabrication process. Class 3 includes structures with defects. Yet, their intended appearance can be recognised. These defects include holes or craters usually attributed to overexposure and subsequent bubble formation. Lattices that do not resemble their intended design are assigned to class four.

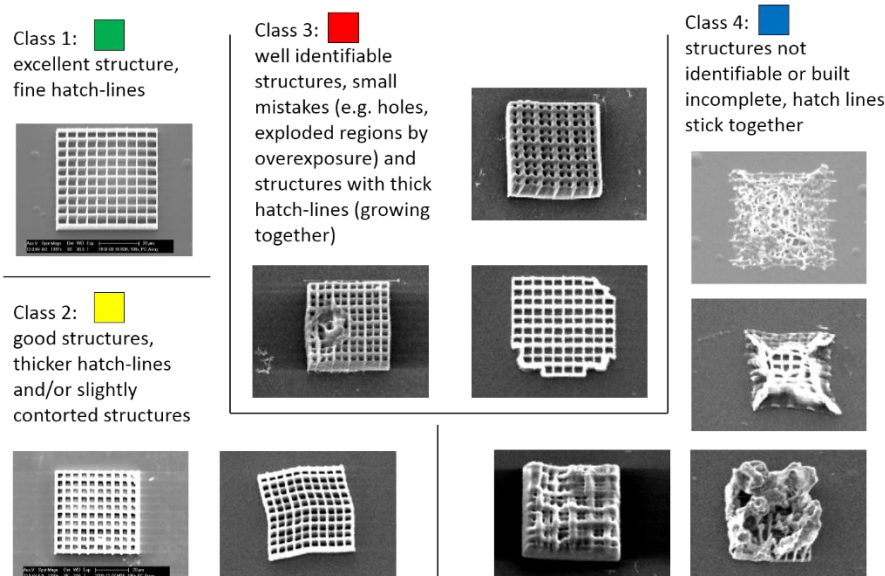


Figure 55 Lattice classes for qualitative optical assessment [176]

The whole speed-power array of M₂CMK can be seen in Figure 56. Almost all structures in the column are pronounced and of good quality. No lattice top left, structured at the lowest speed (1 mm/s) and the highest power (335 mW) can be observed. Presumably, too high intensities caused bubble formation and explosions inside the formulation, which potentially displaced the polymer. Another possibility would be a detachment based on shrinkage of the polymer during development as previously mentioned. Regarding the array from the bottom left, this presumably applies for the structure in row two column two and for the lattice in row three, column three, too. These structures are not there, although elements produced at higher speeds and with higher power are recognisable. Hence, the set parameters were likely suitable for producing lattices. One more evidence of weak attachment is the element in row four, column six, which stands on its side, though it was not produced in that way.

Despite the weak attachment of some structures, the array shows that almost all structures are pronounced and can be classified into the first category (green). Some structures have polymer inclusions and are thus associated to the yellow category. As the yellow structures are randomly distributed within a field of green elements, these inclusions are likely a result of the development process rather than of the structuring parameters. The qualitative assessment shows that defined structures can be produced at laser powers as low as 35 mW at 1 mm/s. Writing speeds of 151 mm/s are reached at 110 mW. At 135 mW, well-defined lattices are fabricated at this speed. The laser power was measured before the 20x NA 0.8 objective. The laser power reaching the sample was 60% of the given values.

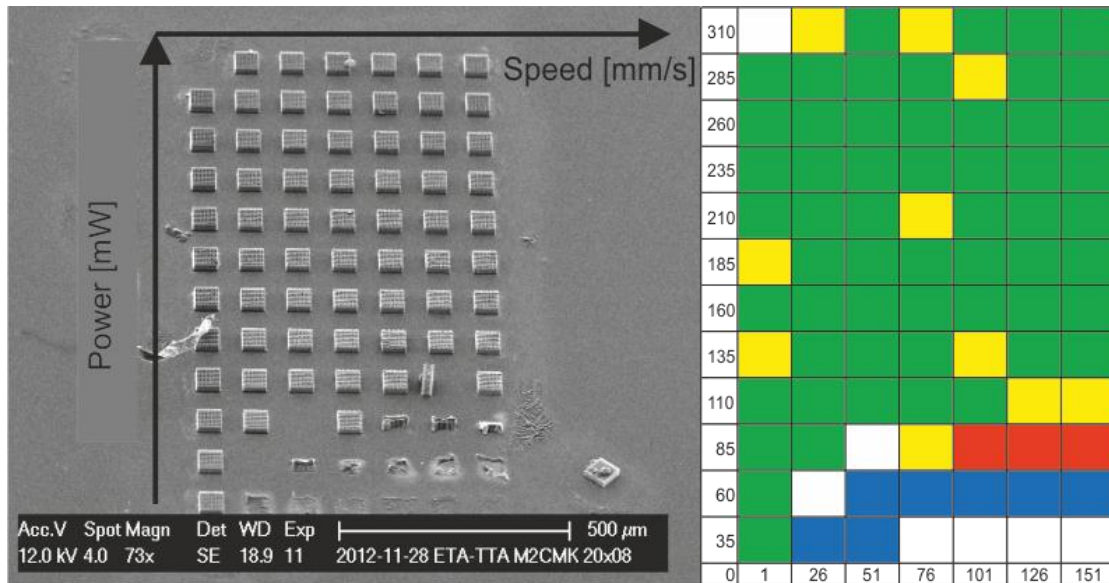


Figure 56 Screening of PI M₂CMK in ETA-TTA and qualitative assessment, 20x NA 0.8 objective; left: SEM image, right: qualitative assessment

The results of this section indicate that M₂CMK in ETA-TTA formulation facilitates precise micro-fabrication at the highest process speeds ever reported in 2PP, which shows that a major goal of this thesis could be achieved.

As a symbol for high writing speed and to show the 3D capabilities of the presented formulation, we structured the model of an indy racecar based on the CAD file in Figure 57a. This structure was 285x130x100 μm^3 in dimensions and consisted of 100 layers at an average of 200 polymer lines each. The distance between the lines was set to 1 μm . Despite the large amount of polymer lines structured in total, the fabrication process only took close to four minutes (see Figure 57b). The Z-axis needed 2/3 of the whole building time to level up. Thus, the total structuring time (the time for fabricating one layer) was only ~2.6 minutes. Taking the time used for positioning the mechanics without inducing any polymerisation, the focal point was traced in the formulation at well above 80 mm/s. Due to inertia problems, this speed was the limitation of the Mipro setup for this specific CAD structure. ETA-TTA including M₂CMK can be likely processed at even higher writing speeds.

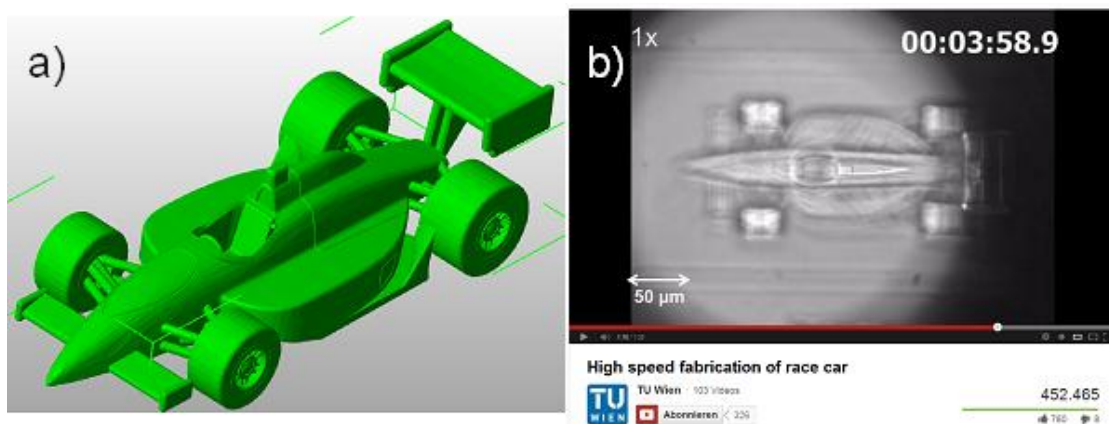


Figure 57 Micro-fabrication of indy racecar; a) CAD file, b) recorded fabrication process

Following a press release showing a video on the fabrication of the racecar, we received a lot of attention all over the world. The full video of the fabrication process has been uploaded to

YouTube (see Figure 57b). From its initial release in March 2012, the fabrication process had more than 450000 viewers.¹³ The SEM images were published in a large variety of magazines and newspapers¹⁴. Two of the images are depicted in Figure 58.

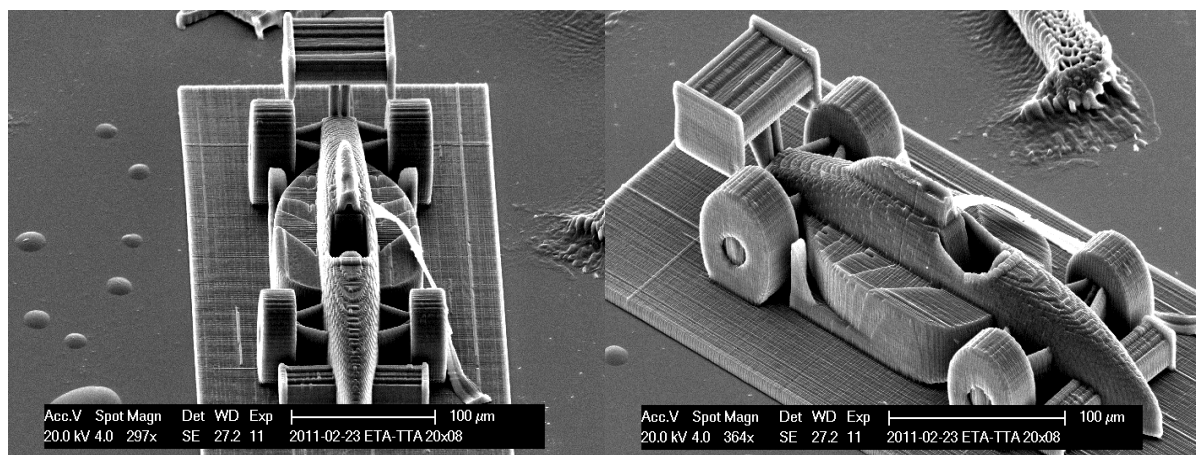


Figure 58 SEM images of racecar, ETA-TTA, M₂CMK, 20x08

The results of this section indicate that the novel efficient initiators from the IAS can be processed at the highest speed reported for 2PP. Together with the fast and precise mechanics of the new Mipro setup, we could fabricate complex structures at a fraction of the time conventional chemistry and mechanics would allow. However, the initiator's capabilities for high-speed fabrication is not yet fully exploited. Martin Schoiswohl, a bachelor student at the time this thesis was written, conducted resolution experiments that revealed fabrication speeds in the m/s range [184]. The initiator used was B₃FL, a compound synthesised by Niklas Pucher and extensively studied by Klaus Cicha [10,116,181,182]. As this compound facilitated similar process windows as M₂CMK [183], we can expect equivalent speeds using this compound. We conclude that the reactivity of PIs synthesised at IAS is, by now, not the limiting factor of 2PP writing speeds in organo-soluble acrylate formulations. As can be seen from the initiator screening in Figure 56, the writing speed is of less influence than the laser power, meaning that a broad spectrum of writing speeds are possible with the same laser power. To tackle the speed issue further, mechanics with higher acceleration capabilities are required.

The second challenge to address is the biocompatibility issue. For processing hydrogel formulations with high water content, it is necessary to find water-soluble PIs that can efficiently cross-link relatively dissolved low-reactive, biocompatible precursors. As the δ of two-photon chromophores drops significantly in water [165], it is interesting to see how the well-performing M₂CMK and its derivatives with different size member rings and the reference compound R1 perform in aqueous solution. In the next section, we will investigate the performance of the M₂CMK derivatives G₂CK, E₂CK, P₂CK and Q₂CK as well as the water-soluble R1 derivative WSPI for cross-linking the water-soluble cross-linker PEG-700-da in an aqueous surrounding.

¹³ Status 8th of February 2013, the full video can be seen on <http://www.youtube.com/watch?v=5y0j191H0kY>

¹⁴ Journals like Popular Mechanics, Science Daily, Materials Today, BBC news, Engadget and Discovery News picked up content from the related press release http://www.tuwien.ac.at/de/aktuelles/news_detail/article/7435/. In total, there were 363 media reports in 20 different languages showing content of this press release all over the world. and picked up content

12.2 Water-soluble 2PP Initiators

For most experiments in this thesis, we used the compound WSPI, (see section 9.1.2) as it was the first one available. Niklas Pucher synthesised this compound in the year 2010 according to a known procedure [165]. It is a derivative from R1 and initially used as high performing chromophore in 2PM. Besides the experiments in this thesis, we do not plan to use this compound further in 2PP. Compared to the 2PIs described recently [183], it requires a difficult multi-step synthesis further challenged by introducing quaternary ammonium salts to make it water-soluble. In this section, we thus explore the easy-synthesisable compounds G₂CK, E₂CK, P₂CK and Q₂CK in respect to WSPI. These experiments will be interesting for PI selection in the future. The chemical structure of the compounds are described in section 9.1.2.

2 wt% of PI was dissolved in a 1:1 ratio of PEG-700-da and deionised water. The sample was prepared according to section 11.1 and screened following section 11.2. The speed parameters were varied from 1 to 30 mm/s by steps of 1 mm/s. The power range was from 20 to 145 mW with process power changing by 15 mW with each element in the plane. In total, 30 elements in the X- and 6 in the Y-plane were fabricated, resulting in a total number of 180 lattices. After fabrication, the structures attached to the slide were rinsed in DI water for 12 hours. Still lying in the water, the sample was observed under the LM and the adhesive strips attaching the coverslip to the spacers underneath, were removed. Special attention had to be paid on the attachment of the structures to the slide (described in detail in section 12.1). Hasty movements of tweezers and/or scalpels inside the water caused fluid flows that potentially pushed the lattices from the glass. Working with aqueous formulations, one had to be even more careful than with the organo-soluble ETA-TTA. Here also, the functionalization of the specimens (see section 11.2) helped a lot and is strongly recommended in future screenings.

After developing and preparing the sample according to section 11.3, we observed it in the laser scanning microscope (LSM). A cw laser with 488 nm was focused through a 10x NA 0.25 objective. Wherever the focal point hit the 2PP-structured polymer, we could observe fluorescence. In the surrounding water, the LSM detector did not record any bright spots. Hence, without any addition of dyes, the fabricated PEGda based polymer showed auto-fluorescence at sufficiently high laser powers. This is in good agreement with previous work observing acrylate polymers in the LSM and allows creating images of the 2PP parts in an aqueous surrounding [185].

Keeping the LSM parameters constant, similar 2PP parts structured at different speeds and laser powers fluoresced differently. With increasing laser power and decreasing writing speed, the polymer appeared brighter, whereas the contrast to the surrounding decreased observing parts structured at lower energy doses. As the polymer is usually more stable and dense when fabricated at higher energy doses (see section 12.1), a higher fluorescence activity obviously indicates denser polymer networks.

It is not clear, which molecules actually contribute to the auto-fluorescence of PEGda hydrogels. As PEG is not expected to fluoresce, the attached acryl group could potentially be responsible for the polymer's visibility in the LSM. However, these groups usually fluoresce at lower wavelengths (280-300 nm) [186]. Thus the PI, although not being bound to the polymer, seems to be the driver for the auto-fluorescence. Its residues may remain within the polymer.

However, rinsing the polymer parts with DI water usually removes at least parts of the remaining PI. The fluorescence would decrease with each rinsing cycle. However, this was not the case in our experiments. Either the PI cannot be removed, or there must be some other molecule driving the auto-fluorescence of PEGda based hydrogels.

To support the hypothesis of attributing high fluorescence to high dense polymers, we observed the same parts in the LM. The structures showing high contrast in the LM tend to show high fluorescence in the LSM (see Figure 59).

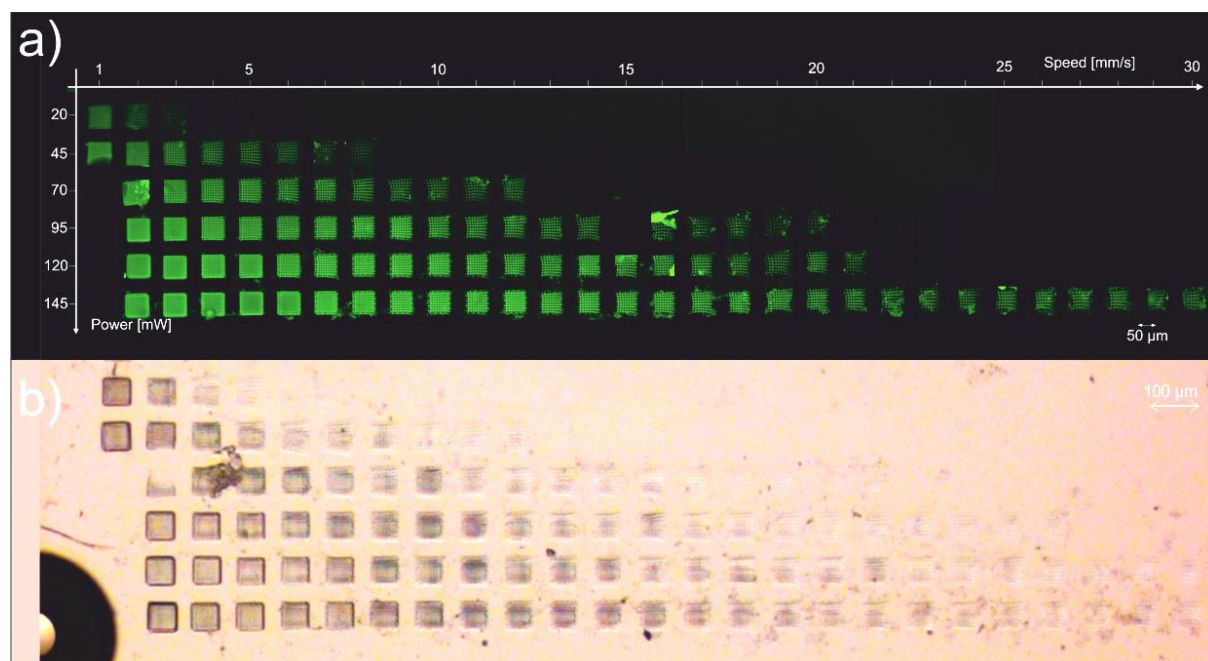


Figure 59 Lattice array screening of 2 wt% WSPI dissolved in a 1:1 PEGda:DI water formulation; a) LSM image, b) LM image

In this thesis, we thus considered the contrast of the parts as sufficient for relatively assessing the impact of laser power and writing speed in one formulation. However, spectroscopy analysis might reveal, which molecules actually contribute to the auto-fluorescence in PEGda based hydrogels.

Applying the same screening for the other initiators G₂CK and Q₂CK, shows that they facilitate different process windows for cross-linking the acrylate based hydrogel formulation (see Figure 60). G₂CK shows the broadest processing window. Using the lowest power of 20 mW, process speeds from 1 mm/s (lowest) until 13 mm/s are possible. Raising the power to 45 mW allows fabrication speeds of up to 30 mm/s (highest). G₂CK is quite sensible to overexposure. At 45 mW, the upper polymerisation threshold is already 4 mm/s, at 145 mW. Too high laser powers potentially caused damage to the structures fabricated at lower speeds than this threshold. This potentially caused damage to the polymer structures which then lost adherence to the glass slide. Yet, the structures produced with 145 mW at 11, 12 and 14 mm/s obviously did not adhere to the glass slide. This might have two reasons; either the initiator was not properly dissolved, the focus point hit an initiator causing overexposure and bubble formation. This might have resulted in a damage to the structure and its subsequent detachment from the slide. Another possibility might have been the lattices' loss of adherence during development. As this did not happen anywhere else than on the edge of the array, I presume the latter cause to be more likely.

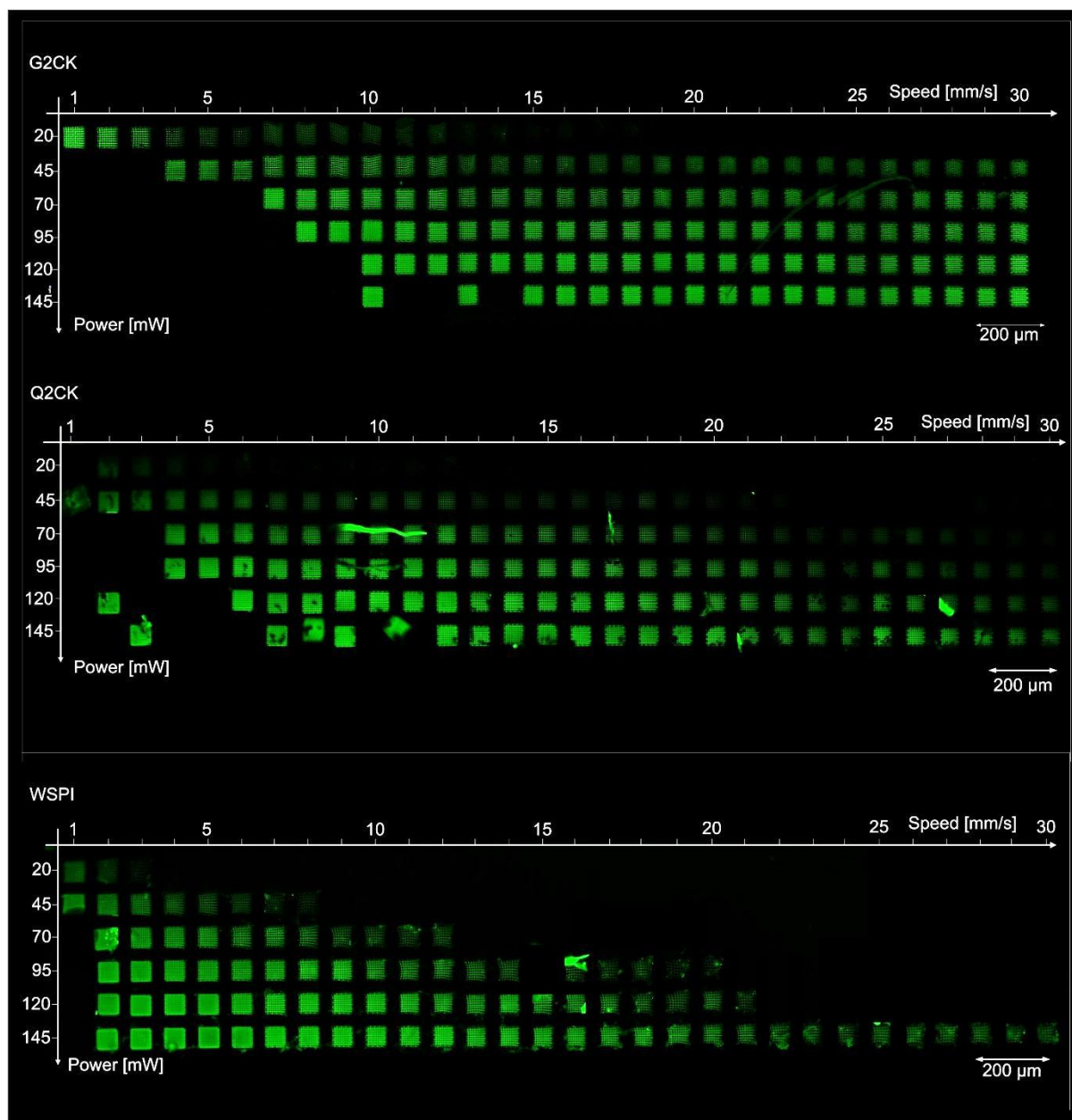


Figure 60 Process window of 2 wt% G₂CK, Q₂CK and WSPI in a 1:1 PEG-700-da: DI water formulation, joined LSM images 10x

Q₂CK shows an almost equally broad processing window. Yet, it is somehow shifted to higher energy doses. Despite that the lattices structured with 20 mW and 1 mm/s cannot be seen, the one produced at the same speed and higher power (45 mW) is there. Yet it seems distorted and not well adhered to the glass. Similarly, the structures at 120 mW, 2 mm/s and 145 mW, 3 mm/s stand alone. If the formulation would have its upper polymerisation threshold at these parameters, structuring at higher speed would have been possible. Yet, there is no structure whatsoever to be seen at higher speeds. This give evidence that the upper polymerisation threshold is not reached as displayed. Obvisouly, a lot of structures lost their attachment. This can potentially be attributed to the bad solubility of Q₂CK. In Figure 60, one can see many structures with errors, bright and dark elements running through the lattices. This is attributed to the initiator impurities that caused unexpected polymerisation and damage to the polymer during fabrication. We thus conclude that Q₂CK, despite its high potential for polymerising water-soluble acrylate formulations, is deficient as two-photon PI.

WSPI shows the smallest processing window of all investigated compounds. Here again, the process window is shifted towards higher laser powers. At 1 mm/s, structures produced with 20 mW and at 45 mW of power are visible. At 2 mm/s, structuring is already possible using the whole investigated power range. The upper right corner reveals the lower polymerisation threshold. 30 mm/s is only reached at the highest applied power (145 mW). With 20 mW, polymerisation until 2 mm/s is possible. At these parameters, however, the quality of the structures is already quite weak. Despite its obviously lower reactivity compared to G₂CK and Q₂CK, WSPIs solubility in the formulation is quite high. There is no evidence of any structure that fell off the glass during polymerisation. Also the attachment to the glass is quite good giving a distinct lower and upper polymerisation threshold.

Concerning the quality of the structures, we had to use a slightly different classification scheme than applied in section 12.1. Due to the nature of the LSM, the above screening gave lower resolution and thus lower insight into the structure's quality than the SEM. We thus decided to associate the lattices to a less distinct classification containing only three categories. Again, the first class included excellent structures with straight fine lines. The single lines were recognisable. Structures of class two are still good but are made of slightly wavy thinner or thicker bars differing from their intended CAD dimensions. Class three includes structures with defects that are still identifiable. These lattices have deviations deriving from burned polymer parts and/or contain holes from overexposure. In addition, some structures of this category contain thick ($\varnothing \geq 5 \mu\text{m}$) polymer lines. In these structures, the single lines are not recognisable. They grow together to form a fully solid polymer with dimensions substantially larger than intended. For water-soluble formulations, we did not consider a class four, as the respective structures were not distinct from those of group three. Figure 61 assigns example structure to the aforementioned categories.

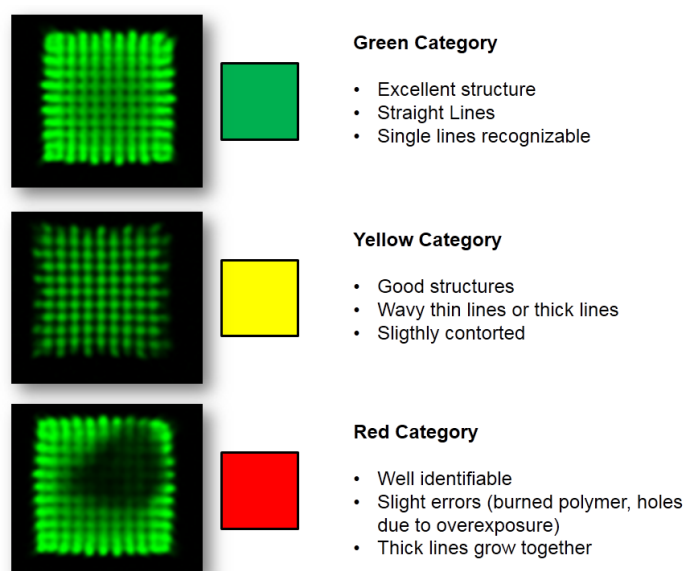


Figure 61 Categories for performance screening of water-soluble PIs with associated example structures

With these criteria in mind, we assigned the lattices of the speed-power array in Figure 60 to these categories. Figure 62 shows a comparison between the initiators. This graph further confirms the above stated bad solubility of Q₂CK in the formulation. Structures attributed to class two and three are randomly distributed within the processing window. Due to the inhomogeneity of this formulation, one cannot expect process parameters found in this screening will work for in a similar formulation as well. Q₂CK thus does not allow reproducible structuring.

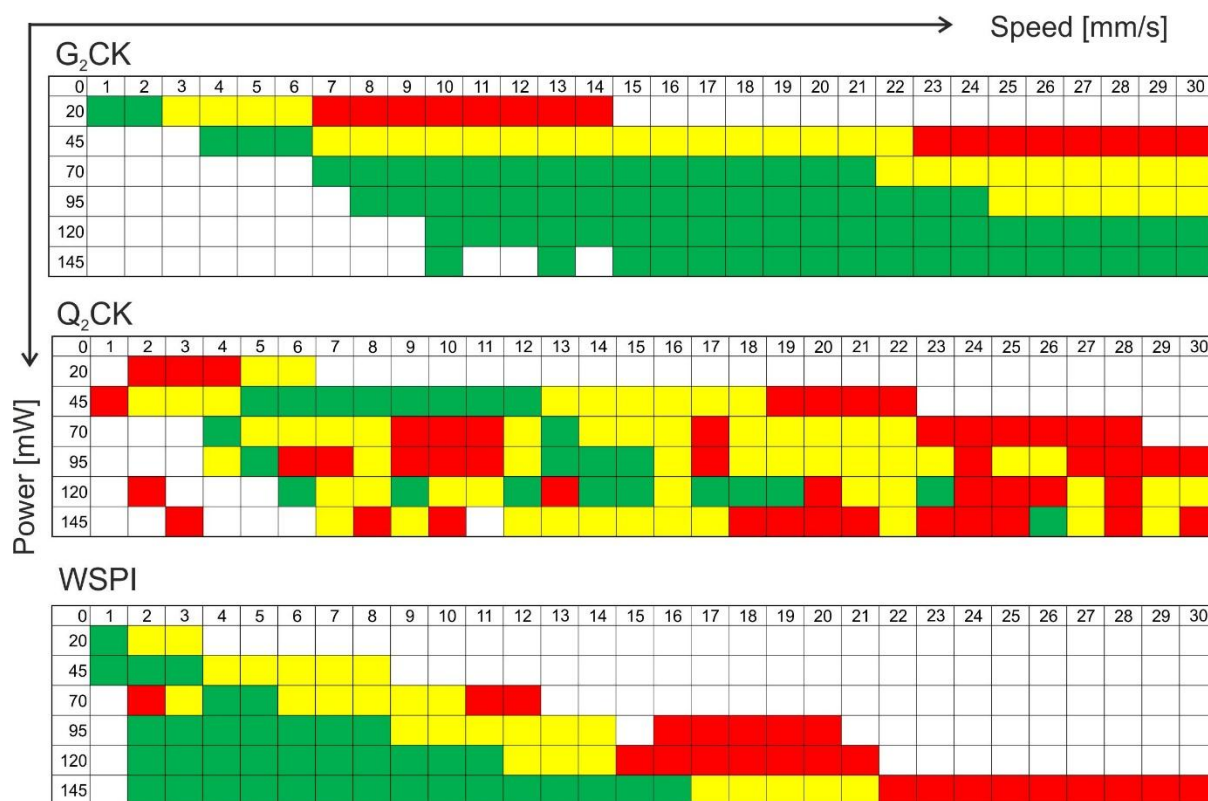


Figure 62 Qualitative assessment of water-soluble PI screening, G₂CK, Q₂CK and WSPI, 2 wt% PI in 1:1 PEGda:DI water formulation, 20x NA 0.8 objective

In November 2011, at the time this screening was done, other water-soluble PIs were not available. As experiments with WSPI were already running, we still concentrated on this compound.

In June 2012, Zhiquan Li synthesised the water-soluble compounds P₂CK and E₂CK, which were based on M₂CMK and similar to G₂CK. In the course of his bachelor thesis, Stefan Fritze (IMST) screened these compounds according to the above-described protocol. The following results were obtained in the course of his thesis [187]. They will soon be published in Zhiquan Li's (IAS) manuscript on these water-soluble two-photon PIs currently in preparation [166].

Besides the length of the alkyl chain attached to the molecule, E₂CK had the same structure as G₂CK. P₂CK was very similar too differing just in the size of its central acceptor. The δ of E₂CK (201 GM) and P₂CK (176 GM) was even higher than for G₂CK (163 GM) in water. The first experiments (not shown) revealed no significant difference in the PIs performance. A larger range of speed and power values was required. After some pre-tests, we found an appropriate power range from 60 to 410 mW increasing by steps of 50 with each element. The speed was varied by 10 mm/s in a range from 1 to 101 mm/s. 11 lattices differing in their fabrication speed were structured in the X-plane, whereas 8 elements were manufactured in the Y-plane at different power values. The other parameters were the same as quoted in section 11.2. The whole array could be observed at once in the LSM. Joining LSM images as in the previous screening was not required. The process window of E₂CK and P₂CK in relation to G₂CK and Q₂CK is shown in Figure 63.

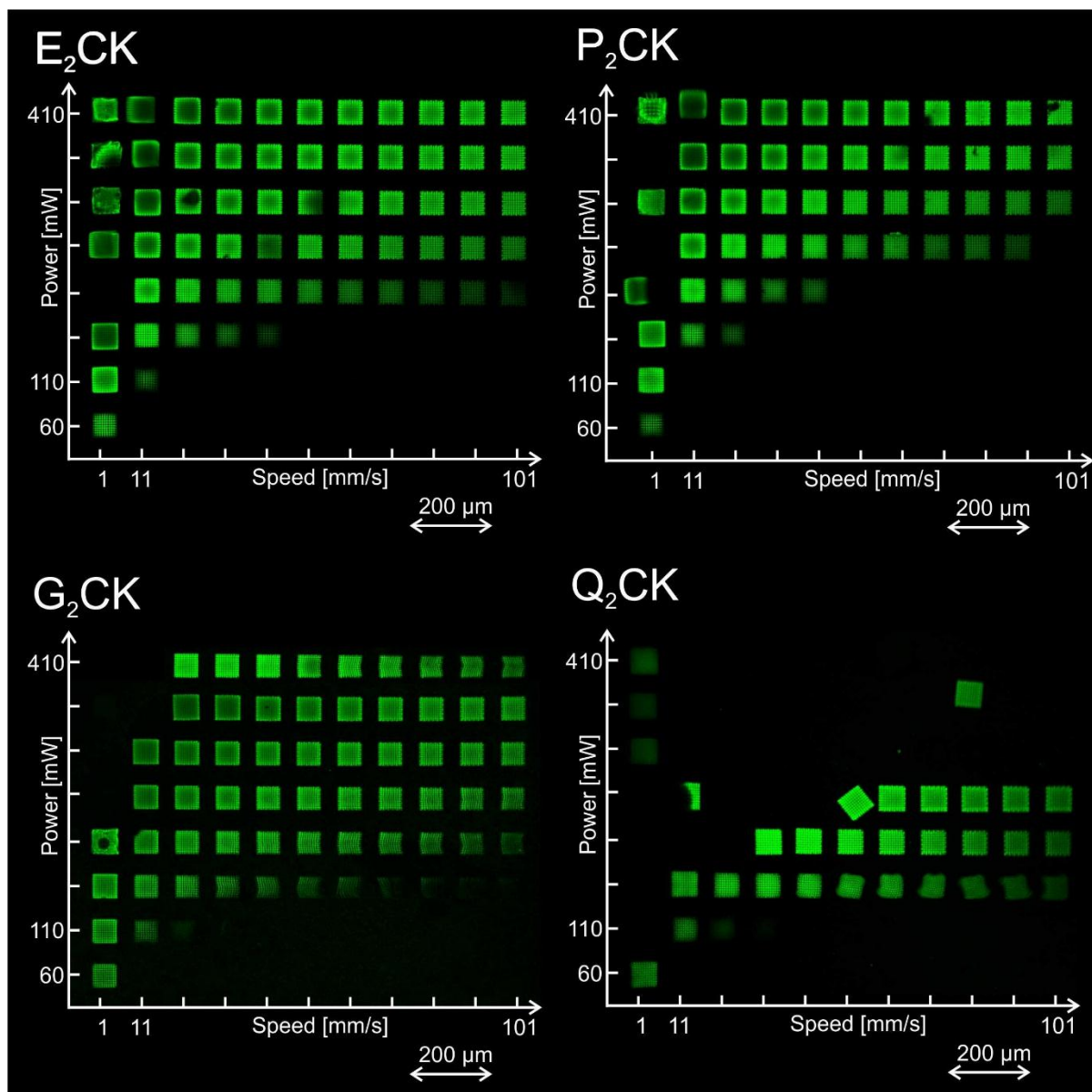


Figure 63 Process window of 2 wt% E₂CK, P₂CK G₂CK and Q₂CK in a 1:1 PEG-700-da: DI water formulation, LSM images 10x

With its central cyclohexanone, E₂CK (top left) is a derivative of M₂CMK (section 9.1.1 and 12.1). As known from the screening of the organo-soluble derivatives, the obtainable process window was already expected larger than those of P₂CK with its central cyclopentanone. This is evident in the bottom right corner of the array, where the applied speed values were high and the power values low. At 110 mW, E₂CK permits fabrication speeds of 11 mm/s, whereas this power is not enough to trigger polymerisation in a similar formulation including P₂CK. 101 mm/s, the highest applied writing speed is possible at 210 mW with E₂CK, whereas 100 mW more are required processing P₂CK. Yet, P₂CK does not shift the process window to higher power values. The upper polymerisation threshold is in fact almost equal to the E₂CK based formulation. E₂CK, thus, seems to be a more efficient 2PP PI facilitating high writing speeds at comparably low laser power.

Comparing this PI to the very similar G₂CK, however, shows that E₂CK's longer alkyl chain attaching the water-soluble moieties to the molecule indeed increase the δ but does not render this PI lower polymerisation threshold. This gets obvious regarding the bottom right of the E₂CK and G₂CK arrays. At 110 mW, for example, the lattice structured at 11 mm/s is bright and thus

well pronounced in the G₂CK array, whereas it is a lot weaker using E₂CK. Taking a closer look at the G₂CK screening, a very dark structure fabricated at 21 mm/s in the same row gets apparent. This proves that the lower polymerisation threshold is higher with E₂CK than with G₂CK. The two lattice rows at higher powers give further evidence to this conclusion. A lot more structures towards high writing speeds are obvious in the row of 160 mW in the G₂CK array. E₂CK's lattice fabricated at 210 mW and 101 mm/s is a lot less pronounced than the one in the G₂CK array.

The upper left part of both arrays, however, illustrates that the longer alkyl chain of E₂CK shifts the process window towards higher powers. The upper polymerisation threshold in E₂CK based formulations thus exceeds the one of an equivalent formulation containing G₂CK. After all, we can conclude that the novel PIs do not outperform the already reported.

At first glance, the reference molecule Q₂CK (bottom-right) does not show a broad processing window at the applied parameters. A closer look, however, shows that this PI favours the lowest polymerisation threshold of all investigated compounds. At 160 mW, already, this formulation facilitates processing at the maximum investigated writing speed (101 mm/s). Though investigated at the same LSM parameters, the lattices at 210 and 260 mW appear brighter than in any other array. However, the structures produced with higher writing speeds cannot be seen. From the online structuring of this formulation, from the LM observation after fabrication (images not shown) and from the previous results expressed in this section, we cannot attribute this to a low upper polymerisation threshold. The dark structures top left in Q₂CK's array constitute a significant larger processing window than displayed. Obviously, the structures detached from the glass, which is again a result of Q₂CK's poor solubility and a damage to the polymer during fabrication. As previously reported, the explosions and formed bubbles in the formulation potentially rendered week attachment of the structures to the glass. In any of our six attempts, we could not prevent the structures from detaching, even with very careful handling. In addition, we observed a significant decline in Q₂CKs solubility with time. Thus we had to order new samples every few weeks, whereas the other PIs stayed dissolved in the formulation over months.

Regardless of its bad solubility, Q₂CK is quite efficient. This is noteworthy since it consists of the same hydrophobic base molecule as P₂CK (see section 9.1.2). As P₂CK is the least performing of all PIs investigated here, we can attribute this performance to the water-soluble moieties of Q₂CK; the quaternary ammonium salts. WSPI uses the same strategy for its water-solubility and is among the best soluble of all compounds. Hence, for future designs of efficient water-soluble PIs, introducing quaternary ammonium salts as water-soluble moieties should be considered.

In Figure 64, we classified the structures according to the three categories mentioned earlier.

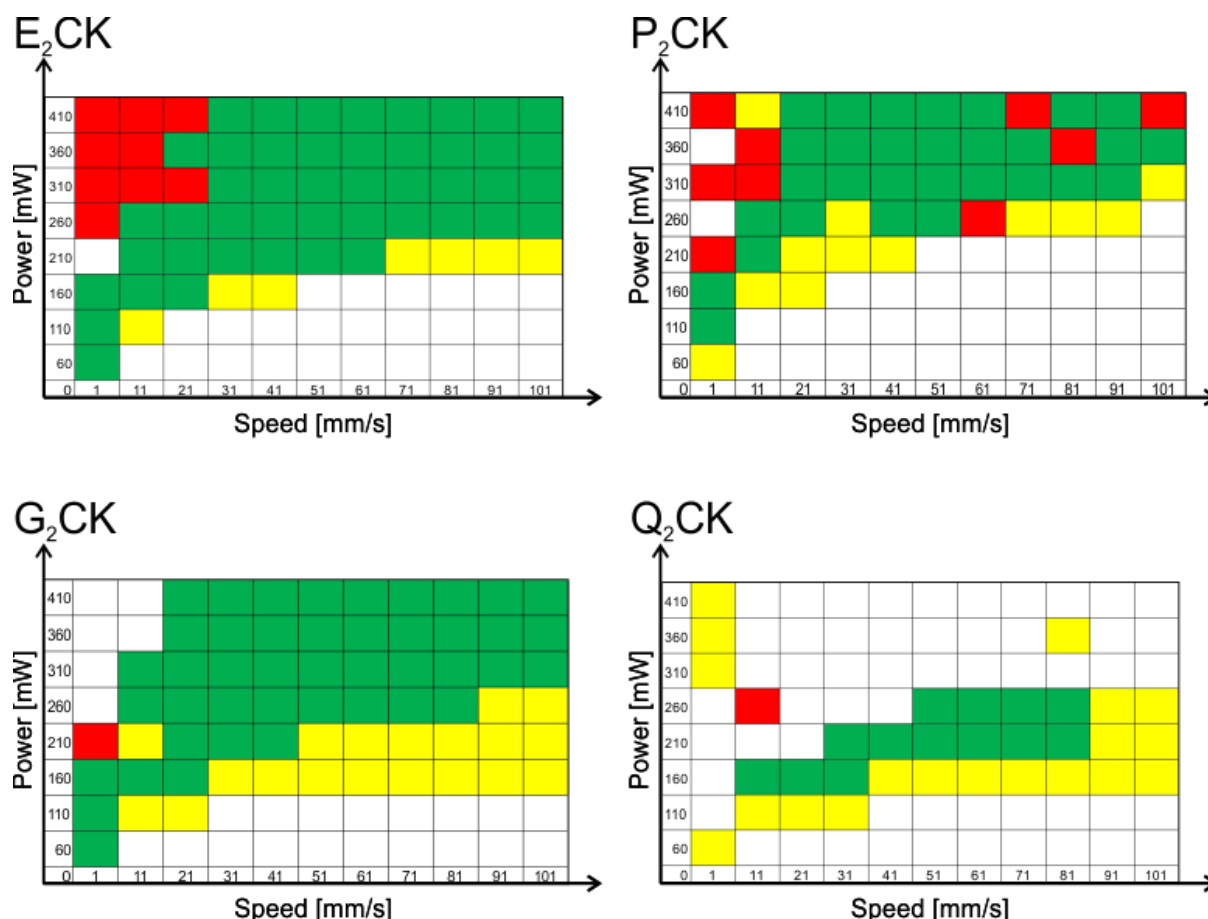


Figure 64 Qualitative assessment of water-soluble PI screening, E₂CK, P₂CK, G₂CK and Q₂CK, 2 wt% PI in 1:1 PEGda:DI water formulation, 20x NA 0.8 objective

Here we clearly see that the lower polymerisation threshold is a lot higher in the formulation including P₂CK than in the one with E₂CK. Regarding the quality of the structures, we do not see any distinct difference in the upper polymerisation of the investigated formulations. In the green marked sections of P₂CK's array, we see some red marked lattices. Usually, the assessment reveals minor but continuous quality changes rather than single elements of bad quality randomly distributed. We thus conclude that the formulation was slightly inhomogeneous. Potentially, the solubility of the cyclopentanone based P₂CK is worse than of its cyclohexanone counterparts. This is quite in agreement with the bad solubility of Q₂CK, which consists of the same hydrophobic core molecule.

Despite its lower polymerisation threshold, the amount of good quality lattices produced with G₂CK is less than with E₂CK. The latter compound's green category even starts at lower energy doses, i.e. at lower laser powers and/or higher writing speeds. Comparing the rows structured at 210 mW, for example, shows that good quality structures can be produced at 61 mm/s using E₂CK, whereas only at 21 mm/s using G₂CK. Also the green category of Q₂CK starts at lower energy doses than the one of G₂CK.

From the results of this section, we conclude that E₂CK is the most suitable PI for cross-linking PEGda. It provides the largest processing window for structuring good quality lattices. G₂CK comes next providing an even larger processing window than E₂CK, although not facilitating the production of high quality structures throughout the whole range. P₂CK offers a much smaller processing window than G₂CK and E₂CK but is still substantially better performing than conventional xanthene dyes. Q₂CK suffers from bad solubility and is not recommended as a 2PP PI. However, the introduction of quaternary ammonium salts as water-soluble moieties as in Q₂CK should not be disregarded. Apart from its bad solubility, this PI seems better

performing than all other compounds despite its presumably low reactive core containing a central cyclopentanone acceptor.

Among the better performing compounds based on M_2CMK and its derivatives, G_2CK was the first one available. Using this initiator, we showed the potential of these kind of initiators for cross-linking hydrogels with high water content in precise 3D shape. As a symbol for high hydrophilicity, we structured complex overhanging parts based on the CAD frog shown in Figure 65a. We used a formulation containing 50% water and 2 wt% G_2CK , the same formulations used for the aforementioned screening. The CADs intended dimensions were $200 \times 170 \times 94 \mu m^3$. As for the PI screening, we used the 20x NA 0.8 objective for structuring. The polymer line distance was set to $0.5 \mu m$, guaranteeing an overlap of the lines and a resulting fully solid structure. The Z-distance was set to $1 \mu m$. The speed was set to constant 15 mm/s, whereas the power was varied from 100-240 mW. The array of hydrogel CAD parts can be seen in Figure 65b.

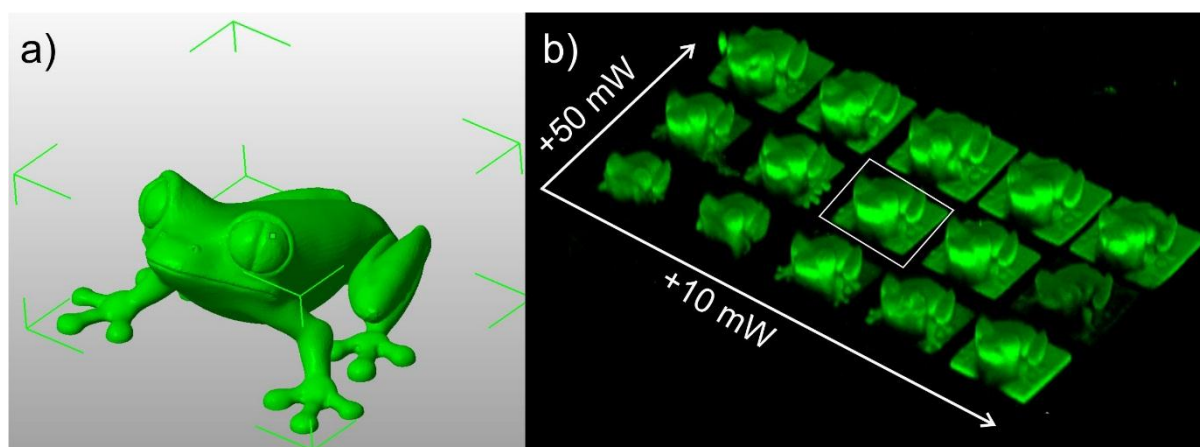


Figure 65 Fabrication of a CAD frog in a 1:1 PEGda: DI water hydrogel formulation containing 2 wt% of G_2CK using a 20x NA 0.8 objective, a) CAD, b) fabricated array at 15 mm/s at different laser powers (100-240 mW), stacked 3D LSM image [166]

For fabricating lattices, the lower polymer threshold of this formulation was not reached at 100 mW and 15 mm/s. For the fabricating the CAD, however, we obtained polymeric parts at these process parameters (Figure 65b first structure from the bottom left). This is attributed to the low polymer line distance. The voxel overlapped during the fabrication process, which still rendered sufficient energy for polymerisation.

In this picture, we also see the broad processing window of G_2CK . We get well-defined structures over the complete applied power range (100-240 mW). However, the cross-linking density gets higher (brighter images due to increased auto-fluorescence) and the parts' dimensions increase with increased laser power. The highlighted structure in Figure 65b is shown in detail in Figure 66. We scanned the cross-sections of the part until the plane of its polymeric base. Thus, it cannot be seen in this picture, whereas it is obvious in Figure 65b. For better resolution, we scanned this part three times and computed the average auto-fluorescence with the LSM software.

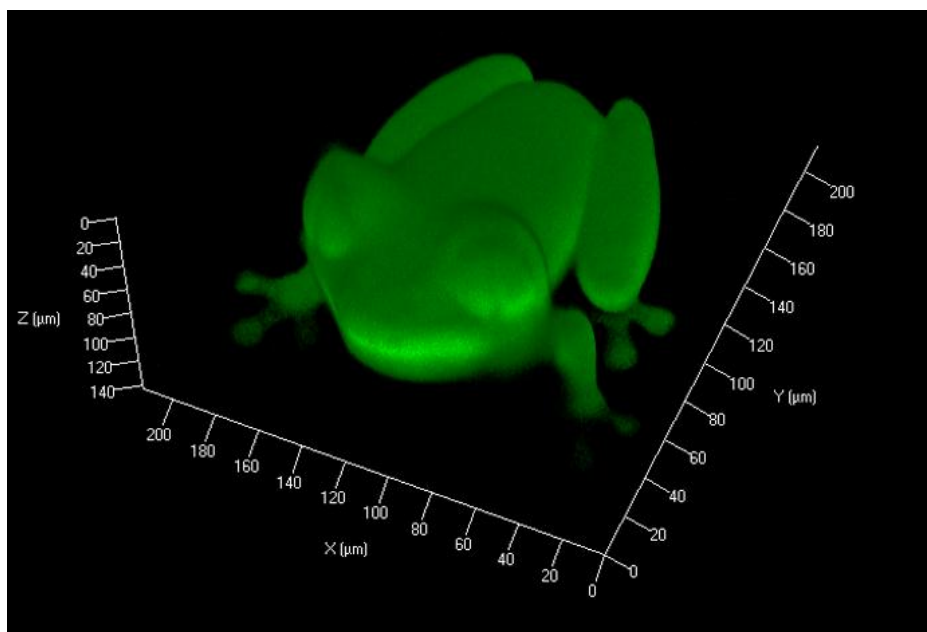


Figure 66 CAD part structured in PEGda based hydrogel formulation, 180 mW, 15 mm/s, 20x NA 0.8 objective, stacked 3D LSM image [50]

In this section, novel optimised 2PP initiators enabled us to fabricate at fabrication speeds of 150 mm/s, the highest speeds reported in 2PP. Modifying these PIs to water-soluble analogues facilitated the processing of formulations with 50% water content. Similarly to the organo-soluble derivatives, these compounds enabled fabrication speeds of over 100 mm/s in a water based formulation. The reactivity is indeed comparable to organic based formulations [116].

12.3 Synthetic Precursor Screening

In the last section, we discussed the efficient initiation of organo-soluble and water-soluble monomers. We exclusively focused on acrylates, attached either to a hydrophobic trimethylolpropane or to a hydrophilic polyethylene glycol. We compared different initiators regarding their reactivity for cross-linking these two precursors but we did not yet characterise the resulting polymer. Moreover, we did not search for alternatives to acrylates. As described in section 8.4.1 and 9.2.1.1, acrylates show a tendency towards Michael addition to polymers and are thus not recommended for biomedical applications.

A major contribution of this thesis was the first application of an optimised 2PP PI for cross-linking aqueous formulations, we will stick to acrylates in the first section of this chapter. We will see how far we can augment the water content inside the formulation while still being able to produce high quality structures at high writing speed. Second, we will search for alternatives to acrylates. The commercially available methacrylates will be the topic of our first investigation. Then we will proceed with vinyl esters and vinyl carbonates, biocompatible monomers suitable for UV polymerisation (see section 9.2.1.2). Finally, we will process protein precursors modified with these biocompatible monomers and show their potential for *in situ* cross-linking in the presence of living cells and tissues.

12.3.1 Polyethylene glycol diacrylate (PEGda)

12.3.1.1 Dimension deviations of manufactured structures compared to the CAD

We initially applied the 2PP PI WSPI for cross-linking PEG-700-da (see section 9.1.2). Four formulations with varying PEGda concentrations were prepared (50, 40, 30, and 20 wt%, respectively). All formulations contained 2 wt% of WSPI. The solvent M9¹⁵ was an aqueous buffer media used to maintain nematodes of the species *Caenorhabditis elegans*. This buffer media did not significantly affect the polymerisation process. Structuring was possible at the same performance as with deionized water. However, the buffer media was important to exclude any solvent-based influences on the biological tissue under investigation. It was thus required for toxicity analysis and polymerisation in the presence of living organisms, which will be part of section 0. For the structuring tests, we left the conditions equal as for *in vivo* polymerisation.

The experiments conducted and results of this section have recently been published in the Journal of Biomedical Optics [49]. This sub-chapter will be an excerpt of this publication.

To measure the influence of the water content in the formulation on the dimensions of the obtained parts, we fabricated $15 \times 140 \times 21 \mu\text{m}^3$ rod-like structures (Figure 67) into the four formulations. For this experiment, we used the M3DL setup (see section 10.1) and the 20x NA 0.4 objective (section 10.3). The focus was traced in the Y-direction only leaving polymer lines parallel to the Y-axis. Nineteen polymeric lines at a distance of $0.8 \mu\text{m}$ to each other (Figure 67 distance a) were structured. As the diameter of one polymer line was thicker, this resulted in an overlap of the exposed volume and in a fully dense polymeric structure. The distance between the six polymer layers was set to $3.5 \mu\text{m}$ (Figure 67 distance b). The writing speed was set to 10 mm/s and the laser powers ranged from 140 mW to 260 mW at an increment of 20 mW. Six elements were structured in each of the four formulations.

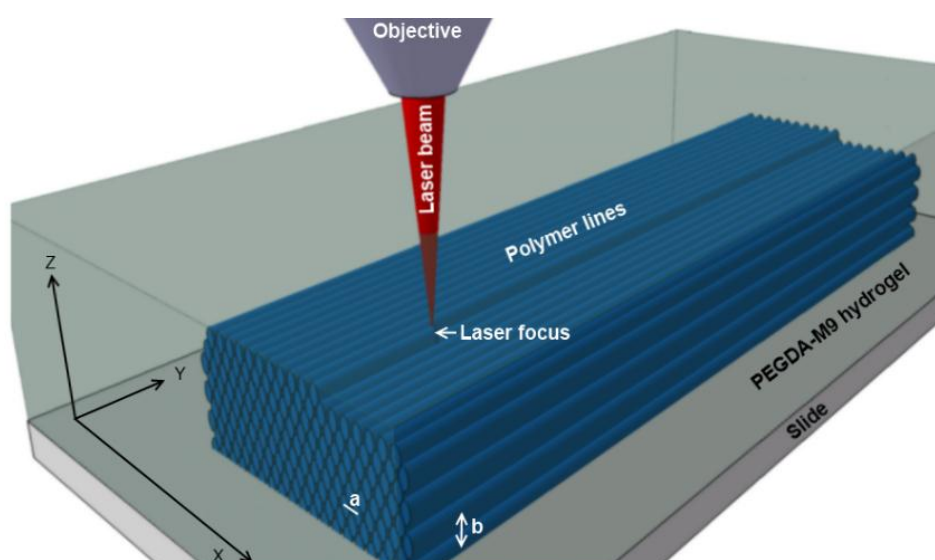


Figure 67 Fabrication of rod-like structures ($15 \times 140 \times 21 \mu\text{m}^3$ X/Y/Z), layer distance $3.5 \mu\text{m}$ (labelled b), layer distance $0.8 \mu\text{m}$ (labelled a), 20x NA 0.4 objective [49]

¹⁵ M9 buffer is a standard media for maintaining *C. elegans*. It contains 3 g KH_2PO_4 , 6 g Na_2HPO_4 , 5 g NaCl, 1 ml 1M MgSO_4 and H_2O to 1 litre [188].

After fabrication, the structures were rinsed with M9 buffer to get rid of monomer residues. Then, they were allowed to swell in the buffer media for 24 hours, to finally reach equilibrium absorption [123]. Every rod structures were observed via LSM individually using a 50x NA 0.8 objective and a cw laser of 488 nm wavelength. The LSM images were joined together to finally show the influence of laser power and water content in Figure 68 [49].

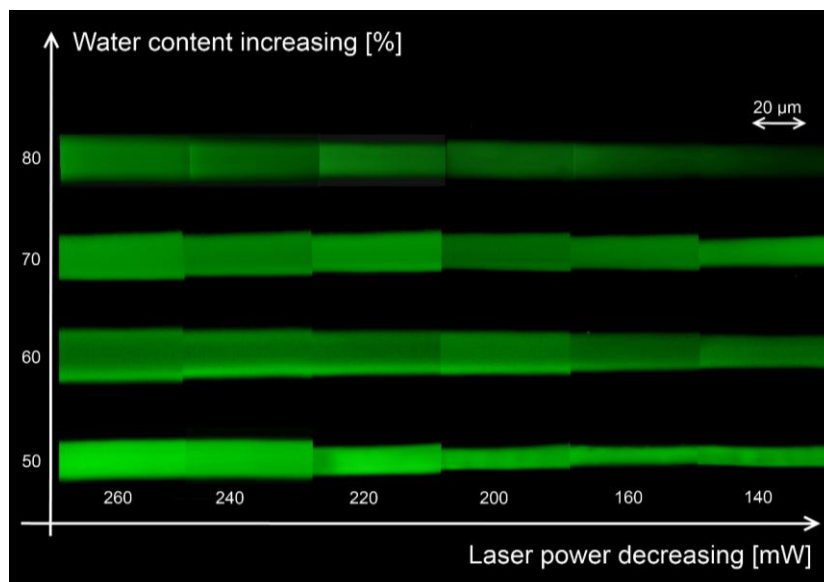


Figure 68 Rods structured using different water contents and average laser powers, LSM images, 50x [49]

The four different formulations are plotted in the Y-plane indicating the impact of the water content. No stable structures could be obtained in formulations with 90% water content. The X-plane shows structures manufactured in the same formulation but at different laser powers. This plane thus shows the impact of the laser power on the rod width. The power was measured before the 20x NA 0.4 objective. The actual power in the focal point is thus 60% less (see efficiency of the 20x NA 0.4 objective in section 10.3).

As the initiator content and the LSM measuring parameters were kept constant in this experiment, we can attribute the fluorescence of structures to the varying monomer contents and laser powers. We thus take the brightness of the structure as an indicator for a difference in the density of the polymer network resulting from the two parameters varied in this experiment.

Qualitatively, an increase in width is obvious with an increase of the intensity applied, which is most striking in the 50% formulation. This is in good agreement with previous work [38] and can be explained with the increase of the 2PA affected zone of the voxel with increasing laser intensity. The larger the voxel, the thicker the polymer lines and the larger the dimensions of the fabricated 3D construct [49].

The deviation changes with increasing water content are not so clear at the first glance. They seem to follow a different, more complicated nonlinear trend. To assess these differences, we further quantitatively investigated the rod widths. For this task, we calculated the width of a polymer line using the LSM fluorescence distribution over the distance of the scanned plane as depicted in Figure 69.

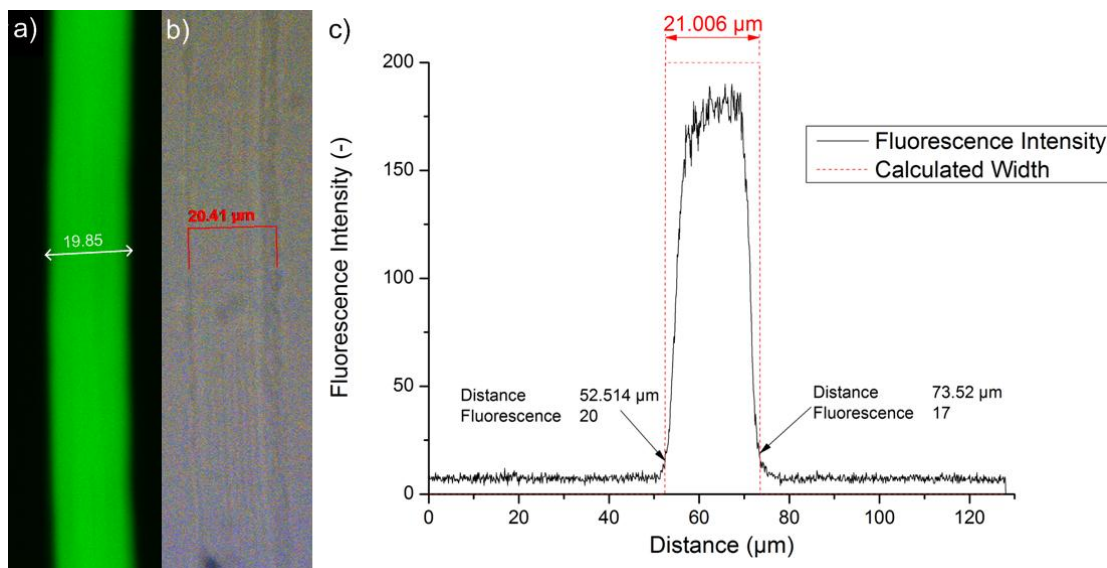


Figure 69 Comparison on rod width measurements, CAD rod structure according to Figure 67, 240 mW, 50% water a) LSM 50x b) LM 50x c) Calculated view over the intensity distribution [49]

The LSM measurements (a) appear thinner than those done with LM (b). The depth of field in the LSM scan is good showing precisely the width of the investigated layer. Layers of other planes could be wider but not quite evident in the image. In contrast, the depth of field in the LM image is weak, showing nearly all layers of the fabricated part. However, the image is blurred making it hard to define the actual interface between the cured hydrogel structure and the surrounding buffer media. This is particularly evident structuring with lower laser power in formulations with higher water content [49].

With lower laser power and higher water content, the cross-linking density gets weaker, making it hard to differentiate the surrounding from the polymer. Therefore, an exact measurement of the width is not possible.

The fluorescence distribution in contrast shows the LSM images in a quantifiable manner. We defined the distance of the scanned plane where 10% of the maximum intensity is observed as the threshold that separates the fluorescence noise from the beginning of the polymeric structure. Similarly, the end of the polymeric structure is defined as the distance where the fluorescence falls below this threshold. Following this principle, the experimental data was evaluated in an automated procedure to exclude any subjective influences [49].

An excel macro automatically created the diagrams shown in Figure 70. Each one of these figures displays the widths of the rods (X-plane) structured at different laser powers (coloured graphs) in terms of their observed fluorescence in the LSM (Y-plane). The difference in the observed fluorescence of the four figures, in contrast, is attributed to the different water content of the four formulations under investigation.

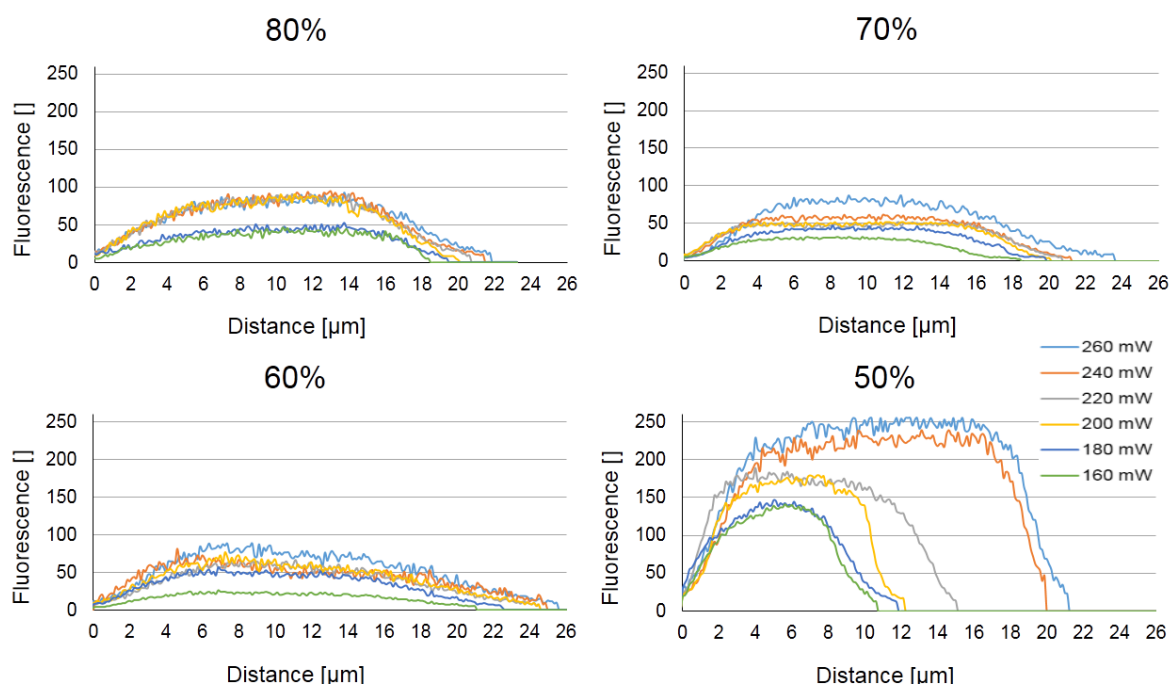


Figure 70 LSM intensity distributions over distance of the scanned plane; each one of the diagrams shows the impact of the laser power on the rod widths of one PEGda/water formulation containing 2 wt% WSPI, the fluorescence is measured in LSM specific dimensionless units

At 50% water content, the observed fluorescence is more than twice as high as in the other formulations (see also Figure 68). In addition, the change in the fluorescence with increasing laser power is only obvious regarding the structures produced in 50% water. The fluorescence changes with both, power and water content are not obvious regarding the structured rods' fluorescence of the other formulations.

The difference between the single graphs' right and left point of intersection with the X-axis constitute the width of one rod. Regarding the rod widths, the impact of the laser power is also most obvious in the formulation containing 50% water. The width of the widest rod, produced with 260 mW of power is ~22 μm; the smallest obtained at 160 mW is only slightly above 11 μm wide. This shows that a decrease in the laser power by 100 mW can result in a width decline of over 100% processing this formulation. There are only minor differences in the width of the rods produced using the formulations with higher water contents. The observed deviations are within 2-3 μm. However, the structures seem to be much wider.

Figure 71 summarises the charts in Figure 70 addressing only the width impact of the laser power and the water content. It specifies the width deviations from the intended 15 μm set in the CAD.

The largest width deviation can be seen in formulations with 60% water content (+70% width increase at 260 mW). Rods fabricated in formulation with 70% and 80% water content show a minor dimension deviation. Formulations with 50% water content, however, facilitate the fabrication of parts with the best agreement to the CAD model (best fit at 220 mW) [49].

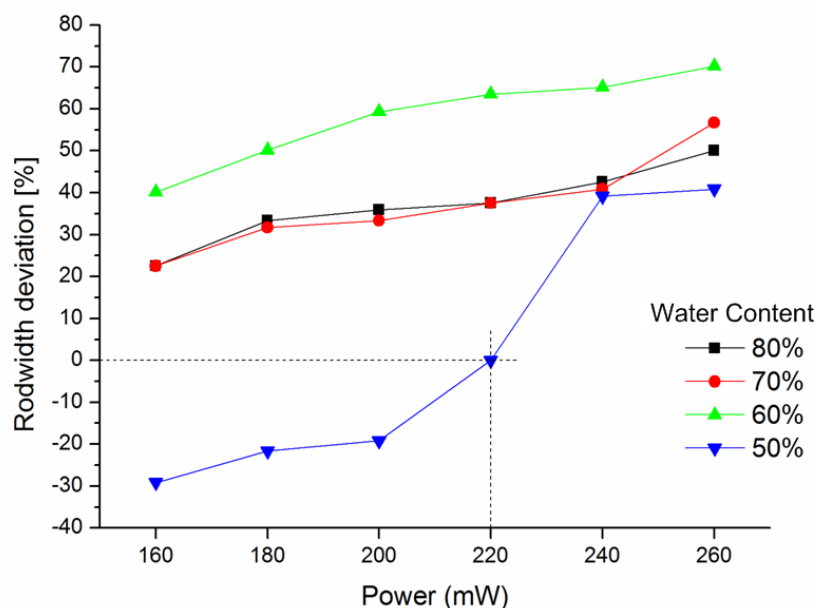


Figure 71 Rod width deviations plotted against laser power in PEGda formulations with different water contents, 2 wt% WSPI [49]

The different dimensions obtained in formulations with different water contents are best explained with the polymeric cross-linking density of the fabricated parts. A high monomer content of 50% renders a stiff network, which absorbs little water. The auto-fluorescence of the observed parts is higher in the LSM (Figure 68 and Figure 70). Defined structures with single polymer lines are visible. The polymer network is stiff; its low elasticity limits the absorption of water.

At 60% water content, the polymer's cross-linking density is still high but the network is more permeable. The restoring force of the polymer's elasticity against water absorption, equilibrium absorption is shifted towards higher water contents. However, formulations with even higher water content (70% and 80%) should render the polymer network even more permeable. Yet, structures fabricated seem to be narrower. This potentially happened as a result of the oligomerisation of the constructs' outer contour polymer lines. The oligomerised monomers can diffuse in the surrounding making the polymer lines thinner reducing the swelling effect.

To conclude, the effects of monomer concentration and laser power are complex and cannot be said to be fully inverted.

The object's deviations from the CAD model due to swelling and shrinking can limit the resolution advantage of 2PP. However, knowing precisely the objects' dimension deviations when processing a specific formulation, one can compensate the CAD model accordingly.

Using commercially available 1PP PIs, the compound PEGda alone was already successfully cross-linked via 2PP at higher energy doses and lower processing speeds without water content in the formulation [121,123]. Here we showed 2PP fabrication of CAD structures at only low laser power and in formulations with only 20% water content. This shows the high efficiency of WSPI showing high efficiency for cross-linking PEGda.

Due to mechanical limitations of the M3DL setup, the maximum writing speed was 10 mm/s. However, the materials presented are likely to be processable at higher writing speeds [49].

In this section, we simply assessed the appearance of the fabricated polymer. We thus decided to manufacture simple structures without overhanging features. For the scope of fabricating

biocompatible parts that provide an adequate surrounding for cells, the question now arises whether we can manufacture complex scaffolds with these formulations.

12.3.1.2 3D structuring

We investigated the differences in the photoreactivity and in the 3D capabilities of two of the aqueous formulations. To get an impression of the changes in the obtainable process window, we chose the lowest (50%) and the highest (80%) water content for our experiment. We designed a porous $280 \times 280 \times 225 \mu\text{m}^3$ large CAD depicted in Figure 72a. This scaffold is a small version of an already successful 2PP scaffold for tissue engineering [149]. We thus considered fabricating according to this design as appropriate for investigating the feasibility of the presented formulations for manufacturing biologically relevant topographies.

As the maximum height of the CAD exceeded the building volume, we had to replace the adhesive strip spacers of the specimen (see section 11.1) with a silicon mask (Sigma-Aldrich) giving us a building volume of $\varnothing 6 \times 1 \text{ mm}^3$ (see Figure 72b). First, we laid the mask in ethanol for $\frac{1}{2}$ hour. Then we put the spacer on the slide and let the ethanol evaporate. This ensured good adherence of the mask to the slide. Afterwards, we pipetted the formulation into the building volume, i.e. the round clearance of the mask. In addition, we put a small drop of liquid on one side of a coverslip. We then carefully placed the coverslip on the silicon mask avoiding the inclusions of air into the building volume. We removed the excess formulation with paper tissues. The specimen was then ready for processing.

The M3DL software did not allow producing an array of CAD structures varying in their writing speed and laser powers. Furthermore, inertia problems limited the processability of the formulations at higher writing speeds. We decided to use the Mipro setup for the experiments described in this section.

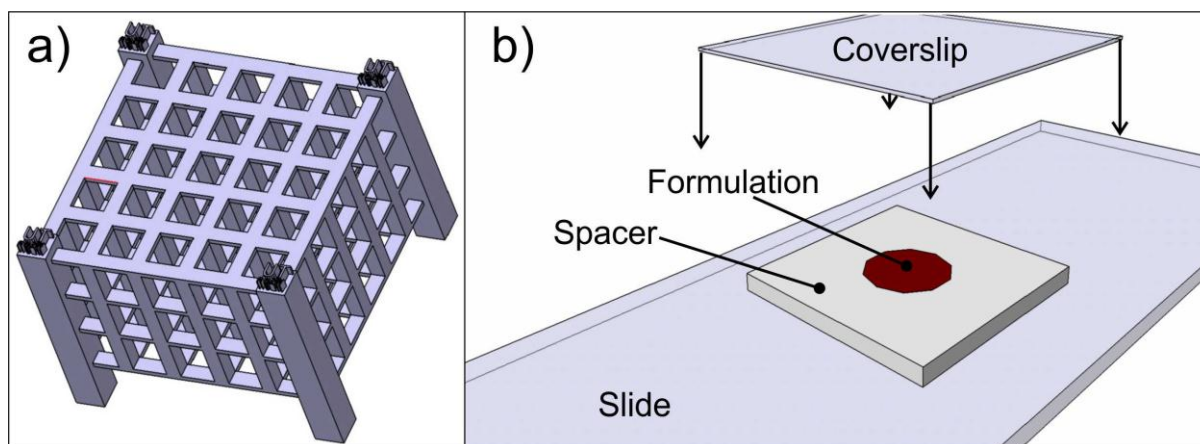


Figure 72 a) CAD scaffold $280 \times 280 \times 225 \mu\text{m}^3$, b) sample preparation for $\varnothing 6 \times 1 \text{ mm}^3$ building volume

To compare the results to those of the previous section, we again applied the 20x NA 0.4 objective for structuring. The polymer line and layer distances, too, were set to the $0.8 \mu\text{m}$ and $3.5 \mu\text{m}$ reported earlier. As for fabricating the rods (see Figure 67), we chose a fabrication strategy, where we traced the focal point only in the Y-axis. Bars of the scaffold extending in the X-direction were thus fabricated of transversely oriented small polymeric lines that were placed next to each other. In total, 21 3D CAD scaffolds were structured at different laser energy doses in the two formulations containing the lowest (50%) and the highest (80%) water

contents, respectively. We altered the laser power (60-300 mW by steps of 40 mW) and the fabrication speed (1-10 mm/s by steps of 3 mm/s).

As stated in the PI screening sections 12.1 and 12.2, we considered the lower threshold as the power value at which we primarily observed polymerisation at a given fabrication speed [116] as well as an appropriate structuring window [133] could be found.

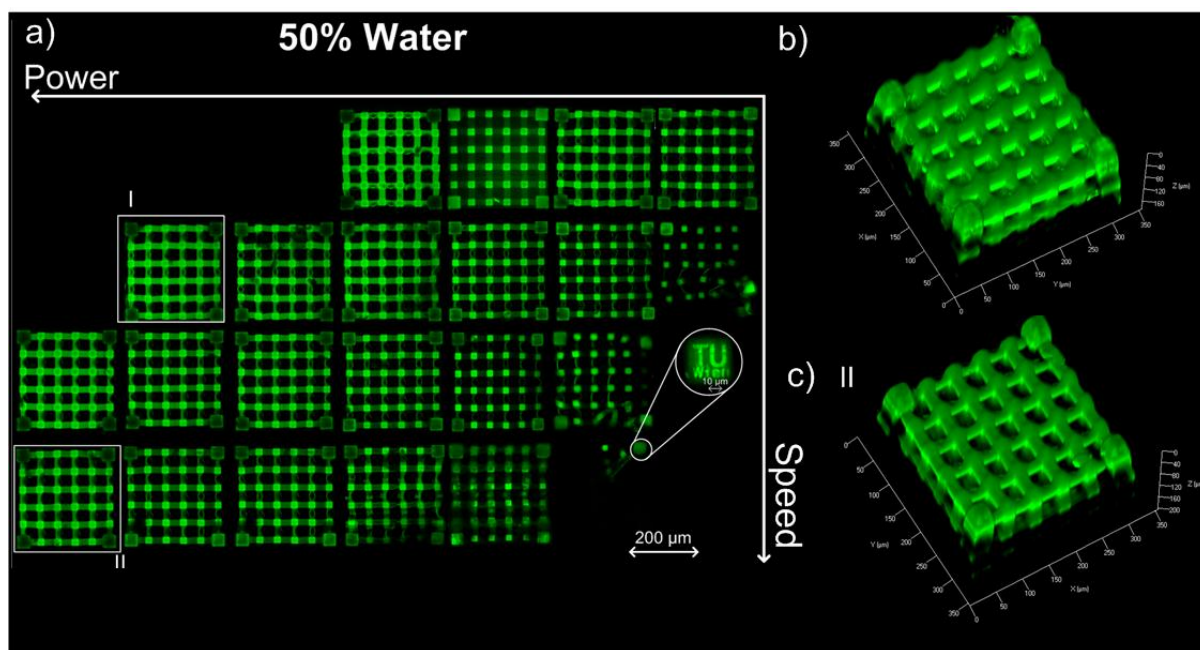


Figure 73 a) Speed power array of fabricated scaffolds in a PEGda formulation containing 50% water; horizontal left to right: 300-60 mW by steps of 40 mW, vertical top down: 1-10 mm/s by steps of 3 mm/s, LSM images 20x b) stacked 3D LSM image of white marked scaffold in a) [49]

Figure 73a illustrated that stable structures were obtained at 60 mW at 1 mm/s, 100 mW at 4 mm/s, 140 mW at 7 mm/s and 220 mW at 10 mm/s, respectively. Below these thresholds, polymerisation was still possible, though the polymeric network was not stiff enough to keep the fabricated part in the preformed shape. At 60 mW and fabrication speeds above 7 mm/s, no polymerisation was obtained. Above 260 mW at 1 mm/s, the energy dose was too high resulting in damage to the structures and their loss of adhesion to the glass slide. Similarly, the energy dose was too high at 300 mW at 4 mm/s.

At low energy doses, only the pillows remained attached to the glass (e.g. at 100 mW, 10 mm/s). The fabricated logos with details in the μm region on the pillows (see detail in Figure 73a), were pronounced in nearly all scaffolds. Yet the freely suspended parts of the structure were not stable enough and therefore deformed and lost their adhesion to the pillows under their own weight.

Some of the connectors appear wavy and thin most distant from the pillows. As every layer of a structure was created line-by-line, the connector was growing in thickness during the fabrication process. Commencing the fabrication, it consisted of one single line and of 50 lines in the end (connector thickness 15 μm divided by line distance 0.3 μm). Thus, the connector is weak at the beginning getting its full strength in the end. This can result in a deformation of single lines during the fabrication process. At higher energy doses, however, the deviation is less [49].

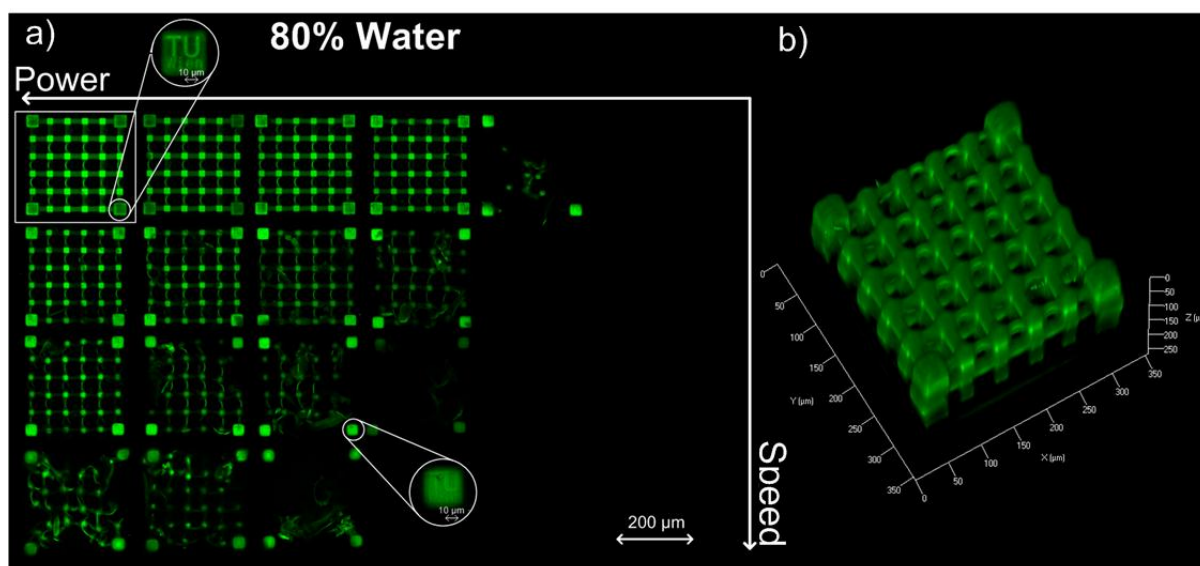


Figure 74 a) Speed power array of fabricated scaffolds in a PEGda formulation containing 80% water; horizontal left to right: 300-100 mW by steps of 40 mW, vertical top down: 1-10 mm/s by steps of 3 mm/s, LSM images 20x b) stacked 3D LSM image of white marked [49]

Figure 74 illustrates the fabrication of scaffolds in formulations containing 80% water. The process window was shifted. Stable structures were obtained above 180 mW at 1 mm/s, 220 mW at 4 mm/s and 300 mW at 7 mm/s, respectively. At 10 mm/s polymerisation was still possible. However, the freely suspended parts are not stiff enough and deform similar to processing formulations with higher monomer content at low energy doses. Here, the deformation of the connectors is more obvious. As described previously, the connectors grow during the fabrication process. Processing formulation with higher water content, the single polymer lines are even weaker and thus the deformation is larger. The longer the fabrication process, the more time available for the construct's deformation. At higher speed and higher power, the structures would thus fit the CAD better. The structure fabricated at 1 mm/s and 300 mW is stable (see 3D stacked LSM image in Figure 74b). No damage resulting from the laser power was recognisable. Thus, the fabrication of scaffolds at higher writing speed is likely possible at higher laser power than 300 mW [49].

Concluding this section, we showed that fabricating complex CAD scaffolds with topographies suitable for biological applications is possible with all of the presented formulations. The objects were fabricated at average laser powers as low as 140 mW at up to 80% water content and at speeds of 10 mm/s.

The performance of the presented formulations is comparable to standard organic-based formulations, where appropriate 3D structures were built at 50 mW and 0.8 mm/s [116] (The experiment was done using the same 20x NA 0.4 objective). The experiments revealed a competitive threshold of 60 mW at 1 mm/s for 3D fabrication in a formulation containing 50% water [49].

However, as we know from section 9.2, the cytocompatibility of acrylates is still in doubt. They are good Michael acceptors which makes them potentially cytotoxic or even carcinogenic [50,169]. Especially for the scope of polymerising *in situ*, living tissue and cells would be exposed to unpolymerised acrylate groups, which would form cytotoxic acrylic acid as degradation product. Although the PEGda formulations presented in this section allow very high water contents in the formulation and perform extremely well in 3D structuring, we have to find more biocompatible precursors.

12.3.2 Polyethylene glycol dimethacrylate (PEGdma)

Methacrylates (MA) are generally less reactive than their acrylate (AC) references. The additional methyl in a MAs increases steric hindrance effects. As a result, the necessary activation energy for breaking the double bonds of ACs is lower. The emerging radicals are more stable and the kinetic and thermal energy during polymerisation is higher, which makes it to proceed much faster. However, MA do not show the AC's tendency towards Michael addition to peptides and are thus less toxic for cells and biological tissue [167].

We conducted preliminary experiments structuring the MA monomers attached to a water-soluble PEG backbone. The molecular masses of the investigated precursors were 600, 700, 800 and 1000 (see section 9.2.1.1 for the chemical structure of PEGdma). We used the M3DL and the 20x NA 0.8 objective for structuring. Similar as in section 9.1, we structured 50x50x40 μm^3 lattices at different laser power and writing speed. Results of the structuring tests are depicted in Figure 75.

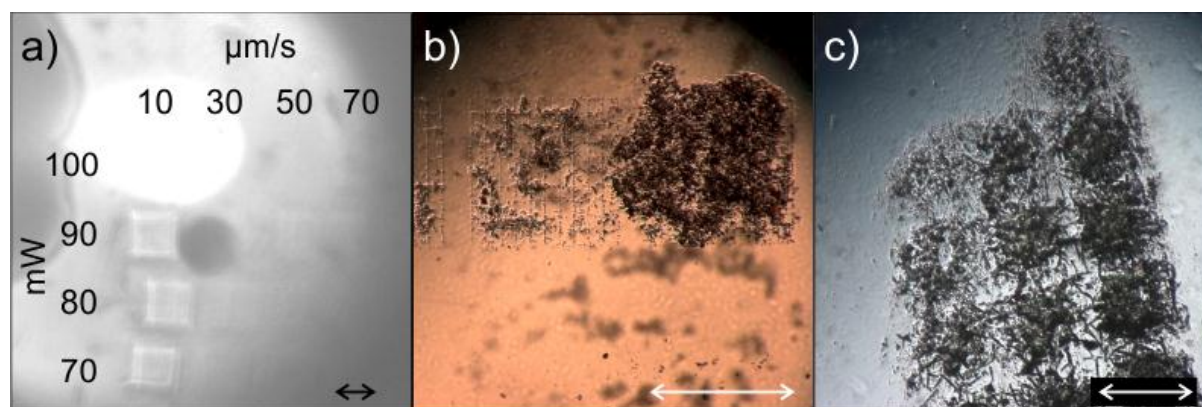


Figure 75 a) PEG-1000-dma, 0.2wt% R1, online process observation b) PEG-800-dma, 0.2 wt% B₃FL, LM image 10x c) PEG-800-dma, 0.2 wt% R1, LM image 5x, scale bars 50 μm

Figure 75a shows an online picture of a structuring attempt with a formulation containing PEG-1000-dma and 0.2 wt% R1. This formulation had to be heated up to 60°C before it could be processed. At room temperature, this formulation rapidly changed its state to solid. Distinct structures could only be obtained at very low writing speed (10 $\mu\text{m}/\text{s}$). Power did not have a strong impact on the processing window. At 70, 80, 90 and 100 mW of power, structuring was possible. Higher processing speeds, however, could not be accessed at any of the power values applied. To get rid of the monomer residue, this sample had to be heated up to 60°C again. In neither of our attempts, the structures withstood this procedure.

Figure 75b shows a LM image of a structuring attempt using PEG-800-dma and 0.2 wt% of the initiator B₃FL. Indeed, this formulation stayed liquid at room temperature, but it was not processable. The power was either too low for polymerisation or too high, which caused damage to the polymer network. Changing the initiator to R1 did not prove any better. The outcome is depicted in Figure 75c.

To increase the reactivity, we decreased the Mw of the PEG backbone to 600. Further, we added 10 wt% of Glycerol-dimethacrylate as comonomer and increased the initiator content to 0.5 wt% R1. 0.1 wt% of the stabiliser Pyrogallol¹⁶ had to be added to avoid PIs precipitation.

¹⁶ Pyrogallol is a derivative of benzol, a trivalent phenol with three vicinal hydroxygroups. In this case, it is used as a stabiliser to prohibit oxidation of thiols with aerial oxygen.

However, this strategy did not bring the desired success. Other than expected, we could not observe any polymerisation at any speed or power.

These discouraging results give evidence that PEGdma alone is not processable, even when applying very efficient 2PP PIs for cross-linking. However, there is evidence that polymerisation occurs processing some of the presented formulations. It is now important to know whether at all, MAs are processable.

12.3.3 Formulation three

Formulation three is a hydrophobic viscous liquid consisting of a 1:1:1 ratio between bisphenol A-diglycerolate dimethacrylate, diurethane dimethacrylate and 1,10-decanediol dimethacrylate known for its applicability in restorative dentistry. The chemical structure of the formulation's components is described in section 9.2.1.1. We added 0.5 wt% of R1 to the formulation. For 2PP processing, we used the M3DL setup and the 20x NA 0.8 objective. We structured a slightly different array to the one described in section 11.2.

The structuring results differed from those of ETA-TTA (section 8.4.1 and 9.1.1). The lateral and the axial dimensions of the obtained polymer line were much larger in formulation three. Hence, we first searched for appropriate design parameters for the lattices for a given writing speed and power rather than investigating the process window. The size of the lattices was initially set to $100 \times 100 \times 30 \mu\text{m}^3$, leaving all other parameters of the lattice equal. Setting the writing speed to constant $300 \mu\text{m/s}$ and the power to 30 mW, we increased the layer distance in X and the line distance in Y. Five elements in the X- and eight in the Y-plane were manufactured at a distance of $50 \mu\text{m}$ to each other, respectively. The height of the structures produced changed from 20 to $68 \mu\text{m}$ in X, the distance between the polymer lines ranged from 5 to $3.3 \mu\text{m}$ in Y. After structuring, we developed the sample in ethanol and investigated the lattices in the SEM. The array is displayed in Figure 76.

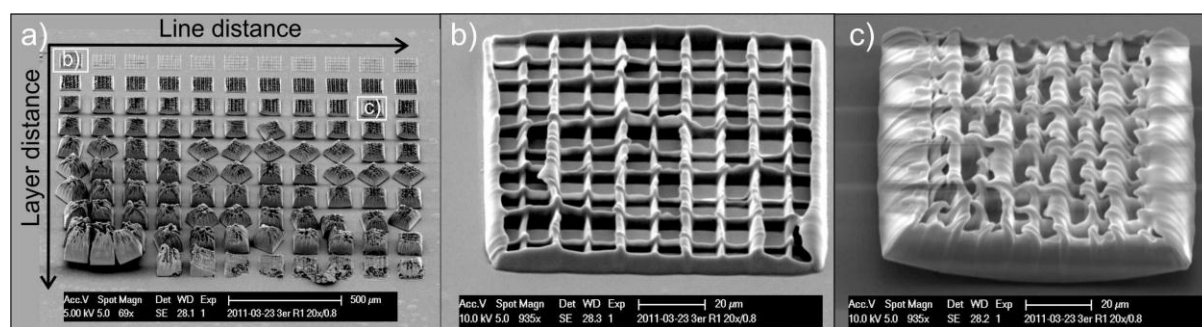


Figure 76 structuring of formulation 3; a) overview of lattice array, layer distance range 1-1.6 μm , line distance changes from 3.3 to $5 \mu\text{m}$, b) layer distance $1 \mu\text{m}$, line distance $5 \mu\text{m}$, c) layer distance $1.5 \mu\text{m}$, line distance $3.3 \mu\text{m}$, 30 mW, $300 \mu\text{m/s}$, 20x NA 0.8 objective

The first lattice produced with $5 \mu\text{m}$ line and $1 \mu\text{m}$ layer distance is shown in Figure 76 b). The element seems well defined. The lines are equidistantly arranged. However, the structure has slight distortions from its intended design. Especially on the top of this lattice, some of the polymer lines seem bent. This effect becomes stronger going from the centre to either of the outer walls of the structure. In addition, the structure appears wider on the bottom, where it was attached to the glass. Hence, the outer walls bend towards the centre of the structure. This characteristic is an indication for a strong shrinkage of the polymer during development. When we look at structure c), this gets even more obvious. The lattice's height increases with

the layer distance. The upper layers are now more distant from the glass and thus, the polymer's support is weaker and it is more exposed to shrinkage. This even leads to the structure's detachment from the glass starting from the outer walls towards the centre. Further increasing the structure's height leads to a complete detachment from the glass as obvious on Figure 76a looking towards the bottom of the array. This is indeed the case with acrylates, too (see section 12.1), but the observed shrinkage of structures produced with formulation 3 by far exceeds that obtained in ETA-TTA.

We can therefore say that processing formulation 3 is generally possible but special modifications to the formulation are required. However, we could not find a processable MA based water-based formulation. From previous experiments we know that Vinyl Esters (VE) show better cytocompatibility than MA and are also more reactive in UV polymerisation [167,169]. Perhaps we can find a VE based formulation with a higher performance than the MA based ones. Potentially, a functionalization of VE with PEG will render a water-soluble low toxic but sufficiently reactive formulation.

12.3.4 Hexandioic acid divinyl ester (4VE)

We prepared a hydrophobic formulation containing 71.5% 4VE and 28.5% Dithiolthreitol (DTT) for increasing the formulation's reactivity. 0.4 wt% of R1 and 0.1 wt% of the stabilizer Pyrogollol was added for 2PP processing. One lattice (300x100x20 μm^3) with a line distance of 5 μm and a layer distance of 3.5 μm was fabricated at a writing speed of 10 $\mu\text{m/s}$ and a power of 100 mW. We used the old M3DL and the 20x Na 0.4 objective for structuring. An online picture shot during the structuring process is depicted in Figure 77a; the structure after the development can be seen in the LM in Figure 77b.

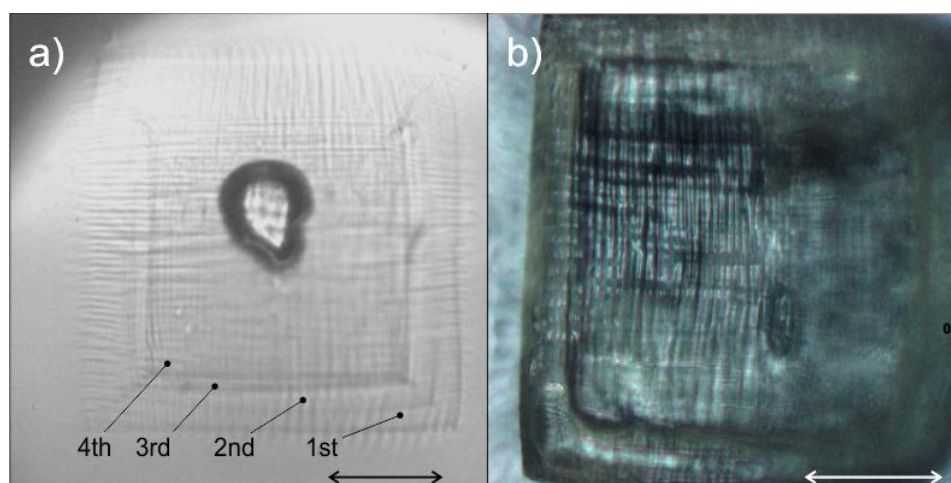


Figure 77 a) Shrinkage of layers during fabrication, online process observation, b) lattice after development, LM 20x, scale bars 30 μm

Here the polymer shrinks already during the fabrication process. Layers that are more distant from the glass (4th layer) are substantially narrower than the layers underneath. The shrinkage is especially obvious between the 1st layer sticking on the glass and the 2nd layer that is only bound to the polymer, i.e. the layer underneath. This is also obvious in the LM image of Figure 77b, where one can clearly see the outer walls bent to the centre of the structure.

Changing the molecular mass of the DTT and changing the ratio between DTT and 4VEs did not give any better results. However, the absence of DTT rendered this formulation completely

unprocessable. As expected, this leads us to conclude that the DTT indeed increase the reactivity of the formulation. As stated in section 9.2.2, Vinyl ester limits the efficiency of chain-growth reactions compared to AC. The thiols additionally favour step-growth reactions while still maintaining the ability of the formulation to perform radical-mediated processes [173]. We could not perform structuring tests with these compounds alone, as they were not stable enough. Yet, they are suitable cytocompatible monomers for increasing the reactivity of a VE based formulation.

It was suggested that the shrinkage effect can potentially be reduced attaching the VE groups to a PEG backbone and moreover, at higher molecular weights, this backbone can also render the precursor water-soluble. Thus, we will investigate the processability of different PEG vinylesters (PEGve) in the next section.

12.3.5 Polyethylene glycol vinyl ester (PEGve)

As it proved successful, we again used DTT in combination with hydrophilic PEG-600-VE in a 2:3 ratio. 0.5 wt% of R1 and 0.1 wt% of Pyrogollol was added for structuring. We structured similar lattices as described in the previous section at 120-300 mW by steps of 15 mW and 10-250 $\mu\text{m/s}$ by steps of 40 $\mu\text{m/s}$ using the M3DL setup and the 20x 0.4 objective. All structures were visible online and did not show any shrinkage. However, the structures dissolved in the formulation after a while and were not visible any more. We thus could not develop the structures. The polymer was too weak. Increasing the PI content to 1 wt% and raising the stabilizer content to 0.5 wt% facilitated higher reactivity and more stable structures. The polymer could be developed and investigated in the LM (not shown). However, the initiator was inhomogeniously dissolved which caused explosions and damage to the polymer.

Decreasing the Mw of the PEG backbone to 250 made the precursor insoluble in water. However, it substantially increased its reactivity. We prepared a 2:3 mixture of DTT and PEG-250-VE including 0.5 wt% R1 and 0.1 wt% Pyrogallol. The obtained structures did not show any substantial shrinkage during structuring. However, after the development, the polymer lines deformed and the structures collapsed. The SEM images can be seen in Figure 78.

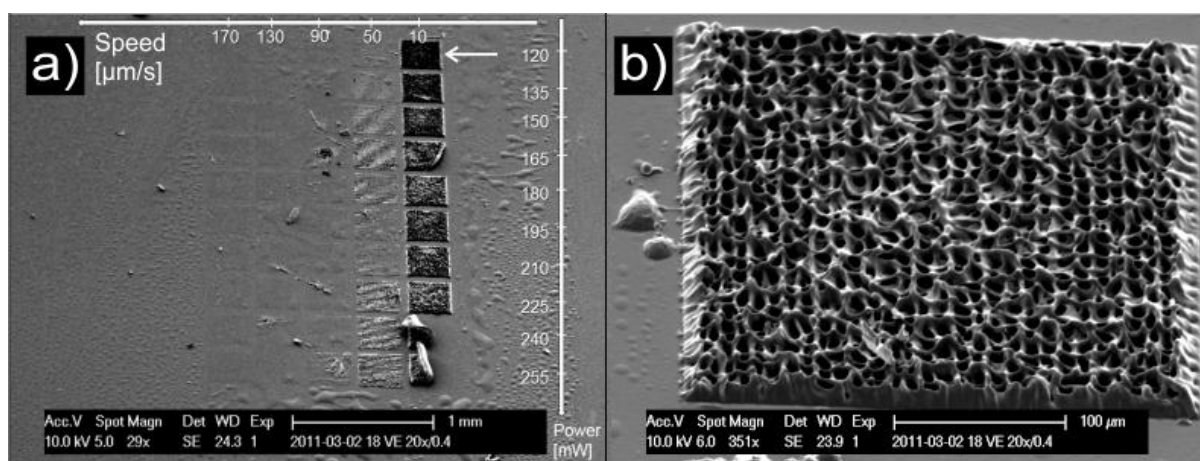


Figure 78 Processing window of 2:3 DTT:PEG-250-VE, 0.5 wt% R1, 0.1 wt% Pyrogollol, 20x NA 0.4 objective, b) structure indicated with white error in a, SEM images

Due to shrinkage, only the contours of the elements produced at speeds higher than 10 $\mu\text{m/s}$ are visible. Increasing the power does not allow for higher writing speeds. The structure produced with 120 mW (labelled with a white arrow) seems in best accordance to the CAD

relative to the other lattices. However, a closer look to Figure 78b, shows that also this lattice collapsed and deformed drastically.

To conclude, 2PP of VE is possible. Although processing 4VE was far from satisfactory, a functionalization of PEG performed substantially better than PEGma, where we could not obtain any developable structure. As VEs do not undergo Michael addition to proteins, they are potential candidates to be covalently bound to native protein-based precursors. These modified natural proteins, described in section 8.4.3 are promising candidates for biocompatible 2PP precursors that can ultimately be applied in the presence of cells and tissues. However, before we continue with VE modified natural proteins in section 12.4, we will first draw our attention to another promising biocompatible polymerisable compound known from stereolithography and digital light processing.

12.3.6 Glycerol Trivinyl Carbonate (GVC)

According to Heller et al. [6,170], the trifunctional cross-linker glycerol trivinyl carbonate (GVC) renders polymer networks with a higher modulus than even TTA. Furthermore, as it is a part of lipids, it is considered cytocompatible. The chemical structure can be seen in section 8.4.1.

For 2PP, we included 1 wt% of B₃FL. As the formulation was provided for an initial proof-of-concept. Hence, we did not process a full speed-power array. Online, presumably suitable processing parameters of 75 mW of power and 100 μ m/s of speed were found. As in the previous section, the size of the structure was 300x300x20 μ m. This time, we used the 20x NA 0.8 objective and a layer distance of 5 μ m. The polymer line distance was again set to 5 μ m. Phase contrast LM images of two elements are depicted in Figure 79.

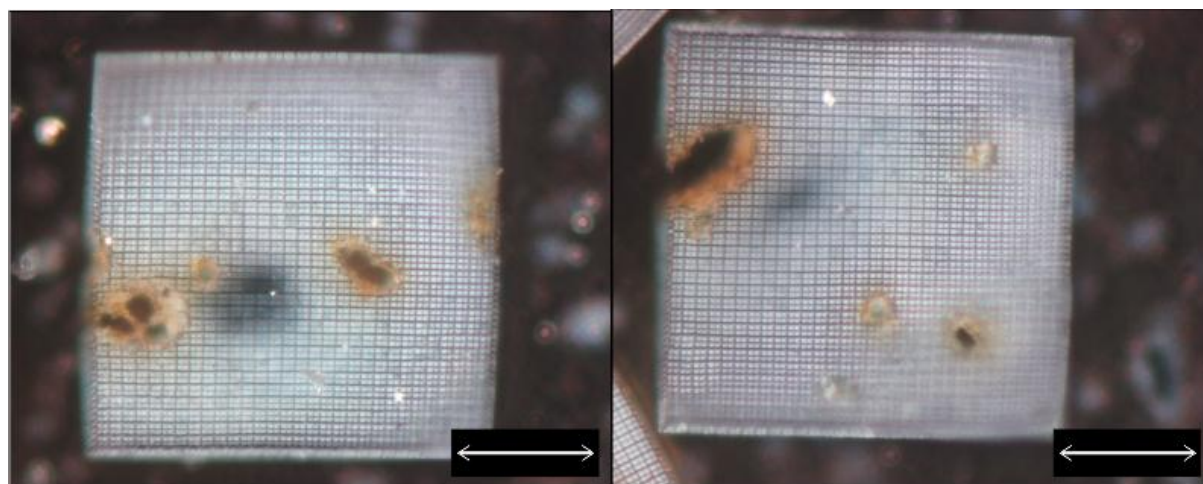


Figure 79 Lattices structured using GVC, 1 wt% B₃FL, 20x NA 0.8 objective, Phase contrast LM, scale bars 100 μ m

Though the process parameters were just rough estimations, we obtained well-defined structures, similar to those obtainable with ETA-TTA. The holes in the lattices are a result of poorly dissolved initiator inside the formulation. Reducing the initiator content and/or changing the initiator will expectedly improve the quality.

From the perspective of structuring, GVC is very promising. Yet, favouring VEs, GVC will not be in the focus of this thesis anymore. However, if this compound is indeed cytocompatible as

described [6] and if its synthesis is easier than that of VEs [170], I would strongly recommend its use as future cross-linking unit in synthetic or modified naturally precursors.

12.4 Modified Natural Precursor Screening

In section 8.4.2, we presented results on cross-linking unmodified natural proteins using water-soluble xanthene dyes. We heard that the first successful two-photon cross-linking of Bovine Serum Albumin (BSA) goes back to the early year 2000 [128], long before synthetic monomers were processed [115]. As any synthetic modification certainly influence the biocompatibility of natural precursors, it should be clarified, which benefits these modified precursors provide compared to their natural derivatives. In this respect, let us assess the different photochemical reactions that can cross-link natural proteins.

12.4.1 Assessment of photochemical reactions in protein cross-linking

Generally, unmodified natural proteins can be cross-linked via two types of reactions:

- In denaturation, proteins or nucleic acids precipitate as they lose their structure present in the native state. External stresses as pH changes, presence of inorganic salts, organic solvents or heat are the cause of such processes [189].
- Protein cross-linking is distinct from a denaturation process. Upon activation of available xanthene dyes, the protein itself acts as co-initiator and cross-linker at the same time. Two radicals are required to make one cross-link.

If we apply too high laser powers, most of the energy is converted to heat and the protein denatures. For this, no initiator is required. Using the 20x NA 0.8 objective, we structured simple lattices with $50 \times 50 \times 20 \mu\text{m}^3$ at $1 \mu\text{m}$ layer distance and $0.5 \mu\text{m}$ polymer line distance in a BSA formulation containing 75% PBS buffer¹⁷. We applied a laser power of 200 mW and a writing speed of 1 mm/s. In the online process observation (

Figure 80 Cross-linking of aqueous protein formulations dissolved in 75% PBS buffer, a) denaturation of BSA, b) Cross-linking of BSA, 0.5 wt% Eosin Y, c) polymerisation of BSA-SH 16% GHve 9% 0.5 wt% WSPI; scale bar $50 \mu\text{m}$, LM images

a), the structure appears significantly different from the surrounding. The precipitation is not limited to the area, where the laser focused was traced through. Moreover, the part is not stable. It deforms within minutes after the fabrication. Besides denaturation, no changes in the protein's appearance at any laser power and writing speed are possible. Adding 0.5 wt% of the commercially Eosin Y to the formulation enables us to induce a different reaction (

Figure 80 Cross-linking of aqueous protein formulations dissolved in 75% PBS buffer, a) denaturation of BSA, b) Cross-linking of BSA, 0.5 wt% Eosin Y, c) polymerisation of BSA-SH 16% GHve 9% 0.5 wt% WSPI; scale bar $50 \mu\text{m}$, LM images

b). At $100 \mu\text{m/s}$ (the lowest speed available at the Mipro setup), we can structure a lattice at 80 mW. Compared to the precipitate structure in Figure 80a, the appearance of this lattice does not significantly contrast from its surrounding. However, after fabrication it does not

¹⁷ Phosphate buffered saline is an isotonic buffer solution widely used in biological research. It is non-toxic to cells and has the ability to maintain their osmolarity, contains sodium chloride and phosphate and sometimes potassium chloride and phosphate [190]

change its shape. From what can be seen in the online picture, the dimensions fit to the CAD. The observed process seems to actually cross-link the BSA protein rather than inducing simply denaturation. However, larger writing speeds are not accessible. They require larger laser powers, which immediately lead to denaturation as shown in Figure 80a.

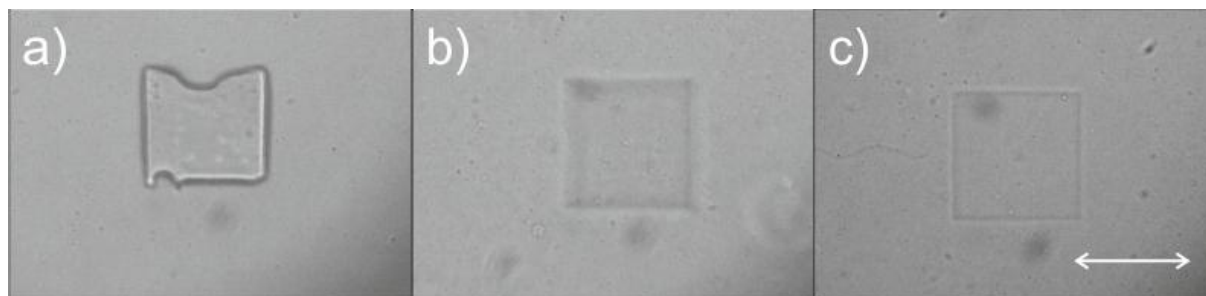


Figure 80 Cross-linking of aqueous protein formulations dissolved in 75% PBS buffer, a) denaturation of BSA, b) Cross-linking of BSA, 0.5 wt% Eosin Y, c) polymerisation of BSA-SH 16% GHve 9% 0.5 wt% WSPI; scale bar 50 μ m, LM images

Real protein polymerisation is shown in Figure 80c. Here, the same lattice was structured in a formulation containing 9% hydrolysed Gelatine modified with VE, 16% of reduced BSA (BSA-SH, see section 9.2.2.1) and 0.5 wt% of WSPI. The structure shows more contrast to the surrounding than the cross-linked BSA structure in Figure 80b. Yet it does not change its shape after the fabrication like the precipitate in a). Although Gelatine is generally less feasible for protein cross-linking than BSA, the presented formulations have been fabricated at 10 mm/s and 80 mW. The underlying chemical reaction in this cross-linking process is obviously more efficient than denaturation or protein cross-linking. In contrast to the other processes, the presented modified natural biopolymers allow for real polymerisation likely involving only one radical to make one cross-link.

However, it is still unclear, if VE polymerisation is just predominantly involved in cross-linking or if it completely replaces this process. Ovsianikov et al. were the first reporting successful 2PP processing of the acrylamide modification of Gelatine (GELmod) at process speeds of 10 mm/s using the commercially available water-soluble 1PP PI Irgacure 2959 [149]. Upon activation, this type I initiator dissolves into radicals that directly break the double bonds of monomers. Mechanisms as direct or indirect hydrogen abstraction from the proteins as (see section 8.3) are unlikely to occur. However, as we could already process GELmod using the type II initiators G₂CK and WSPI at even higher writing speeds and lower laser powers (data not shown), a simultaneous cross-linking of proteins cannot be precluded.

In any case, the modification of proteins is generally a very promising approach for increasing the efficiency of polymer formation. On the one hand, higher accessible writing speeds can lead to the economic fabrication of biological relevant sample sizes. On the other, significantly lower polymerisation thresholds can facilitate processing at only moderate laser powers, not compromising the viability of living tissues and cells.

In what follows, we will present the screening of two native protein based precursors functionalised with polymerisable VE units. First, we will draw our attention to Gelatine. We will see how the reduced Gelatine functionalised with VE (GHve, see section 9.2.2) will perform in 2PP structuring. Furthermore, we will find out, how introducing different amounts of reduced bovine serum albumin (BSA-SH) inside GHve based formulations will change the reactivity and the 3D capabilities of the formulation. In addition, we will investigate how this ratio tailors the mechanical properties and the degradation of the resulting polymer structures.

Furthermore, we will see the impact of different ratios between thiol and -ene groups to assess the efficiency changes in thiol-ene click chemistry¹⁸.

In the second section, we will deal with VE modified Hyaluronic Acid (HAvE) as described in section 9.2.2. As HA is a disulphide-rich protein, it may provide enough anchor points for VE units and may not need a co-monomer for facilitating efficient click-mediated chemistry.

12.4.2 Hydrolised Gelatine Vinyl Ester (GHve)

Gelatine is a proteinaceous polymer hydrolytic degraded from natural collagen, the main constituent of the natural extracellular matrix (ECM). It is soluble in water and proved already as an ideal backbone for creating biocompatible 2PP precursors [50,126,149].

Xiao-Hua (IAS) prepared low Mw Gelatine (Gelatine hydrolisate – GH) functionalised with VE groups. Radical chain-growth VE polymerisation alone is not quite efficient. However, as we know from the results of section 12.3.4, thiol-ene click chemistry can increase the reactivity of the formulation performing radical step-growth via chain transfer reactions [173]. As stated in section 9.2.2, Gelatine can be modified with VE units but it cannot be modified to provide sufficient thiols for such reactions. Another co-monomer is required as model macrothiol. We selected the reduced BSA (BSA-SH) as thiol provider.

For the experiments in this section, the AOM was not available. Instead, we used a mechanical switch based on a hard disc for switching the laser beam and a continuously variable neutral density filter for adjusting the laser power manually (see section 10.2.1, Figure 40). A screening according to section 11.2 was not possible as the fabrication of lattices required fast switching between jump phases (movement of the galvanomirrors to the start position of the next polymer line) and the mark phases (fabrication of the polymer line). Yet to continue with the experiments, we had to test the formulations fabricating specially designed CAD files. The design had to meet the following requirements:

- Short jump phases; in the ideal case, the fabrication of one layer should be possible without switching off the laser beam
- Insufficient switching times, i.e. delays between starting and stopping the fabrication and switching the laser beam on and off should not change the appearance and quality of the structure.
- To demonstrate the 3D capabilities of the formulation, the structure should have overhanging features.

We thus decided to fabricate structures based on a design adapted from a previous reported successful 2PP scaffold used for bone tissue engineering [123]. The CAD file is shown in Figure 81.

¹⁸ see section 9.2.2 for more information on the thiol-ene click chemistry

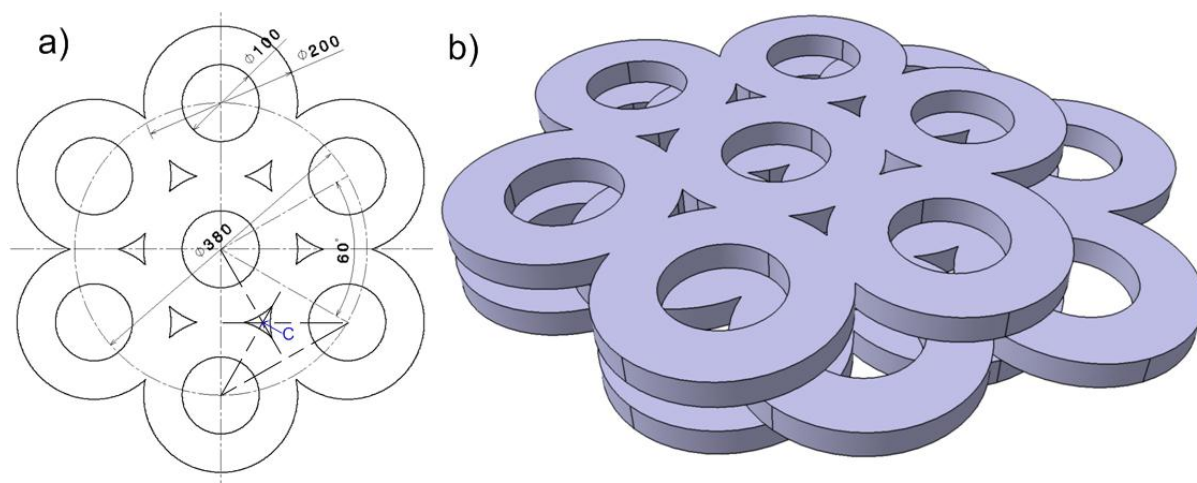


Figure 81 CAD of porous 3D scaffold produced for evaluating GHve/BSA-SH formulations; a) dimensions of one layer in μm , point C is the centre of the next layer; b) 3D picture of produced structure, 3 layers were stacked on top of each other at a defined offset of 94 μm in Y and 50 μm in X

One layer of the structure was made out of seven hollow cylinders. The inner and outer diameter were set to 100 μm and 200 μm , respectively. One cylinder was located in the centre of the layer. The other six cylinders surrounded the central one in a hexagonal-like arrangement. To ensure their attachment to each other, the cylinders overlapped by 5 μm . This geometry rendered the centres of the other cylinders situated on a virtual circle of 190 μm radius from the centre of the layer (see Figure 81a). Hence, the angle between the centres of two outer cylinders from the centre of the layer was 60°. In total, three 25 μm high layers were fabricated at a geometry-defined offset to each other. Connecting the respective centres of two adjacent outer triangles with the layer centre formed an isosceles triangle. The location of its circumcentre defines the centre of the next layer (Figure 81a, point C). The third layer overlaps with the first layer, as shown in Figure 81b. The total dimensions of the whole scaffold was thus $\varnothing 580 \times 75 \mu\text{m}^3$.

Each cylinder was fabricated individually. The linear X- and Y-axes moved to the position of the next cylinder and sequentially placed the structures and layers to the geometry-defined centre positions mentioned earlier. In contrast to previous structures reported in this thesis, these structures were made of polygonal lines. The X- and Y- mirrors moved simultaneously. The fabrication of one cylinder layer started from the inner and finished at the outer diameter. Laser switching was only required at these two positions, which enabled writing speeds far beyond those of lattice type structures when using the mechanical switch. However, an elaborate screening revealing ideal process parameters was not possible. We set the speed to constant 15 mm/s, adjusted the laser power with the density filter and simultaneously regarded the polymerisation process in the online process observation. We increased the power until we reached the upper polymerisation threshold, where we first observed bubble formation. We again lowered the power until we could fabricate at close to this threshold without causing damage to the polymer. Concluding from section 12.3.1, these process parameters likely rendered the stiffest and most dense networks obtainable with the formulation under investigation. However, we can quite likely optimise the quality of structures presented in this section when applying an AOM for switching.

For structuring, we used the Mipro setup and the 20x NA 0.8 objective. The formulations contained 75% PBS buffer¹⁹, 25% GHve/BSA-SH ratio and 0.5 wt% of WSPI. As the long terms

¹⁹ Phosphate buffered saline is an isotonic buffer solution widely used in biological research. It is non-toxic to cells and has the ability to maintain their osmolarity and contains sodium chloride and phosphate and eventually also potassium chloride and phosphate [190].

stability of the formulations was not good, we structured them straight after preparation. We prepared a specimen according to section 11.1 and mounted it to the Z-stage. The polymer line and layer distance of the structure were set to 0.3 μm and 1 μm , respectively, which gave a total number of 333 polymer lines per layer ($100/0.3$) and 25 layers per cylinder. Straight after fabrication, we observed the structures in the LM and carefully developed them in PBS buffer. We prepared the specimen for LSM analysis according to 11.3. All structures were observed in the LSM straight after polymerisation. This was required for G/B1 (see next section) as it degraded within hours. For better comparison between the formulations, we conducted all experiments according to the same protocol. Significant changes in the dimensions observed here are likely to be much larger at equilibrium absorption of the hydrogel (see also 12.3.1.1).

12.4.2.1 Varying the ratio between BSA-SH and GHve

We started with the assessment of formulations differing in their GHve to BSA-SH ratios. The composition of the investigated formulations is shown in Table 3.

Table 3 Formulations with different BSA-SH and GHve ratios

Label	GHve	BSA-SH	WSPI	PBS	Thiol/-ene
G/B 1	15%	10%	0,5wt%	75%	2/10
G/B 2	10%	20%	0,5wt%	70%	1/10
G/B 3	0%	25%	0,5wt%	75%	-

G/B 1 was the least reactive of the investigated formulations. We structured at a power of 330 mW. Though this power already led to bubble formation and damage to the polymer in the intersecting areas between the cylinders, the polymer was very weak and immediately dissolved in the buffer media. In the LSM, the structure was hardly discriminable from its aqueous surrounding (image not shown). We thus tried a different fabrication strategy; we lowered the fabrication power to 305 mW and processed every layer twice. This means that, after the fabrication of one layer, we did not move with any axis. Instead, we traced the focal volume through the already polymerised part again. This strategy provided a considerably higher cross-linked polymer. The 2D and 3D LSM image of the scaffold can be seen in Figure 82.

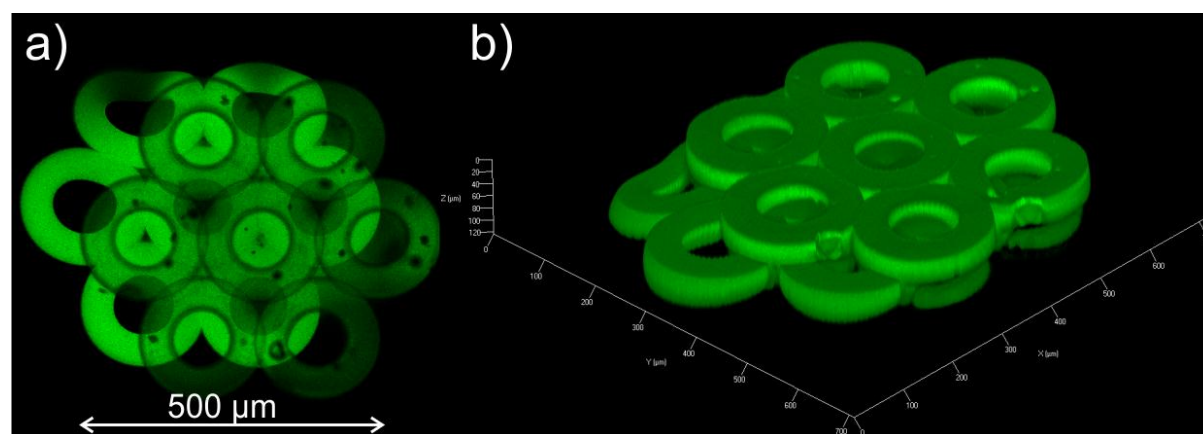


Figure 82 Scaffold produced from formulation G/B 1, a) 2D and b) stacked 3D image, X- and Y-divisions 100 μm , Z division 20 μm , LSM 10x

The structure is in good accordance to the intended CAD. Optical measurements revealed that the outer diameters of the cylinders were 196 μm , the inner diameters was 91 at average. The structure thus shrunk only very slightly from its intended 200 μm and 100 μm outer and inner diameter, respectively. In addition, the dimension of the upper layers did not differ from the ones underneath in any quantifiable manner, which suggests that the cylinders did not bend. The structure stayed in its prescribed 3D shape. We thus conclude that the polymer is stable and does not require any support from the glass slide as other VE based formulations do (see section 12.3.4). However, the standard deviation of the outer and inner diameters is $\pm 13 \mu\text{m}$ and ± 11 , respectively, which is quite large. This can be attributed to the holes inside the polymer. They are randomly distributed within the polymer and are not specifically located at the position of most laser exposure. We would expect an increased probability of damage at the positions of intersection between the cylinders, where the focal point was traced through the formulation 4 times. As this is not the case, we presume that these holes derived either from a deformation of the polymer or from the initiator, which was potentially not homogeneously dissolved in the formulation.

G/B2 contains double the amount of BSA-SH and 5% less of GHve. Thus, the total water content in this formulation is 70%, 5% less than that of the other formulations. In effect, we made a mistake during preparation, which rendered this specimen not really comparable to the others. However, for future research the results are worth mentioning here as an example for increasing the protein content in the formulation above 25%. This formulation was more reactive than G/B1, so we structured every layer only once. The power was set to 200 mW. The outcome is depicted in Figure 83.

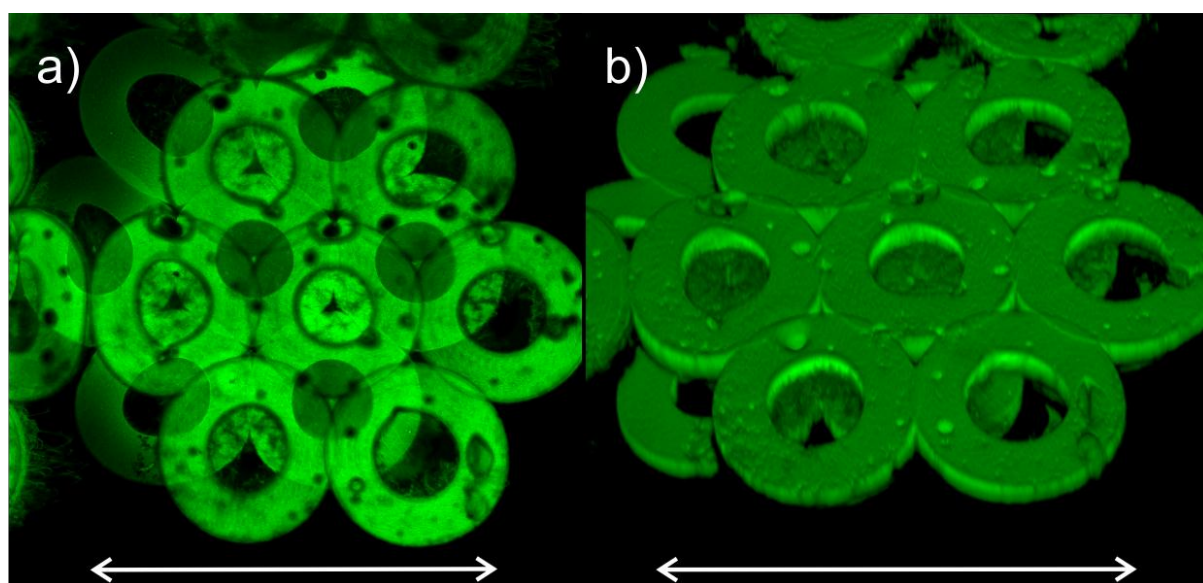


Figure 83 Scaffold produced from formulation G/B2, a) 2D and b) stacked 3D image, scale bars 500 μm , LSM 10x

As can be seen from these pictures, the polymer is rather stable. It holds its 3D shape precisely. The outer diameters are 19 μm larger than intended. The inner diameters, however, are exactly 100 μm . This can have two reasons: On one hand, the applied laser power potentially increased the 2PA-affected zone of the voxel, rendered thick polymer lines and therefore larger cylinder dimensions. On the other hand, the structure could likely have soaked up water between sample development and observation in the LSM. In addition, the overhanging structures probably bent under their own weight causing their deformation. The standard deviation of the outer diameter is less but total deformation is larger compared to the

structure produced from G/B1. The structure obtained with G/B2 has outer and inner diameters that differ by approximately 6 μm . We thus expect the dimension deviations to be a result of swelling and thick polymer lines.

We can see even more holes than in the G/B1 structure. This indicates limited solubility of the initiator in the formulation. Likely, WSPIs solubility decreases with increasing protein content in the formulation. The inner walls of the structure seem to be frayed indicating a deformation of the polymer at the beginning of the fabrication process. The polymer was weak at the beginning of the fabrication getting its full strength in the end. This can result in a deformation of single lines during the fabrication process as observed structuring PEGda in section 12.3.1.2.

G/B3 was a reference formulation consisting of 25% BSA-SH. The power applied was only 100 mW. The result of the structuring can be seen in Figure 84. Only the most overhanging cylinders in the second and in the top layers are a little bent. Similar to G/B2, the outer diameters exceed the intended dimension by 19 μm , whereas the inner diameters show no significant deviations. The structure is thus a little larger than intended. Again, we think this is a result of swelling and thick polymer lines. In contrast to G/B2, the inner walls are not frayed indicating that even single polymer lines in the beginning of the fabrication process are stable enough to hold their shape. In the LSM, this polymer appears very bright. These facts give evidence that not only G/B3 is the most reactive among the formulations investigated. In addition, the polymer consisting of BSA alone also has the highest cross-linking density.

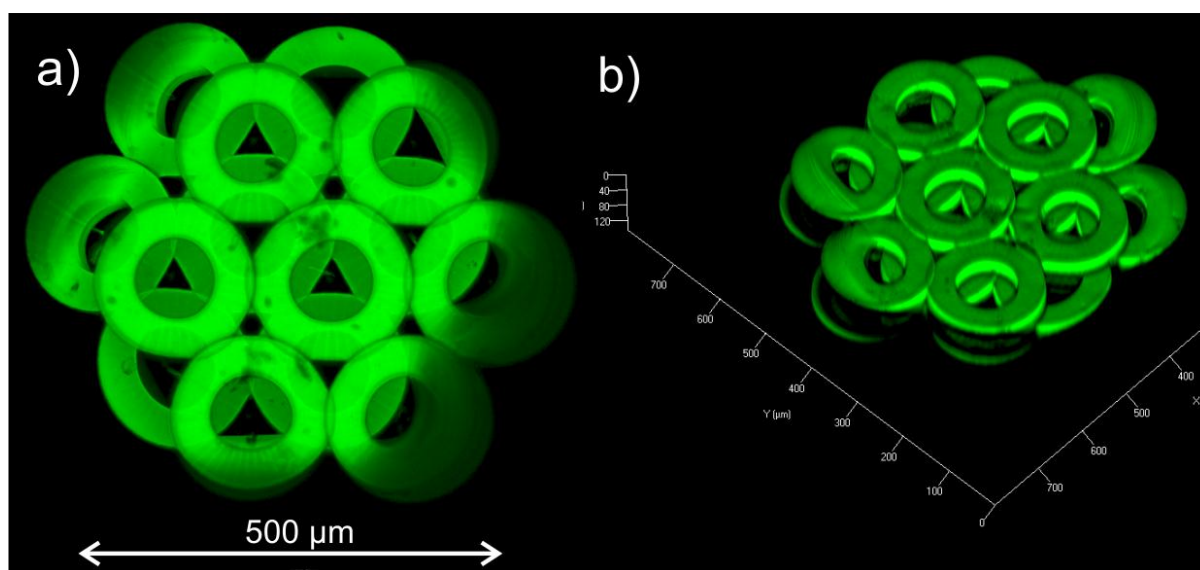


Figure 84 Scaffold produced from formulation G/B3, a) 2D and b) stacked 3D image, X- and Y-divisions 100 μm , Z division 20 μm , LSM 10x

To conclude this section, we see an increased reactivity with increasing BSA-SH content in the formulation. BSA-SH facilitates the best structuring results. Increasing the protein content to over 25% is not recommended as the initiator lacks solubility in formulations with higher protein content.

BSA is already well established in 2PP micro-fabrication (see section 8.4.2). However, BSA based formulations conventionally contain commercially available xanthene dyes as photoinitiators. As a result, BSA could not be processed at writing speeds beyond 1 mm/s [150]. Using WSPI as PI, we here report fabrication speeds of 15 mm/s using an 800 nm

wavelength laser. It is very likely that we can process this formulation at even higher writing speed.

As BSA is known to be a biocompatible component, the question is whether GHve is still attractive for 2PP of biocompatible formulations since it obviously only reduces the reactivity of BSA. However, though BSA is widely used, it is well known that, in contrast to Gelatine, it resists cell adhesion due to the negative charge on its surface [191]. Preliminary cell studies proved that GHve/BSA-SH based hydrogels were cytocompatible with MG63 cells. Cell attachment could be adjusted by tuning the relative ratio between GHve and reduced BSA. These results showed that GHve supported cell adhesion [50,171]. It is thus worth to further improve GHve based formulations as they are potentially suitable to be polymerised in the presence of living cells and tissues. Improving the thiol/-ene ratio potentially increases chain-transfer reactions and thus improves the reactivity of GHve based formulations. With a given content of the macrothiol BSA-SH, we investigated the performance of different thiol/-ene ratios in GHve based formulations. The goal was to increase the reactivity without reducing the biocompatibility.

12.4.2.2 Varying thiol/-ene ratios

We tested formulations with 16% GHve, 9% BSA-SH and 75% water. Again 0.5 wt% of WSPI was added for 2PP. The presented formulations varied in their thiol to carbon-carbon double bonds of the VE units. With the following experiments, we wanted to investigate the impact of this ratio on the efficiency of the thiol-ene click chemistry mediated step-growth reactions. As in the experiments of the last section, we kept all process parameters constant and set the power to slightly below the upper polymerisation threshold. The following Table 4 gives an overview of the investigated formulations. The results of this section will soon be published in Xiao-Hua's (IAS) manuscript currently in preparation [171].

Table 4 Formulations with different thiol/-ene ratios

Label	GHve	BSA-SH	WSPI	Solvent	Thiol/-ene
T/E1	9%	16%	0,5wt%	75wt%	1/10
T/E2	9%	16%	0,5wt%	75wt%	2/10
T/E3	9%	16%	0,5wt%	75wt%	4/10

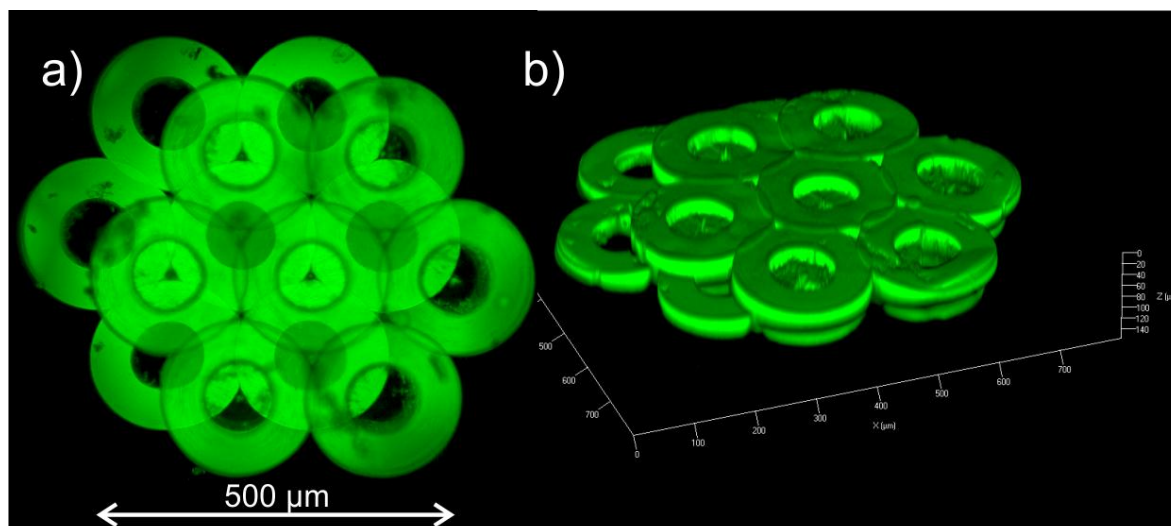


Figure 85 Scaffold produced from formulation T/E1, a) 2D and b) stacked 3D image, X- and Y-divisions 100 μm , Z division 20 μm , LSM 10x [171]

T/E1 was fabricated at 280 mW. The result of the fabrication process can be seen in Figure 85.

The structure appears very bright, which we again attribute to a dense polymer network. The inner walls of the cylinders where the fabrication started seem to be frayed, indicating a deformation of the polymer at the beginning of the fabrication process similar to the formulation G/B2. Some parts of the structure have cracks. However, no cracks can be observed at the overlaps between the cylinders (where the focal point was traced through twice). Therefore, overexposure is not the cause. The cracks either derive from a deformation of the polymer or from inhomogeneous dissolved photoinitiator. The overall structure is swollen. The outer diameter is 22 μm ($\pm 2 \mu\text{m}$) wider than the CAD. The inner diameter is almost 100 μm ($\pm 4 \mu\text{m}$).

TE/2 seemed more homogeneous but less reactive. The highest accessible laser power was 200 mW. The result of the fabrication process is depicted in Figure 86.

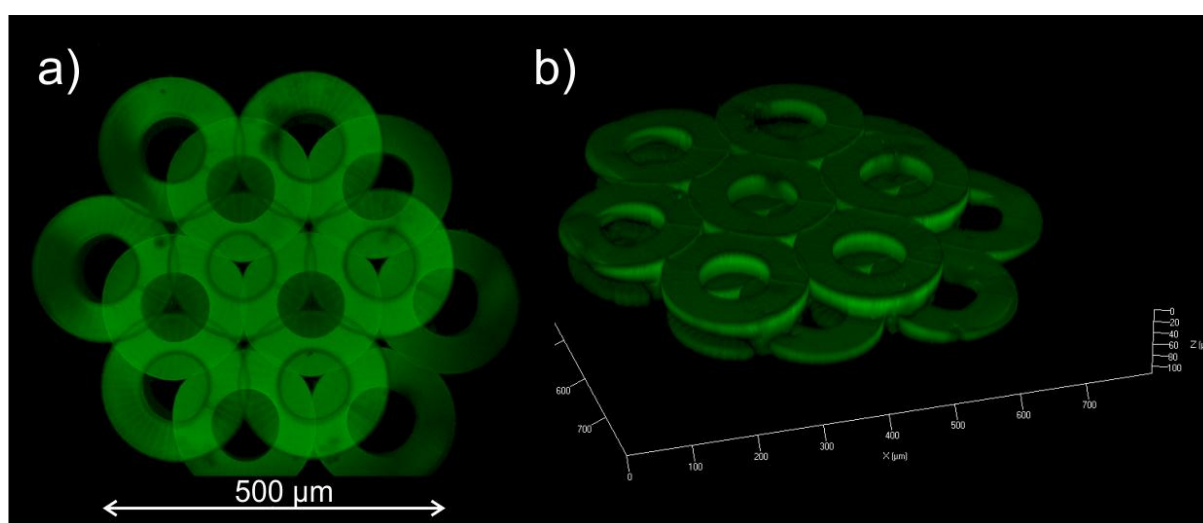


Figure 86 Scaffold produced from formulation T/E2, a) 2D and b) stacked 3D image, X- and Y-divisions 100 μm , Z division 20 μm , LSM 10x [171]

The structure is well defined. The deviations from the CAD are minor compared to formulation TE/1. The outer and inner diameter exceed the CAD dimensions by +12 μm and +1 μm ,

respectively. However, the network is less stable than that of the structure produced with T/E2. The overhangs of the structure flow down. In contrast to TE/1, no cracks or frayed parts can be observed. The polymer seems to be more stable. In addition, the reproducibility is better. The outer and inner diameters vary by 2 μm , respectively.

TE/3 allowed the fabrication of microstructures at a power of only 75 mW, the lowest power used for polymerisation of GHve/BSA-SH formulations so far. However, the produced scaffolds could not be developed due to insufficient long-term stability of the formulation. The unpolymerised proteins fell out rapidly and conglomerated around the produced structures making it impossible to get rid of the monomer residue without destroying the parts. However, we obtained LM images straight after polymerisation, which are shown in Figure 87.

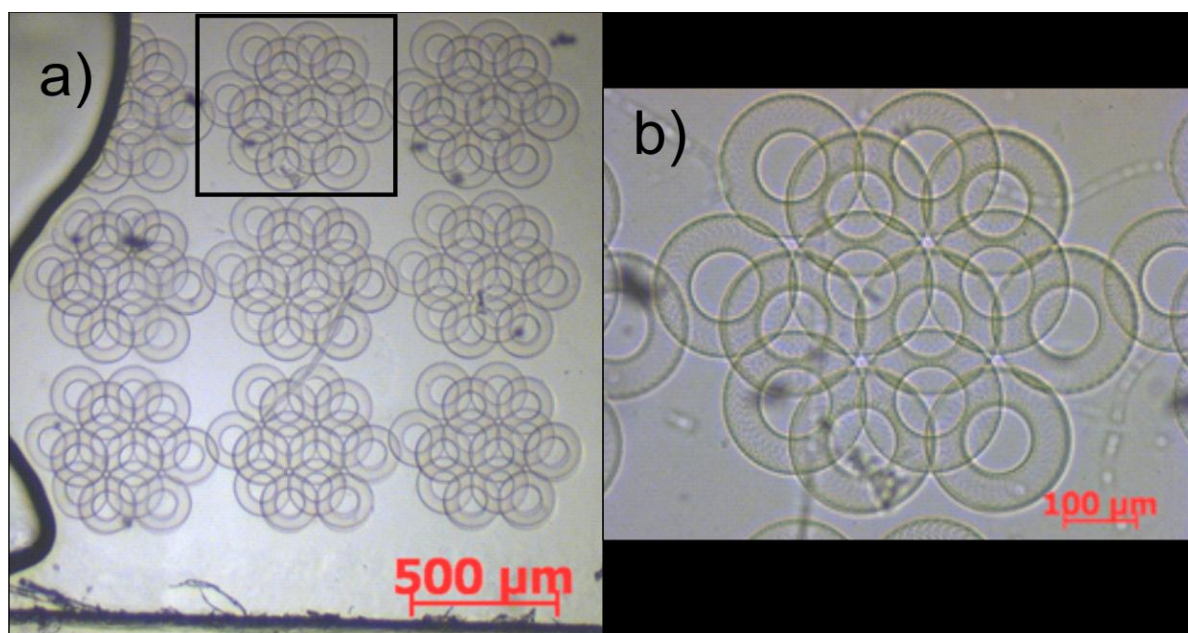


Figure 87 Scaffold produced from formulation T/E3, a) array of scaffolds, LM 2.5x b) close-up of highlighted part in a, LM 10x

From what can be observed in the LM, the part looks quite well. The cylinder layers are perfectly arranged and no deformation can be observed. However, the structure seems quite swollen, as nearby elements already overlap. As the set distance between the structures was 50 μm , it is expected that the structures produced with this formulation swell quite rapidly.

As soon as the AOM was available again, we investigated the lower and higher polymerisation threshold of T/E1, 2 and 3 structuring 50x50x40 μm lattices with 0.3 μm polymer line distance and 1 μm height. To compare the results to those from this section, we set the speed to constant 15 mm/s and varied the power.

Table 5 Lower and upper polymerisation threshold of GHve/BSA-SH formulations with different thiol/-ene ratios [171]

Label.	Thiol/-ene	Lower [mW]	Higher [mW]
T/E1	0.1	75	375
T/E2	0.2	100	300
T/E3	0.4	50	125

Increasing the thiol to –ene ratio, the process window gets narrower. A decrease in the upper polymerisation threshold is obvious. However, the lower polymerisation threshold first raised with increasing the thiol to –ene ratio and then decreases again. This is quite unexpected. Potentially there was a mistake in the experiment and it should be repeated.

What we can conclude from this section is that though the formulations presented are based on natural proteins, the reactivity can be compared to potentially toxic PEGda based hydrogels structured using the same initiator at higher concentrations (see section 12.3.1 and [49]). In contrast to BSA alone, the addition of GHve can increase cell adhesion and render these formulations potential candidates for polymerisation *in vivo*. With varying the thiol/-ene ratios in the formulation, the degradation rate, the stiffness of the polymer and the reactivity and 3D capabilities for 2PP can be tailored.

However, for the experiments in this section, we still required a BSA content of 16%, which might reduce the biocompatibility of the formulation. Maybe we can find a precursor that has a sufficient number of free disulphide bridges acting as macrothiol and at the same time providing sufficient anchor points for cross-linkable VE units.

12.4.3 Hyaluronic Acid Vinyl Ester (HAvE)

According to section 9.2.2.2 and similar to the procedure presented in preparing GHve, Xiao-Hua prepared the low Mw of Hyaluronic Acid and substituted the free lysine units using divinyl adipate. However, the degree of substitution was 0.53 and thus much less than in the GHve based formulations reported before. 0.5 wt% photoinitiator was dissolved in PBS buffer. The HAvE was added to give a 10% concentration. Dithiothreitol (DTT) was added to this solution, making the functionality ratio between thiols and -enes 20%, a similar ratio as for the T/E2 formulation described in section 12.4.2.2. For the proof-of-concept of this formulation, we structured a CAD file of the TU Logo (100x100x20 μm^3) and a Ying-Yang Logo (100x100x10 μm^3) at a polymer line distance of 0.5 μm and a layer distance 1 μm . Both of the structures were produced at a speed of 1 mm/s and a power of 80 mW using the 20x NA 0.8 microscope objective. We did not develop the structures but only observed them online as shown in Figure 88.

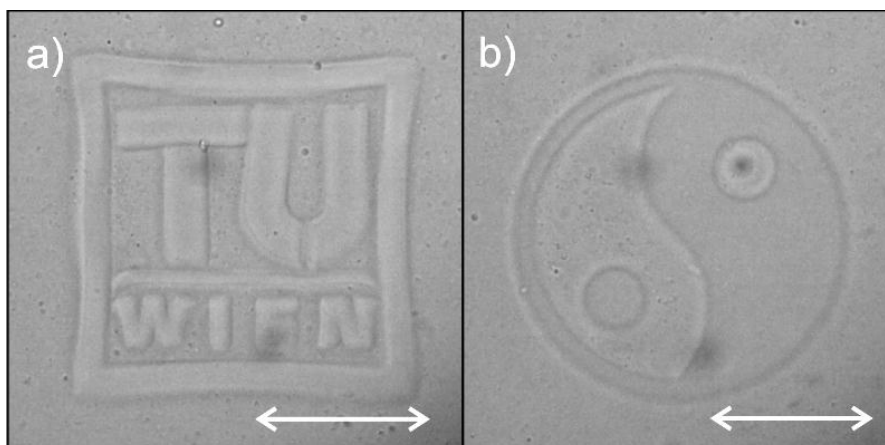


Figure 88 a) TU Logo ($100 \times 100 \times 20 \mu\text{m}^3$) and b) Ying-Yang Logo ($100 \times 100 \times 10 \mu\text{m}^3$) structured in HAVe based formulation, online process observation, 20x NA 0.8 objective, scale bars 50 μm

These structures only represent the very first attempt in the structuring of HAVe. However, we are quite confident that this material has a high potential for *in situ* polymerisation, since HA is one of the major components of the ECM. It favours cell adhesion, proliferation and migration and can be found in various lotions and wound healing bioadhesives. In contrast to GHve formulations presented in the last section, this formulation does not require BSA, which potentially lowers the incentive for cell adhesion and proliferation. Furthermore, only 10% of reactive precursors in the formulation are required, which shows the formulation's high reactivity. The development of modified HA based formulations for 2PP is still at an early stage. We will see how these formulations will unfold their practical potential in future experiments.

By now, we have tested many potential 2PP specialised PIs as well as many precursors, either synthetic or naturally derived that perform differently in 2PP. From other research fields, we know that many of the compounds used for the synthesis of the presented materials are very attractive. Moreover, Gelatine and HA precursors have good applicability for cell encapsulation as well as for creating tissue engineering scaffolds. However, for 2PP in the presence of cells and tissues, we have to prove that all components of this process, PIs, NIR light, precursors and process by-products are biocompatible. Furthermore, we have to prove that our modifications to Gelatine and Hyaluronic Acid did not compromise their biocompatibility and their properties as ECM analogues. It is now important to determine, how cells and/or living biological tissues experience this artificial dynamic environment. In addition to the challenges known from seeding approaches [192], we have to deal with many additional factors potentially compromising the biocompatibility:

- The toxicity of the unpolymerised precursors
- The toxicity of the unpolymerised PI
- The toxicity of the formed radicals upon activation
- Photochemical and/or photothermal effects

Let us thus explore how some of the presented formulations affect the viability of living organisms. The next section will introduce the roundworm *Caenorhabditis elegans*, the test organism of this work. We will see how the ingredients of an unpolymerised formulation in different concentration affects the viability of the animal. Furthermore, we will see at which energy levels, through which mechanisms and on which principle NIR laser light causes stress to the animal.

13 Toxicity analysis

The following chapter was partly published 2012 in the Journal of Biomedical Optics [49].

For any successful *in vivo* application, biocompatibility on cellular, tissue and organism level is essential. Testing is mostly done using cultured cells, but this requires an expensive infrastructure. In addition, stress responses in cells are often not visible via direct microscopic observation and cell viability cannot be easily defined in terms of a single physiological or morphological parameter [112]. Before investing in cell laboratories, employ biologists and adapt machines to fit biological conditions, we had to pre-determine the biocompatibility of the presented materials on biological systems that are easy to maintain and do not need special sterile conditions. Multi-cellular organisms are feasible test organisms that already become popular as pre-screening models [193].

Caenorhabditis elegans (*C.elegans*) is a nematode (roundworm) that can serve as inexpensive and ethically acceptable high-throughput and real-time biosensor for animal organisms in predicting acute lethality in mammals [194]. Several publications focus on the effects of chemicals on wild-type nematode survival (LC)²⁰, development and mutagenicity [195–197]. As *C. elegans* uses chemosensation to find food, avoid noxious conditions, develop appropriately and mate, it has to sense chemicals that penetrate the cuticle, exposing its sensory cilia to the environment [197]. We consider the choice of *C. elegans* as a model organism appropriate to provide the practical basis for a proof of concept for applying 2PP in a biological surrounding [49].

In this chapter, we will examine the topic of biocompatibility from two different perspectives; the materials' side including the impact of the unpolymerised monomers and the initiator on the living animals and the impact of the laser light required for polymerisation. For getting insights into the former, we will perform LC₅₀ assays showing the toxicity of PEG-700-da in different concentrations. Similarly, we will investigate the effects of the initiator WSPI separately at a concentration used for structuring in 12.3.1. In the second section, we will refer to observations from the literature, where a threshold is presented, below which focused pulsed NIR laser light can be applied in the presence of living organisms and cells without compromising their viability. Referring to these results, we will get insights whether photodamage is likely to occur at intensities required for polymerisation. To relate the results of this section to the biocompatibility of 2PP, we will refer to the the Dorland's Medical Dictionary definition for biocompatibility as the "*quality of not having toxic or injurious effects on biological systems*" [198].

²⁰ The average lethal concentration LC is the statistically calculated concentration of a substance that causes death to the exposed animals during and after the investigation period.

13.1 Biocompatibility of monomers and initiators

In this section, we will investigate the biocompatibility of PEGda and WSPI. Pure M9 buffer media and the hydrophobic ETA-TTA (section 9.1.1) will be taken as references, respectively. The toxicity of components other than PEGda are tested on cells and are not part of this thesis. Interested readers will find more information in manuscripts that are currently in preparation [166,171,174].

13.1.1 Preparation and Experimentation

The *C. elegans* animals were cultured using standard techniques [199]. N2 wild type nematodes without any genetic modifications were used for the LC₅₀ assays. To ensure that all animals were of the same age, we had to synchronise the population. Via hypochlorite digestion of worms only the eggs survived. The unstaged *C. elegans* cultures with adults were incubated for 5 min in bleaching solution (10% 5M NaOH, 20% chlorine bleach) until adult worm corpses were completely dissolved. Eggs were collected by centrifugation (3400 g, 2 min, 20°C, Hermle Z383K), washed with M9 buffer and seeded onto fresh plates. After letting worms hatch and grow to adulthood, worms were washed off the plates with M9 buffer.

500 µL of this synchronised population in M9 buffer (15 worms/µL) were pipetted into a centrifuge tube containing 500 µL of double concentrated formulation (without initiator). In total, we investigated 4 different formulations, containing 10%, 20%, 40% and 60% M9 in PEGda, respectively. Mixed with the worm emulsion, this resulted in concentrations of 50%, 60%, 70% and 80% M9 in PEGda formulations, the concentrations used for structuring in 12.3.1. The 3 reference tubes contained 500 µL worm suspension and 500 µL pure M9 buffer. After 15 min of exposure, the emulsion was centrifuged (3400 g, 2 min, 20°C, Hermle Z383K). The pellet was washed with 4 mL M9 buffer and centrifuged. 20 µL of cleaned worm pellet (300-400 worms) were pipetted onto three 35 mm wide agar lawn petri-dishes each.

The biocompatibility of the initiator was investigated separately. 4 wt% of WSPI (double the amount used for structuring) was dissolved in M9 buffer, mixed with the worm emulsion and treated equally.

In addition to the pure M9 references, we also investigated the impact of the organo-soluble formulation ETA-TTA (see section 9.1.1).

We determined the biocompatibility of the compounds employing a movement assay for adverse effects on exposed animals described in [200]. We defined an animal as dead when it completely lacked motion after a recovery phase of 20 minutes. The duration of this phase has been shown to be sufficient to exclude the possibility of non-moving but living animals regaining their mobility [49].

As shown in Figure 89, six petri-dishes carrying the exposed worms (3) were placed into a six-well plate and covered with caps. Three petri dishes contained worms that were exposed to the formulation. The three other were reference probes, containing worms exposed to pure M9 buffer media only.

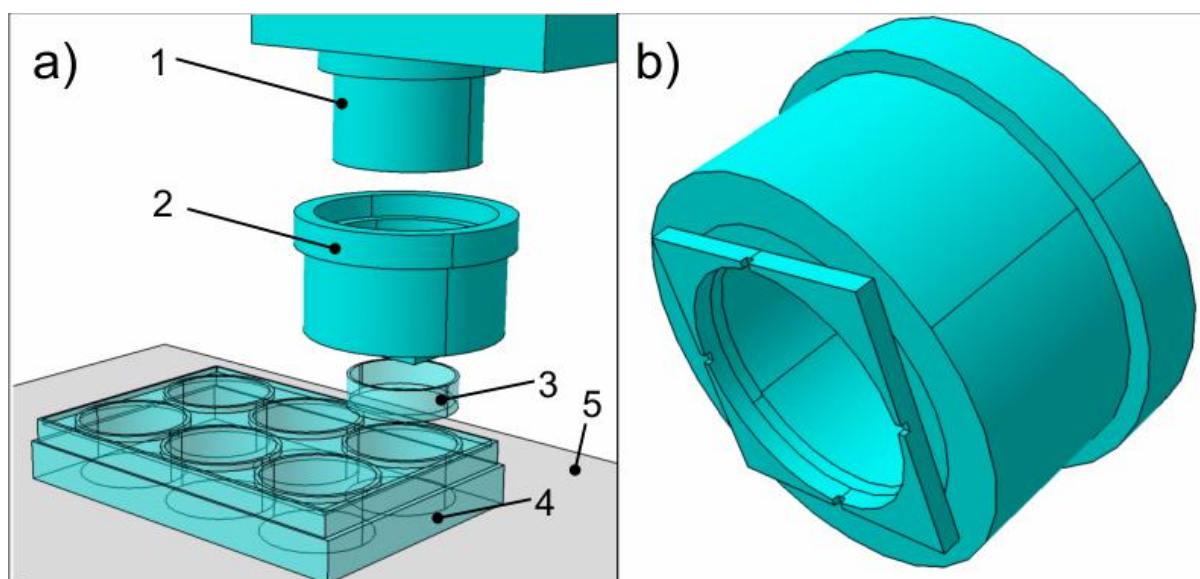


Figure 89 Setup for LC₅₀ analysis, 1) camera, 2) retainer, 3) petri dish carrying exposed animals, 4) 6-well plate, 5) CCD display

A digital camera (Canon Power Shot SX200IS, 1) was mounted to a specially designed retainer (2). This device ensured a constant distance to the specimen (3). Its top (see Figure 89b) facilitated precise fastening of the camera to the six-well plate. When taking a photograph of a specimen, the picture always showed the same spot with the movement of the worms being the only variable. The focus of the camera was set such that the worms moving on the agar plate appeared sharp. A computer screen (15.6" TFT 1920x1080 pixels, 5) showing a white image ensured homogeneous illumination of the sample. Every three minutes after the exposure, the caps of the specimens (3) were removed and two high-resolution (4x3 megapixels) were taken of each specimen, respectively. The delay between the pictures was set to 1 second. During this time, the agar of the petri dish absorbed the liquid leaving the worms on the lawn.

The worm's viability was determined measuring their mobility and impetus to move [200]. Comparing photographs taken at different times, visibly moving worms were considered alive [49].

We repeated this experiment five times, for four formulations with different PEGda concentrations, one formulation with the initiator. Every experiments involved the preparation of six agar plates (three with exposed animals and three reference probes) carrying 300-400 worms each. None of the animals survived the exposure to ETA-TTA in the first experiment. This is quite in accordance with previous work [11] and was thus quite expected. ETA-TTA obviously kills all animals within seconds after the exposure. As this was quite clear, we performed one experiment on one specimen only.

13.1.2 Analysis

We changed all pictures to black and white and sorted them according to the protocol. In the previous section, we mentioned that two pictures each were shot for every specimen and observation time, respectively. We counted the worms present on the first image. After that, we inverted the second image that was shot one second after the first. This reversed black and white of this image. The modified second image was adjusted to 50% opacity and laid over the first one. All details of the image, which did not change within 1 second, became

invisible. Hence, dead worms were not shown on this merged image. Alive worms, however were shown twice, one black worm (worm of first image) and one white worm (worm of second image).

Showing the first image only, we counted the total number of worms. Overlaying the second image, we counted the white worms visible. The ratio between these two values determined the survival rate. Figure 90 shows the necessary steps for preparing the images for analysis.

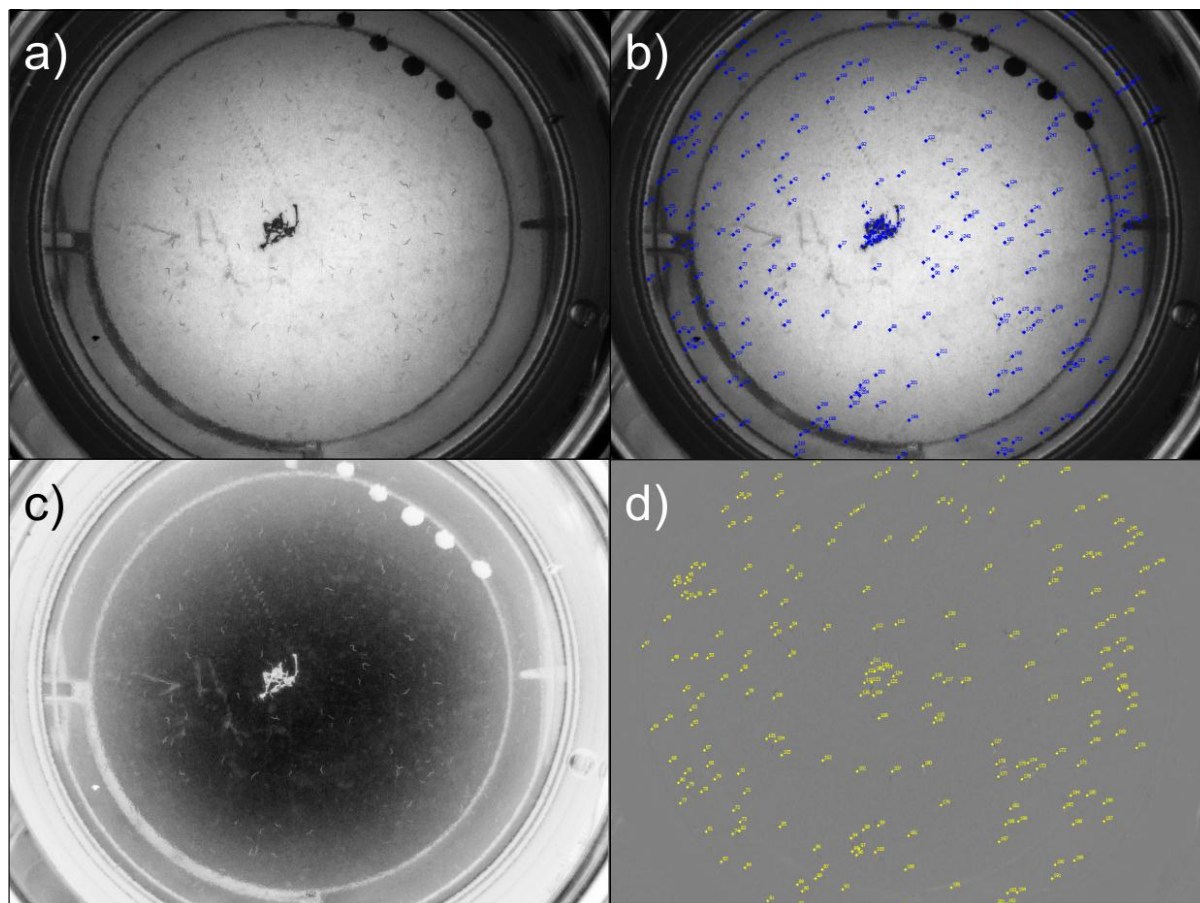


Figure 90 Toxicity analysis a) Monochromatic Image 1, b) Counting total number of worms, c) inverting second image, d) adjusting second image to 50% opacity and overlaying the first image, counting number of alive worms

The ratio of alive worms to their total number determined the survival rate. To simplify the analysis, we only considered two observation times, 15 min and 18 min for each specimen, respectively. As it was expected that worms do not always move, the higher survival rate observed was taken for the LC analysis. Evaluating all pictures would be a slightly more exact determination. However, as the counting was done manually, the effort needed for a thorough assessment does not justify the obtained accuracy benefit. A software tool counting the number of dead or alive worms would facilitate an easy and more accurate LC value.

Each of the 300-400 worms in one specimen can be tracked with this assay. Hence, we believe that a simple live/death statement is just a small fraction of the possible functions such an analysis can provide. Over a period of 18 min, this protocol enables the observer to measure the total distance travelled and to benchmark the kind of movement (random or straight away from the site of exposure). In addition to the movement, this assay allows to evaluate the appearance of the worms (curly or straight) and the time when they increasingly start to move (end of paralysation past exposure). However, quantitative observations of this kind again

require appropriate software tools. As we will not continue our work with *C. elegans* in the future, we shall limit ourselves here to deal with a simple live/death assay. The outcome is presented in Figure 91.

13.1.3 Results of LC assay

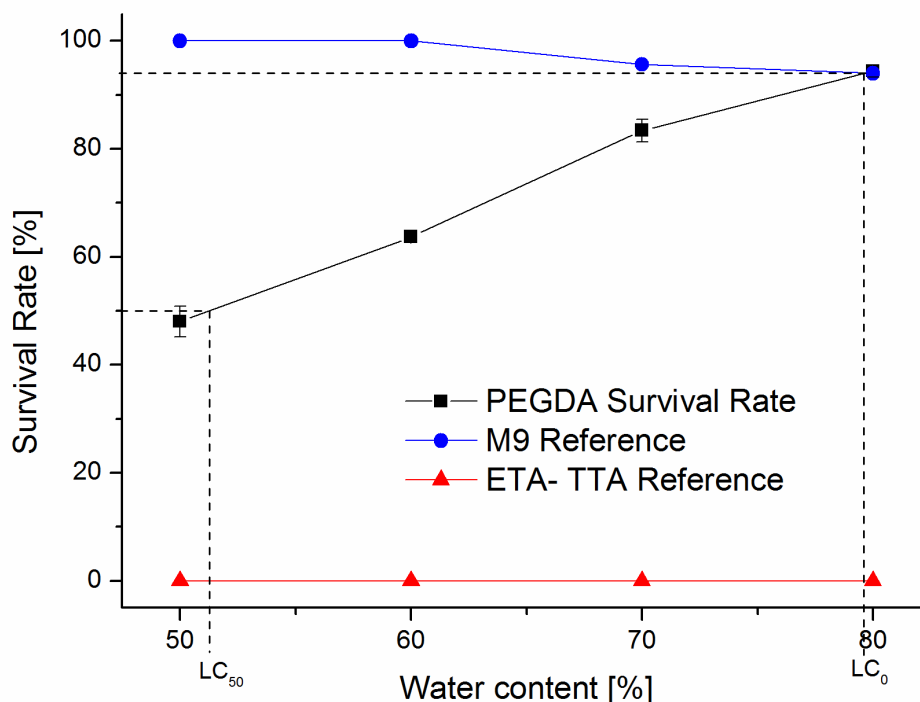


Figure 91 Percentage of worms alive plotted against decreasing concentrations of PEGda in M9, worms kept in the uncured resin for 15 min; black line: PEGda in buffer media at different concentrations (triple measurements), blue line: buffer reference, red line: ETA-TTA reference. Each data point represents an individual measurement performed with 300-400 worms. Data points in one vertical row represent experiments done at the same time with the same population. LC_{50} and LC_0 values are highlighted [49].

As already stated, the non-aqueous ETA-TTA virtually immobilised all worms, whereas the survival rates progressively raised using decreasing amounts of PEGda in buffer media. At approximately 52% water content, 50% of the worms survive when exposed for 15 minutes (LC_{50}). Considering the buffer reference, the survival rate increased by 33%, 35% and 15% when raising the water content from 50- 60%, 60-70% and 70-80%, respectively. At 79% water content, no difference to the reference was found (LC_0).

The biocompatibility of the initiator WSPI was investigated in a control experiment. Worms in buffer media containing 2 wt% of WSPI (the concentration used for structuring in 12.3.1) was 84% (\pm 4%) at an exposure time of 15 min. The survival rate of worms in buffer reference was 93%. The animals showed no quantifiable reaction to the exposure in the investigated period.

These results indicate that, in contrast to standard 2PP formulations like ETA-TTA, PEG-based hydrogels dissolved in buffer media show higher biocompatibility. For the applied exposure time, the toxic influence of the initiator seems low.

The photopolymerisable formulation contains M9 buffer media, the monomer PEGda and the initiator WSPI. From these components, PEGda only has a quantifiable toxic influence in the investigated timeframe. Therefore, we consider the monomer as good proxy for the

total biocompatibility of the formulations for the investigated timeframe. For this work, we will further quantitatively define a material as being biocompatible if the survival rate of *C. elegans* in the investigated formulation exceeds 50% measured against reference animals held in pure M9 buffer media (LC₅₀) at an exposure time of 15 minutes [49].

After getting an insight into the biocompatibility of the individual components of the formulation, we now need to know whether the focused laser beam will compromise the viability of *C. elegans* during polymerisation. Hence, in the next section, we will deal with photochemical and photothermal caused stress for the organism.

13.2 Photodamage

This chapter was published in 2012 in the Journal of Biomedical Optics [49].

Optical absorption coefficients of biological tissues reflect the absorption of proteins, DNA, melanin, haemoglobin and water. The variation of their optical activities is strongly dependent on the wavelength [112]. In the NIR region, water is the most important tissue chromophore. It begins contributing significantly to tissue absorption at $\lambda \geq 900$ nm [111]. Thus, the heating of the tissue increases with the wavelength. Light below 800 nm, however, increasingly causes photochemically induced stress inside biological tissues. The damage caused is significantly higher using light with wavelengths below 800 nm. Hence, compared to UV light, NIR light and light of 800 nm in particular, seems to be more suitable for inducing polymerisation in the near vicinity of biological tissues.

Potentially, laser induced photodamage can have a negative effect on biological material. In previous experiments, researchers investigating cell regulations made use of fs, NIR laser pulses to selectively ablate intracellular components in live cells without altering neighbouring structures or compromising cell viability. Focusing 100 fs pulsed 800 nm wavelength laser light tightly (100x NA 1.4 objective) beneath cell membranes, pulse energies of 1.5 nJ at process speeds of 5 $\mu\text{m/s}$ were reported as being necessary to induce ablation [113]. With laser surgery, pulse energies above 2 nJ of a tightly focussed (64x NA 1.4 objective) fs laser beam are necessary for severing single axons of *C. elegans* [34]. In contrast, it could be shown that two-photon photodegradation of PEG hydrogels with embedded cells can be done at pulse energies below 1.5 nJ, maintaining high cell viability and causing no non-specific intracellular ablation [114].

For our experiments processing PEGda based formulations, we expected laser induced photodamage on the organism to be very unlikely due to the following arguments:

- Given the 30% transmission efficiency of the 20x NA 0.4 objective used for structuring PEGda based formulations in section 12.3.1, the maximum pulse energy in the focal volume is 1.2 nJ at laser power maximum of 300 mW used for structuring, which is well below the reported pulse energy maximum of 1.5 nJ.
- The larger the NA, the smaller the volume illuminated at the focal point and the lower the energy required to reach the intensity threshold for ablation [113]. With the 20x NA 0.4 objective, we can expect a higher energy threshold as that being necessary for non-specific ablation.
- The reported pulse energy threshold of 1.5 nJ was assessed for scanning of 5 $\mu\text{m/s}$. The processing speeds used for cross-linking PEGda was 1-10 mm/s, which means that the exposure time to the beam was shorter by a factor of 200-2000.

To double-check this, we exposed several specimens of *C. elegans* to the focal point of the objective at the maximum intensity for 2-3 seconds. This did not lead to any quantifiable effects compared to non-exposed controls [49].

After knowing appropriate process parameters and formulation compositions to successfully fabricate microstructures in a biological surrounding, we can now bring everything together. In the next section, we will demonstrate polymerisation in the presence of a living organism of the species *C. elegans*.

14 In-Vivo writing

Parts of this section were already published in 2012 in the Journal of Biomedical Optics [49].

A conformable proof of applying 2PP in a biological surrounding requires visual evidence for the formation of a polymerised construct and an evidence for the animal being alive at the same time. Thus, as we investigate the biocompatibility via movement assays of *C. elegans* in the last chapter [200], an online process observation of a 2PP structuring procedure with an embedded *C. elegans* would combine both perspectives. However, as the animal cannot be immobilised for this purpose, the experiment places several requirements to the formulation:

- A stiff and dense polymer network is necessary, which the animal cannot easily damage.
- The viscosity must be high to limit the movement of the worm, facilitating an easier positioning and tracking without the need of the animal's immobilisation.
- The emerging polymer network must have a different refractive index compared to the uncured residue. Otherwise, it would be hard to recognise single polymer lines online.

To meet these requirements, we decided to polymerise a construct around a living *C. elegans* using a formulation containing only 50% water.

A 15 mg droplet of aqueous M9 buffer containing *C. elegans* was mixed with double concentrated PEGda based hydrogel (100% PEGda, 4 wt% WSPI) at a ratio of 1:1 rendering a formulation with 50% water content containing *C. elegans*. A woodpile structure (200x200x35 μm^3 , 10 layers at a distance of 3.5 μm , 50 polymer lines per layer) was fabricated close to the surface of a glass slide and around a living nematode. The speed was set to 10 mm/s and applied the 20x NA 0.4 objective for structuring. During fabrication, the focal point was traced through the animal's body attaching the polymer lines to the cuticle. After fabrication, the specimen was rinsed with M9 buffer. The specimen could swell for 24 hours and was afterwards observed in the LSM. The LSM pictures are depicted in Figure 92 [49].

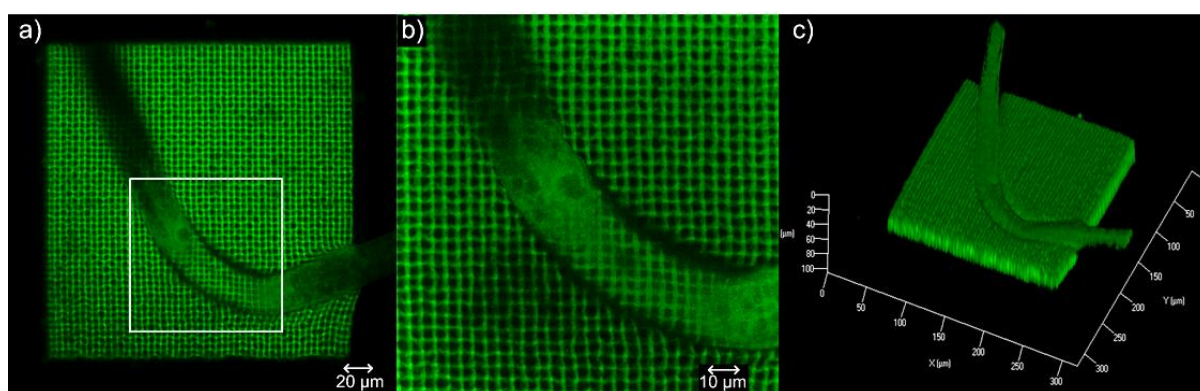


Figure 92 *C. elegans* captured in a woodpile structure with 200 μm side length (line distance 4 μm , layer distance 3.5 μm , 10 layers, writing speed 10 mm/s, laser power 220 mW, 20x NA 0.4 objective, 50% water content) a) LSM image 20x, b) detail of white marked section in a), c) stacked 3D LSM image [49]

As the polymer seems deformed in the bottom right part of Figure 92a, we can assume that the worm moved during the fabrication process and slightly deformed the structure. This indicates that the animal was alive during the fabrication and that the polymer was attached to the outer cuticle. The video of the online process observation of a slightly different structure (supplementary section of [49]) more clearly shows that *C. elegans* survives a ~15 minutes

structuring process in a PEGda formulation containing 50% water and 2 wt% WSPI. Furthermore, it gets evident that the voxel can be traced through the body of the animal without triggering any specific reactions. We can thus assume that the laser light used for structuring does not seem to affect *C. elegans*, as already claimed in the previous section.

Though it is evident that polymerisation in the presence of living organisms is more biocompatible in formulations with 80% water content (see section 13.1.3), the experiment would not clearly show a 2PP process in the presence of a living organism. A higher monomer content is necessary for visual evidence, but not for successful polymerisation in principle [49].

With this final proof-of-concept, we have reported all relevant experiments that were done during this PhD thesis. We have presented the 2PP performance of novel hydrophobic and hydrophilic PIs as well as investigated novel precursors that can potentially render biocompatible polymer constructs suitable for *in vivo* polymerisation. We have described the evaluation protocols developed for optically assessing the quality of the constructed parts. Furthermore, based on PEGda, we have introduced a protocol for toxicity analysis observing the movement of *C. elegans* and have finally attached a PEGda polymer to a living animal. However, there are yet many questions to be answered. Will Gelatine and Hyaluronan based formulations be substantially more biocompatible than PEGda? Do these materials really have properties similar to the natural ECM? Can experiments using *C. elegans* be related to experiments with cells or tissues? Will cells withstand polymerisation and adhere to the formed polymer, grow and proliferate? In other words, are there suitable materials that are bioactive rather than just biocompatible? And finally, will cells respond to dynamic cues provided by 2PP? In the final section, we will provide an outlook on possible research directions.

15 Perspectives

With the highly efficient two-photon PI WSPI dissolved in M9 at concentrations suitable for 2PP micro-fabrication, we have seen no difference in the survival of *C. elegans* compared to the reference. However, we did not investigate the impact of other initiators. Will they be more toxic? A manuscript related to the synthesis, efficiency and the biocompatibility of novel initiators referred to above will be published soon [166].

So far, we focused on the toxicity of a non-active PI in solution; however, we did not investigate the toxic influence of the initiator upon its activation and its interplay with other components during polymerisation. It is quite likely that the necessary radicals for polymerisation cause stress to living biological tissues and cells. Although the model organism in this work survived the polymerisation process and obviously did not show any reactions to the laser exposure, we must consider this issue. Especially the cells and tissues uptake of PI molecules and their subsequent activation in the polymerisation process might be problematic. We will focus on this matter in the short future. Appropriate initiator designs will potentially overcome related toxic effects.

From what is known from literature and from other research fields such as cell encapsulation studies, the natural protein based hydrogels have a very high potential for *in vivo* polymerisation. In this thesis, successful precise micro-fabrication of 3D constructs in Gelatine-based hydrogels has been shown. The same vinyl ester modification of Hyaluronic Acid has been reported and will likely perform similarly in 2PP but will be more biocompatible. However, though the biomaterials Gelatine and Hyaluronan might be well suitable, their modification for 2PP might compromise their applicability as biomaterials. Hence, the respective non-polymerised and polymerised formulations will have to show their biocompatibility first. Toxicity analysis based on MG63 cells are under way [171,174].

For conventional one-photon polymerisation, the materials properties of many presented polymers or, at least, for many components of the presented formulations have been extensively investigated [139,167,169,170]. These results cannot be directly linked to 2PP parts, as the fabrication process is entirely different. For 2PP in particular, we only have presented assessments based on the produced parts' optical appearance in this thesis. Although these protocols are easy to use and fast, their quality relies on the subjective view of the evaluator. Interpreting and concluding the results in respect to material characteristics requires experience and is often prone to speculations. A quantitative measurement that reflects material properties like elastic modulus, stiffness, hardness, strength and the like is quite difficult due to the small sizes of the structures. Klaus Cicha (IMST) has done seminal work in this field [116,181]. Similar protocols have to be developed for 2PP hydrogels, too.

As we were mostly concerned with the suitability of the materials for 2PP, we only scratched the surface of the biological assays that are required. Suitable toxicity assays for investigating the impact of initiator, monomer and laser light independently and in their interaction during polymerisation have to be developed. Furthermore, an examination of their behaviour on the formed constructs is necessary.

Ultimately, if all previous steps were successful, we can tune this environment dynamically changing the cross-linking density locally to finally get a better understanding of the cell-cell and cell-matrix interactions existent in nature.

With these perspectives, we will leave it up to following researchers to tackle *in vivo* writing up further. We hope we could convince the reader that due to its versatility and possible operation at biocompatible wavelengths, 2PP has a high potential for an application in the presence of

living organism and cells. It likely can provide a dynamic control of a biological environment, which will potentially allow building effective ECM analogues.

16 Conclusion

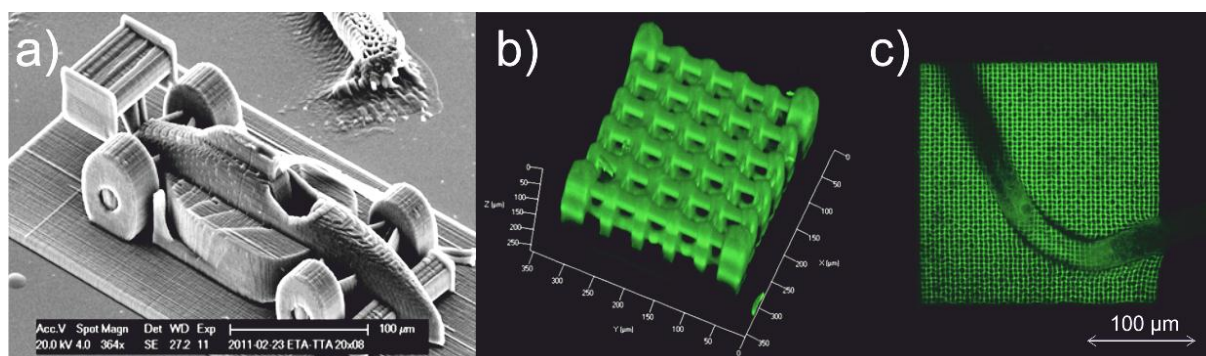


Figure 93 a) Racecar fabricated at high writing speed, ETA-TTA (1:1), 0.2 wt% Initiator M2CMK, SEM image; b) porous scaffold fabricated in formulation containing 80% water, 20% PEGda, 2 wt% initiator WSPI, stacked LSM image; c) capturing of living *Caenorhabditis elegans* in woodpile structure, PEGda formulation containing 50% water, 2 wt% WSPI, LSM image

Two-photon polymerisation (2PP) is a versatile technique that has been used to create microstructures for a variety of applications including optoelectronics, photonics and micro-mechanical devices. Since it allows an operation at biocompatible wavelengths, 2PP has a high potential to induce polymerisation in the presence of living tissues and cells, where dynamic environments similar to the natural extra-cellular matrix (ECM) can be created.

In this thesis, we wanted to get closer to achieving the goal of *in vivo* polymerisation. We dealt with two major bottlenecks of 2PP: the long process times and the limited availability of biocompatible formulations. We designed and realised a novel two-photon polymerisation (2PP) setup based on a galvano-scanner. This novel setup allowed to process a variety of formulations at the highest writing speed reported in the field of 2PP. Together with efficient photoinitiators synthesised at the Institute of Applied Synthetic Chemistry (IAS), precise microstructures could be fabricated at speeds above 100 mm/s (Figure 93a).

The water-soluble derivatives of these initiators enabled us to polymerise complex porous scaffolds in aqueous poly(ethylene glycol diacrylate) (PEGda) formulations with water contents of up to 80%, the highest water contents reported in 2PP. Such structures could be reproducibly fabricated at 1 μm resolution and writing speeds as high as 100 mm/s (Figure 93b).

As acrylate are potentially toxic for cells and tissues, we turned to vinyl ester (VE) and vinyl carbonate based formulations as biocompatible alternatives with sufficient reactivity. We report the successful modification of bioactive natural proteins like gelatine with VE units. Formulations based on these photopolymerisable precursors allowed the precise micro-fabrication of complex 3D scaffolds. Tuning the ratio in this formulation between thiols and -enes allowed us to increase the reactivity of the formulation while tuning the degradation behaviour and cross-linking density of the formed polymer.

Using *C. elegans* as model organisms, we investigated the biocompatibility of a PEGda based hydrogel formulation's individual components. The novel water-soluble initiators presented in this thesis, do not seem to affect the animals. We could perform 2PP in the presence of a living nematode. The structure was attached to the animal, which survived the fabrication process (Figure 93c).

Finally, we highlighted some potentially attractive directions and challenges materials research will face in the future to ultimately create dynamic bioinspired environments, which potential can mimic key attributes of the natural ECM.

17 Abbreviations

1PA	One-photon Absorption
1PP	One-Photon Polymerisation
2PA	Two-photon Absorption
2PM	Two-photon Microscopy
2PP	Two-photon Polymerisation
3D	Three Dimensional
3T3	Standard fibroblast cell line
4VE	Hexandioic Acid Divinyl Ester
AC	Acrylate
AM	Additive Manufacturing
AMT	Additive Manufacturing Technologies
AOM	Acousto-optic modulator
Bis-GMA	Bisphenol A-Diglycerolate Dimethacrylate
BSA	Bovine Serum Albumin
BSA-SH	Reduced BSA
<i>C. elegans</i>	<i>Caenorhabditis elegans</i> is a nematode (roundworm) and a common model organism in biological research and in toxicology
CAD	Computer Aided Design
CAD-CAM	Computer Aided Design-Computer Aided Manufacturing is a procedure, in which the design is directly transferred to manufacturing and where manufacturing problems can be simulated during design.
CCD	Charge-Coupled Device
cw	Continuous Wave
D ₃ MA	1,10-Decanediol Dimethacrylate
DLP	Digital Light Processing
DTT	Dithiothreitol
ECM	Extracellular Matrix
enes	Carbon-Carbon double bonds
ETA	Ethoxylated (20/3)-Trimethylolpropanetri Acrylate
ETA-TTA	1:1 mixture of ETA and TTA
FAD	Flavin Adenine Dinucleotide
FDA	Federal Drug Administration
fs	Femtosecond
GelMOD	Methacrylamide derivatives of Gelatine
GH	Hydrolysed Gelatine
GHve	VE derivative of Gelatine
GM	Göppert-Meyer is a unit for measuring the δ of a molecule, it is measured in $10^{-50} \text{ cm}^4 \text{ photon}^{-1}$
GND	Ground Potential of Electric Circuits
GVC	Glycerol Trivinyl Carbonate
HA	Hyaluronic Acid
HAmA	Methacrylated HA
HAVE	VE derivative of HA
IAS	Institute of Applied Synthetic Chemistry, Vienna University of Technology
IMST	Institute of Materials Science and -technology, Vienna University of Technology
IR	Infrared

LC	Lethal Concentration is a statistically calculated concentration of a substance causing death to exposed animals after the investigation period.
LC ₀	LC for a survival rate of 100%
LC ₅₀	LC for a survival rate of 50%
LM	Light Microscope
LSM	Laser Scanning Microscope
LZH	Laser Zentrum Hannover
M3DL	Micro three-dimensional structuring device
M9	Aqueous buffer media used to maintain nematodes of the species <i>C. elegans</i>
MA	Methacrylate
MG63	Human Osteosarcoma Cell Line
Mw	Molecular Weight
NA	Numerical Aperture
Nd:YAG	Neodymium Doped Yttrium Aluminium Garnet
Nd:YLF	Yttrium Lithium Fluoride
NIR	Near Infrared
PEG	Poly(Ethylene Glycol)
PEGda	PEG diacrylate
PEGdma	PEG dimethacrylate
PEGdve	PEG divinyl ester
PI	photoinitiator
RGD	Arginine-Glycine-Aspartic acid
SEM	Scanning Electron Microscope
SESAM	Semi-saturable absorber mirror
SLA	Stereolithography
STL format	is a data interface that approximates a 3D object's surface via triangles. It is commonly used in AMT
Ti:Sa	Titanium Sapphire
TTA	Trimethylolpropanetriacrylate
TTL	Transistor-Transistor Logic
UDMA	Diurethane Dimethacrylate
UV	Ultraviolet
VC	Vinyl Carbonate
VE	Vinyl Ester
VIS	Visible
Voxel	A Volumetric Pixel is the basic building unit in 2PP
δ	The 2PA cross-section δ is an efficiency measure for a molecule's ability for two-photon absorption.

18 Literature

- [1] Gebhardt A. Generative Fertigungsverfahren: Rapid Prototyping - Rapid Tooling - Rapid Manufacturing. Hanser Verlag; 2007.
- [2] Stampfl J, Baudis S, Heller C, Liska R, Neumeister A, Kling R, Ostendorf A, Spitzbart M. Photopolymers with tunable mechanical properties processed by laser-based high-resolution stereolithography. *Journal of Micromechanics and Microengineering* 2008;18:125014.
- [3] Stampfl J, Liska R. Polymerizable Hydrogels for Rapid Prototyping: Chemistry, Photolithography, and Mechanical Properties. In: Bártolo PJ, herausgeber. *Stereolithography*, Boston, MA: Springer US; 2011, S. 161–82.
- [4] Nič M, Jirát J, Košata B, Jenkins A, McNaught A, herausgeber. *modulus of elasticity*, E. IUPAC Compendium of Chemical Terminology, Research Triangle Park, NC: IUPAC; o. J.
- [5] Liao H, Munoz-Pinto D, Qu X, Hou Y, Grunlan MA, Hahn MS. Influence of hydrogel mechanical properties and mesh size on vocal fold fibroblast extracellular matrix production and phenotype. *Acta Biomaterialia* 2008;4:1161–71.
- [6] Heller C. Biocompatible and Biodegradable Photopolymers by Additive Manufacturing: From Synthesis to In-Vivo Studies. Vienna University of Technology, 2010.
- [7] Decker C. The use of UV irradiation in polymerization. *Polymer International* 1998;45:133–41.
- [8] Ovsianikov A, Mironov V, Stampfl J, Liska R. Engineering 3D cell-culture matrices: multiphoton processing technologies for biological & tissue engineering applications. *Expert Review of Medical Devices* 2012:1–21.
- [9] Bártolo PJ. *Stereolithography: materials, processes and applications*. New York: Springer; 2011.
- [10] Pucher N. Synthesis and evaluation of novel initiators for the two-photon induced photopolymerization process - a precise tool for real 3D sub-micrometer laser structuring. Vienna, Austria: TUW; 2010.
- [11] Torgersen J. *In-vivo-writing using two-photon-lithography*. Vienna, Austria: Vienna University of Technology; 2010.
- [12] Melchels FPW, Feijen J, Grijpma DW. A review on stereolithography and its applications in biomedical engineering. *Biomaterials* 2010;31:6121–30.
- [13] Felzmann R, Gruber S, Mitteramskogler G, Tesavibul P, Boccaccini AR, Liska R, Stampfl J. Lithography-Based Additive Manufacturing of Cellular Ceramic Structures. *Advanced Engineering Materials* 2012;14:1052–8.
- [14] Passinger S. *Two-photon Polymerization and Application to Surface Plasmon Polaritons*. Cuvillier Verlag; 2008.
- [15] Haske W, Chen VW, Hales JM, Dong W, Barlow S, Marder SR, Perry JW. 65 nm feature sizes using visible wavelength 3-D multiphoton lithography. *Opt Express* 2007;15:3426–36.
- [16] Göppert-Mayer M. Über Elementarakte mit zwei Quantensprüngen. *Annalen Der Physik* 1931;401:273–94.
- [17] Kaiser W, Garrett CGB. Two-Photon Excitation in CaF_2 : Eu^{2+} . *Phys. Rev. Lett.* 1961;7:229–31.
- [18] Lee K-S, Kim RH, Yang D-Y, Park SH. Advances in 3D nano/microfabrication using two-photon initiated polymerization. *Progress in Polymer Science* 2008;33:631–81.
- [19] Zipfel WR, Williams RM, Webb WW. Nonlinear magic: multiphoton microscopy in the biosciences. *Nature Biotechnology* 2003;21:1369–77.
- [20] Reinhardt BA, Brott LL, Clarson SJ, Dillard AG, Bhatt JC, Kannan R, Yuan L, He GS, Prasad PN. Highly Active Two-Photon Dyes: Design, Synthesis, and Characterization toward Application. *Chem. Mater.* 1998;10:1863–74.
- [21] Pawlicki M, Collins HA, Denning RG, Anderson HL. Zweiphotonenabsorption und das Design von Zweiphotonenfarbstoffen. *Angewandte Chemie* 2009;121:3292–316.

- [22] Atkins PW. Atkins' Physical chemistry. 7th ed. Oxford ; New York: Oxford University Press; 2002.
- [23] Amos B. Multiple-photon Excitation Fluorescence Microscopy | LOCI. Laboratory for Optical and Computational Instrumentation (LOCI) web site 2012.
- [24] Spangler CW. Recent development in the design of organic materials for optical power limiting. *Journal of Materials Chemistry* 1999;9:2013–20.
- [25] He GS, Gvishi R, Prasad PN, Reinhardt BA. Two-photon absorption based optical limiting and stabilization in organic molecule-doped solid materials. *Optics Communications* 1995;117:133–6.
- [26] Mukherjee A. Two-photon pumped upconverted lasing in dye doped polymer waveguides. *Applied Physics Letters* 1993;62:3423–5.
- [27] Dvornikov AS, Rentzepis PM. Accessing 3D memory information by means of nonlinear absorption. *Optics Communications* 1995;119:341–6.
- [28] Agate B, Brown C, Sibbett W, Dholakia K. Femtosecond optical tweezers for in-situ control of two-photon fluorescence. *Opt. Express* 2004;12:3011–7.
- [29] Lin T-C, Chung S-J, Kim K-S, Wang X, He GS, Swiatkiewicz J, Pudavar HE, Prasad PN. Organics and Polymers with High Two-Photon Activities and their Applications. In: Lee K-S, herausgeber. *Polymers for Photonics Applications II*, vol. 161, Berlin, Heidelberg: Springer Berlin Heidelberg; o. J., S. 157–93.
- [30] He GS, Signorini R, Prasad PN. Two-Photon-Pumped Frequency-Upconverted Blue Lasing in Coumarin Dye Solution. *Appl. Opt.* 1998;37:5720–6.
- [31] Pudavar HE, Joshi MP, Prasad PN, Reinhardt BA. High-density three-dimensional optical data storage in a stacked compact disk format with two-photon writing and single photon readout. *Applied Physics Letters* 1999;74:1338–40.
- [32] Watanabe W, Arakawa N, Matsunaga S, Higashi T, Fukui K, Isobe K, Itoh K. Femtosecond laser disruption of subcellular organelles in a living cell. *Opt. Express* 2004;12:4203–13.
- [33] Shen N, Datta D, Schaffer CB, LeDuc P, Ingber DE, Mazur E. Ablation of cytoskeletal filaments and mitochondria in live cells using a femtosecond laser nanoscissor. *Mechanics chemistry of biosystems MCB* 2005;2:17–25.
- [34] Yanik MF, Cinar H, Cinar HN, Chisholm AD, Jin Y, Ben-Yakar A. Neurosurgery: Functional regeneration after laser axotomy. *Nature* 2004;432:822–822.
- [35] Denk W, Strickler J, Webb W. Two-photon laser scanning fluorescence microscopy. *Science* 1990;248:73–6.
- [36] Helmchen F, Denk W. Deep tissue two-photon microscopy. *Nat. Methods* 2005;2:932–40.
- [37] Dunn KW, Sandoval RM, Kelly KJ, Dagher PC, Tanner GA, Atkinson SJ, Bacallao RL, Molitoris BA. Functional studies of the kidney of living animals using multicolor two-photon microscopy. *Am J Physiol Cell Physiol* 2002;283:C905–C916.
- [38] Sun H-B, Kawata S. Two-Photon Photopolymerization and 3D Lithographic Microfabrication. *NMR • 3D Analysis • Photopolymerization*, Springer Berlin Heidelberg; 2004, S. 169–273.
- [39] Ovsianikov A, Viertl J, Chichkov B, Oubaha M, MacCraith B, Sakellari I, Giakoumaki A, Gray D, Vamvakaki M, Farsari M, Fotakis C. Ultra-Low Shrinkage Hybrid Photosensitive Material for Two-Photon Polymerization Microfabrication. *ACS Nano* 2008;2:2257–62.
- [40] Serbin J, Egbert A, Ostendorf A, Chichkov BN, Houbertz R, Domann G, Schulz J, Cronauer C, Fröhlich L, Popall M. Femtosecond laser-induced two-photon polymerization of inorganic organic hybrid materials for applications in photonics. *Opt. Lett.* 2003;28:301–3.
- [41] Seet KK, Mizeikis V, Juodkasis S, Misawa H. Spiral three-dimensional photonic crystals for telecommunications spectral range. *Appl. Phys. A* 2006;82:683–8.
- [42] Schizas C, Melissinaki V, Gaidukeviciute A, Reinhardt C, Ohrt C, Dedoussis V, Chichkov BN, Fotakis C, Farsari M, Karalekas D. On the design and fabrication by two-photon polymerization of a readily assembled micro-valve. *Int J Adv Manuf Technol* 2010;48:435–41.

- [43] Maruo S, Inoue H. Optically driven micropump produced by three-dimensional two-photon microfabrication. *Applied Physics Letters* 2006;89:144101–144101–3.
- [44] Matsuo S, Kiyama S, Shichijo Y, Tomita T, Hashimoto S, Hosokawa Y, Masuhara H. Laser microfabrication and rotation of ship-in-a-bottle optical rotators. *Applied Physics Letters* 2008;93:051107.
- [45] Maruo S, Ikuta K. Submicron stereolithography for the production of freely movable mechanisms by using single-photon polymerization. *Sensors and Actuators A: Physical* 2002;100:70–6.
- [46] Stadlmann K. Fabrication of Optical Interconnects with Two Photon Polymerization. *Proceedings of LPM 2010- The 11th International Symposium on Laser Precision Microfabrcation*, vol. 10, Stuttgart: K. Sugioka; 2010, S. 6.
- [47] Stampfl J, Inführ R, Stadlmann K, Pucher N, Lichtenegger H, Schmidt V, Liska R. Materials for the fabrication of optical waveguides with two photon photopolymerization. *Lasers in Manufacturing 2009*, vol. S., Munich, Germany: A. Ostendorf; 2009, S. P1–P4.
- [48] Krivec S, Matsko N, Satzinger V, Pucher N, Galler N, Koch T, Schmidt V, Grogger W, Liska R, Lichtenegger HC. Silica-Based, Organically Modified Host Material for Waveguide Structuring by Two-Photon-Induced Photopolymerization. *Advanced Functional Materials* 2010;20:811–9.
- [49] Torgersen J, Ovsianikov A, Mironov V, Pucher N, Qin X, Li Z, Cicha K, Machacek T, Liska R, Jantsch V, Stampfl J. Photo-sensitive hydrogels for three-dimensional laser microfabrication in the presence of whole organisms. *Journal of Biomedical Optics* 2012;17:105008–105008.
- [50] Torgersen J, Xiao-Hua Q, Zhiquan L, Ovsianikov A, Gruber P, Liska R, Stampfl J. Hydrogels for two-photon polymerization: a toolbox for mimicking the extracellular matrix. *Advanced Functional Materials* 2013;accepted.
- [51] Fairbanks BD, Schwartz MP, Halevi AE, Nuttelman CR, Bowman CN, Anseth KS. A Versatile Synthetic Extracellular Matrix Mimic via Thiol-Norbornene Photopolymerization. *Advanced Materials* 2009;21:5005–10.
- [52] Tibbitt MW, Kloxin AM, Dyamenahalli KU, Anseth KS. Controlled two-photon photodegradation of PEG hydrogels to study and manipulate subcellular interactions on soft materials. *Soft Matter* 2010;6:5100–8.
- [53] Allen R, Nielson R, Wise DD, Shear JB. Catalytic Three-Dimensional Protein Architectures. *Analytical Chemistry* 2005;77:5089–95.
- [54] DeForest CA, Anseth KS. Photoreversible Patterning of Biomolecules within Click-Based Hydrogels. *Angewandte Chemie* 2012;124:1852–5.
- [55] Mohr PJ, Taylor BN, Newell DB. CODATA Recommended Values of the Fundamental Physical Constants: 2006. arXiv:0801.0028 2007.
- [56] Sheik-Bahae M, Said AA, Wei T-H, Hagan DJ, Van Stryland EW. Sensitive measurement of optical nonlinearities using a single beam. *IEEE Journal of Quantum Electronics* 1990;26:760–769.
- [57] Birge RR, Pierce BM. Semiclassical time-dependent theory of two-photon spectroscopy. The effect of dephasing in the virtual level on the two-photon excitation spectrum of isotachysterol. *International Journal of Quantum Chemistry* 1986;29:639–56.
- [58] Mongin O, Porrès L, Charlot M, Katan C, Blanchard-Desce M. Synthesis, fluorescence, and two-photon absorption of a series of elongated rodlike and banana-shaped quadrupolar fluorophores: a comprehensive study of structure-property relationships. *Chemistry* 2007;13:1481–98.
- [59] Sun H-B, Kawata S. Two-photon laser precision microfabrication and its applications to micro-nano devices and systems. *Journal of Lightwave Technology* 2003;21:624–633.
- [60] Liu Y, Dong X, Sun J, Zhong C, Li B, You X, Liu B, Liu Z. Two-photon fluorescent probe for cadmium imaging in cells. *The Analyst* 2012;137:1837.
- [61] Hayek A, Bolze F, Nicoud J-F, Baldeck PL, Mély Y. Synthesis and characterization of water-soluble two-photon excited blue fluorescent chromophores for bioimaging. *Photochemical & Photobiological Sciences* 2006;5:102–6.

- [62] Lu Y, Hasegawa F, Goto T, Ohkuma S, Fukuhara S, Kawazu Y, Totani K, Yamashita T, Watanabe T. Highly sensitive measurement in two-photon absorption cross section and investigation of the mechanism of two-photon-induced polymerization. *Journal of Luminescence* 2004;110:1–10.
- [63] Campagnola PJ, Delguidice DM, Epling GA, Hoffacker KD, Howell AR, Pitts JD, Goodman SL. 3-dimensional submicron polymerization of acrylamide by multiphoton excitation of xanthene dyes. *Macromolecules* 2000;33:1511–3.
- [64] Paschotta R. *Encyclopedia of laser physics and technology*. Weinheim: Wiley-VCH; 2008.
- [65] Krueger A. *Getting Practical*. SPIE Newsroom 2004.
- [66] Weinberger P. John Kerr and his effects found in 1877 and 1878. *Philosophical Magazine Letters* 2008;88:897–907.
- [67] *Encyclopedia of physics*. 2nd ed. New York: VCH; 1991.
- [68] Patterson J, Martino MM, Hubbell JA. Biomimetic materials in tissue engineering. *Materials Today* 2010;13:14–22.
- [69] Kleinman HK, Philp D, Hoffman MP. Role of the extracellular matrix in morphogenesis. *Current Opinion in Biotechnology* 2003;14:526–32.
- [70] Drury JL, Mooney DJ. Hydrogels for tissue engineering: scaffold design variables and applications. *Biomaterials* 2003;24:4337–51.
- [71] Melchels FPW, Domingos MAN, Klein TJ, Malda J, Bartolo PJ, Hutmacher DW. Additive manufacturing of tissues and organs. *Progress in Polymer Science* 2012;37:1079–104.
- [72] Liu X, Ma PX. Polymeric Scaffolds for Bone Tissue Engineering. *Annals of Biomedical Engineering* 2004;32:477–86.
- [73] Mikos AG, Lyman MD, Freed LE, Langer R. Wetting of poly(l-lactic acid) and poly(dl-lactic-co-glycolic acid) foams for tissue culture. *Biomaterials* 1994;15:55–8.
- [74] Hoffman AS. Hydrogels for biomedical applications. *Advanced Drug Delivery Reviews* 2012.
- [75] Peppas NA, Hilt JZ, Khademhosseini A, Langer R. Hydrogels in Biology and Medicine: From Molecular Principles to Bionanotechnology. *Advanced Materials* 2006;18:1345–60.
- [76] Lih E, Lee JS, Park KM, Park KD. Rapidly curable chitosan–PEG hydrogels as tissue adhesives for hemostasis and wound healing. *Acta Biomaterialia* 2012;8:3261–9.
- [77] Tomatsu I, Peng K, Kros A. Photoresponsive hydrogels for biomedical applications. *Advanced Drug Delivery Reviews* 2011;63:1257–66.
- [78] Burdick JA, Anseth KS. Photoencapsulation of osteoblasts in injectable RGD-modified PEG hydrogels for bone tissue engineering. *Biomaterials* 2002;23:4315–23.
- [79] Young C-D, Wu J-R, Tsou T-L. High-strength, ultra-thin and fiber-reinforced pHEMA artificial skin. *Biomaterials* 1998;19:1745–52.
- [80] Kobayashi M, Toguchida J, Oka M. Development of the shields for tendon injury repair using polyvinyl alcohol - Hydrogel (PVA-H). *Journal of Biomedical Materials Research* 2001;58:344–51.
- [81] Elisseeff J, McIntosh W, Anseth K, Riley S, Ragan P, Langer R. Photoencapsulation of chondrocytes in poly(ethylene oxide)-based semi- interpenetrating networks. *Journal of Biomedical Materials Research* 2000;51:164–71.
- [82] Bryant SJ, Anseth KS. The effects of scaffold thickness on tissue engineered cartilage in photocrosslinked poly(ethylene oxide) hydrogels. *Biomaterials* 2001;22:619–26.
- [83] Nicodemus GD, Bryant SJ. Cell Encapsulation in Biodegradable Hydrogels for Tissue Engineering Applications. *Tissue Engineering. Part B, Reviews* 2008;14:149–65.
- [84] Chan V, Zorlutuna P, Jeong JH, Kong H, Bashir R. Three-dimensional photopatterning of hydrogels using stereolithography for long-term cell encapsulation. *Lab on a Chip* 2010;10:2062.
- [85] Melchels FPW, Feijen J, Grijpma DW. A review on stereolithography and its applications in biomedical engineering. *Biomaterials* 2010;31:6121–30.
- [86] Leong KF, Cheah CM, Chua CK. Solid freeform fabrication of three-dimensional scaffolds for engineering replacement tissues and organs. *Biomaterials* 2003;24:2363–78.

- [87] Shu XZ, Ahmad S, Liu Y, Prestwich GD. Synthesis and evaluation of injectable, in situ crosslinkable synthetic extracellular matrices for tissue engineering. *Journal of Biomedical Materials Research Part A* 2006;79A:902–12.
- [88] Ahmed TAE, Griffith M, Hincke M. Characterization and inhibition of fibrin hydrogel-degrading enzymes during development of tissue engineering scaffolds. *Tissue Engineering* 2007;13:1469–77.
- [89] Balakrishnan B, Jayakrishnan A. Self-cross-linking biopolymers as injectable in situ forming biodegradable scaffolds. *Biomaterials* 2005;26:3941–51.
- [90] Chenite A, Chaput C, Wang D, Combes C, Buschmann M, Hoemann C, Leroux J, Atkinson B, Binette F, Selmani A. Novel injectable neutral solutions of chitosan form biodegradable gels in situ. *Biomaterials* 2000;21:2155–61.
- [91] Horn EM, Beaumont M, Shu XZ, Harvey A, Prestwich GD, Horn KM, Gibson AR, Preul MC, Panitch A. Influence of cross-linked hyaluronic acid hydrogels on neurite outgrowth and recovery from spinal cord injury. *Journal of Neurosurgery: Spine* 2007;6:133–40.
- [92] Stosich MS, Mao JJ. Adipose tissue engineering from human adult stem cells: clinical implications in plastic and reconstructive surgery. *Plastic and reconstructive surgery* 2007;119:71–83; Discussion 84–85.
- [93] Dadsetan M, Szatkowski JP, Yaszemski MJ, Lu L. Characterization of photo-cross-linked oligo[poly(ethylene glycol) fumarate] hydrogels for cartilage tissue engineering. *Biomacromolecules* 2007;8:1702–9.
- [94] Qiu Y, Park K. Environment-sensitive hydrogels for drug delivery. *Advanced Drug Delivery Reviews* 2001;53:321–39.
- [95] Liu Y, Shu XZ, Prestwich GD. Osteochondral defect repair with autologous bone marrow-derived mesenchymal stem cells in an injectable, in situ, cross-linked synthetic extracellular matrix. *Tissue Engineering* 2006;12:3405–16.
- [96] Desai ES, Tang MY, Ross AE, Gemeinhart RA. Critical factors affecting cell encapsulation in superporous hydrogels. *Biomedical Materials* 2012;7:024108.
- [97] Miller JS, Stevens KR, Yang MT, Baker BM, Nguyen D-HT, Cohen DM, Toro E, Chen AA, Galie PA, Yu X, Chaturvedi R, Bhatia SN, Chen CS. Rapid casting of patterned vascular networks for perfusable engineered three-dimensional tissues. *Nature Materials* 2012;11:768–74.
- [98] Lu Y, Mapili G, Suhali G, Chen S, Roy K. A digital micro-mirror device-based system for the microfabrication of complex, spatially patterned tissue engineering scaffolds. *Journal of biomedical materials research. Part A* 2006;77:396–405.
- [99] Arcaute K, Mann BK, Wicker RB. Stereolithography of three-dimensional bioactive poly(ethylene glycol) constructs with encapsulated cells. *Annals of biomedical engineering* 2006;34:1429–41.
- [100] Lin H, Zhang D, Alexander PG, Yang G, Tan J, Cheng AW-M, Tuan RS. Application of visible light-based projection stereolithography for live cell-scaffold fabrication with designed architecture. *Biomaterials* 2013;34:331–9.
- [101] Kim K, Yeatts A, Dean D, Fisher JP. Stereolithographic Bone Scaffold Design Parameters: Osteogenic Differentiation and Signal Expression. *Tissue Engineering. Part B, Reviews* 2010;16:523–39.
- [102] Khademhosseini A, Langer R. Microengineered hydrogels for tissue engineering. *Biomaterials* 2007;28:5087–92.
- [103] Melchels FPW, Tonnarelli B, Olivares AL, Martin I, Lacroix D, Feijen J, Wendt DJ, Grijpma DW. The influence of the scaffold design on the distribution of adhering cells after perfusion cell seeding. *Biomaterials* 2011;32:2878–84.
- [104] Moroni L, Schotel R, Hamann D, De Wijn JR, Van Blitterswijk CA. 3D Fiber-Deposited Electrospun Integrated Scaffolds Enhance Cartilage Tissue Formation. *Advanced Functional Materials* 2008;18:53–60.
- [105] Kino-Oka M, Maeda Y, Yamamoto T, Sugawara K, Taya M. A kinetic modeling of chondrocyte culture for manufacture of tissue-engineered cartilage. *Journal of bioscience and bioengineering* 2005;99:197–207.
- [106] Stankus JJ, Guan J, Fujimoto K, Wagner WR. Microintegrating smooth muscle cells into a biodegradable, elastomeric fiber matrix. *Biomaterials* 2006;27:735–44.

- [107] Schuurman W, Khristov V, Pot MW, Van Weeren PR, Dhert WJA, Malda J. Bioprinting of hybrid tissue constructs with tailorable mechanical properties. *Biofabrication* 2011;3:021001.
- [108] Rezende RA, Azevedo F de S, Pereira FD, Kasyanov V, Wen X, De Silva JVL, Mironov V. Nanotechnological Strategies for Biofabrication of Human Organs. *Journal of Nanotechnology* 2012;2012:1–10.
- [109] Spivey EC, Khaing ZZ, Shear JB, Schmidt CE. The fundamental role of subcellular topography in peripheral nerve repair therapies. *Biomaterials* 2012;33:4264–76.
- [110] Sinha RP, Häder DP. UV-induced DNA damage and repair: a review. *Photochem. Photobiol. Sci.* 2002;1:225–36.
- [111] Vogel A, Venugopalan V. Mechanisms of Pulsed Laser Ablation of Biological Tissues. *Chemical Reviews* 2003;103:577–644.
- [112] Leitz G, Fällman E, Tuck S, Axner O. Stress response in *Caenorhabditis elegans* caused by optical tweezers: wavelength, power, and time dependence. *Biophysical Journal* 2002;82:2224–31.
- [113] Shen N, Datta D, Schaffer CB, LeDuc P, Ingber DE, Mazur E. Ablation of cytoskeletal filaments and mitochondria in live cells using a femtosecond laser nanoscissor. *Mechanics chemistry of biosystems MCB* 2005;2:17–25.
- [114] Tibbitt MW, Kloxin AM, Dyamenahalli KU, Anseth KS. Controlled two-photon photodegradation of PEG hydrogels to study and manipulate subcellular interactions on soft materials. *Soft Matter* 2010;6:5100–8.
- [115] Doraiswamy A, Jin C, Narayan RJ, Mageswaran P, Mente P, Modi R, Auyeung R, Chrisey DB, Ovsianikov A, Chichkov B. Two photon induced polymerization of organic–inorganic hybrid biomaterials for microstructured medical devices. *Acta Biomaterialia* 2006;2:267–75.
- [116] Cicha K, Li Z, Stadlmann K, Ovsianikov A, Markut-Kohl R, Liska R, Stampfl J. Evaluation of 3D structures fabricated with two-photon-photopolymerization by using FTIR spectroscopy. *Journal of Applied Physics* 2011;110:064911–064911–5.
- [117] Ovsianikov A, Schlie S, Ngezahayo A, Haverich A, Chichkov BN. Two-photon polymerization technique for microfabrication of CAD-designed 3D scaffolds from commercially available photosensitive materials. *Journal of Tissue Engineering and Regenerative Medicine* 2007;1:443–9.
- [118] Klein F, Striebel T, Fischer J, Jiang Z, Franz CM, Von Freymann G, Wegener M, Bastmeyer M. Elastic Fully Three-dimensional Microstructure Scaffolds for Cell Force Measurements. *Advanced Materials* 2010;22:868–71.
- [119] Schafer KJ, Hales JM, Balu M, Belfield KD, Van Stryland EW, Hagan DJ. Two-photon absorption cross-sections of common photoinitiators. *Journal of Photochemistry and Photobiology A: Chemistry* 2004;162:497–502.
- [120] Huang S, Heikal AA, Webb WW. Two-Photon Fluorescence Spectroscopy and Microscopy of NAD(P)H and Flavoprotein. *Biophysical Journal* 2002;82:2811–25.
- [121] Weiß T, Schade R, Laube T, Berg A, Hildebrand G, Wyrwa R, Schnabelrauch M, Liefelth K. Two-Photon Polymerization of Biocompatible Photopolymers for Microstructured 3D Biointerfaces. *Advanced Engineering Materials* 2011;13:B264–B273.
- [122] Ovsianikov A, Gruene M, Pflaum M, Koch L, Maiorana F, Wilhelmi M, Haverich A, Chichkov B. Laser printing of cells into 3D scaffolds. *Biofabrication* 2010;2:014104.
- [123] Ovsianikov A, Malinauskas M, Schlie S, Chichkov BN, Gittard S, Narayan R, Löbner M, Sternberg K, Schmitz K-P, Haverich A. Three-dimensional laser micro- and nano-structuring of acrylated poly(ethylene glycol) materials and evaluation of their cytotoxicity for tissue engineering applications. *Acta Biomater* 2011;7:967–74.
- [124] Spivey EC, Ritschdorff ET, Connell JL, McLennon CA, Schmidt CE, Shear JB. Multiphoton Lithography of Unconstrained Three-Dimensional Protein Microstructures. *Advanced Functional Materials* 2012:n/a–n/a.
- [125] Jhaveri SJ, McMullen JD, Sijbesma R, Tan L-S, Zipfel W, Ober CK. Direct Three-Dimensional Microfabrication of Hydrogels via Two-Photon Lithography in Aqueous Solution. *Chem. Mater.* 2009;21:2003–6.

- [126] Ovsianikov A, Deiwick A, Van Vlierberghe S, Pflaum M, Wilhelmi M, Dubruel P, Chichkov B. Laser Fabrication of 3D Gelatin Scaffolds for the Generation of Bioartificial Tissues. *Materials* 2011;4:288–99.
- [127] Farsari M, Filippidis G, Sambani K, Drakakis TS, Fotakis C. Two-photon polymerization of an Eosin Y-sensitized acrylate composite. *Journal of Photochemistry and Photobiology A: Chemistry* 2006;181:132–5.
- [128] Pitts JD, Campagnola PJ, Epling GA, Goodman SL. Submicron Multiphoton Free-Form Fabrication of Proteins and Polymers: Studies of Reaction Efficiencies and Applications in Sustained Release. *Macromolecules* 2000;33:1514–23.
- [129] Basu S, Rodionov V, Terasaki M, Campagnola PJ. Multiphoton-excited microfabrication in live cells via Rose Bengalcross-linking of cytoplasmic proteins. *Opt. Lett.* 2005;30:159–61.
- [130] Wan X, Zhao Y, Xue J, Wu F, Fang X. Water-soluble benzylidene cyclopentanone dye for two-photon photopolymerization. *Journal of Photochemistry and Photobiology A: Chemistry* 2009;202:74–9.
- [131] Seidlits SK, Schmidt CE, Shear JB. High-Resolution Patterning of Hydrogels in Three Dimensions using Direct-Write Photofabrication for Cell Guidance. *Advanced Functional Materials* 2009;19:3543–51.
- [132] Pitts JD, Howell AR, Taboada R, Banerjee I, Wang J, Goodman SL, Campagnola PJ. New Photoactivators for Multiphoton Excited Three-dimensional Submicron Cross-linking of Proteins: Bovine Serum Albumin and Type 1 Collagen. *Photochemistry and Photobiology* 2002;76:135–44.
- [133] Li Z, Siklos M, Pucher N, Cicha K, Ajami A, Husinsky W, Rosspeintner A, Vauthey E, Gescheidt G, Stampfl J, Liska R. Synthesis and structure-activity relationship of several aromatic ketone-based two-photon initiators. *Journal of Polymer Science Part A: Polymer Chemistry* 2011;49:3688–99.
- [134] Burdick JA, Prestwich GD. Hyaluronic Acid Hydrogels for Biomedical Applications. *Advanced Materials* 2011;23:H41–H56.
- [135] Weiß T, Hildebrand G, Schade R, Liefelth K. Two-Photon polymerization for microfabrication of three-dimensional scaffolds for tissue engineering application. *Engineering in Life Sciences* 2009;9:384–90.
- [136] LaFratta CN, Fourkas JT, Baldacchini T, Farrer RA. Multiphoton Fabrication. *Angewandte Chemie International Edition* 2007;46:6238–58.
- [137] Bryant SJ, Anseth KS. Controlling the spatial distribution of ECM components in degradable PEG hydrogels for tissue engineering cartilage. *Journal of Biomedical Materials Research Part A* 2003;64A:70–9.
- [138] Drury JL, Mooney DJ. Hydrogels for tissue engineering: scaffold design variables and applications. *Biomaterials* 2003;24:4337–51.
- [139] Nguyen QT, Hwang Y, Chen AC, Varghese S, Sah RL. Cartilage-like mechanical properties of poly (ethylene glycol)-diacrylate hydrogels. *Biomaterials* 2012;33:6682–90.
- [140] Berg A, Wyrwa R, Weisser J, Weiss T, Schade R, Hildebrand G, Liefelth K, Schneider B, Ellinger R, Schnabelrauch M. Synthesis of Photopolymerizable Hydrophilic Macromers and Evaluation of Their Applicability as Reactive Resin Components for the Fabrication of Three-Dimensionally Structured Hydrogel Matrices by 2-Photon-Polymerization. *Advanced Engineering Materials* 2011;13:B274–B284.
- [141] Hoffmann JC, West JL. Three-dimensional photolithographic patterning of multiple bioactive ligands in poly(ethylene glycol) hydrogels. *Soft Matter* 2010;6:5056–63.
- [142] Santos E, Orive G, Hernández RM, Pedranz JL. Cell-Biomaterial Interaction: Strategies to Mimic The Extracellular Matrix. In: Pramatarova L, herausgeber. *On biomimetics*, Rijeka, Croatia: InTech; 2011.
- [143] Lee S-H, Moon JJ, West JL. Three-dimensional micropatterning of bioactive hydrogels via two-photon laser scanning photolithography for guided 3D cell migration. *Biomaterials* 2008;29:2962–8.
- [144] Leslie-Barbick JE, Shen C, Chen C, West JL. Micron-scale spatially patterned, covalently immobilized vascular endothelial growth factor on hydrogels accelerates

- endothelial tubulogenesis and increases cellular angiogenic responses. *Tissue engineering. Part A* 2011;17:221–9.
- [145] Kloxin AM, Kasko AM, Salinas CN, Anseth KS. Photodegradable hydrogels for dynamic tuning of physical and chemical properties. *Science* 2009;324:59–63.
 - [146] DeForest CA, Anseth KS. Cytocompatible click-based hydrogels with dynamically tunable properties through orthogonal photoconjugation and photocleavage reactions. *Nature Chemistry* 2011;3:925–31.
 - [147] Lasagni AF, Yuan D, Shao P, Das S. Periodic Micropatterning of Polyethylene Glycol Diacrylate Hydrogel by Laser Interference Lithography Using Nano- and Femtosecond Pulsed Lasers. *Advanced Engineering Materials* 2009;11:B20–B24.
 - [148] Gittard SD, Ovsianikov A, Akar H, Chichkov B, Monteiro-Riviere NA, Stafslien S, Chisholm B, Shin C-C, Shih C-M, Lin S-J, Su Y-Y, Narayan RJ. Two Photon Polymerization-Micromolding of Polyethylene Glycol-Gentamicin Sulfate Microneedles. *Advanced Engineering Materials* 2010;12:B77–B82.
 - [149] Ovsianikov A, Deiwick A, Van Vlierberghe S, Dubruel P, Möller L, Dräger G, Chichkov BN. Laser Fabrication of Three-Dimensional CAD Scaffolds from Photosensitive Gelatin for Applications in Tissue Engineering. *Biomacromolecules* 2011;12:851–8.
 - [150] Ritschdorff ET, Nielson R, Shear JB. Multi-focal multiphoton lithography. *Lab on a Chip* 2012;12:867–71.
 - [151] Kaehr B, Shear JB. Multiphoton fabrication of chemically responsive protein hydrogels for microactuation. *Proceedings of the National Academy of Sciences* 2008;105:8850–4.
 - [152] Harper JC, Brozik SM, Brinker CJ, Kaehr B. Biocompatible Microfabrication of 3D Isolation Chambers for Targeted Confinement of Individual Cells and Their Progeny. *Analytical Chemistry* 2012;84:8985–9.
 - [153] Kaehr B, Allen R, Javier DJ, Currie J, Shear JB. Guiding neuronal development with in situ microfabrication. *Proceedings of the National Academy of Sciences of the United States of America* 2004;101:16104–8.
 - [154] Kuetemeyer K, Kensah G, Heidrich M, Meyer H, Martin U, Gruh I, Heisterkamp A. Two-photon induced collagen cross-linking in bioartificial cardiac tissue. *Optics Express* 2011;19:15996–6007.
 - [155] Cunningham LP, Veilleux MP, Campagnola PJ. Freeform multiphoton excited microfabrication for biological applications using a rapid prototyping CAD-based approach. *Optics Express* 2006;14:8613–21.
 - [156] Basu S, Campagnola PJ. Properties of crosslinked protein matrices for tissue engineering applications synthesized by multiphoton excitation. *Journal of Biomedical Materials Research Part A* 2004;71A:359–68.
 - [157] Hawkins JW, Dugaiczky A. The human serum albumin gene: structure of a unique locus. *Gene* 1982;19:55–8.
 - [158] Fancy DA, Kodadek T. Chemistry for the analysis of protein–protein interactions: Rapid and efficient cross-linking triggered by long wavelength light. *Proceedings of the National Academy of Sciences* 1999;96:6020–4.
 - [159] Basu S, Cunningham LP, Pins GD, Bush KA, Taboada R, Howell AR, Wang J, Campagnola PJ. Multiphoton Excited Fabrication of Collagen Matrixes Cross-Linked by a Modified Benzophenone Dimer: Bioactivity and Enzymatic Degradation. *Biomacromolecules* 2005;6:1465–74.
 - [160] Fraser JRE, Laurent TC, Laurent UBG. Hyaluronan: its nature, distribution, functions and turnover. *Journal of Internal Medicine* 1997;242:27–33.
 - [161] Khripin CY, Brinker CJ, Kaehr B. Mechanically tunable multiphoton fabricated protein hydrogels investigated using atomic force microscopy. *Soft Matter* 2010;6:2842–8.
 - [162] Van Den Bulcke AI, Bogdanov B, De Rooze N, Schacht EH, Cornelissen M, Berghmans H. Structural and Rheological Properties of Methacrylamide Modified Gelatin Hydrogels. *Biomacromolecules* 2000;1:31–8.
 - [163] Rumi M, Ehrlich JE, Heikal AA, Perry JW, Barlow S, Hu Z, McCord-Maughon D, Parker TC, Röckel H, Thayumanavan S, Marder SR, Beljonne D, Brédas J-L. Structure–Property Relationships for Two-Photon Absorbing Chromophores: Bis-Donor

- Diphenylpolyene and Bis(styryl)benzene Derivatives. *Journal of the American Chemical Society* 2000;122:9500–10.
- [164] Li Z, Pucher N, Cicha K, Torgersen J, Ligon SC, Ajami A, Husinsky W, Rosspeintner A, Vauthey E, Scherzer T, Stampfl J, Liska R. A Straightforward Synthesis and Structure-Activity Relationship of Highly Efficient Initiators for Two-photon Polymerization. *Macromolecules* 2012;accepted.
 - [165] H.Y. Woo, B. Liu, B. Kohler, D. Korystov, A. Mikhailovsky, G.C. Bazan. Solvent Effects on the Two-Photon Absorption of Distyrylbenzene Chromophores o. J.
 - [166] Li Z. Initiation Efficiency and Cytotoxicity of Novel Water-soluble Two-photon Photoinitiators for Direct 3D Microfabrication of Hydrogel. manuscript in preparation 2013.
 - [167] Husár B, Heller C, Schwentenwein M, Mautner A, Varga F, Koch T, Stampfl J, Liska R. Biomaterials based on low cytotoxic vinyl esters for bone replacement application. *Journal of Polymer Science Part A: Polymer Chemistry* 2011;49:4927–34.
 - [168] Husár B, Liska R. Vinyl carbonates, vinyl carbamates, and related monomers: synthesis, polymerization, and application. *Chemical Society Reviews* 2012;41:2395–405.
 - [169] Heller C, Schwentenwein M, Russmueller G, Varga F, Stampfl J, Liska R. Vinyl esters: Low cytotoxicity monomers for the fabrication of biocompatible 3D scaffolds by lithography based additive manufacturing. *Journal of Polymer Science Part A: Polymer Chemistry* 2009;47:6941–54.
 - [170] Heller C, Schwentenwein M, Russmüller G, Koch T, Moser D, Schopper C, Varga F, Stampfl J, Liska R. Vinylcarbonates and vinylcarbamates: Biocompatible monomers for radical photopolymerization. *Journal of Polymer Science Part A: Polymer Chemistry* 2011;49:650–61.
 - [171] Qin X-H, Torgersen J, Ovsianikov A, Mühleder S, Pucher N, Zhiquan L, Holnthoner W, Saf R, Stampfl J, Liska R. 3D Microfabrication of Protein Hydrogels via Two-photon-excited Thiol-Vinyl ester photopolymerization. in preparation 2013.
 - [172] Mautner A, Qin X, Wutzel H, Ligon SC, Kapeller B, Moser D, Russmueller G, Stampfl J, Liska R. Thiol-ene photopolymerization for efficient curing of vinyl esters. *Journal of Polymer Science Part A: Polymer Chemistry* 2012;n/a–n/a.
 - [173] Hoyle CE, Bowman CN. Thiol–Ene Click Chemistry. *Angewandte Chemie International Edition* 2010;49:1540–73.
 - [174] Qin X-H, Torgersen J, Zhiquan L, Ovsianikov A, Stampfl J, Liska R. 3D Microfabrication of Hyaluronic Acid based hydrogels. in preparation 2013.
 - [175] Köwitsch A, Yang Y, Ma N, Kuntsche J, Mäder K, Groth T. Bioactivity of immobilized hyaluronic acid derivatives regarding protein adsorption and cell adhesion. *Biotechnology and Applied Biochemistry* 2011;58:376–89.
 - [176] Cicha K. Struktur-Eigenschaftskorrelation von 3D-Mikrostrukturen, hergestellt mit Hilfe von Zweiphotonenpolymerisation. Vienna University of Technology, 2012.
 - [177] Stadlmann K-P. Herstellung von Lichtwellenleitern mittels Zweiphotonenlithographie. Vienna University of Technology, 2011.
 - [178] Zeiss C. Objektiv LD Plan-Neofluar 20x/0.4 Korr Ph2 2005.
 - [179] Zeiss C. Objektiv Plan-Apochromat 20x/0.8 SF25 2005.
 - [180] Patel A, Mequanint K. Hydrogel Biomaterials. In: Fazel R, herausgeber. *Biomedical Engineering - Frontiers and Challenges*, InTech; 2011.
 - [181] Cicha K, Koch T, Torgersen J, Li Z, Liska R, Stampfl J. Young's modulus measurement of two-photon polymerized micro-cantilevers by using nanoindentation equipment. *Journal of Applied Physics* 2012;112:094906–094906–6.
 - [182] Pucher N, Rosspeintner A, Satzinger V, Schmidt V, Gescheidt G, Stampfl J, Liska R. Structure–Activity Relationship in D- π -A- π -D-Based Photoinitiators for the Two-Photon-Induced Photopolymerization Process. *Macromolecules* 2009;42:6519–28.
 - [183] Li Z, Pucher N, Cicha K, Torgersen J, Ligon SC, Ajami A, Husinsky W, Rosspeintner A, Vauthey E, Naumov S, Scherzer T, Stampfl J, Liska R. A Straightforward Synthesis and Structure–Activity Relationship of Highly Efficient Initiators for Two-Photon Polymerization. *Macromolecules* 2013;46:352–61.

- [184] Schoiswohl M. Der Einfluss der Laserpulslänge auf die Abmessung von Zweiphotonenlithographie-Strukturen. Vienna: Vienna University of Technology; 2013.
- [185] Gittard SD, Miller PR, Boehm RD, Ovsianikov A, Chichkov BN, Heiser J, Gordon J, Monteiro-Riviere NA, Narayan RJ. Multiphoton microscopy of transdermal quantum dot delivery using two photon polymerization-fabricated polymer microneedles. *Faraday Discuss* 2011;149:171–245.
- [186] Liska R. PEGda auto-fluorescence at 488nm. 2013.
- [187] Fritze S. Wasserlösliche Photoinitiatoren für die Laserverarbeitung von biokompatiblen Hydrogelen mittels Zweiphotonenlithographie. Vienna: Vienna University of Technology; 2013.
- [188] Stiernagle T. Maintenance of *C. elegans*. *WormBook the online review of C elegans biology* 2006;15:1–11.
- [189] Anfinsen CB, Edsall JT, Richards FM. *Advances in protein chemistry*. Volume 24. New York; London: Academic Press; 1970.
- [190] Medicago AB. PBS Buffer Datasheet. Uppsala, Sweden: Medicago SB; o. J.
- [191] Murphy MC, Howell NK. Functional properties of native and positively and negatively charged modified bovine serum albumin. *Journal of the Science of Food and Agriculture* 1991;55:489–92.
- [192] Langer R, Vacanti JP. Tissue engineering. *Science* 1993;260:920–6.
- [193] Clarke JDW, Jayasinghe SN. Bio-electrosprayed multicellular zebrafish embryos are viable and develop normally. *Biomedical Materials* 2008;3:011001.
- [194] Williams PL, Dusenbery DB. Using the Nematode *Caenorhabditis Elegans* To Predict Mammalian Acute Lethality To Metallic Salts. *Toxicology and Industrial Health* 1988;4:469–478.
- [195] Donkin S, Dusenbery D. A soil toxicity test using the nematode *Caenorhabditis elegans* and an effective method of recovery. *Archives of Environmental Contamination and Toxicology* 1993;25.
- [196] Donkin SG, Dusenbery DB. Using the *Caenorhabditis elegans* soil toxicity test to identify factors affecting toxicity of four metal ions in intact soil. *Water, Air, & Soil Pollution* 1994;78:359–73.
- [197] Bargmann C. Chemosensation in *C. elegans*. *WormBook* 2006.
- [198] Dorland WAN. *Dorland's Medical dictionary* / introd. by Franz J. Ingelfinger. Philadelphia, Pa. : New York :: Saunders Press ; distributed by Holt, Rinehart & Winston; Philadelphia, Pa. : Saunders Press ; New York : distributed by Holt, Rinehart & Winston, c1980.
- [199] Brenner S. The genetics of *Caenorhabditis elegans*. *Genetics* 1974;77:71–94.
- [200] Bischof LJ, Huffman DL, Aroian RV. Assays for Toxicity Studies in *C. elegans* With Bt Crystal Proteins. In: Strange K, herausgeber. *C. elegans*, Humana Press; 2006, S. 139–54.

19 Curriculum Vitae

Name: Jan Torgersen
Academic degree: Dipl.-Ing.
Nationality: Austrian
Date of birth: 06. Aug 1984
Place of birth: Vienna
Email: jan.torgersen@tuwien.ac.at
Tel.: +43-(0)1-58801-30869
Fax: +43-(0)1-58801-30895



Employment

05/2010-present: Project Assistant at the Institute of Material Science and Technology (Group of Prof. J. Stampfl) Vienna University of Technology, Favoritenstrasse 9-11, 1040 Vienna, Austria

Education

05/2010-present: PhD Student at the Institute of Materials Science and Technology (Group of Prof. J. Stampfl) Vienna University of Technology
2004-2010: Student at the Vienna University of Technology, graduated with Dipl.-Ing. in Industrial Engineering
1995-2003: High School, Vienna

Academic Appointment

05/2010-present: Scientific researcher at the Institute of Material Science and Technology

Publications in Scientific Journals

- [1] **J. Torgersen**, X. Qin, Z. Li, A. Ovsianikov, P. Gruber, R. Liska, J. Stampfl: "Hydrogels for two-photon polymerisation: a toolbox for mimicking the extracellular matrix. Advanced Functional Materials", Advanced Functional Materials (**invited**), accepted 2013
- [2] Z. Li, N. Pucher, K. Cicha, **J. Torgersen**, S.C. Ligon, A. Ajami, W. Husinsky, A. Rosspeintner, E. Vauthey, S. Naumov, T. Scherzer, J. Stampfl, R. Liska: "A Straightforward Synthesis and Structure–Activity Relationship of Highly Efficient Initiators for Two-Photon Polymerisation"; Macromolecules, 46 (2013), 352-361.
- [3] **J. Torgersen**, A. Ovsianikov, V. Mironov, N.U Pucher, X.H. Qin, Z. Li, K. Cicha, T. Machacek, V. Jantsch-Plunger, R. Liska, J. Stampfl: "Photo-sensitive hydrogels for threedimensional laser micro-fabrication in the presence of whole organisms"; Journal of Biomedical Optics, 17 (2012), 10; 1 - 10.
- [4] R.A. Rezende, F.D.A.S Pereira, V. Kasyanov, A. Ovsianikov, **J. Torgersen**, P. Gruber,

- J. Stampfl, K. Brakke, J.A. Nogueira, V. Mironov, J.V.L. da Silva: "Design, physical prototyping and initial characterisation of "lockyballs""; Virtual and Physical Prototyping, 7 (2012), 287-301.
- [5] A. Ovsianikov, Z. Li, A. Ajami, **J. Torgersen**, W. Husinsky, J. Stampfl, R. Liska: "3D grafting via three-photon induced photolysis of aromatic azides"; Applied Physics A: Materials Science & Processing, 108 (2012), 1; 29 - 34.
- [6] A. Ovsianikov, Z. Li, **J. Torgersen**, J. Stampfl, R. Liska: "Selective Functionalization of 3D Matrices Via Multiphoton Grafting and Subsequent Click Chemistry"; Advanced Functional Materials, 22 (2012), 16; 3429 - 3433.
- [7] K. Cicha, T. Koch, **J. Torgersen**, Z. Li, R. Liska, J. Stampfl: "Young's modulus measurement of two-photon polymerised microcantilevers by using nanoindentation equipment"; Journal of Applied Physics, 112 (2012), 094906.
- [8] **J. Torgersen**, A. Baudrimont, N.U Pucher, K. Stadlmann, K. Cicha, C. Heller, R. Liska, J. Stampfl: "In Vivo Writing using Two-Photon-Polymerisation"; Laser Precision Micro-fabrication 2010, Stuttgart, D; 2010-06-07 - 2010-06-10; in: "Proceedings of LPM2010", K. Sugiyoka (ed.); (2010), #10-42.

Talks and Poster Presentations

- [1] A. Ajami, Z. Li, A. Ovsianikov, **J. Torgersen**, J. Stampfl, W. Husinsky: "Effect of Concentration of Chromophores on Two-photon Absorption Cross Section"; Poster: 50 years of nonlinear optics, NLO 50 International Symposium, Barcelona/Spain; 2012-10-08 - 2012-10-10.
- [2] A. Ovsianikov, **J. Torgersen**, X.H. Qin, Z. Li, S. Mühleder, W. Holthöner, H. Redl, R. Liska, J. Stampfl: "Laser fabrication of cell-containing hydrogel constructs"; Talk: International Conference on Biofabrication, Manchester; 2012-10-29 - 2012-10-31.
- [3] J. Stampfl, **J. Torgersen**, A. Ovsianikov, X.H. Qin, L. Zhiquan, V. Mironov, R. Liska: "Photo-sensitive Biocompatible Hydrogels Structuring Extracellular Environments by Two Photon Polymerisation"; Poster: 2012 MRS Spring Meeting & Exhibit, San Francisco; 2012-04-09 - 2012-04-13.
- [4] **J. Torgersen**: "The race at the bottom: speeding up nanotechnology"; Talk: TEDx Vienna, Wien (**invited**); 2012-11-03.
- [5] **J. Torgersen**, A. Ovsianikov, V. Mironov, N.U Pucher, X.H. Qin, Z. Li, K. Cicha, T. Machacek, V. Jantsch-Plunger, R. Liska, J. Stampfl: "High Speed 3D laser micro-fabrication of biocompatible hydrogel scaffolds"; Keynote Lecture: CAIM III Tercier Congreso Argentino de Ingeniería Mecánica, Buenos Aires (**invited**); 2012-10-02 - 2012-10-05.
- [6] K. Cicha, Z. Li, K. Stadlmann, **J. Torgersen**, R. Markut-Kohl, R. Liska, J. Stampfl: "Fabrication and evaluation of 3D-micro-structures produced using two-photon-induced photopolymerisation (TPIP or 2PP) by means of optical assessment and FTIR-spectroscopy"; Talk: 16. Tagung Festkörperanalytik, Wien; 2011-07-04 - 2011-07-06.
- [7] Z. Li, X.H. Qin, A. Ovsianikov, **J. Torgersen**, A. Ajami, W. Husinsky, S. Mühleder, W. Holthöner, J. Stampfl, R. Liska: "Water-soluble Initiators for Two-photon Polymerisation"; Poster: The 3rd TERMIS World Congress 2012, Vienna; 2012-09-05 - 2012-09-08; in: "Journal of Tissue Engineering and Regenerative Medicine 2012", John Wiley & Sons, Ltd., 6/Supplement s1 (2012), ISSN: 1932-7005; 369.
- [8] X.H. Qin, Z. Li, **J. Torgersen**, A. Ovsianikov, S. Mühleder, W. Holthöner, J. Stampfl, R. Liska: "Developing Biodegradable 3D Hydrogels Scaffolds: From Synthesis to Two-photon Polymerisation"; Poster: The 3rd TERMIS World Congress 2012, Vienna; 2012-09-05 - 2012-09-08; in: "Journal of Tissue Engineering and Regenerative Medicine

- 2012", John Wiley & Sons, Ltd., 6/Supplement s1/ (2012), ISSN: 1932-7005; 369.
- [9] X.H. Qin, **J. Torgersen**, N.U Pucher, A. Mautner, Z. Li, A. Ovsianikov, J. Stampfl: "Multiphoton Fabrication of Protein Hydrogels in 3-dimensions via Thiol-ene Photo-click Reactions"; Talk: The 9th World Biomaterials Congress, Chengdu, China; 2012-06-01 - 2012-06-05; in: "9th World Biomaterials Congress", (2012), 1.
 - [10] X.H. Qin, Z. Li, S. Ligon, **J. Torgersen**, A. Ovsianikov, S. Mühleder, W. Holnthoner, J. Stampfl, R. Liska: "Biodegradable 3D Hydrogel Scaffolds: Synthesis and Two-photon Polymerisation"; Poster: E-MRS 2012 FALL MEETING (European Materials research Society), Warschau; 2012-09-17 - 2012-09-21; in: "E-Mrs 2012 Fall Meeting", (2012).
 - [11] S. Ligon, B. Husar, H. Wutzel, H. Hoffmann, **J. Torgersen**, R. Liska: "Assessing anti-oxygen inhibition strategies for LED-based wood coatings by FTIR"; Talk: European Symposium of Photopolymer Science - ESPS 2012, Torino; 2012-09-04 - 2012-09-07; in: "European Symposium of Photopolymer Science - Book of Abstracts", (2012).
 - [12] X.H. Qin, Z. Li, A. Ovsianikov, **J. Torgersen**, S. Mühleder, W. Holnthoner, J. Stampfl, R. Liska: "Developing biodegradable 3D hydrogel scaffolds: from synthesis to two-photon polymerisation"; Poster: European Symposium of Photopolymer Science - ESPS 2012, Torino; 2012-09-04 - 2012-09-07; in: "European Symposium of Photopolymer Science - Book of Abstracts", (2012), 19.
 - [13] Z. Li, X.H. Qin, A. Ovsianikov, **J. Torgersen**, S. Mühleder, W. Holnthoner, A. Ajami, W. Husinsky, J. Stampfl, R. Liska: "Water-soluble Initiators for Two-photon Polymerisation"; Poster: European Symposium of Photopolymer Science - ESPS 2012, Torino; 2012-09-04 - 2012-09-07; in: "European Symposium of Photopolymer Science - Book of Abstracts", (2012), 26.
 - [14] Z. Li, X.H. Qin, A. Ovsianikov, **J. Torgersen**, A. Ajami, J. Stampfl, R. Liska: "3D site-specific functionalization of matrices via multi-photon grafting and subsequent click reaction"; Poster: European Symposium of Photopolymer Science - ESPS 2012, Torino; 2012-09-04 - 2012-09-07; in: "European Symposium of Photopolymer Science - Book of Abstracts", (2012), 25.
 - [15] Z. Li, A. Ovsianikov, **J. Torgersen**, J. Stampfl, R. Liska: "3D site-specific functionalization of matrices via multi-photon grafting and subsequent click reaction"; Poster: International Symposium on NanoPhotonics 2012, Beijing; 2012-02-12 - 2012-02-14; in: "International Symposium on NanoPhotonics 2012", (2012).
 - [16] X.H. Qin, Z. Li, **J. Torgersen**, A. Ovsianikov, S. Mühleder, W. Holnthoner, J. Stampfl, R. Liska: "Development of biocompatible 3D hydrogel scaffolds: From synthesis to two-photon-polymerisation"; Poster: 5th Biomaterialsymposium, Vienna; 2012-11-19 - 2012-11-21; in: "Abstracts", J. Stampfl (ed.); (2012), 65.
 - [17] Z. Li, X.H. Qin, A. Ovsianikov, **J. Torgersen**, A. Ajami, W. Husinsky, S. Mühleder, W. Holnthoner, J. Stampfl, R. Liska: "Novel water-soluble two-photon initiators for 3D scaffold micro-fabrication"; Talk: 5th Biomaterialsymposium, Vienna; 2012-11-19 - 2012-11-21; in: "5th Vienna Biomaterialsymposium 19.11.-21.11.2012", J. Stampfl (ed.); (2012), 95.
 - [18] F. Höller, A. Ovsianikov, **J. Torgersen**, T. Koch, D. Dekel, S. Levenberg, S. Nürnberger, H. Redl, R. Liska, J. Stampfl: "Laser micro-fabrication of elastic 3D scaffolds"; Poster: 5. Wiener Biomaterialsymposium, Wien; 2012-11-19 - 2012-11-21; in: "Abstracts 5th Biomaterialsymposium Vienna", (2012), 107 - 108.
 - [19] A. Ovsianikov, **J. Torgersen**, X.H. Qin, Z. Li, S. Mühleder, W. Holnthoner, R. Liska, J. Stampfl: "Engineering 3D cell-culture matrices with femtosecond laserinduced photochemistry"; Keynote Lecture: 5. Wiener Biomaterialsymposium, Wien (invited); 2012-11-19 - 2012-11-21; in: "Abstracts 5th Biomaterialsymposium Vienna", (2012), 15 - 16.

- [20] S. Gruber, **J. Torgersen**, A. Neumeister, R. Felzmann, R. Liska, J. Stampfl: "Advanced Photopolymer-based Additive Manufacturing Systems Using High Performance Light Sources"; Talk: 7th International Symposium on Emerging and Industrial DLP® Applications, Frankfurt; 2012-10-30; in: "7th International Symposium on Emerging and Industrial DLP® Applications", (2012).
- [21] J. Stampfl, **J. Torgersen**, A. Ovsianikov, X.H. Qin, Z. Li, S. Mühleder, W. Holthöner, R. Liska: "Photo-stimulation of low-toxicity biopolymers in additive manufacturing"; Talk: Materials Science and Engineering 2012, Darmstadt, Deutschland; 2012-09-25 - 2012-09-27; in: "MSE Programme", (2012), 22.
- [22] A. Ovsianikov, S. Nürnberger, **J. Torgersen**, Z. Li, H. Redl, R. Liska, J. Stampfl: "Fabrication of elastic 3D scaffolds by two-photon polymerisation"; Talk: Materials Science and Engineering 2012, Darmstadt, Deutschland; 2012-09-25 - 2012-09-27; in: "MSE Programme", (2012), 37.
- [23] **J. Torgersen**, A. Ovsianikov, V. Mironov, N.U. Pucher, X.H. Qin, K. Cicha, Z. Li, T. Machacek, V. Jantsch-Plunger, R. Liska, J. Stampfl: "Biocompatible Hydrogels for the Three-dimensional Micro-fabrication of Extracellular Environments"; Talk: Bio-inspired Materials, Potsdam; 2012-03-20 - 2012-03-23; in: "Bio-inspired Materials International School and Conference on Biological Materials Science", DGM Programme, (2012), 20.
- [24] R. Liska, M. Schwentenwein, S. Baudis, S. Ligon, A. Mautner, A. Gugg, Z. Li, C. Gorsche, N.U. Pucher, **J. Torgersen**, F. Nehl, H. Bergmeister, K. Macfelda, T. Koch, G. Russmüller, J. Stampfl: "3D-Printing of Advanced Biomaterials by Additive Manufacturing Technologies"; Talk: UPAC 9th International Conference on Advanced Polymers via Macromolecular Engineering (APME 2011), Cappadocia, TR (invited); 2011-09-05 - 2011-09-08; in: "IUPAC 9th International Conference on Advanced Polymers via Macromolecular Engineering (APME 2011) - Program and Abstract Book", (2011), 101.
- [25] A. Ovsianikov, **J. Torgersen**, R. Liska, J. Stampfl: "3D photofabrication by femtosecond laser pulses and its applications in biomedicine"; Talk: 4th European Conference on Applications of Femtosecond Lasers in Materials Science FemtoMat & Nano and Photonics, Mauterndorf; 2011-03-14 - 2011-03-18; in: "4th European Conference on Applications of Femtosecond Lasers in Materials Science- Femto Mat", (2011), 4.
- [26] A. Ovsianikov, **J. Torgersen**, Z. Li, J. Stampfl: "3D photofabrication by femtosecond laser pulses and its applications in biomedicine"; Talk: Laser Precision Micro-fabrication 2011, Takamatsu, Kagawa, Japan; 2011-06-07 - 2011-06-10; in: "Tagungsband Laser Precision Micro-fabrication 2011", (2011), 121.
- [27] K. Cicha, Z. Li, A. Mautner, K. Stadlmann, **J. Torgersen**, N.U. Pucher, R. Markut-Kohl, R. Liska, J. Stampfl: "Fabrication and evaluation of 3D-micro-structures produced using two-photon-induced photopolymerisation (TPIP or 2PP) by means of optical assessment and FTIR-spectroscopy"; Talk: Euromat 2011, Montpellier, France; 2011-09-12 - 2011-09-15; in: "Conference Proceeding Euromat 2011", (2011), 0453.
- [28] **J. Torgersen**, A. Baudrimont, N.U. Pucher, K. Stadlmann, C. Heller, R. Liska, J. Stampfl: "Biocompatible Materials structured in-vivo using high-resolution AMT"; Talk: Euro Biomat, Jena; 2011-04-13 - 2011-04-14; in: "Euro Biomat - European Symposium on Biomaterials and Related Areas", 22 (2011), 18.
- [29] **J. Torgersen**, A. Baudrimont, N.U. Pucher, K. Stadlmann, K. Cicha, C. Heller, R. Liska, J. Stampfl: "In Vivo Scaffold Fabrication"; Poster: ESAO-ASAIO Winter School 2011, Semmering; 2011-01-26 - 2011-01-29; in: "Advancing Roles: Biomaterials in Artificial Organs and Regenerative Medicine", D. Falkenhagen, E. F. Leonard, S. Mikhalevsky (ed.); (2011), 70.

- [30] X.H. Qin, **J. Torgersen**, L. Zhiquan, A. Ovsianikov, C. Heller, M. Schwentenwein, G. Russmüller, J. Stampfl, R. Liska: "Two-photon induced polymerisation for 3D fabrication of Biocompatible and Biodegradable hydrogels"; Poster: 4. Wiener Biomaterialsymposium: Von der Werkstoffentwicklung bis zur klinischen Anwendung, TU Wien, Wien; 2010-11-15 - 2010-11-17; in: "Tagungsband", (2010), 56.
- [31] X.H. Qin, **J. Torgersen**, C. Heller, M. Schwentenwein, G. Russmüller, J. Stampfl, R. Liska: "Two-photon induced Polymerisation for 3D Micro-fabrication of Biocompatible and Biodegradable Hydrogels"; Poster: European Symposium of Photopolymer Science, Mulhouse, France; 2010-11-28 - 2010-12-01; in: "European Symposium of Photopolymer Science - Abstract Book", (2010).
- [32] **J. Torgersen**, A. Baudrimont, N.U Pucher, K. Stadlmann, K. Cicha, C. Heller, R. Liska, J. Stampfl: "In-Vivo-Writing mittels Zweiphotonenlithographie"; Talk: 4. Wiener Biomaterialsymposium, Wien; 2010-11-15 - 2010-11-17; in: "Tagungsband- 4. Wiener Biomaterialsymposium", (2010), 24.
- [33] **J. Torgersen**, A. Baudrimont, N.U Pucher, K. Stadlmann, K. Cicha, C. Heller, J. Stampfl, R. Liska: "Poster F5-64 In-Vivo Writing using Two-Photon-Polymerisation as Enabling Technology for Making Use of Bio-inspired Structures"; Poster: Materials science and engineering MSE 2010, Darmstadt; 2010-08-24 - 2010-08-26; in: "Tagungsband Material science and engineering 2010", (2010), 45.
- [34] **J. Torgersen**, A. Baudrimont, N.U Pucher, K. Stadlmann, K. Cicha, C. Heller, R. Liska, J. Stampfl: "In Vivo Nanostructuring of Biocompatible Materials"; Poster: BioNanoMed 2010, Krems a.d. Donau; 2010-11-02 - 2010-11-03; in: "BioNanoMed 2010", (2010), 12.
- [35] **J. Torgersen**, A. Baudrimont, N.U Pucher, K. Stadlmann, K. Cicha, C. Heller, R. Liska, J. Stampfl: "In Vivo Writing using Two-Photon-Polymerisation"; Talk: 11th International Symposium on Laser Precision Micro-fabrication, LPM 2010, Stuttgart, D; 2010-06-07 - 2010-06-10.

Diploma Thesis:

- [1] **J. Torgersen**: "In-Vivo-Writing using Two-Photon Lithography"; Supervisor: J. Stampfl, R. Liska; TU Wien, 2010; final examination: 2010-03-24.